

Prof. Dr. May-Britt Kallenrode

Fachbereich Physik

Modeling Transport

Osnabrück, 13th November 2006

Contents

1	What is Transport?	1
1.1	What is transport? – A Guided Tour	1
1.2	Help, I still can't define Transport	9
1.2.1	Definition	9
1.2.2	Classification – Questions on our Way to a Transport Model	10
1.2.3	Why should I Model at All?	10
1.3	Orientation	12
2	Modeling	14
2.1	Outline	15
2.1.1	Types of Models	16
2.1.2	When Not to Model	17
2.2	Creating a model	19
2.2.1	Make a Sketch	19
2.2.2	Draw an Envelope	19
2.2.3	Simplifying Assumptions	19
2.2.4	Closure	22
2.3	Examples	24
2.3.1	Discharge of a Plant Effluent into a River	24
2.3.2	Newton's Law of Cooling	25
2.3.3	Evaporation of a Pollutant into the Atmosphere	26
2.3.4	Thermal Balance of a Building	28
2.4	If Inspiration Refuses to Help	36
2.4.1	Mass Conservation	36
2.4.2	Energy Conservation	38
2.4.3	Conservation of Momentum (Equation of Motion)	38
2.5	Selling and Borrowing	38
3	Constant Flow with Reactions	41
3.1	Chemical Reactor in Steady-State	41
3.1.1	The Problem	42
3.1.2	The Model	42
3.1.3	Solving the Problem	43
3.1.4	Closure	45
3.2	Time-Dependent Reactor	46
3.2.1	Numerical Method 1: Implicit Method	47
3.2.2	Numerical Method 2: Crank–Nicolson	48
3.2.3	Closure	50
3.3	Compartment Models in Natural Systems	51

4	Diffusion and Heat Conduction	55
4.1	Diffusion – The Basics	55
4.1.1	Examples	56
4.1.2	Formal Description of Diffusive Processes	57
4.1.3	Diffusion and Dispersion	62
4.2	Diffusion/Heat Conduction – Simple Cases	63
4.2.1	Stationary Heat Transport in a Plate	63
4.2.2	The Time-Dependent Problem	69
4.3	Diffusion–Convection Model	71
4.3.1	The Transport Equation	71
4.3.2	Simple Analytical Solution	71
4.3.3	Numerical Solutions	71
4.4	Diffusion–Reaction Model	72
4.4.1	Turing Patterns	73
4.4.2	Other Application of Diffusion–Reaction Models	73
4.5	Diffusion in Porous Media	74
4.5.1	A Simple Example: Ground Penetration from an Oil Spill	75
4.6	Phase Transitions: The Stefan Problem	76
4.6.1	The Shrinking Core Model and Quasi-Steady State	76
4.6.2	Solidification in Heat Transfer	78
4.6.3	Traffic Jam and Phase Transition	79
5	Finite Differences with Splitting	81
5.1	The Problem	81
5.2	The Model	82
5.2.1	Physical Basis	83
5.2.2	Focusing in the Large Scale Interplanetary Magnetic Field	83
5.2.3	Pitch Angle Diffusion	84
5.2.4	Diffusion in Momentum Space	85
5.2.5	Wave–Particle Interactions	85
5.2.6	Solar Wind Effects	87
5.2.7	The Transport Equation	87
5.2.8	Boundary and Initial Conditions	88
5.3	The Numerical Scheme	89
5.3.1	The Splitting Scheme	89
5.3.2	The Spatial Transport $L(s)$	89
5.3.3	The Pitch-Angle Transport $L(\mu')$	89
5.3.4	The Momentum Transport $L(p')$	91
5.4	Closure	91
5.5	Extensions	93
5.5.1	The Shock as a Moving Source of Particles	93
5.5.2	Magnetic Cloud and Modified Focusing	95
5.5.3	The Numerics behind the Shock	97
5.5.4	Extension: Perpendicular Diffusion	97
5.6	Particle Motion going Extreme	98
6	Dikes: Finite Element Modeling	100
6.1	Finite Elements	100
6.1.1	Introductory Example	101
6.1.2	FEM – The Idea	102
6.1.3	FEM – The Scheme	103
6.2	Simple 1D Examples	105
6.2.1	First Encounter with π	105
6.2.2	Longitudinal Tank	106
6.3	Application: Dikes	107

6.3.1	The Problem	107
6.3.2	The Model	108
6.3.3	Finite Elements Applied	112
6.3.4	Results	113
7	Panta Rei: Computational Fluid Dynamics (CFD)	118
7.1	The Physics of the Flow: Navier–Stokes Equation	118
7.1.1	Pressure-Gradient Force	119
7.1.2	Equation of Motion: Euler and Navier–Stokes	120
7.1.3	Stress Tensor and Viscosity	120
7.1.4	Fictitious Forces in Rotating Systems	121
7.1.5	Electromagnetic Forces	122
7.1.6	Putting it all Together	122
7.2	Boundary Layer Problem: Motion of Fluid Layers	123
7.2.1	The Model	123
7.2.2	Numerical Solution: Finite Centered Differences in Time and Space	124
7.2.3	Closure	125
7.3	Typical Examples from CFD	126
7.3.1	Flow around a Body	126
7.3.2	Fire and Smoke Modeling	127
7.3.3	Magnetohydrodynamics	128
7.4	Literature	135
8	Monte Carlo Simulation	136
8.1	Monte Carlo – A first Encounter	136
8.1.1	Numerical Integration	136
8.1.2	Accuracy of a Monte Carlo Result	139
8.1.3	How Random are Random Numbers?	139
8.2	Monte Carlo Simulation – First Steps	140
8.2.1	Radioactive Decay	140
8.2.2	Convection and Decay	142
8.2.3	Longitudinal Tank	142
8.3	Energetic Charged Particles in the Atmosphere	142
8.3.1	Modeling Individual Events	144
8.3.2	Monte Carlo Simulation of Atmospheric Ionization	146
8.3.3	Applications of the Model	151
8.4	Some other Examples	158
8.4.1	Nuclear Physics: GEANT 4	158
8.4.2	Medical Applications	159
8.4.3	Complex Environments: Stochastic Differential Equations	160
8.5	Summary	162
9	Unconventional Transport Processes	163
9.1	Small Networks	163
9.1.1	Why do we need the Small World Concept?	166
9.1.2	From Small World to Scale-Free Nets	167
9.1.3	Not a Test: Disease and Money	169
10	Projects	171
10.1	Rules of the Road	171
10.2	Project 1	172
10.2.1	Idea	172
10.2.2	Definition of the Project	172
10.2.3	Details	172
10.3	Project 2	173

10.3.1	Idea	173
10.3.2	Definition of the Project	173
10.3.3	Details	174
10.4	Project 3	174
10.4.1	Definition of the Project	174
10.4.2	Details	175
10.5	Project 4	175
10.5.1	Idea	176
10.5.2	Definition of the Project	176
10.5.3	Details	177
11	Closure	178
11.1	Transport Modeling in General	178
11.2	Numerical Methods	179
11.3	Finite Difference Method: Schemes	179
11.4	Some Final Words	181
A	Useful Things	182
A.1	List of symbols	182
A.2	List of Acronyms	184
A.3	Useful Numbers	185
A.4	Exponential Function and Related Stuff	185
A.5	Vector Calculus	185
B	A Little Mathematical Reminder	187
B.1	Analytical Strategies for Ordinary Differential Equations	187
B.2	Partial Differential Equations – Classification	189
B.2.1	Characteristics of a PDE	189
B.2.2	Types of PDEs – Examples	190
B.2.3	Summary 2D	192
B.3	Laplace Transformation	192
B.3.1	Integral Transforms	192
B.3.2	Properties of the Laplace Transform	193
C	A Little Remainder on Some Physics Basics	196
C.1	Some Fundamental Laws	196
C.2	Distributions and Phase Space Density	198
C.2.1	Phase space density	198
C.2.2	Averaging	199
C.2.3	Maxwell’s Velocity Distribution	199
C.2.4	Distribution Function and Measured Quantities	200
C.3	Fundamental Transport Equations in Phase Space	201
C.3.1	Boltzmann equation	201
C.3.2	Fokker–Planck equation	202
C.3.3	Vlasov equation	203
C.4	Excursion: Collisions	204
C.4.1	Collisions Between Neutrals	205
C.4.2	Collisions Between Charged Particles	206
C.5	Scale Analysis	207
C.5.1	Equation of motion in Oceans and in the Atmosphere	207

D A Little Remainder on Some Numeric's Basics	210
D.1 Discretization	210
D.1.1 First- and Second-Order Derivatives	210
D.1.2 Consistency and Accuracy	211
D.1.3 Stability	212
D.2 Numerical Integration – The Basics	213
D.3 Numerical Solutions of ODEs – Finite Differences	213
D.4 Numerical Solutions of PDEs – Finite Difference Methods	215
D.4.1 Linear Hyperbolic Equations	215
D.4.2 Linear Parabolic Equations	216
D.4.3 Linear Elliptic Equations	217
D.4.4 Diffusion–Convection Equation	218
D.5 Thomas Algorithm for Tridiagonal Matrices	218
E Solutions to some questions	220

Chapter 1

What is Transport?

Transport is related to the (re-)distribution of matter (or other properties of space) with time. Formally, in the simplest case this is described by a partial differential equation (PDE), in the more interesting applications by a system of PDEs. This introduction gives some general ideas of transport processes, the underlying physics and the mathematical description.

Goals: after working through this chapter you should be able:

- to give examples for transport processes and to appreciate the manifold of different transport processes as well as the manifold of applications of one particular transport process to entirely different (physical) problems.
- to get a first glimpse on models embedded in models embedded in models embedded in models and to understand the importance of well defined goals and boundaries of a model.
- to classify transport problems.

1.1 What is transport? – A Guided Tour

Give me a break – let’s start with a more basic question: **What can be transported?** That is (a) matter, (b) momentum and energy, and (c) information. For a start, let us limit ourselves to the transport of matter and browse through a few examples with a short pictorial guide.

In it’s daily meaning, transport most likely is associated with traffic; an autobahn can serve as illustration for transport. This kind of transport is basically 1D (coordinate is the autobahn-km) and directed. The particle flow can be described in different ways. In the most simple case, we assume that all particles move at the same speed. This approach resembles a cold fluid, thus the flow can be described by Bernoulli’s law. Consequently, the flow will speed up at an obstruction and slow down if the autobahn widens (e.g. an additional lane). No traffic jam will ever occur.



A different approach should consider the particles individual speeds. These can be described by some distribution added to the average flow speed. The resulting transport can be modeled as a 1D-diffusion-convection model – and this model even allows for the build-up of a traffic jam.¹ If your special interest in transport is in this kind of transport, you might consider a closer look into *Modeling Transport* by Ortúzar and Willumsen [124].

¹Amazingly, traffic jams do not necessarily require a construction site or an accident that slows down the traffic flow but can build-up out of nothing just due to the gradients in speed. Information on traffic modeling can be obtained at <http://www.traffic.uni-duisburg.de/>; traffic jams as a form of a phase transition will be briefly discussed in sect. 4.6.3; project 2 allows you to study this topic in more detail.

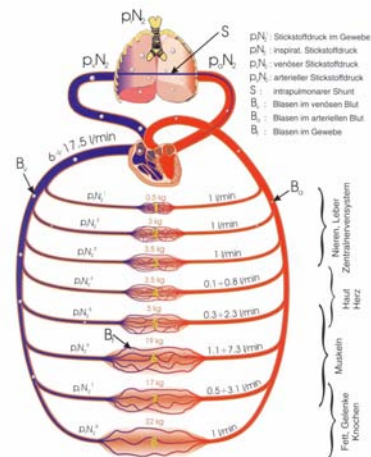
Side question 1 Is traffic a continuous, incompressible fluid or made up of discrete cars? Is the requirement for a fluid/gas to be in equilibrium fulfilled in traffic?

A pipeline also is an example for directed transport. As in an autobahn, the goal is to move matter from A to B as fast as possible. But not too fast: if the flow becomes turbulent, energy is converted from bulk motion via turbulence into heat. Thus pumping becomes expensive. Although we are still in a 1D geometry, Bernoulli probably would not be sufficient to describe this mode of transport: first of all, all the twists and bends in a pipeline will generate a certain amount of turbulence. And secondly, the fluid transported through the pipeline might sediment its more solid parts eventually modifying the flow. This is of particular concern in oil refineries; the interested reader might consult *Advanced transport phenomena* [157].



Side question 2 Recapitulate Bernoulli and related laws. Are they sufficient to explain the turbulence created in the bend of a pipe? Do they account for turbulence at constrictions or behind obstacles?

A very similar, although natural system is the cardiovascular system. Again, a fluid is transported through pipes which vary in diameter. These pipes also branch and connect. In addition, the problem of congestion by ‘fall-out’ from the fluid is also known; here it is called arteriosclerosis. The main challenges in modeling the cardiovascular system are the time-dependent complex pumping system (heart, supportive indirect pumping by valves in the extremities) and the varying diameter of the vessels: in the main aorta blood certainly can be regarded as a liquid; the small capillary vessels, however, have diameters of the order of the diameter of a red blood cell – thus blood no longer is a fluid but consists of discrete vehicles. Some of the more interesting topics on the subject are discussed in *The physics of heart and circulation* by Strackee and Westerhoff [161].



Some in-between calculation 1 If blood in some vessels can be regarded as simple flow and in others as particulate matter – how is it described in vessels with diameters in between. Or in other wording: where does the transition happen, what are the consequences of this transition for modeling?

But not even such a simple liquid as pure water behaves always as a fluid if transport is concerned. Instead, interesting transport phenomena can be created if a droplet of water hits the surface of a body of water: surface waves travel from the impact site outwards. They transport energy and the information about the impact to remote sites. Thus we get an entirely different physical situation: first, the droplets potential energy is converted to kinetic energy during its fall. After impact this energy is converted to wave energy. The energy transport in the first part is coupled to the motion of the droplet (and its heating since friction cannot be neglected). In the second part, energy is also coupled to the motion of water, nonetheless, while the energy is transported away from the impact site the matter stays at rest – except for small motions around the rest position to allow for wave propagation. Formally, this is described



by a 2D wave equation – a transport mode that will not be discussed in more detail in this text. Although the Indian ocean tsunami has drawn the public attention to surface waves only recently, coastal engineers consider them an important topic, in particular at times of climate change. This interest is also reflected in the large number of good textbooks on ocean surface wave, such as [38, 39, 108, 111]. Freak waves are another special version of ocean surface waves and also make it into the press sometimes: for a long time they were regarded as sailor’s folk tale, however, they occasionally swallow even larger ships and their existence has been confirmed by automatized measuring buoys; for further information you might consult http://www.math.uio.no/~karstent/waves/index_en.html, which also offers pdf’s of some papers, or the more popular site <http://www.saevert.de/2freakwaves.htm>. A pretty good resource, also in Norwegian only, is Dysthe’s talk in modeling of freak waves (<http://www.math.uio.no/~karstent/waves/vitenskapsakademiet.pdf>).

Although also related to water and surfaces, an entirely different transport phenomenon can be observed at a window pane when droplet meets droplet during a rain shower. Here the transport is not as simple as one might expect. Naively, the dominating force on the droplet should be gravitation, pulling it down. However, intermolecular forces between the water molecules and the pane’s surface determine not only shape and size of any of the droplet individually but also influence its motion. As a droplet follows the pull of gravity it often follows the path left by an earlier droplet. And a droplet might not necessarily stay a droplet but interact and coalescence with another droplet.



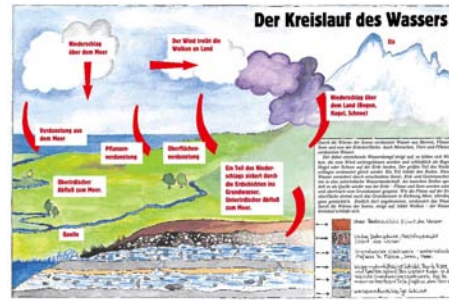
Side question 3 Is it possible to model such kind of processes? And if so, what would be a reasonable approach – deterministic or stochastic?

While the last example had the individual droplet in its focus, this example for transport in some respect resembles the autobahn – but still contains the droplet aspect. At least in its upper parts (almost hidden from the view) the flow is channeled by the structure of the underlying rock. Although this is a channeled transport, it is also turbulent transport. With increasing fall, the flow divides into a large number of partially interacting sub-streams which partly even resolve into droplets. Here the boundary condition, that is the surface of the rock beneath the stream, determines the structure and character of the flow. Although it looks pretty difficult to model, this is a very simple example for a natural water flow: the rock is a static boundary condition, at least on time scales that are not concerned with the erosion of mountain ranges. Thus this boundary condition can be implemented into any numerical model easily even if the expenditure of work is large. If the stream passes over porous rock or runs in a sand bed the situation is different: fluid can be exchanged across this boundary, thus the bottom of the stream is not a closed boundary but right in the middle of the simulation volume and the medium below the stream bed must be considered. This is one prominent example for transport modeling related to human needs: fresh water, which often is groundwater. Such a reservoir should not be depleted faster than nature can replenish it; thus transfer through porous rocks and soil is an important topic in resources management. The basics have been described by Bear [9] in its legendary *Dynamics of fluids in porous media*; standard textbooks on modeling groundwater reservoirs and pollution are [10, 62, 95, 96].



Side question 4 Is the turbulence in the flow required for droplet formation or could an accelerating stream resolve into droplets without its aid? Think about it – Bernoulli’s law and the tap in you kitchen might help you with the answer.

The water resources manager at your local waterworks might be happy with one of the above models. However, these models need some additional input: the flow carried by the stream. This can be taken as average of the observations during the last three decades.² A concerned water resources manager might decide that nature does not necessarily know about three-decade-standards and follows its own path. Thus he orders a different set of data to be fed into his model: the simulation of the present-day global hydrological cycle. Since climate change and the looming climate catastrophe has become a concern to him, he also orders the model results for the future hydrological cycle.



Note, we are starting to encounter intertwined models: the hydrological cycle (model 1) feeds the rivulet feeding the reservoir (model 2), however, that flow is determined by the interaction between water and rock bed (model 3). All models run on different spatial scales. And if we model for long enough a time, we even need more sophisticated models, because model 3 leads to erosion which in turn influences run-off into the reservoir (model 2).

But not only the water resources manager is concerned about the river's runoff – also the dike-reeve is interested in water runoff and water level. Dikes are not only a concern at the low-lying marshes of the Netherlands and the German North Sea coast but also at rivers. Sea dikes are damaged during a storm surge by waves washing over the dike and undermining it from the back. This is a mechanical problem rather than a transport phenomenon. The situation is quite different for river dikes: wave activity is unimportant but high water levels last for days or weeks, soaking the dike and making it less stable. In addition, the water might contain an extremely high amount of pollutants from flooding urban or industrial areas or even waste pits somewhere upstream. Thus not only the dike-reeve looks at the flood but also the farmer living behind the dike: he not only dislikes the idea of the river flooding his living room but also is concerned whether pollutants might infiltrate the dike in such an amount that his sheep cannot graze it after the flood has receded. These combined points, water and pollutant diffusion into the dike, are treated in a numerical model in [37]. We will turn back to this topic in detail in chapter 6.



The hydrological cycle simulation, at least on a global scale, becomes tricky because water exists in different states: as liquid and vapor but also as solid, kept in the arctic ice shields and in glaciers. A closer look on a glacier reveals that it also flows and, at least in Mark Twain's opinion, can be used as a means of transportation.³ Whether a means of transportation or not, glaciers move. And they move in a particular way, first described by Tyndall [168]: slower at the sides and faster in the middle – resembling the velocity distribution in a river. But glaciers also show a discontinuous behavior with their bergschrunds and crevasses. They modify the rock bed and transports



²Three decades often are used to define averages in natural systems, in particular in weather and climate. Unfortunately, this standard does not relate to any typical time scales of the systems. Instead, as scientists decided to describe average quantities in climate and water management, at most locations observations were available for only a few decades – thus the three decades magically appeared as standard.

³'... so I resolved to take passage for Zermatt on the great Gorner Glacier. and took up as good a position as I could upon the middle of the Glacier – because Baedeker said the middle part travels the fastest. As a measure of economy, however, I put some of the heavier baggage on the shoreward parts, to go as slow freight. ... the passenger-part of the glacier, – the central part, – the lightning-express part, so to speak, – was not due Zermatt till the summer of 2378, and the baggage, coming along the slow edge, would not arrive until some generations later.' [167]

debris and boulders, depositing it in moraines. Thus modeling glaciers is modeling transport, but in a complex way: we are modeling the flow of a crystalline material that also modifies its boundary conditions. The relevant physical concepts and models are described in Hooke [63].

Side question 5 Make a simple sketch of the hydrological cycle containing the different spatial and temporal scales (including the polar ice caps and the glaciers). Think about questions to be answered with such a model. Which part should be modeled in detail? What about the other parts/scales of the model?

Who limited water's states to solid, liquid and vapor? Besides from the fact that solid might be quite fluid as in a glacier, solid might also be quite granular and water can become a powder. Powder snow is a thrill for skiers and snowboarders (and occasionally even for snowshoe-goers) but it is also a threat to them if all the powder suddenly follows the gravitational pull. Avalanches and avalanche prediction also are topics for transport modelers. Prediction is requested on different spatial and temporal scales: the daily prediction for the outdoor activities, which might tell people to stay indoors to avoid getting caught in one of the likely avalanches, normally is made on a crude spatial grid such as a region and considers basically only the snowfall of the last days and the stability conditions of the underlying snow pack. The long term prediction on the other hand uses refined topographic models to understand the spatial evolution of an avalanche [148] and the risk of avalanches at certain places which are prone to avalanches. This information is relevant for development plans – not everybody likes the thrill of living in an avalanche path. The Eidgenössisches Institut für Schnee- und Lawinenforschung SLF in Davos provides not only a wealth of information for the layman but also is active in avalanche research and modeling and has examples on its web page: www.slf.ch. A good overview on numerical methods for equations relevant to avalanche simulation is given in [92].



Stability on a slope of granular matter is not only a problem in avalanches but also in dunes and in particular in shifting sand dunes. Dunes are a common feature at places with lots of sand and wind to move it around. Most dunes are rather stationary because vegetation develops fast enough to stabilize the dune. Only if sand transport is faster than vegetation development, the dune becomes a shifting dune. This is the case in deserts and in some parts of the Baltic, in particular the Kurische Nehrung and the Frische Haff. There sand supply is abundant because the sand delivering currents in the Baltic are deflected from their west–east orientation towards the north and, on being slowed down, deposit large amounts of sand at the coast. The prevailing western winds then blow this sand onshore creating high dunes which march along and swallow cultivated land and the occasional village. A readable primer on dunes is provided by Herrmann [60].



A related problem is coastal evolution. Here the dominating processes are erosion, transport of sand with the flow and deposition. Coastal evolution [26, 27, 114] is an important topic because human settlement on coastlines and in particular at river mouths is dense and vulnerable to both a retreating coast (your living room moves from the top of the cliff with the nice views suddenly to the bottom of the sea) as well as an advancing coast (a formerly busy harbor suddenly sits high and dry in the middle of the land). Consequently, coastal defence [35, 46, 153] is an important topic. But since one man's erosion is another man's deposition, subsisting coastal defence requires advanced modeling considering large stretches



of a particular shoreline to avoid the negative side effects of a working coastal stabilization [45]. In addition, dunes can exist on both sides of the shore line: on the land in the sense discussed above and on the sea bed. Close to the shoreline, these latter are visible as small ripples in the sand, at the ocean bottom they can extend for kilometers. Recently shorelines have gained even more interest because climate variability with changing ocean flows, winds, and rising sea levels threat costal habitats even more.

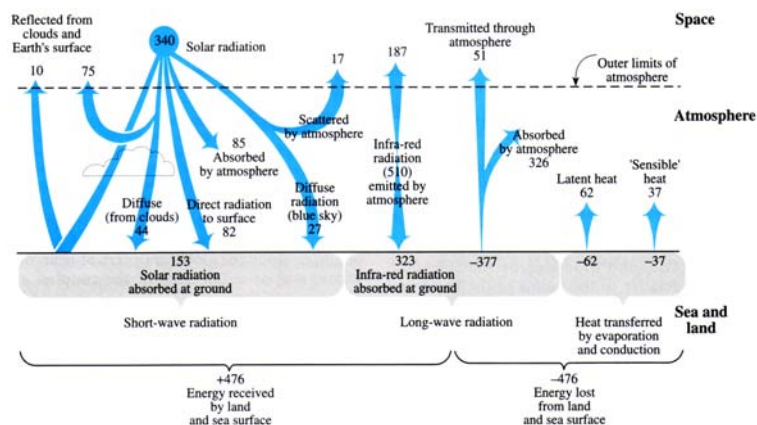
From a more philosophical point, coastal evolution also is interesting: it is still not understood whether coastal evolution is a continuous process (the daily dose of sand removed or added) or a catastrophic one (the cliff collapsing during a winter storm. This is not even a neither–nor scenario: the occasional catastrophe might be required to allow the daily transport to become effective which in turn allows for the next catastrophe. For modelers, this problem is quite a threat and leads to fundamentally different approaches on coastal models.

Transport processes are not limited to liquids but are also common in gases. Liquids and gases are fluids in the sense that they adjust the shape to the vessel that contains them. They differ in such that a gas fills the entire space provided by its container while liquids only use that part of space that corresponds to their volume. The expansive behavior of gases leads to one fundamental difference in all transport models: while the basic processes of diffusion and convection are the same as in liquids, transport in gases always is three-dimensional – and the diffusion part normally is isotropic. While the latter certainly is good news, the former requires some additional efforts in modeling. The examples in this text therefore show a strong preference for liquids over gases.



So far, we have only transported matter. What with energy and information? Both have been mentioned in connection with the surface wave, thus waves are suitable to transport these immaterial properties. But energy transport also can be related to the transport of matter. For instance, all climate models basically are energy transport models, combining material and immaterial aspects of energy transport.

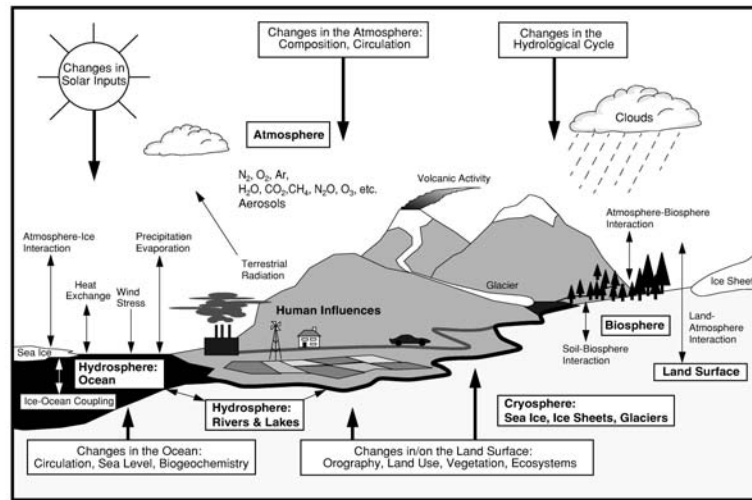
Earth's only source of energy is the Sun; geothermal energy and the heat conduction from the core to the surface make up less than 1 in 1000 of the energy incident from the Sun. The energy flux incident on the top of the terrestrial atmosphere is the solar constant. All the energy absorbed by Earth and its atmosphere must be



radiated back into space because otherwise Earth would heat up or cool down. Thus the atmosphere basically can be understood as a medium in which energy transport occurs from the top of the atmosphere to the surface of Earth and back to the top of the atmosphere. The incident energy is electromagnetic radiation with short wave lengths. Its transport has to be modeled as radiation transport including reflection, absorption and scattering, as suggested in the left part of the figure. Part of the short wave radiation is directly reflected back into space (contributing to the terrestrial albedo), part is absorbed in the atmosphere (heating it and being radiated isotropically into space and towards the terrestrial surface) and the bulk of the incident energy is absorbed by the terrestrial surface. The resulting heating leads to evaporation of water, convective motions and the emission of long-wave thermal radiation. Thus energy transport out of the atmosphere is not only limited to radiation transport but

also includes sensible heat (convection) and latent heat (water vapor). In these cases energy transport is related to the transport of matter.

But that is only vertical transport. The non-homogenous distribution of energy between equator (high solar zenith angle, most of the radiation is absorbed by oceans and rainforest) and poles (low solar zenith angle, most of the incident radiation is reflected by the ice caps) drives a redistribution of energy, normally called the global circulation. The atmosphere contributes to



about 2/3 of the energy transport, the remaining 1/3 is redistributed by the oceans, in particular the thermohaline circulation – in middle and northern Europe we appreciate the heat transport by the Gulf stream that leads to rather mild winters. The energy balance of the atmosphere therefore also requires to model the global circulation and thus also the driving forces for weather, in particular the polar front that guides the pressure systems. In addition, modeling the energy balance of the atmosphere requires an ocean model. Thus a climate model automatically becomes a global coupled ocean–atmosphere model. To make modeling more interesting (and challenging), we should also add a hydrological cycle to the model and some aspects of human activity, such as deforestation and carbon dioxide emission. And finally our simple energy transport model requires Tokyo’s Earth Simulator for even the simplest estimates.

There are also some less pictorial but very common transport phenomena. One has already been mentioned in connection with the transport of energy in the atmosphere: heat transport. Heat transport has many technical applications (power plants, chemical reactions, heating engineering [115, 182]) but is also related to our comfort inside the building: the radiative heat exchange with the walls and the radiator, the exchange of sensible heat by convection and the cooling effects of evaporation. Basically these are the very same processes also considered in the atmosphere’s energy balance. Since the governing equations are rather simple (heat transport and diffusion can be described by the same equation⁴) there exists a wealth of literature on heat transport. Modern and accessible texts for instance are the books by Jaluria and Torrance [76] and Potting [133].

Momentum transport is a common phenomenon on boundary layers. Momentum is transferred from the wind to the sand (as e.g. in dunes) or from the ocean flow to the sand (as e.g. in dunes on the ocean floor or erosion and deposition). We have encountered this idea already in the context of sand transport in dunes and coastal evolution. But momentum is also transported from the atmosphere to the ocean to drive surface waves and surface currents. And momentum is also transported between the oil spill on a lake and the lake’s water.⁵ Thus also invisible, momentum transport is quite frequent and can be considered as driving force in the subsequent transport of matter. But this driving occurs at the expense of the flow, thus momentum transport results in the redistribution of kinetic energy in the two media. Part of the energy, however, is lost during the process, resulting

⁴Both processes rely on stochastic collisions between molecules – so why expect a difference? See also chap. 4

⁵Oil often has been used to dampen surface waves on the sea by a vessel in distress or by rescuers trying to aid a grounded or wrecked ship. However, oil would not help to fight a freak wave.

in heating (and partly also in damaging structures as the coherence between sand grains or even between molecules on a rock bed).

Side Remark: Are all Transport Modelers Catastrophists?

Our tour through transport phenomena included some less pleasant examples like avalanches, dike breaks, tsunamis, nuclear explosions etc. Thus modelers, at least modelers concerned with the natural environment, apparently have a preference for catastrophe. But do modelers like catastrophe? “YES, of course,” many modelers do, and “NO, of course not,” the same modelers do not like catastrophe. Personally, modelers do not have more preference for catastrophe than other people because they have the same fears and like a quiet live.⁶ But modelers take advantage of catastrophe as do many geophysicists. Nature is a complex system and any observable, such as the flow speed of an glacier, is influenced by many present (and often also past) observables and partly also unobservables. Thus cause and consequence are not directly related in a natural system. In contrast, in any natural process there is a lot of (often quite loud) noise from undesired side effects. The study of the influence of one observable on the system becomes much more simple if this one sticks far out of the noise such that it determines most of the systems reaction. In that case, a rather direct cause–effect relation can be established (and hopefully also quantified). But any natural quantity which clearly sticks out of its usual range often leads to catastrophe.⁷

In a more mathematical terminology we can also say that nature is a roughly stable system with lots of noise in any quantity. In such a system, catastrophe provides some kind of δ -stimulus and nature’s reaction gives its Green’s function. In addition, it gives a good test case for our model results. In this case, catastrophe is very welcome to the modeler (as well as to the observer). This understanding only comes by a price: both modelers as well as observers have to be patient and to take the answers nature gives voluntarily. But they are not experimentalists: they might be a catastrophe in themselves but they do not cause catastrophe or even long for it. Often it is not the modeler that looks for catastrophe but the catastrophe that looks for the modeler. Fire simulation is a good example: in principle, it can be done experimentally. But what was the influence of the open kitchen door in this particular case? Or the bursting of the front window? How the hell can a flash-over occur and how can a fire-fighter survive in the hell of such an event. Simulation is slightly less expensive and more controlled than the experiment; it also allows for some kind of parameter study.

In addition, modelers help to avoid that an inevitable natural catastrophe (in the sense of a signal sticking out of its natural variation, a Jahrhundert event) becomes a human disaster by deriving the parameters for a suitable protection against damage from this Jahrhundert event. For instance, the high risk of a flooding of New Orleans in a class 5 hurricane had been predicted already in 2001, even with detailed calculations of the weak spots in the dike system. Katrina only confirmed the model results – although the modelers would have preferred a different scenario: believe the predictions of the model, take the advised steps and never get your bad prediction confirmed because the weak spots have been strengthened.

⁶In contrast, the awareness of the risk of catastrophe also contributes to survival. This well-known relation between fear and the ability to survive in uncomfortable environments also drives some of our leisure activities: “Wenn ich in der Natur allein bin und über Gletscher gehe, bin ich ununterbrochen wach - die Angst hilft mir, nicht umzukommen. In der Wildnis wird man mit einer sehr greifbaren Form der Furcht konfrontiert.” (R. Messner)

⁷Please keep in mind, catastrophe is not the correct term: catastrophe always implies harm to humans – thus a strong earthquake in some remote areas which does not affect humans is not a catastrophe while an earthquake of much smaller magnitude in a densely populated area with inadequately constructed housing and thus a large number of fatalities is termed catastrophe. The same is true for avalanches: a typical small avalanche in the Himalaya shifts a certain mass/volume over a pretty large height range – but most of these avalanches are not even observed let alone harm some unexpected mountaineer. In the Alps, a much smaller avalanche almost inevitably would swallow some skiers or even a village and therefore would be regarded as catastrophe. In such sense, the modeler does not use catastrophe but only large signals. Only in a fragile and densely populated habitat these strong signals also (can) turn to catastrophe.

Catastrophe not only shapes our world but also our view of the world – in the layman's terms as well as in the modeler's view.

Sneer remark: Modeling supports itself

Experience shows that autobahns create traffic and thus the requirement for more autobahns. Or for short: autobahns create the need for autobahns. The above examples suggest something quite similar: (transport) models in natural systems create the need for (transport) models. Presently, the looming threat of climate catastrophe fuels the research in consequences of climate change. Thus models for coastal evolution and protection, recession of glaciers and the resulting landslides and consequences for water resources, stability of dikes against unusual water levels and many other models are motivated by the results from climate models: increasing temperatures, redistribution of precipitation, increased frequency of extreme weather and climate events, the rising sea level and many other predictions.

1.2 Help, I still can't define Transport

Ok, let's try to be a little more systematically.

1.2.1 Definition

The above examples allow for a brief glance at transport only. They are examples, the only thing in common is that a property $\varepsilon(\vec{r}, t)$, which might be a scalar such as mass or energy or a vector such as momentum, is redistributed in space and time.

Definition 1 Transport is the redistribution of a property ε of space \vec{r} with time t .

The definition makes the mathematical requirements obvious: since $\varepsilon = \varepsilon(\vec{r}, t)$, any change in ε will be described by a partial differential equation (PDE) – except in the limit of a 1D geometry in steady-state. Solutions of such a transport model (TM) therefore can be viewed in two ways, representing cross-sections in different 'dimensions' of the model:

- the temporal development $\varepsilon(t)$ at a fixed position $\vec{r} = \text{const}$ or
- the spatial distribution $\varepsilon(\vec{r})$ at fixed time $t = \text{const}$.

Solutions of PDEs can be obtained analytically only under special circumstances, in particular in steady-state, limiting geometries or under the (oversimplifying) assumption that parameters are constant. Often these attempts use convolutions of Green's functions because the systems response can be determined only for a δ -forcing. Under more realistic conditions, numerical solutions are required.

Numerical solutions also can circumvent some physical nonsense evident in some analytical ones. For instance, the analytical solution of the isotropic diffusion equation

$$\frac{\partial U}{\partial t} = D\Delta U$$

for a δ -injection at position $\vec{r} = 0$ and time $t = 0$ is

$$U(r, t) = \frac{U_0}{\sqrt{4\pi Dt}} \exp\left(-\frac{r^2}{4Dt}\right).$$

For $t > 0$, the particle number density U is different from zero at all points \vec{r} , even if $t = 0.1$ s and $r = 300\,000$ km, implying a propagation speed of $10c$ – which might frustrate Einstein a little bit. A numerical solution, on the other hand, advances in the grid provided by the numerical scheme and thus leads to finite propagation speeds, although these sometimes have to be adjusted by flux correction techniques (flux corrected transport FCT).

Side question 6 Think about this problem. What is the mistake? Is the transport equation wrong? Is the solution wrong? Does the problem result from the unphysical δ -injection? Is the problem academic?

1.2.2 Classification – Questions on our Way to a Transport Model

First of all we should define the property $\varepsilon(\vec{r}, t)$ to be transported. Thus we have to ask the question **What is transported?**. We can classify this as

- matter,
- energy/momentum,
- information.

Our second question regards the mode of transportation, that is **How is ε transported?** Answers can be classified into three main categories:

- directed transport, for instance with a flow,
- stochastic transport, e.g. diffusion,
- wave-like transport: information and energy is transported but no matter.

A fourth category arises from the human infrastructure: the spread/transport of diseases as well as rumors can be traced along the pathways of humans (such as flight routes in SARS) or information (such as the Web). We will come back to this point in chap. 9.

Our third question is concerned with sources and sinks, or **Can ε change inside a volume without being transported across its boundaries?** Sources and sinks can be chemical reactions, (radioactive) decay, adsorption or removal from the fluid due to a phase transition. From the viewpoint of a running river, the oozing away of water through the silt into the groundwater also can be regarded as a sink. The groundwater reservoir, of course, would regard this water as a source. However, if the transport from the river to the groundwater is our main concern, we would model the transport of exactly these water molecules – may be with the river parameterized as a source.

This remark introduces our last question: **What are the scales, spatial as well as temporal, of our transport problem?** This question probably is the most relevant question and should be asked right as second question when starting to model.⁸ The temporal scale often is obvious: as Mark Twain already realized, glacier motion should be modeled on time scales of decades to centuries rather than on time scales of minutes to hours.⁹ On the other hand, modeling a tsunami on time scales of days to weeks also is not useful because in this case the modeling time extends well beyond the live time of the phenomenon to be modeled.

The choice of the spatial scale is less obvious, as can be demonstrated with the hydrological cycle or coastal evolution. The hydrological cycle is a global phenomenon including also glaciers, rivers and the oozing off of water into groundwater reservoirs. While glaciers and groundwater reservoirs can be modeled for themselves, it certainly would be too much detail to use these models as submodels in the hydrological cycle. Instead, their results will be parameterized in some suitable way and fed into the global model. Coastal evolution is similar: one can model the processes of erosion and deposition on a molecular level – but not for a 50 km long stretch of coast. In the latter case, the flow is modeled and erosion and deposition are parameterized.

Thus before we start any modeling, we have to define the purpose of the model precisely and then develop it accordingly.

1.2.3 Why should I Model at All?

But why should we be interested in modeling? Some applications of modeling are rather technical, for instance drag on a new car design or the thermal balance of a building. These models are used as aid in construction or to determine threshold values. Such models are well established and often approved by the government, for instance models to calculate the radiative exposure of aircraft crews or the energy efficiency of a building.

⁸The first question always is a task: define your goals (or better the goals to be achieved with your model).

⁹This could be of interest only in a model with sufficiently fine spatial scales that also treats all individual seracs and aims to predict icefall or changes in smaller structures close to the glacier's snout. Or in model concerned with the run-off of melting water and the associated risk of a glacier lake suddenly emptying through a crevasse into a lower-lying, unsuspecting valley.

Other models are developed to gain a better understanding into a complex system. For instance, systematic variation in different parameters might help to determine whether a given process has a strong influence on the system or not. This kind of modeling is a tricky business: modeling might be simple but the test of the model is quite difficult or almost impossible. If it were not, we would not have any need to model.

For a large natural system modeling serves a similar purpose as experiments do in laboratory physics. It is not possible to do the ‘experiment’ climate change or river runoff in a laboratory setting. With a working numerical model, however, it is possible to test the reaction of the system to certain stimuli or to determine changes in its state for changes in boundary conditions or initial conditions. These large models sometimes are also used for predictions, for instance of climate change or on a much shorter time scale for weather forecast: most climate models have evolved from weather forecast models.

Thus models can be basic as well as applied science – and in case of environmental modeling even can have a strong, sometimes controversially discussed impact on society. In particular in the climate debate but also in insurance cases this is a fundamental problem: modeling is only the minor part of the job – model validation and communication of the results can be much more time consuming.

Modeling also has an educational aspect: the modeler has to learn to view the natural system under study in its entire complexity and then to reduce the system to the relevant processes and the relevant parameters. Thus modeling combines a rather holistic approach with brute-force reductionism. But this is also the salient part of science: realizing the complexity (and beauty) of nature and still being able to create working models to cope with it. This is the same process we do in social interactions – albeit there we do it instinctively. But in both spheres the emphasis is on ‘working model’: the model must contain enough aspects of the system to allow for reliable prediction but also must be as small as possible to be executed fast enough: normally, a partner in a social interaction is not prepared to wait two hours to get my answer to a question such as “milk and sugar with your tea or better lemon?”. As in social interaction, modeling requires a lot of abstraction and generalization – otherwise a model can be as autistic as a person.

Sneer Remark: Does Modeling allow for Predictions?

But can modeling have an impact on society? Can modeling really allow or predictions? Isn't there Lorentz' butterfly effect¹⁰ [106]: “Does the flap of a butterfly's wing in Brazil set off a tornado in Texas?”

While Lorentz made the experience of the small error in initial conditions, Alan Turing [165] had made a similar statement about two decades earlier out of reasoning about computers and in particular the later so-called Turing test: “The system of the ‘universe as a whole’ is such that quite small errors in the initial conditions can have an overwhelming effect at a later time. The displacement of a single electron by a billionth of a centimeter at one moment might make the difference between a man being killed by an avalanche a year later, or escaping.”

Turing's statement is even more fatal than Lorentz' because it retracts to the quantum mechanical level. If the world model or the general model of the universe including details down to the atomic and sub-atomic level is the target, Turing's objections most likely are correct. However, whether a model allows for a prediction or not, depends on the question and the model. A dike reeve, for instance, wants to know whether a certain stretch of dike will hold or break – it does not matter in detail where and how it will break.¹¹ Thus if we

¹⁰The tale goes that Lorentz discovered this effect after a computer breakdown in his lab at MIT. Lorentz was a pioneer in numerical weather forecast. One day, he restarted a run after a computer breakdown with the last saved data set as initial conditions for the run's continuation. When he compared the results to the results from a complete run, obvious differences appeared. He concluded that the rounding errors made as the saved data were fed back into the program were large enough to affect the program's output strongly. To illustrate that such a small deviation can make a strong effect, he created the above statement.

¹¹Probably nobody in New Orleans cared about which part of the dike broke – the fact that some dike broke was fatal enough.

judge a model in its ability to reproduce the intimate details of the process under study, most models probably will fail. But if we ask the more general question, the model, at least if it is a good working model, probably will give a reasonable answer. The same is true for climate models. The large number of different climate models also can be used to confirm the trends in the results: although all models lead to different predictions about the exact temperature evolution until 2100 under the constraint of increased carbon dioxide levels, all models agree on the warming effect and all models lead to predictions in a rather small range of temperature changes, see e.g. [69]. And this agreement despite the differences in the models suggests that it might be time to think about measures to take even if models are not perfect. This problem is discussed in detail in Pollack's book *Uncertain science ... uncertain world* [130].

In sum, although models do not predict the future in all detail, good models give quite reasonable ideas about it. For instance, weather forecast is well advanced and gives pretty reliable predictions for the general weather pattern over Germany for about five days in advance – also it always almost fails to tell me whether I will need an umbrella on my way to the mensa or not. The path of hurricane Katrina has been predicted fairly well – as had been the inability of New Orleans' dike system to withstand such a hurricane. Tsunami prediction in the Pacific works reasonably well and is greatly appreciated by the surrounding countries. And even the rather crude models two decades ago made reasonable predictions about the fall out following the Chernobyl accident and the burning oil fields in the first Iraqi war.

1.3 Orientation

The goal of this text is not to give you a comprehensive overview over all transport models. Instead, its aim is to introduce into some models in more detail.

The script is structured as follows: chapter 2 introduces some general aspects of modeling. It should guide you through the process of abstraction and formalization; some examples for the abstraction process will be given. The chapter also addresses the limitations of modeling.

Chapter 3 describes a very simple approach on modeling, the compartment approach. Because this is a rather graphical kind of model, it also repeats and illustrates the fundamentals of model building. Examples are chemical reactions in a steady flow (some of these ideas later will be needed in groundwater and dikes) and atmospheric chemistry. The compartment approach allows for 1D models and thus relatively clearly arranged numerical schemes. Therefore we can limit ourselves to finite difference models and introduce the centered finite difference scheme for the spatial and the Crank–Nicolson scheme for the combined spatial and temporal transport.

The most important transport process, diffusion, is discussed in detail in chapter 4. We will start from the basics of the process and a simple diffusion model and continue to the diffusion-convection model. Examples will be the propagation of pollutants and heat transfer; in fact, even the simple example from chapter 3 has been a diffusion-convection model. The heat conduction equation also will introduce the Stefan problem: heat conduction in a liquid might reduce temperatures in parts of the liquid such that a phase transition to a solid occurs. Thus the simulation volume contains an inner boundary that shifts in time. Such a Stefan problem also can be used to describe and model the development of a traffic jam.

Chapter 5 picks up a particular transport equation for the propagation of energetic charged particles from the Sun through the interplanetary medium. Again, the model is 1D because particle propagation essentially is along the magnetic field. Using this transport equation we will illustrate the method of finite differences in detail, in particular the splitting into different schemes if different types of PDEs are involved in the TM.

Chapter 6 discusses a model to evaluate the stability of dikes during sustained high water levels. As in chapter 5, we will learn about the underlying physics and construct the model from the basic equations. In this case, the solution is obtained by a finite-element method which will be described in detail. Thus this chapter also serves as an introduction into finite element modeling.

Chapter 7 briefly introduces into computational fluid dynamics (CFD): the flow is not prescribed as in chapters 3 and 6 but the equation of motion has to be solved in three dimensions instead. We will solve some rather simple problems using finite difference and finite element schemes. CFD finds its applications in natural systems (ocean and atmosphere models, coupled ocean–atmosphere models, global climate models), in technical design (drag of a flow around a body, car design) as well as in accident investigation (fire modeling).

Chapter 8 introduces a different kind of numerical modeling, Monte-Carlo modeling. We will introduce this method with the example of energetic particles in the atmosphere. Part of that chapter also will be devoted to more general remarks on Monte-Carlo methods. Monte carlo methods rely on throwing a dice. Consequently, they are useful only if the underlying process is stochastic rather than deterministic. Since this is the case in e.g. diffusion, heat conduction and turbulent transport, Monte-Carlo methods face a vast array of applications in transport modeling.

In chapter 9 we will encounter some entirely different transport processes, such as the spread of diseases or rumors or the path of ants across a stretch of land.

The remaining chapter 10 summarises some open problems that can be used for end-of-term projects. The closure in chapter 11 loops back to this introduction and summarizes some of the more important aspects of this text.

Modeling requires knowledge in physics, mathematical methods and numerical methods. To keep the text readable, detailed explanations or derivations of equations are missing as are some basic numerical or mathematical methods. The appendices try to cover up for a few of these omissions. Appendix A contains the usual lists of symbols and abbreviations, some useful numbers and a little bit vector calculus. Appendix B contains some useful mathematical basics such as analytical solution strategies for ordinary differential equations, the classification of partial differential equations, and the Laplace transform. Appendix C contains some physical basics, that is a list of standard equations and a formal introduction into (and recapitulation of) some fundamental concepts of statistical mechanics, such as distribution functions, averaging and basic transport equations, e.g. the Fokker–Planck equation. Appendix D gives some background on numerical methods, such as discretization, numerical integration, standard numerical schemes for ODEs and PDEs. And finally appendix E gives solutions to a few of the questions and exercises.

Literature

I do not have a recommendation for a book that can cover the entire lecture. Instead, I will give recommendations at the end of each chapter. And I strongly recommend to consult literature beyond this text. As a lecture note it suffers from some limitations: it reflects my personal preferences on the topic, it has been written under deadline pressure and it contains a large number of smaller and larger errors.

Good scientific conduct requires credit not only for the text sources but also for pictures. Normally this should not be done in a footnote.¹²

¹²This figures in the pictorial guide are taken from the following sources: (1) autobahn from <http://www.hotskiing.com/photogallery.htm>, (2) pipeline from <http://www.arisi.it/images/imptec/Pipeline-.jpg>, (3) cardiovascular system from http://www.tc-interlaken.ch/fundgrube/pic_anatomie/kreislauf_gewebearten_aladin.JPG, (4) falling drop from <http://www.3dhifi.de/pics/tropfen.jpg>, (5) drops on a window pane from <http://twoday.net/static/desideria/images/tropfen.jpg>, (6) cascade at a tributary to the Mattmark reservoir, Valais, (7) hydrological cycle from <http://archiv.greenpeace.de/wassergeist/images/wasserkreislauf100.gif>, (8) dike break during the Mulde flood from <http://muldehw.ufz.de/album/fotos/foto11.jpg>, (9) Eigergletscher, Bernese Alps, (10) induced avalanche, SLF Davos, from <http://www.slf.ch/>, (11) Hohe Düne at Nidden from <http://home.arcor.de/ralf.brandstetter/neringa/hoheduen.jpg>, (12) Darss from <http://www.hansaluftbild.de/>, (13) nuclear explosion from <http://www.worldthreats.com/images/nuclear-bomb-explosion.jpg>, (14) the energy balance of the atmosphere from IPCC [69], (15) components of a climate model from IPCC [69]. The choice of sources does not reflect any personal preferences for or opinions about these pages – instead most of them were Google’s choices.

Chapter 2

Modeling

*To see a world in a grain of sand
And a heaven in a wild flower
Hold infinity in the palm of the hand,
and eternity in an hour.*
Blake – Auguries of Innocence

This chapter deals with modeling in general. It will present some guidelines on how to develop a model as well as a few examples. The latter will be described qualitatively without delving into equations or the underlying physics more deeply than absolutely necessary.

For model development I will adhere to my personal view on the modeling of natural processes. And this includes two seemingly contradictory definitions

Definition 2 Modeling *requires the apprehension of nature in its entire complexity.*

In face of this complexity modeling might appear to be the impossible. It would be, were it not for the second definition:

Definition 3 Modeling *is brute (but hopefully intelligent) reductionism.*

Thus successful modeling requires the awareness of complexity with the simultaneous reduction to the essential. And the modeler has to be aware of this reductionism. The examples discussed in the chapter should help to understand these points.

A second focus in this chapter is the test of a model. We will learn that a model is worthless as long as it is not tested. First tests might be against simple physical concepts such as the conservation of mass or energy; more advanced tests include the comparison to experiments and/or reality.

Goals: after working through this chapter you should be able:

- to analyze and describe a (physical) problem in such a way that it can be converted into a mathematical model (at least if the relevant equations are known and a numerical scheme has been developed).
- to develop a test procedure for a model.
- to develop a checklist for the modeling process from the very onset of the verbal description of the problem to the communication of the result. This can be regarded as quality assurance.

2.1 Outline

Compared to the above definitions, Basmadjian [5] offers a more conventional approach on modeling:

Definition 4 Modeling *is the assembling of mathematical expressions as a description of a system or process. A mathematical model therefore consists of the assembled equations that describe a physical system or process.*

To get the essence of modeling let us forget about the details of equations for a moment: assume we have a construction kit of equations, some kind of Lego set. We are not concerned with the details of the bricks but we know what they are for: wheels are for driving, the slanted bricks are ideal for roofs and rounded bricks are a poor choice for plain walls that intersect at right angles. Thus our first step is to identify which kind of bricks is required: we want to build a house, thus we discard everything that has wheels on it since as middle Europeans we are not used to mobile homes. We then can specify which slanted bricks and which standard bricks are needed, assemble them and check whether the assembly meets our pre-occupations regarding the essential features of a house.

Side question 7 What are the essential features of a house? Right-angled walls? Hundertwasser would be disappointed. Slanted roofs? Doors and Windows? Who defines what an essential feature is?

Successful modeling is pretty similar to playing with Lego. It requires the following ingredients:

- an understanding of the *underlying physics* of the system and the laws that govern them. Conservation laws always are a good starting point; some fundamental laws are summarized in appendix A in table C.1, conservation laws are also discussed in section 2.4.
- the ability to make suitable *simplifying assumptions* to reduce the system's complexity while retaining a valid and realistic description of its behavior. For instance: a house needs some top boundary against sun, rain and so on. But this must not be a slanted roof.
- expression of the model in *mathematical terms*. This part often can be delegated to a textbook or a handbook.
- analytical or numerical *solutions*. This often can not be delegated to standard schemes.
- *closure*: analysis of the results obtained. **If you forget about this, you did not model at all!**

Of these requirements, the simplification process is the most difficult one. Often it only leads to bracketing the solution, that is only lower and upper bounds can be given. This often is also called a best-case–worst-case scenario: a process depends on a parameter which cannot be determined exactly. But the upper and lower bounds of the parameter are known and thus two model runs can be performed, bracketing the solution.

Side question 8 Is this approach valid for all kinds of models or only under special assumptions/limitations? Justify your answer.

Basmadjian [5] links simplifying to an art as much as to science: it requires a certain feel for the importance of parameters and processes. Such skill cannot be learned from a text(book), however, examples from many different fields of science might help the reader to get at least an idea about it. Such an advantage comes only by a price: some examples might require a little bit additional reading to understand them because the physical basics are rather unfamiliar. On the other hand, this approach also illustrates that often different physical processes lead to similar, if not identical, mathematical models. This chapter is concerned mainly with the first two points: underlying processes and suitable simplification. In the subsequent chapters, models with increasing complexity will be discussed.

Note that simplification might lead to different models of a system depending on the problem under study. The atmosphere is a suitable example. A researcher in the field of

climate change needs a different model atmosphere than a researcher in air pollution: the relevant processes are different, the spatial and temporal scales also, as are the suitable averaging procedures. But neither the climatologist nor the researcher in air pollution are happy with a model atmosphere that focuses on numerical weather forecast:¹ the meteorologist attempts to predict the weather on time scales of a view days with a spatial resolution of a few hundred km. Thus the meteorologist assumes the properties of the ocean and the terrestrial surface to be constant during the simulation interval. The climatologist, on the other hand, is concerned with the very changes in exactly these parameters and thus requires a model with larger spatial scales and in particular longer time scales. Thus the oceans and their variation are important to him – as a consequence, all modern climate models are coupled ocean–atmosphere models. For an introduction to climate modeling see e.g. von Storch et al. [173] or Washington and Parkinson [174].

The next two steps, the expression in terms of equations and their numerical solution, are specific to a certain model. Thus we will not discuss these steps in general, except for very fundamental processes, such as diffusion. Instead we will discuss the details of the mathematical model and its numerical treatment in an exemplary way in the following chapters.

The last step, the closure, loops back to the first two steps: only if the results make sense and fit to the underlying physics, the model can be valid – otherwise, at least one of the steps must be wrong. Testing or validating of models is at least as important as model development. A battery of tests is much better than one test only because neither expected nor unexpected results proof a model right or wrong: a single agreement between model and expectation might be accidental. In addition, an agreement between model and expectation might result from our interpretation of the scenario: the processes we think are relevant in the system under study determine our expectations – but if the processes are wrongly identified, model and expectations both are wrong. Thus a comparison to fundamental physical laws and observations is helpful. On the other hand, a disagreement between model and expectation might not necessarily prove the model wrong: our expectations might be wrong but the model is correct. Again, an experiment or observations might be helpful. Thus testing is not only important but also a tricky business.

2.1.1 Types of Models

Models can be divided into three different types, representing different modeling philosophies.

Models based on first principles are derived from first principles such as the conservation laws. The typical example is the energy conservation

$$\frac{\partial \varepsilon}{\partial t} + \nabla \vec{S} = q \quad (2.1)$$

with ε being the energy density [J/m^3], \vec{S} being the energy flux density [$\text{J}/(\text{m}^2\text{s})$] and q being sources and sinks [$\text{J}/\text{m}^3\text{s}$]. Such models preferentially are used to understand the inner relationships in a system or to perform a sensitivity analysis. The latter shows the dependence of system variables on certain parameters and therefore allows to identify the parameters most important for the understanding of a system.

From a philosophical point of view (at least from one school), models based on first principles are the best ones since they work in an axiomatically closed space. Thus they do not rely on assumptions and observations and other stuff involving the human and its imperfect brain. Modeling than is clean, almost sterile, and axiomatic – (un)fortunately, nature is complex and resists such a perfect axiomatic description.

Although many simple physical models fall into this category, often first principle models are combined with a phenomenological ansatz: relations between physical quantities derived

¹This is certainly true for the present state of modeling. Nonetheless, most climate models have been developed from meteorological models. The relation between climate and weather is described by Pollack [130] as: “Climate is what you expect ... weather is what you get.”

from experiment instead of first principles are added. The energy equation is an example for such phenomenological model, now in the form of the heat conduction equation

$$\rho c \frac{\partial T}{\partial t} = -\lambda \Delta T . \quad (2.2)$$

Here we consider the phenomenologically derived energy density $\varepsilon = c\rho T$ with ρ as mass density and c as specific heat. The second phenomenological ansatz is the energy flux density $-\lambda \nabla T$ as being proportional to the gradient of the temperature and the thermal conductivity. Most models used for predictions, in particular in natural systems, belong to the group of phenomenological models.

A third kind of model is neither concerned with predictions nor phenomenological relationships but starts from the data. These data models basically are a skillful visualization and combination of data to obtain phenomenological laws from observations. They are required for instance in oceanography to describe the global circulation which cannot be modeled in other ways owing to the complexity of the boundary conditions such as sea floor topography and continents. These data models then enter into a coupled ocean-atmosphere model to predict the future climate.

Within this text we will encounter models of the first two classes. They lead to mathematical models and can be solved analytically or numerically.

2.1.2 When Not to Model

Although modeling often is the only means to understand a complex system such as climate, modeling is not the panacea to solve problems. Instead, owing to the modeling process outlined above, modeling bears its own problems. As a consequence, there are also a lot of occasions when modeling is not advised (see also [5]):

1. the answer is required within hours.
2. the answer may be obtained by a simple and inexpensive experiment.
3. the client is suspicious of theory and prefers the experiment, such as in court cases.
4. the system is too complex to be modeled in a meaningful way, for instance the determination of drag or transport coefficients.
5. the answer is self-evident.
6. modeling for the sake of modeling (sterile or post-facto modeling).

Asides from being a general problem (if I only had time, only had time), the lack of time (1) might be of particular importance in an industrial process or during catastrophe – it is too late to set up, run and validate a model if a river already is running high water or when Katrina is approaching New Orleans. Although a detailed model certainly is out of range in such a case, a very simple model might allow for some guideline or lower and upper bound. For instance, in the high running river in- and outflow still might be in balance: thus water levels will not rise above dike level (no need for immediate evacuation) but dikes might break after a few days due to soaking (keep an eye on them). But such a result does not require an advanced dike model as discussed in chap. 6. Instead, the equation of continuity is sufficient; and this can be solved analytically.

If a simple and inexpensive experiment (2) is possible within the time frame and cost limits, it is preferable to modeling because a model or its mathematical solution might be faulty. Although this can also be the case in an experimental setting, skilled experimentalists and the repetition of the experiment should avoid errors (or at least discover existing ones) much easier than this can be done in a numerical model because *to code is to err*. And this also implies: *to model is to err*. And an error in modeling can have more sources than only the errors in coding. The error also might be on the side of the identification of the relevant processes, their mathematical description or the parameters entering them.

Modeling is not only limited to scientific questions but model results also are used in political decisions (all the climate debate) or in court. In the latter case often experiments are preferred to modeling as mentioned in point (3). Consider an insurance case in a fire

or explosion. Judge and jury know about law but not about the physics and chemistry of a spreading fire and the possibility of a flash-over or even a backdraft. Thus a model is very abstract and the results of the prosecutor's model contradict that of the defender's model. While scientists might be able to sort this problem out by going into the details of both models, the layman will not be able to follow their reasoning and might prefer the experiment. Selling new regulations to the public is a similar situation: the motion of a crash test dummy is a better motivation to use the safety belt than any refined model could be.

An illustrative example has been given by nobel laureate Richard Feynman in the investigation of the explosion of space shuttle Challenger in 1986. Almost all aspects of the space shuttle are modeled to the last detail: in manned spaceflight the crew's safety is of utmost importance, thus detailed knowledge of the shuttles behavior is required. Since the demands of the payload require a crew on board, unmanned flights with the shuttle were not reasonable (although in principle possible). For the safety of the crew modeling to understand the system Space Shuttle was important. Despite these efforts, in 1986 Challenger exploded 73 s after launch – embrittlement in a gasket in the liquid fuel boosters allowed a small flame to burn like a welding torch into the hydrogen tank and ignite it. This sequence even could be reconstructed from the photos/films taken during launch and prior and during the explosion. Temperatures at the launch pad had been below zero centigrade, nonetheless, the technicians had approved the launch. In the subsequent investigation the embrittlement in the gasket was easily identified as the cause of the accident. A debate arose on whether this was foreseeable or not. Without relying on any modeling, Richard Feynman, a member of the investigation panel, just took a sample of the gasket under question and held it into his glass of iced water to demonstrate that the gasket loses all its elasticity even at temperatures around zero centigrade. A short version of the accident investigation is given in http://de.wikipedia.org/wiki/STS-51-L#Das_Challenger-Ungl.C3.BCck or http://en.wikipedia.org/wiki/Space_Shuttle_Challenger_disaster.

The complexity of the system (4) is of particular importance in the simulation of large natural systems. For instance in modeling coastal dynamics one of the main problems is the deposition and pick-up of sand by the current. This process depends on the currents speed, turbulence and the composition of the sediment. It is difficult to obtain these coefficients experimentally: on the one side, they depend on too many parameters and on the other hand, experiments in some kind of flow tunnel are not useful because the grain sizes cannot be scaled to the flow speed like a ship or an automobile. Thus one might be tempted to model the molecular processes at the ocean's bottom. Such a model is way to complex for two reasons: (a) the underlying physical processes are very complex and (b) the parameter depends on many other parameters (see above). And since these parameters cannot be determined experimentally, the model cannot be validated. In a coastal dynamics model this problem can be overcome by some stochastic trick: the parameter is varied stochastically. Variation of a parameter in bracketing the solution gives upper and lower boundaries. In the stochastic version, the parameter is varied in time and/or space stochastically to reflect its natural variability. We will turn back to this topic in chap. 8. In other cases, such as reaction rate constants in chemical modeling, the parameters cannot be modeled (otherwise we would have to model the atom and the interaction between electrons of different atoms) but are known fairly well from experiment.

Post-facto or sterile modeling addresses the following situation: the physics of the system is understood, all parameters are measured experimentally and the system has been studied experimentally. Thus modeling does not provide any new insight. Modeling for the sake of modeling also occurs if a model cannot be implemented in practice, either because its output cannot be compared to the real system or because it is too complex. Modeling for the sake of modeling has only one useful purpose: education. Since in such case everything is known and measured, we can focus completely on the mathematical model and its analytical or numerical solution. And both even can be tested against each other as well as against observations.

2.2 Creating a model

Although the creation of a model is as much art as science, as in art a systematic approach can be helpful. Basic steps are:

1. Make a sketch.
2. Draw an envelope.
3. Introduce simplifying assumptions.
4. Closure.

2.2.1 Make a Sketch

The first step is essential to identify the relevant variables and the relation between them, in particular flows of mass and energy. In particular a novice might be so concerned with the mathematical description of individual processes that he thinks the sketch might be trivial. But this is not true. The sketch is the flow chart of the system, it allows to classify variables of the system according to input, output and system variables. Note that input and output variables also can be system variables while the system variables often are internal variables that describe the evolution of the system but do not show up for an observer outside the system.

Two examples can illustrate this point: a low pass filter can be realized as a series of resistor and capacitor with the input signal lying over the series and the output over the capacitor. In- and output variables are the signal to be filtered and the filtered signal. System variables are, for instance, the voltage drops at the resistor and the capacitor – the latter is also the output signal. Instead of the voltage drop at the resistor also the current through it could be used as system variable. Both do not show up at the outside but each of them can be used to describe the evolution of the system completely – at least if an initial condition is given.

The second example is from chemistry. In a chemical reaction, the input might be hydrogen and oxygen and the expected output is water vapor. The corresponding system variables then are the concentrations of these components. Nonetheless, since the reaction is exothermal, the temperature T of the tank also is an important system variable: it defines the amount of input material reacting to give the output.

If you feel uncomfortable with a formal flow chart as sketch, start with a graphical sketch – in time it often develops into a flow chart.

2.2.2 Draw an Envelope

The second step, the envelope, defines the system and its exchange of matter and energy with the environment. Occasionally, the envelope is directly suggested by the system, for instance the tank in which the reaction happens.

In other cases, no obvious envelope can be identified. If a conservation law is involved in the model, a differential segment can be drawn into this envelope and all in- and outgoing quantities can be marked. Note that this is not necessarily unambiguous because envelopes sometimes can be divided into sub-envelopes or can be put together into a larger envelope.

An envelope might be subdivided into compartments which can be defined as subsystems, for instance because they do not exchange mass or energy with the environment. The heating system in the thermal balance of the building in section 2.3.4 is an example for such a closed subsystem: do we really need to model the burning of oil and oxygen and the convection of the heated water through the pipes or do we treat this subsystems just as a source of heat at a given (time-dependent) rate.

2.2.3 Simplifying Assumptions

Once the subsystems and system variables are established, simplifying assumptions can be made. These can either make or break the model. The main tools include:

1. Reduce the number of unknown dependent variables.
2. Reduce the number of independent variables.
3. Reduce the number of terms in an equation.
4. Simplify the terms in the equation.
5. Bracketing the solution.
6. Dimensional analysis.

Successful simplifying allows an efficient handling of the mathematical model while still retaining all relevant features of the system. Even if the simplification is not required to formulate the numerical model and its solution it might be useful because it leads to a much faster code without too much loss in accuracy.

Reduce the number of unknown dependent variables

Formally, the reduction of the number of unknown dependent variables is equivalent to a reduction in the number of equations because the number of variables generally matches the number of equation. This process requires the identifications of variables that do not change the outcome of the process significantly: either because the variable itself is almost constant or because the system's behavior does not change significantly with a variation of this particular variable. For instance, the rate of a chemical reaction in most cases depends on temperature. Temperature can be dropped as a variable if (a) our system stays at almost constant temperature or (b) the reaction rate only weakly depends on temperature.

The latter approach might hold for the atmosphere: here the chemical reactive species also are the minor constituents and thus do not affect the thermal balance. The situation is different in a chemical plant. Here the reaction between the two species is the dominant process and thus modifies the temperature – which in turn modifies the reaction rates. Thus besides from the mass balances of the two species an energy balance must be considered. Here a reduction of variables is possible if the reaction is carried out with a large excess of one of the species: the reaction will lead to only minor variations in that species and thus the mass balance of that species can be dropped, reducing the system to one mass balance and the energy balance. The large water tank in section 2.3.2 is an example.

Whether this simplification is justified or not requires careful judgement – that is the art of modeling.

Reduce the number of independent variables

Formally, the reduction of the number of independent variables is equivalent to a lower dimension of the model – for instance, a PDE of two independent variables might be reduced to an ODE. Typical examples are the stirred tank concept and the one-dimensional pipe. Both reduce the spatial dimension of the problem. The stirred tank concept often is used in heat transfer, modeling of chemical processes or in mixing processes, such as in the examples in sect. 2.3.1 and 2.3.2.

The stirred tank, also called compartment concept, is applied in situation where spatial gradients can be neglected. In sect. 2.3.1 we will discuss a chemical plant that releases an effluent containing copper into a river. While in reality the concentration of Cu will vary around the discharge, we will assume that mixing with the environment is instantaneous – the river is stirred well. Models of chemical processes often also use the stirred tank: reactants as well as the products are well mixed in the entire volume. In heat transfer the stirred tank concept might be reasonable, too. Although it is difficult to stir a copper rod, a high thermal conductivity has the same effect: heat is distributed evenly in the metal body although heat losses occur only on the surface.

The one-dimensional pipe model also reduces the number of independent variables. Here we allow for one spatial variable, the length s along the pipe and assume steady-state conditions: there is no variation with time. In such a model, a stream carrying mass, energy or momentum enters a conduit and the associated variables (temperatures, concentration,

pressure) undergo a continuous variation in the direction of the flow. Changes in radial direction (perpendicular to the flow) are summarized into a boundary layer or effective film near the wall. In this film, gradients are assumed to be linear. Thus the differential operator ‘gradient’ is replaced by a simple difference, reducing the dimensionality of the problem.

And of course, the limitation to the steady-state always is a means to reduce the number of independent variables – here time t is omitted.

Reduce the number of terms in an equation

The former two steps are formal simplifications. The reduction of the number of terms digs more deeply into the physics: neglecting a term in an equation omits the physical effect formalized by it.

A good modeler with a broad scope of applications in mind attempts to work with a few general equations instead of a large number of equations only applicable in special cases. Thus the transport equation for a continuous medium (ocean, atmosphere, river, bath tub) will contain, for instance, the pressure gradient, friction, gravitation, the centrifugal force and the Coriolis force. In the atmosphere the Coriolis force certainly is important: combined with the pressure gradient, it allows the generation of the weather systems, in particular high and low pressure regions. Ocean currents, too, are subject to the Coriolis force. However, the distribution of cream in my mug of tea (or coffee) certainly is an entertaining problem in transport processes in a continuous medium, however, the scale is way too small to allow Coriolis to become effective – thus the force (and the corresponding term in the equation) can be omitted.

Friction also is a process that should be evaluated carefully. A frictional term is part of the equation of motion. Nonetheless, the relevance of friction for the system often can be evaluated much easier in terms of an energy balance: if the kinetic energy is much larger than the losses due to friction, friction can be ignored. If we drop a stone from a bridge, we can neglect friction – if we drop a parachutist from an airplane it is more sensible to consider friction. Both are clear-cut examples, the tricky business are the cases in between. For instance, what about the parachutists in free fall before the parachute opens?

Scale analysis is a tool to judge the relative importance of different terms in an equation as demonstrated for the equation of motion in oceans and in the atmosphere in sect. C.5.

Simplify the terms in the equation

The basic tool for simplifying terms is linearizing. This can be done in two ways. In the simplest case, we find a suitable linear relation for our problem and assume that this linearity is valid in the pertinent range of operation. Some typical linear relations are Ohm’s law, Fick’s law, Fourier’s law, Newton’s viscosity law, Hooke’s law, Stoke’s law, the convective heat transfer or the equation for a first-order chemical reaction.²

If the dynamical range is small, it might be useful to assume some parameters as constant: for instance, if reaction rates depend on temperature but temperature can be kept fairly steady in the experiment, it might be useful to assume the reaction rates as constant.

The most common way of linearizing is the simple mathematical approach to expand the nonlinear term and to discard all higher order terms.

Bracketing the solution

As mentioned before, the procedure of bracketing the solution does not reduce the complexity of the model but attempts to determine upper and lower boundaries of the solution. In an industrial process, these boundaries might be a sufficient information for the design of a plant and thus modeling of the full complexity of the system is not even required.

Bracketing the solution also can be considered as a best-case–worst-case scenario. However, we must be careful with this term: using the upper and lower bounds of a parameter

²These equations all are well-known, most of them are also given in Tab. C.1

gives upper and lower (or vice versa) bounds of the solution only in a linear system. In a non-linear system, upper and lower bounds might lead to almost the same results while some value in between gives an entirely different solution.

Dimensional analysis

This is a tool that should be considered if a problem becomes too complex to be modeled in a quantitative way. One of the first examples of dimensional analysis encountered in physics is the Reynolds' number, the ratio of viscous and inertia forces. The Reynolds' number is a dimensionless quantity which allows a qualitative description of processes. For instance, we introduce a critical Reynolds' number that indicates when a flow changes from laminar to turbulent. Thus with the dimensional analysis we describe the basic processes qualitatively without considering all the nasty details of, for instance, drag on a body as a car is exposed to a turbulent flow.

As can be guessed from the above example, this technique is quite common in fluid dynamics (see e.g. [42]). It is helpful to determine not only one solution of the differential equation but an entire manifold of solutions which can be scaled to the situation under study. This is particularly helpful in hydrodynamics when the solution for a certain size of syringe or nozzle is known and we are looking for a dynamically similar flow on a different scale. It is also the formal equivalent for experimental design aids such as flow channels.

The idea is quite simple: all equations representing scientific laws can be expressed such that both sides are dimensionless. In its simplest case, just divide one side of the equation by the other: the result, one, is dimensionless. To take advantage of dimensionless variables, first identify the physical variables relevant to the problem and combine them into dimensionless groups A, B, C, \dots . These groups have to be independent of one another. If the groups are dimensionless, combinations of groups such as AB or A/B^2 are dimensionless, too. But they are not independent of either A or B , though any one of them might be included instead of A or B if this seems advantageous. If the groups are chosen in such a way that the quantity of interest occurs in only one of them, it can be expressed by the function $A = f(B, C, \dots)$. The nature of this unknown function can be determined analytically or by computational methods. In an analytical solution, the advantage of the use of dimensionless variables is small; it only shows which parameters are important in scaling. If the solution has to be obtained by numerical simulations, the advantage of this method is more obvious: the procedure to determine a solution for one particular set of parameters can be quite time consuming. Each other set of parameters would require a new run. If dimensionless variables are used instead, the nature of the solution becomes obvious and it can be scaled to suit different sets of parameters.

2.2.4 Closure

Closure is as important as identifying the relevant processes and simplifying the equations. It is required to test the model. The validation of the model should not rely on one test only but on a larger number of tests. Reasons are twofold: in one test only, agreement might be accidental, that is a wrong model might provide roughly correct results for this special case and in consequence is adapted to model all other cases were results are completely nonsense. In addition, the final test might require an expensive or time-consuming experiment; thus it should be performed only if we are pretty sure that the model is corrected, that is, if we have tested it with a large number of basic tests..

Before starting an overkill of expensive and/or time-consuming tests, we should check very simple crucial points:

1. dimensions,
2. unphysical results,
3. order of magnitude,
4. asymptotic behavior,

5. unusual behavior for certain values of variables or parameters,
6. unexpected results.

The first question, ‘are the dimensions correct?’ should not only be asked at the end of the modeling process but during the entire process of model building from the very first sketches up to the final solution. Basically, a disagreement in dimensions implies that something is wrong with the equations or the values and parameters inserted into them. In particular during the reduction of the number of variables or linearization some parameters might not have been adjusted to the new conditions and still carry their original dimensions and values. Here the check on the dimensions points to an error – which hopefully might help to detect the error in the number, too.

The second question, ‘is the solution physically possible?’, is concerned with the fundamental laws of physics. For instance, flow speeds exceeding the speed of light suggest a faulty model. As do total masses of products of a chemical reaction exceeding that of the reactants. Both questions are basic and can be answered easily. They therefore should be checked frequently during model development, in particular also during validation of the numerical code. And, of course, in the interpretation of the results obtained with the model.

The third question, ‘is the order of magnitude reasonable?’, can be answered only after a solution is obtained from the model. Often experience or rough calculations help to answer the question; an example is given in sect. 2.3.1.

All three of the above questions are important also from the viewpoint of scientific reputation: only a very few things are more embarrassing than to present results that are patently absurd. And since the above question tackle very basic problems, all interested readers/listeners can ask them and simply estimate whether the model has obvious flaws or not. In fact, a good scientist might not even ask the question consciously but might identify a model as faulty simply by her gut feeling [49]. If the modeler has failed at this point, his reputation is seriously damaged: not because of the mistake in the model but because of his apparent un-ability to evaluate and validate his own work.

The asymptotic behavior can be studied by asking the question ‘what is the behavior of the result for large or small values of the variables or parameters?’. The procedure is similar to the upper- and lower-bounds method. A special case arises for $t \rightarrow \infty$: this often gives the steady-state solution. This case often can be checked easily: all temporal derivatives in the governing equations vanish and thus an ODE might become an algebraic equation. Or a PDE might become an ODE which can be solved analytically; see the example of the longitudinal tank in sect. 3.1. If the steady-state is not met by our model, the simulation of the transient phase, the development towards the steady-state, will be faulty, too. If the modeler discovers only at this state that the steady-state solution is the only solution he is interested in, he might re-think his approach on the problem: a model should be as complete as necessary but as small and simple as possible. And if only steady-state interests, the full transient solution is overkill and the governing equations should have been simplified long before starting their numerical or analytical solution.

The quest for unusual behavior for some parameters also is some kind of asymptotic analysis. Assume a solution that contains a difference in the denominator, such as

$$f(x) \sim \frac{1}{x - a} .$$

A critical situation arises if x approaches a : $f(x)$ will increase enormously. Such runaway may be a beneficial or catastrophic event, such as a resonance catastrophe. These runaways should be checked carefully: since they are easily observed in a system, they can validate or disprove the numerical solution. An exponential term e^{ax} also leads to a runaway and should be checked carefully.

The last question is a little bit more tricky: unexpected results might disprove a system (in particular if they do not make any sense physically) but they also can be the salt of modeling: it is the unexpected that provides new insight.³ Unexpected results therefore

³Always remember that information I is defined by probability p : the least expected signal has the highest

tell us that a model is either flop or top: flop if the unexpected result points to an error in modeling and top if it points to a new fact or phenomenon. This is better than just a working descriptive model because the encounter with the new is what drives science. Thus an expected result has to be analyzed carefully: even if the gut feeling suggests that the unexpected result points to a flaw in the model, it might be a correct result (and model), as is illustrated in sect. 2.3.3.

2.3 Examples

We will now start to sketch very simple models to get a feeling for the first two steps of modeling: describing the underlying physics and simplifying the model.

2.3.1 Discharge of a Plant Effluent into a River

The problem: a chemical plant discharges an effluent containing a concentration $c_{Cu} = 10 \text{ mg/l}$ of copper at a rate of $f_{Cu} = 150 \text{ l/min}$ into a nearby river with a flow f_R varying between 2300 and 5000 l/s. Environmental regulations allow for a maximum concentration of $c_{Cu, \max} = 1.0 \text{ } \mu\text{g/l}$ in the river. Is the river flow sufficient to reduce the effluent's concentration below the permitted values?

Analysis of the Problem

Here we can start with a graphical sketch. The spatial target is a part of the river containing the plant's discharge – this is also our envelope. Our target property is the copper concentration, thus the conservation law under consideration is the mass balance for copper.

To set up the basic equation we will simplify our model. The copper concentration inside the envelope will vary locally in a rather complex manner but with the highest values close to the discharge. The river's flow rate suggests a fast running river which implies enough turbulence for efficient mixing. Thus we can use the concept of the stirred tank or compartment and work with an average concentration, ignoring all the local fluctuations. And in a slow moving river? Locally we will have large aberrations from the average concentration, however, further downstream the mixing process was efficient enough to keep copper values below permitted values.

Another simplification regards the river flow. Since the regulatory limit must be met at all time we only have to consider the lower flow of 2300 l/s.

And our target quantity? We are only interested whether the copper concentration stays below the permitted value. Thus we can start from the simplified mass balance:

$$\text{Rate of copper in} - \text{Rate of copper out} = 0. \quad (2.3)$$

Mathematical Formulation and Analytical/Numerical Solution

Equation 2.3 is a simple algebraic equation, thus its solution should pose no difficulties. We only have to be careful to write the terms correctly:

$$c_{Cu} f_{Cu} - c_R (f_R + f_{Cu}) = 0; \quad (2.4)$$

Just a moment: where is the inflowing flow? Since this is not a mass balance for the water, it is not required. But if you want to see it written down add it to the first term in 2.3:

$$c_{Cu, \text{clean river}} f_R + c_{Cu} f_{Cu} - c_R (f_R + f_{Cu}) = 0 \quad (2.5)$$

information: $I = -\ln p$.

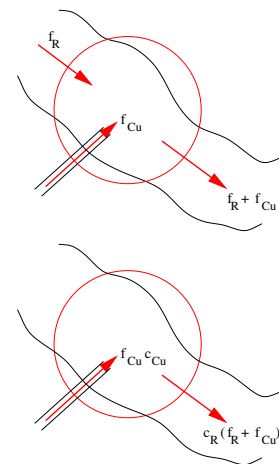


Figure 2.1: Mass and copper balance

with $c_{\text{Cu, clean river}} = 0$. c_{R} is the unknown quantity, the copper concentration in the well stirred river. Inserting the values given in the problem description, we obtain

$$c_{\text{R}} = 10.9 \mu\text{g/l} \gg c_{\text{Cu, max}} . \quad (2.6)$$

The river's flow is not sufficient to dilute the effluent below the permitted value. Thus copper must be removed before discharging the effluent into the river – or the effluent must be diluted.

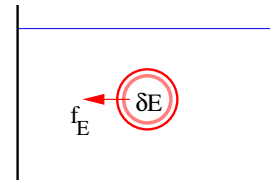
Some in-between calculation 2 How do the results change if the upstream flow already carries a substantial copper concentration $c_{\text{Cu, clean river}}$?

2.3.2 Newton's Law of Cooling

The problem: A copper ball has a diameter of 1 cm and a temperature of 100°C . At time $t = 0$ the ball is dropped into a large water basin with a temperature of 30°C . The water basin is large enough to retain this temperature. After 3 min the ball's temperature has dropped to 70°C . After which time has the temperature dropped to 31°C , that is just 1° above the water's temperature?

Analysis of the Problem

The sketch is a simple one: we have a large water reservoir with the ball inside and heat exchange between water and ball. There is no exchange between the water and its surroundings. Since the problem description suggests that the water retains its temperature, we can apply the concept of the stirred tank: the water is at constant temperature everywhere in the tank and thus the temperature gradient at the ball's surface, which drives the heat transport, only changes due to changes in the ball's temperature. Although we do not apply any stirring to the tank, the high thermal conductivity of water supports this assumption. We make the same assumption for the copper ball: while it transfers heat to the water its temperature shows no spatial gradient although the transport occurs only on the surface – but copper also has a very high thermal conductivity, thus the approximation is valid.



The basic concept in our model is a conservation law, the energy balance. The envelope can be drawn around the ball and we can formulate the required equation verbally as

$$\text{Rate of energy in} - \text{Rate of energy out} = \text{Rate of change in energy content} , \quad (2.7)$$

with the first term on the left hand side vanishing.

Mathematical Formulation

We can either derive the heat transfer equation by inserting the relevant terms from Tab. C.1 into (2.7) or by directly referring to Newton's law of cooling

$$- \kappa(T - T_s(t)) = \frac{dT}{dt} \quad (2.8)$$

with k being the rate with which heat is absorbed by the body and $T_s(t)$ being the temperature of the surroundings, in our case $T_s = \text{const}$.

Analytical/Numerical Solution

Since (2.8) is an ordinary differential equation of first-order it can be solved analytically. Both an exponential ansatz or separation of variables will work. With the latter approach we can rewrite (2.8):

$$- \frac{dT}{T - T_s} = k dt . \quad (2.9)$$

We can now proceed in different ways, depending on our personal preferences. For instance, we can first obtain the general solution, than insert the 3 min value to obtain the value of k and finally insert this and the end temperature to obtains the time required for cooling. Or we do the same steps without the first one by choosing the integration limits accordingly. In the latter case we get

$$-\int_{370}^{340} \frac{dT}{T-300} = k \int_0^3 dt \Rightarrow \ln \frac{370-340}{340-300} = 3k \Rightarrow k = 0.187 \text{ h}^{-1}. \quad (2.10)$$

Here all temperatures are absolute temperatures, units are omitted to avoid typos from my side. Changing the integration limits yields the time required to cool the ball down to the given value of 31° :

$$-\int_{100}^{31} \frac{dT}{T-300} = 0.187 \text{ h}^{-1} \int_0^t dt \Rightarrow \ln \frac{370-300}{31-30} = 0.187 t, \quad (2.11)$$

and solved for t

$$t = \frac{\ln 70}{0.187} \text{ h} \approx 22.8 \text{ min}. \quad (2.12)$$

Side question 9 Would it make a difference if degrees centigrade were used instead of absolute temperatures?

Closure

Reasoning: cooling down is a kind of decay, thus it follows an exponential law. We should see this from the structure of the differential equation; it would be more obvious if we had first obtained the general solution of (2.8) and performed our calculations afterwards – if you don't 'see' the exponential, just obtain the general solution. Thus a drop by 69 K instead of 30 K should require significantly more time than the $\frac{69}{30} \times 3$ minutes. Thus 23 min does not contradict our expectations.

Experimental confirmation: just do it.

2.3.3 Evaporation of a Pollutant into the Atmosphere

The problem: a pollutant in a body of water may be partly released into the atmosphere.⁴ For simplification we assume that at time $t = 0$ the pollutant's concentration in the water is c_{poll} . It is well mixed with the water and there is no in- or outflow of water and/or pollutant. Which amount of the pollutant remains in the water?

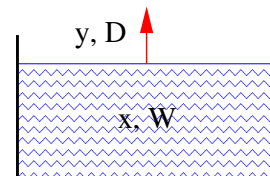
Analysis of the Problem, Mathematical Formulation & Analytical Solution

The problem is incomplete. Normally, we would simply determine the pollutant concentration with time, $c_{\text{poll}}(t)$. But that would require data on evaporation rates which in turn depend on temperature and wind speed. Thus detailed modeling is not possible.

What else to do? Let us start with a sketch and check wether we can eliminate the unknown data from the problem. Therefore let us start with something very fundamental, in this case the mass balances. Here they are formulated for moles rather than mass because the physical laws involved here, such as the ideal gas law or the phase equilibrium relations, are formulated for moles. Balances are obtained for the total mass/moles and the pollutant mass/moles:

$$\text{Rate of moles in} - \text{Rate of moles out} = \text{Rate of change of moles}. \quad (2.13)$$

⁴Other processes of pollutant removal from the water such as absorption on or reaction with the bottom sediment or biodegradation through bacterial action are ignored in this scenario.



With D as the total moles evaporating per unit time and W as the total moles in the water body, we obtain for the total mole balance

$$D = \frac{dW}{dt} . \quad (2.14)$$

The pollutant mole balance is

$$yD = \frac{dxW}{dt} \quad (2.15)$$

with y and x being the pollutant concentrations in the vapor and aqueous phase. So far, we have four dependent variables but only two equations. One variable, D , can be eliminated by dividing both equations:⁵

$$y = x + W \frac{dx}{dW} . \quad (2.16)$$

If we assume that the water vapor leaving the liquid is locally in equilibrium with the liquid, we get a third equation: $y = f(x)$. This is permissible because the thermodynamics of phase equilibria suggest for sparsely soluble, low volatility substances

$$p_p = \frac{xp_w}{x_s} \quad (2.17)$$

with p being the partial pressure of the pollutant in the vapor phase, p_w the vapor pressure of the pure pollutant and x_s the solubility of the pollutant in water. Thus the pollutant concentration p in the vapor increases with the liquid phase concentration x and with the water pressure of the pure pollutant. Partial pressure can be converted into moles using the ideal gas law, $p \sim n$. Using Dalton's law we get

$$y = \frac{n}{n_{\text{tot}}} = \frac{p}{p + p_{0,\text{H}_2\text{O}}} \approx \frac{p}{p_{0,\text{H}_2\text{O}}} \quad (2.18)$$

with n being the number of moles of the pollutant, n_{tot} the total number of moles, and $p_{0,\text{H}_2\text{O}}$ the pure component water pressure. Thus (2.16) can be written as

$$\frac{xp}{x_s p_{0,\text{H}_2\text{O}}} = x + W \frac{dx}{dW} . \quad (2.19)$$

Integration yields

$$\left[\frac{p}{x_s p_{0,\text{H}_2\text{O}}} - 1 \right] \ln \frac{W}{W_0} = \ln \frac{x}{x_0} . \quad (2.20)$$

We will examine the solution for one particular pollutant, mercury, with a solubility of $3 \cdot 10^{-2}$ mg/l and a vapor pressure of 0.173 Pa, both values taken at 25°. Water has a vapor pressure of 3170 Pa.

Since we still do not have any information about evaporation rates, we start with an assumption: a small fraction of the water basin, 0.01%, evaporates. Substitution into (2.20) yields

$$\frac{x}{x_0} = 0.133 , \quad (2.21)$$

thus 87% of the original mercury has evaporated into the atmosphere – although only 0.01% of the water pool has evaporated.

⁵Both equations are first-order ODEs, therefore this procedure is permitted.

Closure

This result certainly is unexpected. Without any further assumptions we would not be surprised to get values of about 0.01% evaporated Mercury; values an order of magnitude different, that is 0.1% or 0.001% probably would surprise us, but still are somehow plausible – at least, we would try to make up some explanation for them. The calculated disagreement of about 4 orders of magnitude, on the other hand, is unexpected and unplausible. At first hand, it suggests a fault in the model. Alternatively, it can suggest some new insight (at least new to us). Looking into the properties of mercury, we can justify the result on physical grounds: Mercury has an extremely low solubility in water and consequently exhibits an unusual high fugacity or “escaping tendency” – therefore the high rate of transfer into the atmosphere.

The lesson to be learned from this example: results that appear to be completely out of the ordinary should not call for automatic disbelief or dismissal. Instead, a careful review of the solution process should be undertaken and if the result persists, the underlying physical processes should be closely scrutinized.

2.3.4 Thermal Balance of a Building

The following problem is much more complex and requires a full-fledged numerical model. However, since it has some application in ordinary life and digs a little bit deeper into a more complex problem, we will discuss it here.

The problem: the heating system in a public building, such as a seminar room in an university building, shall be optimized to conserve energy while simultaneously providing the necessary comfort for the user. The standard method is either night- and weekend-setback or even night- and weekend-set off. In the latter case, the heating system is switched-off completely for the night hours or the weekend while in the former case only the flow temperature is reduced.

The goal: keep the user thermally comfortable⁶ (as e.g. defined in Figs. 2.2 and 2.3) in the seminar room under the constraint of minimizing the energy input into the building/heating system. The user exchanges heat with the room through different processes. The room as part of the building experiences the very same heat exchange processes with the remaining parts of the building while the building exchanges heat with the environment – its a system of nested subsystems and we have to evaluate quite carefully down to which detail each (sub-)system is simulated. The optimization problem requires to determine a temporal dependence of the flow temperature T_{flow} such that energy consumption is small and during working hours room conditions are within the comfort range.

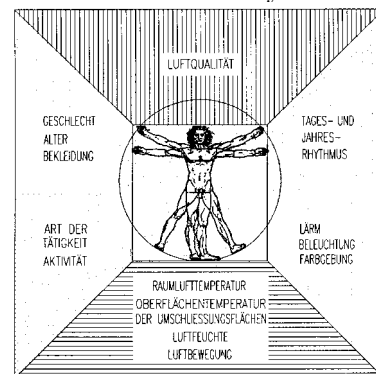


Figure 2.2: Parameters influencing comfort [129]

The processes determining the comfort range can be summarized as follows:

- heat conduction to the surrounding air or contact surfaces (such as chair, desk, floor).
- convection which is related to the motion of the air.
- radiative heat transfer, in particular with walls, floor and ceiling but also with windows and radiators,
- evaporation.

⁶Comfort in this case is not defined as the subjective impression of comfort but on a physiological basis: a person always has to adjust his metabolism to his surroundings with the main goal to keep his body temperature constant. In the comfort zone neither excessive heat production by the body to keep the person warm nor excessive sweating to cool down an overheated body is required. Physiological adaptation processes to the environment are different from person to person, nonetheless, comfort ranges can be defined for at least a certain percentage of the population. For a more detailed discussion see e.g. [129, 182] or the regulations in the DIN.

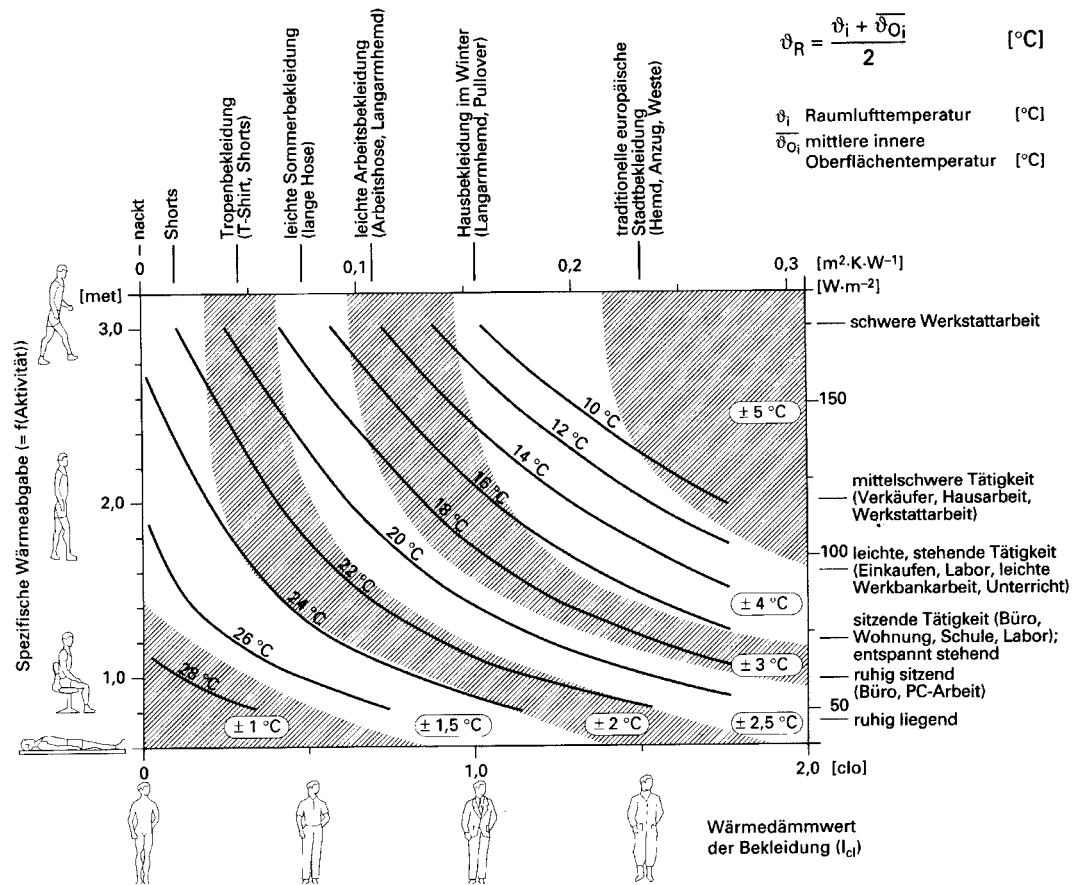


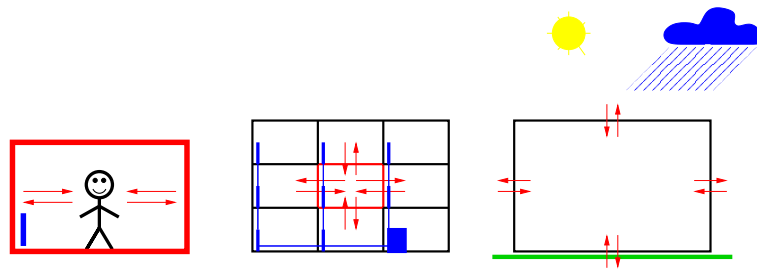
Figure 2.3: Comfort temperature depending on activity and clothing [182]

These processes relate to different parameters of the room. In heat conduction, the heat flux depends on air temperature and on the temperatures of the contact surfaces. The heat flux in convective transport is related to air temperature and speed; for outdoor applications the latter is referred to as wind-chill. Radiative transfer is determined by the surface temperatures of all objects within sight. Heat fluxes due to evaporation, in turn, depend on temperature and humidity. The different room parameters influencing the comfort range are summarized qualitatively in the left panel of Fig. 2.2.

Figure 2.3 shows the necessary ambient temperature for a person in a room to feel thermally comfortable. This ambient temperature depends on the persons activity M (unit met for metabolism, 1 met corresponds to 60 W/m^2) and clothing I_{cl} (unit clo for clothing, 1 clo corresponds to a thermal resistance of $0.155 \text{ m}^2 \text{ K/W}$; 1 clo roughly corresponds to the insolation provided by the clothing for a thermally comfortable person sitting still at an ambient temperature of 21°C , a relative humidity of 50% and an air speed of 0.1 m/s). The temperatures given in Fig. 2.3 are determined for a relative humidity of 50% and an air speed of 0 m/s for $M \leq 1$ and $0.3(M - 1) \text{ m/s}$ for $M > 1$. Such an approach is reasonable because a person totally at rest will not feel comfortable in the presence of convective cooling (except for ambient temperatures exceeding body temperature). On the other hand, with increasing M the mechanical work load on the person increases and thus its own motion will induce air motion. The solid lines in Fig. 2.3 give optimum ambient temperatures: 95% of the persons in the room should feel thermally comfortable under these conditions. The shaded areas show the allowed deviation from the optimum ambient temperature where less than 10% of the population will feel thermally uncomfortable.

It should be noted that ambient temperature is not the air temperature in the room. Since

Figure 2.4: Thermal balance of a building as matryoshka problem



radiative exchange with the walls and any other surfaces in the room contributes as much to the heat exchange as heat conduction, ambient temperature is defined as the average of air temperature and temperature of the room's surfaces. It should be noted that this approximation is valid if ambient temperature and temperature of the surfaces differ by a few degrees only. Even in a well-insulated building, this requirement only is met if temporal variations (time scales of hours to days) in temperature are small. Short-term temperature fluctuations are less important: walls have a rather high heat capacity and therefore a rather long time scale to adjust to changes in air temperature. Thus the short-term fluctuations are averaged out.

Analysis of the Problem

The problem resembles a little bit a Russian matryoshka: the only processes are heat exchange processes. In the target room, it is the heat exchange between the user of the room and its walls, air, window and radiator. Kindly note the wording in German and English: the English word radiator describes the main heat exchange process while the German word Heizkörper describes the function but not how it is performed. Thus we often forget that a radiator only works if it views most of the room but not if it is hidden under a desk or behind a couch.

But the room is not thermally isolated from the other rooms in the building: heat fluxes here are mainly due to heat conduction but convection and radiative transport also contribute. And the outer shell of the building exchanges heat with the environment: heat conduction to the ground, radiative transport, heat conduction and evaporative losses to the atmosphere. This nesting is sketched in Fig. 2.4.

Figure 2.4 however is not the sketch we are asked to start with in modeling. Before we draw that sketch we have to simplify our problem. Thus let's ask some questions:

1. do we need to simulate the heat transfer between a user and the room in all details?
2. do we need to consider heat transfer to adjacent rooms or from the building's shell to the environment?

To decide on these questions, it might be worthwhile to look at the feasibility of their modeling as well as on their relative importance and relevance to the problem under study. Thus we have to scrutinize each transport mechanism and decide whether modeling in detail is both possible and reasonable.

Heat conduction is based on collisions between particles in fluids or the vibration of atom rumps around their rest position in solids. Thus a direct contact is required for heat conduction to become effective. For a person in a room, heat conduction can be divided into two parts: (1) the heat transfer to solid bodies such as chair, floor and desk (see also Fig. 2.5) and (2) the heat transfer to the air directly in contact with the body and the clothing. While the first part of this heat transfer in principle can be modeled easily, the second part becomes more tricky. If a person is completely at rest in a room where air motion is negligible, a thin film of heated air will develop around her reducing the heat flux and increasing the person's thermal comfort. With increasing motion relative to the ambient air, this thermal film is destroyed and heat fluxes

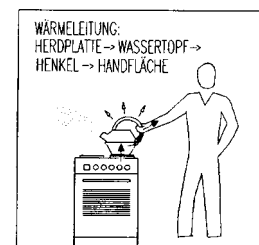


Figure 2.5: Heat conduction [129]

increase. The motion can be due to draught, the convective motion of the air or the person's motion. Thus the latter part is difficult to model: either assumptions have been made and average parameters are used or this process has become too complex to be modeled, see also sect. 2.1.2. In addition, that process would not be heat conduction but turbulent transport with a flow. The other part of the heat transfer is rather conventional, however, compared to the body's surface, the contact surfaces to solids are rather small and normally also well insulated.

The situation is different if we do not consider the person in the room but the room as part of a building or the building's outer shell as boundary to the environment. In these cases the direct heat conduction dominates over convective cooling and thus a formal description is simple and possible. In addition, since the wall strongly reduces convective exchange between the room and the atmosphere, heat conduction from the inside of the wall/window to its outside will be a pretty relevant process.

Heat conduction is described by Fick's or Fourier's law (see also Table C.1). In general form the heat flow density \vec{j}_Q is given as

$$\vec{j}_Q = -\lambda \nabla T \quad (2.22)$$

with λ as thermal conductivity and T as temperature.

Convection (convective cooling, transport of sensible heat) already has been mentioned in connection with the difficulties in modeling heat conduction between the person and the ambient air. It is related to the bulk motion of air. It is the basic principle of the heating system: first, convection transports heat from the boiler through the pipes to the radiator (in modern heating systems supported by a pump) with water as the transporting medium. Secondly, convection transports heat from the radiator through the room, creating a kind of convection cell with heated air rising close to the radiator and sinking at the opposite wall. All kinds of draught or opening that allow for air motion (door, windows) modify this convection pattern. The presence of people in the room can also modify it: the people themselves form obstacles for the air flow and their motion might add turbulence and momentum to the flow. Thus the difficulties in modeling the second part of heat conduction also appear in modeling convective effects. The general formal description of convection is quite simple: the heat flow density is

$$j_{\text{conv}} = \alpha(T_2 - T_1) \quad (2.23)$$

with α being the heat transfer coefficient and $T_2 - T_1$ the difference between the temperatures of the surface and the air. The problem is that the heat transfer coefficient α depends on flow speed and surface properties. The formal simplicity of convection suggests its consideration in modeling. The high variability of α can be circumvented by either using average values or by bracketing the solution.

The last mechanism is radiative heat transfer. Every body radiates heat. Its amount depends on temperature and the properties of the surface of the body. The radiative flow of a black body is given by Stefan-Boltzmann's law as $q = \sigma T^4$ with $\sigma = 5.67 \cdot 10^{-8} \text{ W}/(\text{m}^2\text{K}^4)$ as Stefan-Boltzmann constant. Stefan-Boltzmann's law can be extended to non-black bodies. Here we introduce an effective temperature T_{eff} , also called mean radiant temperature. This is the temperature, a black body must have, to emit the same total radiation flow as the body under consideration. It can be related to the temperature by a modified version of Stefan-Boltzmann's law for the gray body:

$$q = \sigma T_{\text{eff}}^4 \approx \bar{\epsilon} \sigma T^4 \quad (2.24)$$

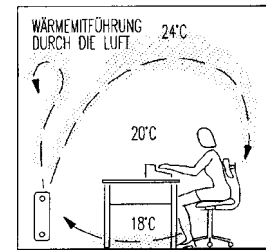


Figure 2.6: Convection [129]



Figure 2.7: Radiative transfer [129]

with $\bar{\varepsilon}$ being the average emissivity.⁷

The emission of radiation is not coupled to the presence of an environment as is the process of radiative transfer does not require matter. This is most obvious in the radiation received from the Sun – the thermal conductivity of interplanetary space is almost zero due to the extremely low densities. Since the emission of radiation does not require an environment it also does not depend on the properties of the environment: while the heat flows in convection and conduction are determined by a temperature gradient or a difference between temperatures at a boundary, the radiative flux emitted from a body is only determined by its temperature.

Nonetheless, there is also heat exchange with the environment due to radiative transfer. The radiation emitted by body B1, e.g. a person in a room, hits body B2, for instance a wall of that room. The heat transfer from B1 to B2 then is determined by that part of B1's radiation that hits B2 and by the absorption coefficient of B2. And in turn, part of the radiation emitted by B2 is also absorbed by B1.

The heat flow \dot{Q}_{12} from body B1 at higher Temperature T_1 to body B2 at $T_2 < T_1$ is given by

$$\dot{Q}_{12} = c_{12} A_1 (T_1^2 - T_2^2). \quad (2.25)$$

Here A_1 is the area of the emitting surface of B1 and c_{12} is the radiation exchange coefficient. The latter considers the average emissivities of the bodies and their geometry, that is the relative amount of B1's emitted radiation absorbed by B2 and vice versa. The general form of the radiation exchange coefficient is

$$c_{12} = \frac{\bar{\varepsilon}_1 \bar{\varepsilon}_2 \sigma \varphi_{12}}{1 - (1 - \bar{\varepsilon}_1)(1 - \bar{\varepsilon}_2) \frac{A_1}{A_2} \varphi_{12}^2}. \quad (2.26)$$

The difficult part of the geometry is concealed in the 'einstrahlzahl'

$$\varphi_{12} = \frac{1}{\pi A_1} \int_{A_1} \int_{A_2} \frac{\cos \beta_1 \cos \beta_2}{r^2} dA_1 dA_2 \quad (2.27)$$

with β_i being the 'richtungswinkel' between the beam's direction and the normal to A_i .

Figure 2.8 shows radiation exchange coefficients for some simple geometries. Before attempting to calculate the radiation exchange coefficients for each situation by hand, we should have a look at that table to identify situations that can be described by these special geometries. The parallel surfaces in the upper example are not relevant for our particular problem but they are relevant for instance in the calculation of heat transfer coefficients for windows with double or triple glazing (see example in [84]). The convex surface enclosing a concave surface can be used as a very simple model for a person inside a room – at least in cases where radiation transfer is not strongly influenced by furniture and window area is small compared to the surface of the entire room. We can use this coefficient also to illustrate the

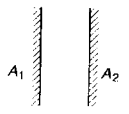
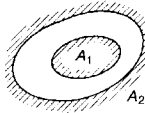
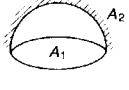
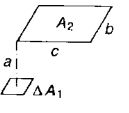
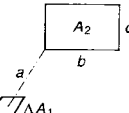
Geometrie	Strahlungsaustauschkoefizient
 parallele Flächen	$C_{12} = \frac{\sigma}{\frac{1}{\varepsilon_1} + \frac{1}{\varepsilon_2} - 1}$
 konvexe Fläche A_1 von konkaver Fläche A_2 um- schlossen	$C_{12} = \frac{\sigma}{\frac{1}{\varepsilon_1} + \frac{A_1}{A_2} \left(\frac{1}{\varepsilon_2} - 1 \right)}$
 Halbraum A_2 über ebener Fläche A_1	$C_{12} = \frac{\varepsilon_1 \varepsilon_2 \sigma}{1 - \frac{1}{2} (1 - \varepsilon_1)(1 - \varepsilon_2)}$
 Rechteckfläche parallel zum Flächenelement ΔA_1	$C_{12} = \sigma \varepsilon_1 \varepsilon_2 \frac{1}{2\pi} \left(\frac{b}{\sqrt{a^2 + b^2}} \arctan \frac{c}{\sqrt{a^2 + b^2}} + \frac{c}{\sqrt{a^2 + c^2}} \arctan \frac{b}{\sqrt{a^2 + c^2}} \right)$
 Rechteckfläche senkrecht zum Flächenelement ΔA_1	$C_{12} = \sigma \varepsilon_1 \varepsilon_2 \frac{1}{2\pi} \left(\arctan \frac{b}{a} - \frac{a}{\sqrt{a^2 + c^2}} \arctan \frac{b}{\sqrt{a^2 + c^2}} \right)$

Figure 2.8: Radiation exchange coefficients [59]

⁷Many building materials (e.g. wood, concrete, stone, glass, lacquer, roofing felt or synthetic materials) have average emissivities above 0.9 – a crude approximation thus might even use Stefan–Boltzmann's law for the black body. Water has an average emissivity of 0.95. Metallic surfaces, however, have a smaller average emissivity; here Stefan–Boltzmann's law for the black body should only be used if an emergency estimate is required.

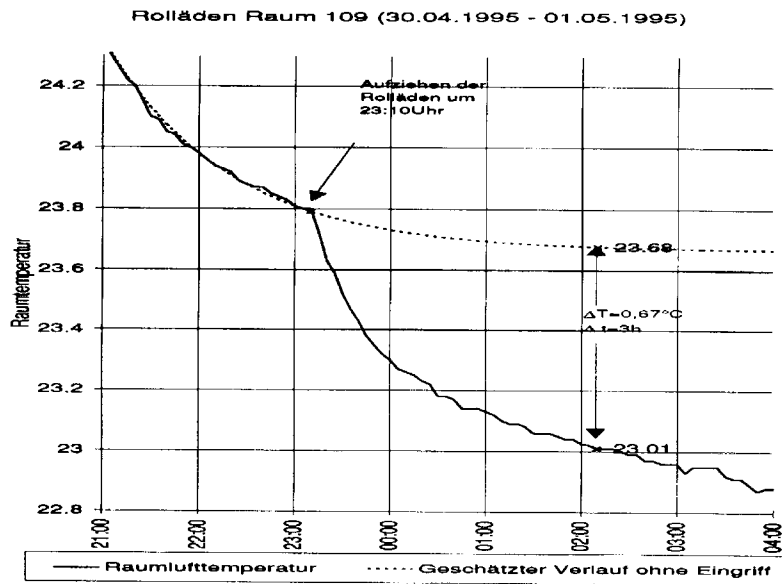


Figure 2.9: Changes in room temperature due to radiative losses through a window during night (solid curve). The dashed curve shows higher temperatures (and thus increased losses) if darkening is used [150]

importance of radiative transfer for thermal comfort. The heat flow for this special geometry is

$$\dot{Q}_{12} = \frac{\sigma A_1 (T_1^4 - T_2^4)}{\frac{1}{\bar{\varepsilon}_1} + \frac{A_1}{A_2} \left(\frac{1}{\bar{\varepsilon}_2} - 1 \right)}. \quad (2.28)$$

The person's parameters are: surface area $A_1 = 1.8 \text{ m}^2$, average emissivity $\bar{\varepsilon}_1 = 0.95$ and surface temperature $T_1 = 32^\circ \text{C}$ (only shorts and light T-shirt). The room has the following parameters: surface area $A_2 = 68 \text{ m}^2$ (height 2.5 m, floor $3 \times 4 \text{ m}^2$), average emissivity $\bar{\varepsilon}_2 = 0.93$ and surface temperature $T_2 = 16^\circ \text{C}$. The heat flow from the person to the room's surface then is 162.3 W. Increasing the room's surface temperatures to 20°C gives a heat flow of 124 W; a decrease to 12°C increases the heat flow to 199 W – the excess heat flow has to be created by internal heating, that is an increased metabolism and/or shivering.

The third geometry in Fig. 2.8 describes heat exchange between a surface and a half-sphere above. This geometry is a good approximation on any radiation exchange with the outer world: the exchange between a solar collector and the night sky or the exchange between the buildings outer shell and the sky. The remaining two geometries can be applied to many different situations. Examples are the radiative exchange between a radiator and a wall, between different surfaces in the room or between a person in the room and the night sky visible through the window. Figure 2.9 illustrates the importance of radiative losses through a window during nighttime.

Mathematical Formulation and Solution

We have described and discussed all processes qualitatively and quantitatively but still we have not decided on the model. But from the discussion of thermal comfort we can learn that the relevant parameters which can be influenced by the operator of the heating system is the ambient temperature, defined as the average of the surface temperature and the air temperature. Air temperature is regulated automatically by the thermostat; the temperature of the surfaces is regulated by heat conduction to adjacent rooms, radiative losses through windows and losses to the atmosphere through the buildings outer shell. In the latter case, the relevant processes are heat conduction and radiative losses. The most problematic process, convection, is not considered inside a room because it strongly depends on the behavior of the people inside the room (and, at least to a certain extend, can be regulated by them). In addition, convection inside a room can be regarded as advantage in modeling: convection

tend to equalize the spatial distribution of temperature and thus allows to treat each room like a stirred tank. Thus the details of the room do not enter the simulation. Convection is also not important for heat transfer inside the building because for a public building we can assume all doors and windows to be closed during night and weekends. The convective losses only are relevant at the outer shell of the building.

Our main problem is that we have to model at different scales. We can attempt some finite difference or finite element model for the entire building by the price of huge grids and computational efforts. Or we can use nested models, that is we model the inside of the seminar room separately from the rest of the building. In each time step, the surface temperatures of our target room are used to calculate the heat transfer to adjacent rooms and afterwards are adjusted accordingly.

Before going into more detail let us take a step back and start with some simple estimates. What is more important: heat conduction through the wall between two rooms or heat conduction through an outer wall? Basically all heat transfer processes depend on the difference in temperature: either as gradient in conduction, as difference in convection or as difference of the forth powers of temperatures in radiative exchange. Inside a building temperature gradients in general are small, the largest gradient in general is that between a person and the building. Temperature gradients to the outside, however, can be quite large. In a cold and clear winter night, air temperatures are well below zero and almost all emitted thermal radiation escapes through the atmosphere without being reflected back. Thus radiative losses are very large. The consequence for modeling: we have to start with the outer shell. Thus our model must consider the floor plan and the properties of all walls, roofs and the building's ground plate.

In a very simple approach, the entire inside of the building is assumed to be in thermal equilibrium. For a more detailed approach, we can specify the rooms according to the ground plan or make a compromise and identify zones inside the building: there are some rooms with relatively low temperatures (bed rooms, corridors, landings, porches), some well-tempered rooms (living rooms, offices) and some rather warm rooms (bathroom, kitchen). Heat exchange is only considered between zones: heat exchange is only relevant in the presence of temperature gradients but since the rooms inside a zone are at comparable temperature, gradients vanish and consequently also the heat exchange.

For the physics building such zoning would be very simple, almost concentric: the well-tempered offices all view the inner court. This inner 'ring' is surrounded by a ring of low-tempered corridors which in turn is surrounded by a ring of low-tempered laboratories. Thus why should we distinguish between corridor and laboratory? They are different zones for two reasons: in contrast to corridors, laboratories are connected to the heating systems. And, more important, laboratories (as offices) have users (any person emits roughly 100 W and thus has to be considered as a heat source) and often also other internal heat sources (machines running inside the laboratories, even computers and printers). Such internal heating sources should be considered in a transient simulation of a building, too. In addition to these internal heat sources we also have to consider the heat provided by the heating system and, if relevant, the removal of heat by ventilation.

Thus the building is specified. Since we have argued that heat exchange across the outer shell is the most important process regulating the ambient temperature inside a room and thus the thermal comfort, we also have to consider the local weather or climate parameters such as air temperature (important for heat conduction), cloudiness (important for radiative transfer), wind speeds (important for convective losses from the building's outer shell and for undesired heat losses by air leakage through joints) and average precipitation (important for evaporative losses – these should not be underestimated because the large heat capacity of water absorbs quite a large amount of heat).

With these parameters and boundary conditions, the relevant equations discussed above can be solved numerically. Such a model cannot be developed within the framework of a lecture although it might be an interesting end-of-term project. To give an example for a result of such kind of simulation, we resort to a commercial program, in this case TRNSYS/IISiBat.

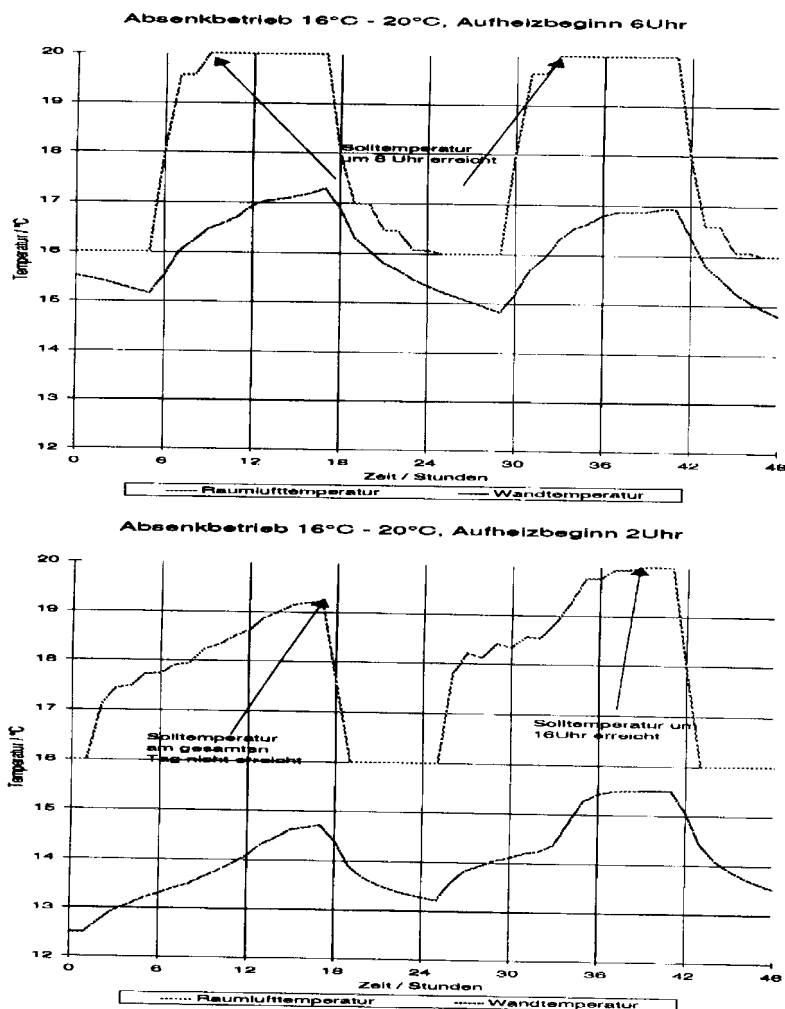


Figure 2.10:
Transient simulation of a building: air and wall temperatures for night setbacks [150]

Figure 2.10 shows a sample result related to the question of this section. The model was used to calculate room and wall temperatures for two scenarios of night- and weekend setbacks. In both panels, setbacks reduce air temperature from 20° to 16°; both simulation runs start at a Monday morning after a weekend setback to 16°. The target air temperature is 20° because the operator of the heating system does not distinguish between ambient temperature and air temperature.

The upper panel is for relatively mild outside temperatures: wall temperatures are around 15° at night. Setback mode has been set back to normal mode at 6 in the morning. This leads to a rapid rise in air temperature and, owing to their larger heat capacity, a slower rise in the temperature of the walls. Target air temperature is acquired at 8 in the morning – right at the start of the working hours. Nonetheless, since wall temperatures still are well below 20°, ambient temperatures are only around 18°. According to Fig. 2.3 this is ok for normal clothing with $I_{cl} = 1$ clo and $M \approx 1$ met, corresponding to instruction.

The lower panel of Fig. 2.10 starts from the same assumptions except that the outside temperature does not correspond to a mild but to a cold day. To compensate for this, the heating is switched on at 2 in the morning instead of 6: the control of the heating panel includes a temperature sensor for outside temperatures. The system thus can adapt its setback times and the switching-on of the heating automatically. However, in spite of this adaption results are a little bit disappointing: the target air temperature is not met during the entire working day. In addition, the wall temperature has dropped below 13°C during the weekend and rises only slowly during the day. Monday at noon, ambient temperatures

thus are only slightly above 16°C, which according to Fig. 2.3 requires an increase in clothing and/or metabolism. The target air temperature only is acquired Tuesday afternoon. Since also the walls start to heat up, the ambient temperature now exceed 17°, approaching a reasonable value for lessons.

Side remark: The old german regulations (Wärmeschutzverordnung) only ask for the total energy consumption during the year. To calculate the heat fluxes, stationary models are sufficient and average climate parameters are assumed. This is absolutely no problem for very conventional architecture and materials. However, if a building involves a different architecture (large windows for passive heating combined with automatic darkening to reduce radiative losses during nighttime), a different usage pattern (long periods of setbacks because of only periodical use, strong temperature gradients within the building due to special usage in some parts) or different materials (such as transparent thermal insulation), a more detailed analysis is required. Thus the modeling of heat transfer in buildings has gained much attention during the recent two decades because on the one side regulations become stronger and stronger and on the other side the architecture and materials become increasingly varied and unconventional. And the introduction of the Gebäudepass will increase the demand for (and probably also on) the simulation of buildings.

2.4 If Inspiration Refuses to Help

Sometimes a problem seems to be too complex to be squeezed into a model. Or the modeler finds that she has not a very good intuitive understanding of the problem. Thus the approach on modeling as art fails – or the modeler feels not very confident with it. In this case she should resort to the simple fundamentals: the conservation laws. Good choices always are mass (or charge), energy and momentum.⁸

Independent of the property ε under study, a conservation law always has the same form: a change in the property ε inside a volume V can result from the convergence of a flux $\vec{C}(\varepsilon) = \varepsilon \vec{u}$ into or out of the volume or sources and sinks $S(\varepsilon)$ inside the volume. It can be written as:

$$\frac{\partial \varepsilon}{\partial t} + \nabla \vec{C}(\varepsilon) = S(\varepsilon) . \quad (2.29)$$

With the relation between partial and total differential obtained with the chain rule

$$\frac{d\varepsilon}{dt} = \frac{\partial \varepsilon}{\partial t} + \frac{dx}{dt} \frac{\partial \varepsilon}{\partial x} + \frac{dy}{dt} \frac{\partial \varepsilon}{\partial y} + \frac{dz}{dt} \frac{\partial \varepsilon}{\partial z} = \frac{\partial \varepsilon}{\partial t} + \vec{u} \nabla \varepsilon \quad (2.30)$$

the left hand side can be rewritten as

$$\frac{\partial \varepsilon}{\partial t} + \nabla(\varepsilon \vec{u}) = \frac{\partial \varepsilon}{\partial t} + \vec{u} \nabla \varepsilon + \varepsilon \nabla \vec{u} = \frac{d\varepsilon}{dt} + \varepsilon \nabla \vec{u} , \quad (2.31)$$

giving the equation of continuity in the form

$$\frac{d\varepsilon}{dt} + \varepsilon \nabla \vec{u} = S(\varepsilon) . \quad (2.32)$$

2.4.1 Mass Conservation

Mass conservation is described by an equation of continuity. Since we are dealing with continuous media, the mass balance is formulated for the mass density ρ instead of mass m .

⁸Note that there is a qualitative difference between these quantities: mass and energy are scalars while momentum is a vector. In the more conventional German literature, conservation laws often are limited to scalar quantities. The conservation of momentum or momentum balance always is termed transport equation. I will adhere to the modern international approach and consider the transport equation also as a conservation law. Even if the reader does not adhere to this approach, he probably agrees with me that the transport equation is rather fundamental in transport modeling.

The equation of continuity for the mass then reads

$$\frac{d\rho}{dt} + \rho \nabla \vec{u} = S(\rho) . \quad (2.33)$$

Mass balances come in different disguise, depending on the situation under study. In the simplest case, we are only concerned with the motion of a fluid without consideration of different components. Then we have one mass balance for the total mass of the fluid. In addition, the sources/sinks term vanishes and the mass balance reduces to

$$\frac{d\rho}{dt} + \rho \nabla \vec{u} = 0 \quad \text{or} \quad \frac{\partial \rho}{\partial t} + \nabla(\rho \vec{u}) = 0 . \quad (2.34)$$

More often, however, the fluid consists of more than one component and the components have different fates, for instance different rates of evaporation or absorption. In this case, a mass balance for each component exists:

$$\frac{d\rho_i}{dt} + \rho_i \nabla \vec{u}_i = S_i(\rho_i) . \quad (2.35)$$

Here the mass balances of all n components are decoupled (no component is a sink or source for another component) and we obtain n independent equations.

Side question 10 Why (or under which assumptions) are evaporation and absorption loss terms? In the latter case, the matter even stays inside the volume element, in the former it is transported as vapor across the simulation volume. Shouldn't it show up as the flux instead of a sink?

The situation is different if chemical reactions couple different components. In this case a sink for component A might be the source for component B with the transfer regulated by component C which is the reaction partner of A : $A + C \rightarrow B$. In this case, again we obtain a mass balance for each of the n components but these mass balances are coupled by the sources/sinks term:

$$\frac{d\rho_i}{dt} + \rho_i \nabla \vec{u}_i = S_i(\rho_1, \rho_2, \dots, \rho_n) . \quad (2.36)$$

Thus we have to solve a coupled system of partial differential equations.

As mentioned above, such a system of equations often can be simplified if one reactant is overabundant. In that case, its concentration is assumed to be constant and the mass balance of the second reactant can be described by some kind of loss factor or decay constant. This approach will be used in the stationary compartment model in sect. 3.1 and in its time-dependent extension in sect. 3.2.

Note that (2.36) also covers the simpler situation of the chemical tank: in that case the terms $\rho_i \nabla \vec{u}_i$ are prescribed flows j_i and the system of coupled PDEs reduces to a system of coupled ODEs.

Charges also obey an equation of continuity. If only one charge is considered, the standard equation of continuity is used with the charge density ρ_c instead of mass density ρ . Such a charge balance is sufficient in one-fluid magnetohydrodynamics. In two-fluid magnetohydrodynamics two separate charge balances are obtained without coupling:

$$\frac{\partial \rho_{c,i}}{\partial t} + \nabla(\rho_{c,i} \vec{u}) = 0, \quad i = \text{i, e} . \quad (2.37)$$

There is neither ionization out of a neutral component nor recombination, thus the source term vanishes. If the components are coupled by such a process, this coupling is provided by the source term. An additional mass balance for the neutral component is required, too.

2.4.2 Energy Conservation

We have encountered energy conservation already in this chapter, although not in the conventional way as conservation of mechanical energy but in connection with the conservation of internal energy, that is heat. Formally, the energy balance is written in the same way as the mass balance by substituting the energy density ε for the mass density ϱ , see also sect. C.1. The crucial point is the correct identification of all kinds of energy involved in the system. The main forms of energy are mechanical, electromagnetic and inner energy (heat). Energy conversion occurs into the direction of inner energy: in a flow, turbulence and friction convert energy from the directed flow to heat. The relevant equations for the different forms of energy are given in Tab. C.2.

Since we are often dealing with fluids, you should keep in mind that Bernoulli's law also is a consequence of energy conservation:

$$p + \frac{1}{2}\varrho u^2 + \varrho gh = \text{const} . \quad (2.38)$$

Note that Bernoulli's law corresponds to the conservation of mechanical energy – it does not consider the conversion of energy into heat and thus it is reversible.

Energy conservation becomes more tricky if heat is concerned. Here we do not only have to consider the heat fluxes and inner energies but also friction as source of additional heat and the heat released or required for phase transitions. We will come back to this in detail in sect. 4.6.2. Some energy transport processes have already been introduced in sect. 2.3.4. A very detailed discussion of heat, heat transfer and heat exchange is given in [157].

2.4.3 Conservation of Momentum (Equation of Motion)

The conservation of momentum is expressed in Newton's second law and thus in the equation of motion. This equation is fundamental to all transport processes. However, the terms used in this equation strongly depend on the situation under study and thus no general form for the transport equation can be given. One example, the momentum balance for the atmosphere and the oceans, is briefly described (and discussed in connection with a scale analysis) in sect. C.5; it is introduced in more detail in chapter 7.

Conservation of momentum gives the equation of motion. This should not be confused with transport of momentum, a typical phenomenon in boundary layers: momentum is transported from the atmosphere to the ocean's surface creating wind-driven waves. Momentum also is transported from a coast-parallel current to the seabed leading to erosion or from one fluid layer to another as described in sect. 7.2.

2.5 Selling and Borrowing

Once a model has been developed and tested, the modeler will be keen to apply it to the particular question that gave rise to model development. However, a look beyond one's own nose might be worthwhile: a model is a simplification and thus an abstraction. Abstraction is important to develop an understanding not of details but underlying processes. Physics itself is an example for abstraction. And the strength of abstraction (as of physics) lies in the existence of basic concepts that can be applied in different situations/circumstances. Such as Newton's realization that Earth's orbit around the Sun is governed by the same basic process as the fall of an apple. As a consequence, models often can be applied to different systems. The best know example probably is Bohr's model of the atom: it is just recycling of Newton's model of the solar system (and thus even his apple) on a slightly different scale.

With some awareness of physical processes working in other fields, a modeler might be able to apply his model to an entirely different problem. For instance, homogeneous heat conduction is essentially the same as isotropic diffusion – asides from the different symbols in the governing equations. Thus a modeler might be able to 'sell' his model. We will encounter another example for 'selling': phase transitions occur if a substance is heated or cooled down.

Basically, phase transitions are due to a change in mobility of the molecules. On an autobahn, such phase transitions occur if the mobile phase suddenly converts to a solid phase in a traffic jam. We will come back to this example in sect. 4.6.3.

But a modeler might also be able to ‘borrow’: either an existing and already validated model that can be applied to his problem without or after only slight adaption. Or he might be able to borrow observations to test his model. For instance, since it can be performed with solids and simple instruments, it might be easier to use temperature distributions in a metal block to validate the diffusion model than to use a water volume and allow the diffusion process to work.⁹

Literature

This text is on modeling in physics. Since it occasionally traverses to geophysics and natural systems, models become complex. Thus some models extend beyond a simple system of partial differential equations and require different approaches. A very readable (and not necessarily academic) text is *Modeling Reality – How Computers mirror Life* by Bialynicki-Birula and Bialynicki-Birula [15]: its just fun to read and points out possibilities.

A more conservative text is *Mathematical Modeling – Case Studies and Projects* by Caldwell and Ng [20]. As the subtitle states, the book is organized around case studies. For each case study, model development as well as solution is described. Most models are rather simple, nonetheless, it is a nice text for training the model developer skills.

And since modeling of natural processes requires a good look at the processes themselves, some texts of earlier scientists such as Humboldt [65], Minnaert [113] or Tyndall [168] might help to step back from the equations to descriptions – the important part in the first two steps of model development: **The physics is in the description and understanding – the equation is important for the abstraction and transfer to other applications but it is not the physics!**

Questions

Frage 1 Sketch the relevant steps in model development.

Frage 2 Recapitulate standard methods for the simplification of a model.

Frage 3 What to do in case a model gives an unexpected result?

Frage 4 Discuss differences and similarities for models based on first principles and phenomenological models.

Frage 5 Can a model of a natural system ever be complete or is there always some effect/influence to add? If so, is this really necessary?

Frage 6 Explain the concept of dimensional variables and dimensional analysis. Give examples for its application (ask Google or a physics textbook).

Frage 7 Explain the stirred tank concept. Give examples and limits.

Frage 8 Discuss implications of Lorentz’ butterfly and Turing’s avalanche for modeling. Give examples in which these statements pose a problem and in which they do not.

Frage 9 Review test methods for models.

⁹Sorry, this is an oversimplified example: in a fluid asides from the diffusion there is also turbulent motion. Thus strictly heat conduction and diffusion work on a different scale. However, the transport by turbulent motion in a fluid often can be described as eddy diffusion – thus again a diffusive process albeit at a different scale.

Problems

Aufgabe 1 Shortly after the explosion of the first atomic bomb in New Mexico in 1945, Nobel laureate Enrico Fermi went outside the protective dugout with some paper strips. As the explosions blast wave arrived, he released the strips and allowed them to be carried away until they fell to the ground. He measured the distance to where the strips came to rest, made some quick calculations and announced a yield of the bomb remarkably close to the later established value of 10 000 t of TNT. Was any modeling involved? If so, what were the principles used in the model? Was modeling necessary? Or was Fermi's result just lucky coincidence?

Aufgabe 2 Return to section 2.3.1 and calculate the maximum allowed concentration of copper in the effluent under the assumption that its flow stays the same. Also calculate the maximum allowed discharge under the assumption that the concentration of the copper does not change.

Aufgabe 3 Develop a simple mathematical model for population growth according to Malthus' law: a population $p(t)$ growth with a rate a as long as it is not too large. If a population becomes sufficiently large, its evolution is described by the logistic law, which adds a "loss term" proportional to p^2 and a decay constant b . Formulate the mathematical law, classify the equation and solve it.

Aufgabe 4 Develop a simple model for the following situation (from [139]): At 7 a.m. in the morning I make my partner a cup of tea using boiling water. After adding some milk it is about 90°C . When we leave for the station at 7:30 a.m. the tea is still drinkable at about 45°C . When I get back home at 8 a.m. the neglected tea has cooled to about 30°C . Determine the temperature in the house.

Aufgabe 5 Develop a simple model for the following situation (also from [139]): a dead body is found outside on a winter's morning at 7 a.m.; its temperature is measured to be 20° . Measured an hour later it has dropped to 15° . The air temperature fluctuation was $T(t) = 3 - 5 \cos(\omega(t - 2))$ with t measured in hours after midnight ($t=0$) and $\omega = \pi/12$. Determine the time of death (assuming a body temperature of 37°C at that time).

Aufgabe 6 Develop a simple model for the following situation: a continuous flow of a fluid has to be heated from a temperature T_1 to a temperature T_2 while the flow is inside a limited length of a shell-and-tube heat exchanger. In the latter, the cold fluid pipe is surrounded by a pipe containing the hot fluid; both fluids are streaming into opposite directions.

Constant Flow with Reactions: Stacked Compartment Models

We have encountered compartment models in the examples in the last chapter. Basically, a compartment model is the equation of continuity inside a limited volume: the change in a quantity inside the volume is defined by in- and outflow as well as sources and sinks. Compartment models often use the stirred tank concept to avoid spatial gradients. As a consequence, the resulting equations are either algebraic or simple ODEs; in most cases solutions can be obtained analytically. Alternatively, the stirred tank concept might be applied such that compartments are aligned along one axis (stacked compartments). Thus the model is 1D and the transport equation is a PDE. Here we will also present the centered difference method as one example for a finite difference method (FDM); a solution with a finite element method (FEM) will be given in sect. 6.2.2.

This chapter starts with an example from chemical engineering. A reactor is designed such that a reaction can take place in a safe and well defined way. We will discuss and analyze the model, formulate the PDE and solve it for both steady-state and the time-dependent version. We will discuss this model in detail to introduce the concept of a compartment model and the basic ingredients and assumptions. The chapter continues with examples for compartment models in natural systems. These examples also provide some graphic introduction to the extensions required to solve the full PDE.

Goals: after working through this chapter you should be able:

- to sketch and apply simple numerical schemes to ODEs and 1D-PDEs,
- to explain the centered difference scheme, the FTCS scheme and the Crank–Nicolson scheme,
- to evaluate the accuracy of the scheme, in particular its order and stability.

3.1 Chemical Reactor in Steady-State

As introductory example we will take the mass balance of a reactor in steady state, closely following the same example in [20]. With a reactor in steady-state we are concerned with the change of the concentration c a substance in a volume (the reactor). The substance can flow into the volume at a certain rate, flow out of it at a different rate, and can be generated inside the reactor at another rate.

Here we assume a cylindrical reactor of length L with a single exit and a single entry point, extending from $x = 0$ (entry) to $x = L$ (exit). The reactor is a well stirred tank, thus any radial and lateral gradients vanish. To ensure mixing, turbulence is required. The motion of individual water volumes therefore results from the direct flow as well as turbulent

mixing. To simplify the problem, we do not attempt to simulate a complex reaction but only calculate the mass balance of one of the reactants by formulating its reduction as a decay.

Side question 11 Explicitly state the assumptions about reactants and reaction products inherent in this approach.

3.1.1 The Problem

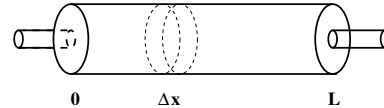
Problem: Give the variation of the concentration c of the chemical substance with length along the cylindrical axis. Instead of using the set of basic equations in table C.1, we first derive the governing equation.

In the general approach assume that until $t = 0$ the reactor is filled with water without the chemical. From $t = 0$ on the chemical is injected into the reactor's inflow at a constant rate c_{in} .

For a start assume steady-state conditions. Thus the above initial condition is not required and the PDE reduces to an ODE.

3.1.2 The Model

To derive the governing equation, we start with a segment of the tube of width Δx (that is one well-stirred compartment) and apply the mass balance to it. For the most general case, any change of concentration inside this volume element is due to (a) the in- and outflow, (b) dispersion due to turbulent mixing and (c) decay. We will come back to dispersion in sect. 4.1.3. For the moment it should suffice that dispersion is related to turbulence. Dispersion is required in our model because it assures that the fluid is well mixed inside the compartment and thus the radial and lateral gradients vanish.



With these processes the mass balance for the length element or compartment becomes

$$V \frac{\Delta c}{\Delta t} = F c(x) - F \left[c(x) + \frac{\partial c(x)}{\partial x} \Delta x \right] - DA_c \frac{\partial c(x)}{\partial x} + DA_c \left[\frac{\partial c(x)}{\partial x} + \frac{\partial}{\partial x} \frac{\partial c(x)}{\partial x} \Delta x \right] - \gamma V c. \quad (3.1)$$

Here V [L^3] is the volume, c [moles/L^3] the concentration, F [L^3/T] the flow rate, D [L^2/T] the dispersion coefficient, γ [T^{-1}] the first-order decay coefficient, and A [L^2] the tank's cross-sectional area. The dispersion term is based on Fick's first law: $\vec{J} = -D\nabla c$ [$\text{moles}/(\text{L}^4\text{T})$]. It specifies that turbulent mixing tends to move mass from regions of high to low concentration.

The partial differential equation can be obtained from (3.1) by letting Δx and Δt approach zero:

$$\frac{\partial c}{\partial t} = D \frac{\partial^2 c}{\partial x^2} - u \frac{\partial c}{\partial x} - \gamma c \quad (3.2)$$

with $u = F/A_c$ [L/T] being the speed of the water flowing through the tank. The mass balance (3.1) thus has led us to a parabolic PDE.¹ The particular equation (3.2) sometimes is referred to as the advection-dispersion equation with first-order reaction. We will encounter most of its terms again in the diffusion-convection equation in sect. 4.3.

In steady-state, the left hand side of (3.2) vanishes and we are left with a second order ODE:

$$D \frac{\partial^2 c}{\partial x^2} - u \frac{\partial c}{\partial x} - \gamma c = 0 \quad \text{for } 0 < x < L. \quad (3.3)$$

¹According to the characteristics of their solutions, PDEs are classified as hyperbolic, elliptic or parabolic, see also sect. B.2. The purpose of this text is modeling not PDEs. Thus if the classification of (3.2) as a parabolic PDE does not mean anything to you, either consult sect. B.2 or ignore it as an irrelevant bit of information – you will still be able to understand the text.

Boundary conditions are

$$F c_{\text{in}} = F c(0) - D A_c \frac{dc(0)}{dx} \Rightarrow c_{\text{in}} = c(0) - \frac{D}{u} \frac{dc(0)}{dx} \quad \text{and} \quad c'(L, t) = 0. \quad (3.4)$$

The first condition considers that the flow at the inlet is determined by the external flow and the flow due to dispersion. The second condition indicates that the chemical leaves the reactor as a function of flow through the outlet pipe only and that dispersion does not affect the exit rate.

3.1.3 Solving the Problem

A differential equation can be solved by different means. While an analytical solution is not always possible, numerical solutions, such as finite difference or finite element methods, always work. Because this example is simple enough to be understood and solved easily, we will use it to briefly recapitulate the first two methods; we will encounter other methods throughout the text in sect. 6.2.2 and chap. 8. The finite difference method FDM will be discussed in detail in the more complex examples in later sections.

Analytical Solution

The focus of this text is on numerical models. However, we will also consider analytical solutions because they can be used to test the numerical model.

An exponential ansatz $c(x) = e^{\lambda x}$ is a general tool to solve a 2nd order ODE. With it we obtain from (3.3) the characteristic equation

$$D\lambda^2 - u\lambda - \gamma = 0. \quad (3.5)$$

The solution is a real one:

$$c(x) = B_1 e^{\lambda_1 x} + B_2 e^{\lambda_2 x} \quad \text{with} \quad \lambda_{1,2} = \frac{u}{2D} \pm \sqrt{\frac{u^2}{4D^2} + \frac{\gamma}{D}}. \quad (3.6)$$

The integration constants B_1 and B_2 can be determined from the boundary conditions (hopefully without too many typos):

$$\begin{aligned} B_1 &= \frac{2D\lambda_2 e^{\lambda_2 L}}{N} u c_{\text{in}}, \\ B_2 &= \frac{2D\lambda_1 e^{\lambda_1 L}}{N} u c_{\text{in}}, \\ N &= e^{\lambda_2 L} \left(u^2 - u\sqrt{u^2 + 4D\gamma} + 2D\gamma \right) - e^{\lambda_1 L} \left(u^2 + u\sqrt{u^2 + 4D\gamma} + 2D\gamma \right). \end{aligned} \quad (3.7)$$

As expected, the concentration decreases along the length of the tank due to the decay reaction. The gradient of the decrease is modified by turbulent mixing: in case of weak mixing ($D \rightarrow 0$), the decay term dominates and the decrease is almost exponential. With increasing turbulent mixing, this gradient become flatter.

Side question 12 Explain why!

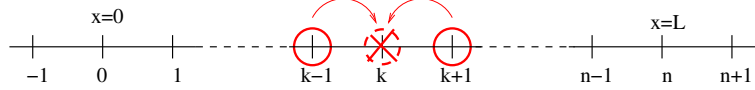
The flux can be derived using Fick's law:

$$J = -D \frac{\partial c}{\partial x} = -D (B_1 \lambda_1 e^{\lambda_1 x} + B_2 \lambda_2 e^{\lambda_2 x}). \quad (3.8)$$

Numerical Solution: Finite Differences

A finite difference scheme divides the simulation volume into n equidistant steps of size Δx . Some possible numerical solvers for finite differences are sketched in sect. D.3. The simple forward or backward discretizations are accurate to first order only, the simplest second order scheme is an implicit centered difference. Here we will adopt this latter scheme to discretize the ODE, see also Fig. 3.1. The basic ideas in discretization are sketched in sect. D.1. The

Figure 3.1: Centered finite difference scheme



derivatives are obtained by Taylor expansion, which is also sketched in sect. D.1. With this additional information we obtain for from the stationary differential equation the following difference equation:

$$D \frac{c_{k+1} + 2c_k + c_{k-1}}{(\Delta x)^2} - u \frac{c_{k+1} - c_{k-1}}{2\Delta x} - \gamma c_k = 0. \quad (3.9)$$

Ordering by nodes, the equation can be rewritten as

$$-\left(\frac{1}{2} + \frac{D}{u\Delta x}\right)c_{k-1} + \left(\frac{\gamma\Delta x}{u} + \frac{2D}{u\Delta x}\right)c_k - \left(-\frac{1}{2} + \frac{D}{u\Delta x}\right)c_{k+1} = 0 \quad (3.10)$$

or in a more compact form

$$Ac_{k-1} + Bc_k + Cc_{k+1} = 0 \quad (3.11)$$

with the abbreviations

$$A = -\left(\frac{1}{2} + \frac{D}{u\Delta x}\right), \quad B = \frac{\gamma\Delta x}{u} + \frac{2D}{u\Delta x} \quad \text{and} \quad C = -\left(-\frac{1}{2} + \frac{D}{u\Delta x}\right). \quad (3.12)$$

All nodes of the system from c_0 at $x = 0$ to c_n at $x = L$ must be center of such a step. Thus the method introduces two additional nodes outside the system: c_{-1} at the inflow and c_{n+1} at the outflow, as also indicated in Fig. 3.1. In the resulting difference equation at the inflow

$$-\left(\frac{1}{2} + \frac{D}{u\Delta x}\right)c_{-1} + \left(\frac{\gamma\Delta x}{u} + \frac{2D}{u\Delta x}\right)c_0 - \left(-\frac{1}{2} + \frac{D}{u\Delta x}\right)c_{+1} = 0 \quad (3.13)$$

the outside node c_{-1} can be removed using the first boundary condition (3.4) and replacing the derivative by a finite difference:

$$Fc_{\text{in}} = Fc_0 - DA_c \frac{c_1 - c_{-1}}{2\Delta x} \quad \Rightarrow \quad c_{-1} = c_1 + \frac{2u\Delta x}{D}c_{\text{in}} - \frac{2u\Delta x}{D}c_0. \quad (3.14)$$

Inserting into (3.13) yields

$$\left(\frac{\gamma\Delta x}{u} + \frac{2D}{u\Delta x} + \frac{u\Delta x}{D} + 2\right)c_0 - \left(\frac{2D}{u\Delta x}\right)c_1 = \left(\frac{u\Delta x}{D} + 2\right)c_{\text{in}} \quad (3.15)$$

or in a more compact form

$$B_{\text{in}}c_0 + C_{\text{in}}c_1 = R_{\text{in}}c_{\text{in}} \quad (3.16)$$

with the abbreviations

$$B_{\text{in}} = \frac{\gamma\Delta x}{u} + \frac{2D}{u\Delta x} + \frac{u\Delta x}{D} + 2, \quad C_{\text{in}} = -\frac{2D}{u\Delta x} \quad \text{and} \quad R_{\text{in}} = \frac{u\Delta x}{D} + 2. \quad (3.17)$$

A similar procedure for the difference equation at the outlet and the boundary condition there yields $c_{n-1} = c_{n+1}$. Thus the difference equation at the outlet becomes

$$-\left(\frac{2D}{u\Delta x}\right)c_{n-1} + \left(\frac{\gamma\Delta x}{u} + \frac{2D}{u\Delta x}\right)c_n = 0 \quad (3.18)$$

or in a more compact form

$$A_{\text{out}}c_{n-1} + B_{\text{out}}c_n = 0 \quad (3.19)$$

with the abbreviations

$$A_{\text{out}} = -\frac{2D}{u\Delta x} \quad \text{und} \quad B_{\text{out}} = \frac{\gamma\Delta x}{u} + \frac{2D}{u\Delta x}. \quad (3.20)$$

Equations (3.10), (3.15) and (3.18) form a system of $n + 1$ equations with $n + 1$ unknowns

$$\begin{array}{rcccccc}
 B_{\text{in}}c_0 & C_{\text{in}}c_1 & & & & = & R_{\text{in}}c_{\text{in}} \\
 Ac_0 & Bc_1 & Cc_2 & & & = & 0 \\
 & Ac_1 & Bc_2 & Cc_3 & & = & 0 \\
 & & Ac_{n-2} & Bc_{n-1} & Cc_n & = & 0 \\
 & & & A_{\text{out}}c_{n-1} & B_{\text{out}}c_n & = & 0.
 \end{array} \tag{3.21}$$

A more compact formulation results in tridiagonal matrix:

$$\begin{bmatrix}
 B_{\text{in}} & C_{\text{in}} & & & & \\
 A & B & C & & & \\
 & A & B & C & & \\
 & & \ddots & \ddots & \ddots & \\
 & & & A_{\text{out}} & B_{\text{out}} &
 \end{bmatrix}
 \begin{bmatrix}
 c_0 \\
 c_1 \\
 c_2 \\
 \vdots \\
 c_n
 \end{bmatrix}
 =
 \begin{bmatrix}
 R_{\text{in}}c_{\text{in}} \\
 0 \\
 0 \\
 \vdots \\
 0
 \end{bmatrix}. \tag{3.22}$$

Thus the solution of the ODE is reduced to the inversion of a sparse matrix, that is a matrix that contains mainly zeros.

Before we apply the scheme, we have to decide on the step-size δx . On the one hand, the step size should be small enough, to assure numerical accuracy and the stability of the scheme, on the other hand it should be as large as possible to allow for a fast model. Mathematically, the centered difference scheme is of second-order accuracy² in space; stability³ of the scheme is obtained for

$$\Delta x \leq \frac{2D}{u}. \tag{3.23}$$

Is there also some physics hidden in the stability criterion? The mathematical expression basically is the ratio between the dispersion coefficient and the flow speed. The dispersion coefficient is the product of a characteristic length scale L (in diffusion, this would be the mean free path λ) and the flow speed u (see also sect. 4.1.3):

$$D = \frac{1}{2}Lu \quad \text{in 1D} \quad \text{or} \quad D = \frac{1}{3}Lu \quad \text{in 3D}.$$

Thus from the viewpoint of physics the stability criterium suggest the step size to be less equal to the characteristic scale length of the physical process. As a consequence, we should code the scheme in such a way, that the spatial step size Δx is not fixed but determined from the parameters flow speed u and dispersion coefficient D such that the stability criterion is met. A fixed Δx would require an extremely small step size to account also for some of the rare occasions in which the scale length is unusually small. This extremely small fixed Δx would lead to very long execution times of the code for the (hopefully more frequent) situations with average or even large scale length – just a waste of resources.

3.1.4 Closure

Here we can divide the test into two clearly distinguishable parts: implementation of the solution and development of the model. Since we have developed two different solutions for our model, their comparison will point to any errors made in the analytical solution or in coding the numerical solutions. Exercise 7 is concerned with this problem.

Here we will presume a successful comparison of the different solutions and now use one of them to check whether the results of our model are reasonable.⁴

Figure 3.2 shows concentration versus distance along the vertical axis of the cylindrical reactor in steady-state for a chemical that decays with first-order decay kinetics. It is a

²The order of accuracy basically means that if you cut the step size in half, the scheme will be more accurate by a factor of 2 to the power of the accuracy's order. Or in other words, the same increase in accuracy can be obtained by dividing the spatial step in a first-order scheme by a factor of 4 or in a second order scheme by a factor of 2. Accuracy is determined by Taylor expansion of the numerical scheme, see also sect. D.1.2.

³Stability means that the truncation error can be kept in charge by the scheme. The stability criterion normally relates the step sizes in the discretization scheme to each other and the coefficients in the equation;

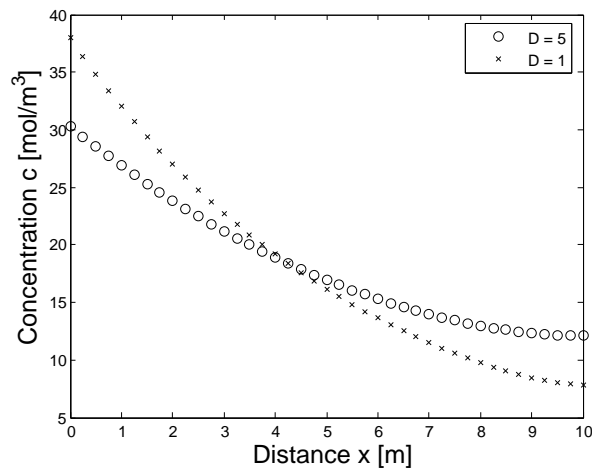


Figure 3.2: Concentration versus distance along vertical axis of a cylindrical reactor in steady-state for different values of the dispersion coefficient

numerical solution (centered finite differences as described above) for $u = 1$ m/h, $\Delta x = 0.25$ m, $L = 10$ m, $c_{\text{in}} = 100$ moles/m³, and $\gamma = 0.2$ h⁻¹. The dispersion coefficient is $D = 1$ m²/h for the crosses and $D = 5$ m²/h for the circles. Results for a fixed dispersion coefficient are reasonable: the concentration decreases with increasing distance from the inflow due to the decay. This decrease is roughly exponential because the constant flow speed u translates distance into time. It is not exactly the decay function because dispersion mixes neighboring volume elements and thus tends to smear out the gradient along the cylinder axis. This can be seen best in the comparison between the runs for different dispersion coefficients because dispersion reduces the spatial gradients. In case of a strong gradient, a volume with a high concentration is transferred from cell k to cell $k + 1$ while a volume with only low concentration is transported into the opposite direction. Thus the gradient is reduced efficiently, leading to a flatter profile along the spatial coordinate as is obvious in Fig. 3.2.

Some in-between calculation 3 Solve the numerical scheme for different Δx . What happens, if the stability criterion is violated? Is the resulting error obvious or would it probably go unnoticed during testing?

Side question 13 Imagine you are a designer for chemical plants and have to defend the assumptions/methods of your model to the production company. State all the relevant assumptions, try to anticipate the critical questions and defend against them – or develop a more elaborate model to meet the criticism.

Side question 14 What happens if dispersion goes to zero. Discuss consequences for the PDE and the numerical scheme. Can the latter still be applied, can it be modified or is an entirely different scheme required? Substantiate your answer.

3.2 Time-Dependent Reactor

Let us now turn back to the problem and consider the time-dependent solution. In consequence, we have to solve the PDE rather than an ODE. We briefly repeat the model assumptions: (1) the chemical being modeled is subject to first-order decay. (2) The tank is well mixed vertically and laterally. (3) Dispersion in the reactor does not affect the reaction rate. (4) For $t < 0$ the reactor is filled with water that contains no chemical. (5) For $t \geq 0$ the chemical is added to the reactors inflow at a constant rate c_{in} .

see also sect. D.1.3

⁴This approach is ok for a lecture. In real model development one should not sketch a model, find more than one solution and decide that the technical aspects of the solutions are ok only to find afterwards that the model does not describe the situation under study.

The resulting PDE, the boundary conditions (5) and the initial condition (4) than can be summarized as the initial boundary value problem

$$\begin{aligned} \frac{\partial c}{\partial t} &= D \frac{\partial^2 c}{\partial x^2} - u \frac{\partial c}{\partial x} - \gamma c & 0 < x < L \\ c(0, t) &= c_{\text{in}} + \frac{D}{u} c'(0, t) & t > 0 \\ c'(L, t) &= 0 & t > 0 \\ c(x, 0) &= 0 & 0 < x < L \end{aligned} \quad (3.24)$$

As in the steady-state ODE, the parabolic⁵ PDE can be solved by a finite difference method. In this case, however, spatial as well as temporal derivatives must be discretized.

3.2.1 Numerical Method 1: Implicit Method

Numerical integration must be performed in two dimensions, space and time. In the implicit method, the spatial derivatives are approximated at an advanced time step $k + 1$; the forward in time and centered in space or FTCS scheme, see also sect. D.4.4. The concentration (or more generally the quantity under study) thus has two indices c_k^l : a lower one, k , indicating the position in space and an upper one, l , indicating that in time.

The time derivative is approximated by a forward finite difference with an error of $\mathcal{O}(\Delta t)$:

$$\frac{\partial c}{\partial t} = \frac{c_k^{l+1} - c_k^l}{\Delta t} . \quad (3.25)$$

The spatial derivatives again are approximated by centered finite differences. This method is accurate to second order $\mathcal{O}((\Delta x)^2)$. The discretized PDE can be written as

$$\frac{c_k^{l+1} - c_k^l}{\Delta t} = D \frac{c_{k+1}^{l+1} - 2c_k^{l+1} + c_{k-1}^{l+1}}{(\Delta x)^2} - u \frac{c_{k+1}^{l+1} - c_{k-1}^{l+1}}{2\Delta x} - \gamma c_k^{l+1} . \quad (3.26)$$

As in the steady-state case, this difference equation contains several unknowns and cannot be solved by simple algebraic rearrangement. Again, the entire set of linear algebraic equations must be solved simultaneously under consideration of the boundary conditions.

Rearrangement of (3.26) according to nodes yields

$$\left(\frac{D}{(\Delta x)^2} + \frac{u}{2\Delta x} \right) c_{k-1}^{l+1} - \left(\frac{1}{\Delta t} + \frac{2D}{(\Delta x)^2 + \gamma} \right) c_k^{l+1} + \left(\frac{D}{(\Delta x)^2} - \frac{u}{2\Delta x} \right) c_{k+1}^{l+1} = -\frac{1}{\Delta t} c_k^l$$

or in a short form

$$A c_{k-1}^{l+1} + B c_k^{l+1} + C c_{k+1}^{l+1} = E c_k^l \quad (3.27)$$

with the abbreviations

$$A = \frac{D}{(\Delta x)^2} + \frac{u}{2\Delta x}, \quad B = -\left(\frac{1}{\Delta t} + \frac{2D}{(\Delta x)^2 + \gamma} \right), \quad C = \frac{D}{(\Delta x)^2} - \frac{u}{2\Delta x} \quad \text{and} \quad E = -\frac{1}{\Delta t} .$$

The structure of this equation is similar to the equation (3.11) for steady-state except for the term on the right hand side containing the concentration c at the earlier time step – which is irrelevant in a steady-state solution – and the details of the coefficients A , B and C .

Since this equation is valid for all nodes of the tank, we get an additional outer node at each end: c_{-1}^l and c_{n+1}^l . As demonstrated for the centered finite differences in sect. 3.1, these additional nodes can be eliminated by considering the boundary conditions. Thus the difference equations for the first and last node read

$$-\left(\frac{1}{\Delta t} + \frac{2D}{(\Delta x)^2} + \gamma + \frac{2u}{\Delta x} + \frac{u^2}{D} \right) c_0^{l+1} + \frac{2D}{(\Delta x)^2} c_1^{l+1} = -\left(\frac{2u}{\Delta x} + \frac{u^2}{D} \right) c_{\text{in}} - \frac{1}{\Delta t} c_0^l \quad (3.28)$$

⁵The classification of PDEs in parabolic, hyperbolic etc. follows their characteristics and is discussed in more detail in sec., B.2.2.

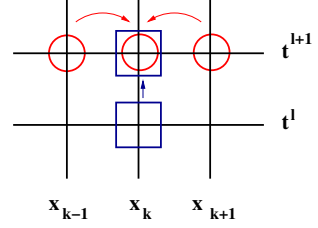


Figure 3.3: FTCS scheme

and

$$\frac{2D}{(\Delta x)^2} c_n^{l+1} - \left(\frac{1}{\Delta t} + \frac{2D}{(\Delta x)^2} + \gamma \right) c_n^{l+1} = -\frac{1}{\Delta t} c_n^l. \quad (3.29)$$

The equations in short form can be written as

$$B_{\text{in}} c_0^{l+1} + C_{\text{in}} c_1^{l+1} = R_{\text{in}} c_{\text{in}} + E_{\text{in}} c_0^l \quad \text{and} \quad A_{\text{out}} \frac{2D}{(\Delta x)^2} + B_{\text{out}} c_n^{l+1} = E_{\text{out}} c_n^l \quad (3.30)$$

with the abbreviations

$$B_{\text{in}} = -\left(\frac{1}{\Delta t} + \frac{2D}{(\Delta x)^2} + \gamma + \frac{2u}{\Delta x} + \frac{u^2}{D} \right), \quad C_{\text{in}} = \frac{2D}{(\Delta x)^2}, \quad R_{\text{in}} = -\left(\frac{2u}{\Delta x} + \frac{u^2}{D} \right) \quad (3.31)$$

and

$$E_{\text{in}} = E, \quad A_{\text{out}} = \frac{2D}{(\Delta x)^2}, \quad B_{\text{out}} = -\left(\frac{1}{\Delta t} + \frac{2D}{(\Delta x)^2} + \gamma \right) \quad \text{and} \quad E_{\text{out}} = E. \quad (3.32)$$

As in the corresponding steady-state situation we get a system of $n+1$ equations for the $n+1$ unknowns:

$$\begin{bmatrix} B_{\text{in}} & C_{\text{in}} & 0 & 0 & \dots & 0 & 0 \\ A & B & C & 0 & \dots & 0 & 0 \\ 0 & A & B & C & \dots & 0 & 0 \\ \vdots & \vdots & \vdots & \vdots & \ddots & \vdots & \vdots \\ 0 & 0 & 0 & 0 & \dots & A_{\text{out}} & B_{\text{out}} \end{bmatrix} \begin{bmatrix} c_0 \\ c_1 \\ c_2 \\ \vdots \\ c_n \end{bmatrix} = R_{\text{in}} \begin{bmatrix} c_{\text{in}} \\ 0 \\ 0 \\ \vdots \\ 0 \end{bmatrix} + E \begin{bmatrix} c_0^- \\ c_1^- \\ c_2^- \\ \vdots \\ c_n^- \end{bmatrix}. \quad (3.33)$$

The main difference to the steady-state system of equations (3.22) is the second term on the right hand side that contains the concentrations c^- at the earlier time step.

The matrix (3.33) is tridiagonal and thus again can be solved by the Thomas algorithm under consideration of the initial condition $c(x, 0) = 0$ or expressed in terms of nodes $c_k^l = 0$ for all $k = 0, 1, \dots, n$ and $l = 0$.

3.2.2 Numerical Method 2: Crank–Nicolson

An alternative numerical scheme is the Crank–Nicolson method. It has the advantage of being of second order in both space and time $\mathcal{O}((\Delta t)^2, (\Delta x)^2)$; see also sect. D.4.2. To get this accuracy, spatial approximations are derived at the midpoint of the time interval, $t_k^{l+1/2}$. The time derivative than is approximated as in the implicit method by

$$\frac{\partial c}{\partial t} \approx \frac{c_k^{l+1} - c_k^l}{\Delta t}. \quad (3.34)$$

The spatial derivatives at the midpoint are determined as the average of the difference approximations at the beginning and at the end of the time step as follows:

$$\frac{\partial c}{\partial x} \approx \frac{1}{2} \left(\frac{c_{k+1}^l - c_{k-1}^l}{2\Delta x} + \frac{c_{k+1}^{l+1} - c_{k-1}^{l+1}}{2\Delta x} \right) \quad (3.35)$$

and

$$\frac{\partial^2 c}{\partial t^2} \approx \frac{1}{2} \left(\frac{c_{k+1}^l - 2c_k^l + c_{k-1}^l}{(\Delta x)^2} + \frac{c_{k+1}^{l+1} - 2c_k^{l+1} + c_{k-1}^{l+1}}{(\Delta x)^2} \right). \quad (3.36)$$

Substituting into (3.24) yields

$$\frac{c_k^{l+1} - c_k^l}{\Delta t} = \frac{D}{2} \left(\frac{c_{k+1}^l - 2c_k^l + c_{k-1}^l}{(\Delta x)^2} + \frac{c_{k+1}^{l+1} - 2c_k^{l+1} + c_{k-1}^{l+1}}{(\Delta x)^2} \right)$$

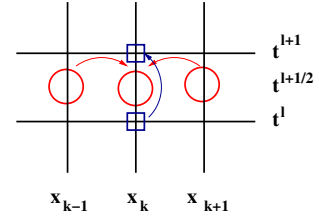


Figure 3.4: Crank–Nicolson scheme

$$-\frac{u}{2} \left(\frac{c_{k+1}^l - c_{k-1}^l}{2\Delta x} + \frac{c_{k+1}^{l+1} - c_{k-1}^{l+1}}{2\Delta x} \right) - \gamma \frac{c_k^l + c_k^{l+1}}{2} \quad (3.37)$$

or ordered by node

$$\begin{aligned} & \left(\frac{D}{2(\Delta x)^2} + \frac{u}{4\Delta x} \right) c_{k-1}^{l+1} - \left(\frac{1}{\Delta t} + \frac{D}{(\Delta x)^2} + \frac{\gamma}{2} \right) c_k^{l+1} + \left(\frac{D}{2(\Delta x)^2} - \frac{u}{4\Delta x} \right) c_{k+1}^{l+1} \\ & = - \left(\frac{D}{2(\Delta x)^2} + \frac{u}{4\Delta x} \right) c_{k-1}^l - \left(\frac{1}{\Delta t} - \frac{D}{(\Delta x)^2} - \frac{\gamma}{2} \right) c_k^l - \left(\frac{D}{2(\Delta x)^2} - \frac{u}{4\Delta x} \right) c_{k+1}^l. \end{aligned} \quad (3.38)$$

In short form, this equations reads

$$A_{\text{adv}} c_{k-1}^{l+1} + B_{\text{adv}} c_k^{l+1} + C_{\text{adv}} c_{k+1}^{l+1} = A c_{k-1}^l + B c_k^l + C c_{k+1}^l \quad (3.39)$$

with the abbreviations

$$A_{\text{adv}} = \frac{D}{2(\Delta x)^2} + \frac{u}{4\Delta x}, \quad B_{\text{adv}} = - \left(\frac{1}{\Delta t} + \frac{D}{(\Delta x)^2} + \frac{\gamma}{2} \right), \quad C_{\text{adv}} = \frac{D}{2(\Delta x)^2} - \frac{u}{4\Delta x}$$

and

$$A = -A_{\text{adv}} \quad B = - \left(\frac{1}{\Delta t} - \frac{D}{(\Delta x)^2} - \frac{\gamma}{2} \right) \quad \text{and} \quad C = - \left(\frac{D}{2(\Delta x)^2} - \frac{u}{4\Delta x} \right).$$

Since the scheme for the spatial coordinates remains unchanged, we get additional outer nodes that can be eliminated using the boundary conditions as described above. The resulting difference equations are for the inlet node

$$\begin{aligned} & - \left(\frac{1}{\Delta t} + \frac{D}{(\Delta x)^2} + \frac{\gamma}{2} + \frac{u}{\Delta x} + \frac{u^2}{2D} \right) c_0^{l+1} + \frac{D}{(\Delta x)^2} c_1^{l+1} \\ & = - \left(\frac{1}{\Delta t} - \frac{D}{(\Delta x)^2} - \frac{\gamma}{2} - \frac{u}{\Delta x} - \frac{u^2}{2D} \right) c_0^l - \frac{D}{(\Delta x)^2} c_1^l - 2 \left(\frac{D}{\Delta x} + \frac{u}{2} \right) \frac{u}{D} c_{\text{in}} \end{aligned} \quad (3.40)$$

and for the outlet node

$$\frac{D}{(\Delta x)^2} c_{n-1}^{l+1} - \left(\frac{1}{\Delta t} + \frac{D}{(\Delta x)^2} + \frac{\gamma}{2} \right) c_n^{l+1} = - \frac{D}{(\Delta x)^2} c_{n-1}^l - \left(\frac{1}{\Delta t} - \frac{D}{(\Delta x)^2} - \frac{\gamma}{2} \right) c_n^l. \quad (3.41)$$

In short form, these equations read

$$B_{\text{adv,in}} c_0^{l+1} + C_{\text{adv,in}} c_1^{l+1} = B_{\text{in}} c_0^l + C_{\text{in}} c_1^l + R_{\text{in}} c_{\text{in}} \quad (3.42)$$

and

$$A_{\text{adv,out}} c_{n-1}^{l+1} + B_{\text{adv,out}} c_n^{l+1} = A_{\text{out}} c_{n-1}^l + B_{\text{out}} c_n^l \quad (3.43)$$

with the abbreviations

$$\begin{aligned} B_{\text{adv,in}} &= - \left(\frac{1}{\Delta t} + \frac{D}{(\Delta x)^2} + \frac{\gamma}{2} + \frac{u}{\Delta x} + \frac{u^2}{2D} \right), \quad C_{\text{adv,in}} = \frac{D}{(\Delta x)^2}, \\ B_{\text{in}} &= - \left(\frac{1}{\Delta t} - \frac{D}{(\Delta x)^2} - \frac{\gamma}{2} - \frac{u}{\Delta x} - \frac{u^2}{2D} \right), \quad C_{\text{in}} = - \frac{D}{(\Delta x)^2}, \\ R_{\text{in}} &= -2 \left(\frac{D}{\Delta x} + \frac{u}{2} \right) \frac{u}{D}, \quad A_{\text{adv,out}} = \frac{D}{(\Delta x)^2}, \quad B_{\text{adv,out}} = - \left(\frac{1}{\Delta t} + \frac{D}{(\Delta x)^2} + \frac{\gamma}{2} \right), \\ A_{\text{out}} &= - \frac{D}{(\Delta x)^2} \quad \text{and} \quad B_{\text{out}} = - \left(\frac{1}{\Delta t} - \frac{D}{(\Delta x)^2} - \frac{\gamma}{2} \right). \end{aligned}$$

Again we get a system of linear equations that can be described by a tridiagonal matrix and thus can be solved efficiently:

$$\begin{aligned}
 & \begin{bmatrix} B_{\text{adv,in}} & C_{\text{adv,in}} & 0 & 0 & \dots & 0 & 0 \\ A_{\text{adv}} & B_{\text{adv}} & C_{\text{adv}} & 0 & \dots & 0 & 0 \\ 0 & A_{\text{adv}} & B_{\text{adv}} & C & \dots & 0 & 0 \\ \vdots & \vdots & \vdots & \vdots & \ddots & \vdots & \vdots \\ 0 & 0 & 0 & 0 & \dots & A_{\text{adv,out}} & B_{\text{adv,out}} \end{bmatrix} \begin{bmatrix} c_0 \\ c_1 \\ c_2 \\ \vdots \\ c_n \end{bmatrix} \\
 &= R_{\text{in}} \begin{bmatrix} c_{\text{in}} \\ 0 \\ 0 \\ \vdots \\ 0 \end{bmatrix} + \begin{bmatrix} B_{\text{in}} & C_{\text{in}} & 0 & 0 & \dots & 0 & 0 \\ A & B & C & 0 & \dots & 0 & 0 \\ 0 & A & B & C & \dots & 0 & 0 \\ \vdots & \vdots & \vdots & \vdots & \ddots & \vdots & \vdots \\ 0 & 0 & 0 & 0 & \dots & A_{\text{out}} & B_{\text{out}} \end{bmatrix} \begin{bmatrix} c_0^- \\ c_1^- \\ c_2^- \\ \vdots \\ c_n^- \end{bmatrix}. \quad (3.44)
 \end{aligned}$$

Stability requires for the step sizes

$$\Delta t \leq \frac{(\Delta x)^2}{2D + \gamma(\Delta x)^2}. \quad (3.45)$$

If we neglect decay, that is $\gamma \rightarrow 0$, the stability condition is exactly the same as for the steady-state reactor in (3.1.3):

$$\Delta x \leq \frac{2D}{u} = \frac{2D}{\Delta x/\Delta t} \quad \leftrightarrow \quad \Delta t \leq \frac{(\Delta x)^2}{2D}. \quad (3.46)$$

Spatial and temporal step sizes thus are not decoupled but coupled by the speed $u = \Delta x/\Delta t$.

And stability in the presence of decay: the reaction term γ tends to make the time step smaller. The denominator in (3.45) contains the sum of (twice) the dispersion coefficient and $\gamma(\Delta x)^2$. Consequently, the latter term also can be interpreted as some kind of transport coefficient with Δx as the relevant length scale and $\gamma\Delta x$ as a velocity, although here the velocity is a measure for the importance of decay during one spatial interval Δx .

Side question 15 Is the stability criterion (3.45) also valid for the FTCS solution?

3.2.3 Closure

As in the steady-state case, we have different mathematical solutions for one model; thus we can easily check for coding errors by comparing the solutions (see also exercise 10). The model also can be tested by letting t approach infinity, which technically means for late times: in this case, the tank should be in steady-state and the solution should be the same as in sect. 3.1.

Figure 3.5 shows concentrations along the x-axis for different times calculated with the implicit scheme. For comparison, the blue crosses give the steady-state solution. The results are reasonable: with increasing time the chemical is transported into the tank: therefore for early times concentrations decay fast with distance. In addition, the concentration at the inlet is rather small since the large spatial gradients are smeared out by dispersion – at the cost of reduced concentrations. The result must be correct for late times because we obtain the same solution as in steady state.

Some in-between calculation 4 Test the model for different step sizes in Δt and Δx , different combinations of both and in particular step sizes violating the stability criterion. Again, are the errors obvious in the latter case?

Further validation of the numerical model could come from a comparison of solutions obtained with the implicit and with the Crank–Nicolson schemes. It should be noted, however, that these tests only check the numerical implementation but not the mathematical model. The latter can be checked by studying the behavior of solutions for different parameters as sketched for the steady-state model.

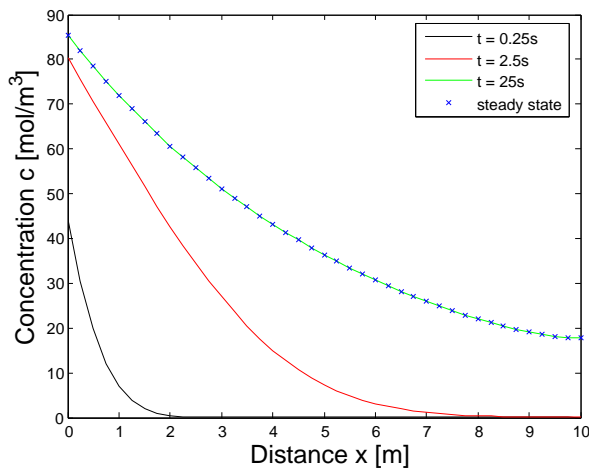


Figure 3.5: Concentration versus distance along the vertical axis of a cylindrical reactor for different times after begin of the injection

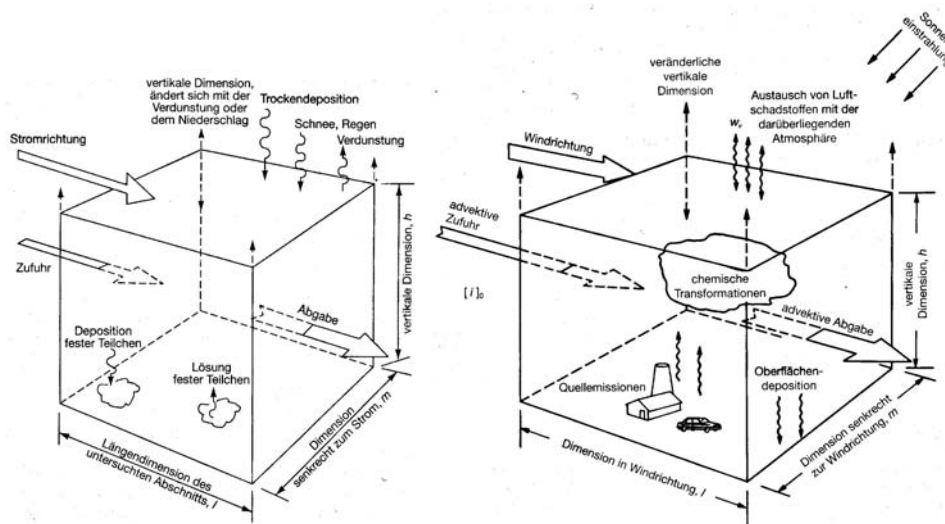


Figure 3.6: 0D compartment models: water (left) and atmosphere (right) [52]

Side question 16 Further checks should be performed varying D , γ and u . Before you do this ask yourself: which results would I expect?

3.3 Compartment Models in Natural Systems

The early models for chemistry in a natural environment (atmosphere or a body of water) also have been compartment models. The simplest model is the 0D compartment model, see the left side in Fig. 3.6, here depicted for a body of water. Again, the main assumption is a well-stirred volume: all components are distributed equally. The 0D compartment model is the direct application of the equation of continuity: any change of a quantity inside the compartment is determined by advection with the river's flow (in- and outflow), precipitation (snow or rain), evaporation and dry deposition. Sources and sinks inside the volume are deposition at the bottom layer and solution of particles from the bottom layer. Whether both processes are considered as sources or sinks depends on the question: are we interested in the total amount of the pollutant in the flow or in the volume.

The 0D compartment model for the atmosphere basically has the same structure, see right side in Fig. 3.6. The main difference is the inclusion of chemical reactions (transformations) inside the volume. Since most of these reactions require energy, also the energy flow into

the volume has to be considered. Atmospheric chemistry is driven by the incoming solar radiation, in particular its hard part, such as UV.

Both examples exhibit one difference compared to classical compartment models such as the tank in a chemistry model: the volume can be variable because the body of water/air might expand or contract, depending on in- and outflows, precipitation or evaporation or on temperature. This variability exists in the vertical only (the horizontal dimensions of the compartment are fixed). For the atmosphere one can get rid of this “breathing” of the volume element due to temperature changes by using a certain pressure as the top of the volume instead of a geometrical height. This is the standard procedure in all modern models of the atmosphere in chemistry, meteorology and climatology: the vertical structure of the atmosphere/ocean is determined by pressure levels rather than by geometrical height.

Side question 17 The use of pressure levels instead of geometrical height gives the atmosphere a structure in which the amount of matter (kg/m^2 is the unit of pressure!) above a certain pressure level serves as relevant physical quantity. Does this make any sense for modeling, meteorology or atmospheric physics? Why?

A compartment model mathematically is simple because in- and outflow are prescribed and the compartment is well stirred. While such an approach is valid in a fish pond or to a certain extent in a small segment of a river, see for instance the example in sect. 2.3.1, it certainly does not allow to describe the entire river or even an ocean self-consistently. This would require the solution of the equation of motion, see also chapter 7. Nonetheless, also a longer stretch of a river can be described by a series of compartments: each compartment is described as above, the coupling between the compartments is due to the in- and outflows: the outflow from compartment j into the direction of compartment $j+1$ also is the inflow into compartment $j+1$ from the direction j . Thus a compartment model also can be understood as some kind of graphical version of a finite difference scheme with mathematically unacceptable large step sizes. Nevertheless, compartment models can be quite useful, in particular if in relatively large spatial segments properties are only weakly variable compared to the variation between adjacent components. A typical natural example are the different layers in the atmosphere: the temperature inversion between troposphere and stratosphere prevents mixing across the tropopause thus both atmospheric layers can be regarded as decoupled, at least as long as transport of matter is concerned. Energy (and also momentum) is transported across the tropopause nonetheless.

For the atmosphere, a division into layers is indicated, see Fig. 3.7, because the atmospheric density decreases with height. Such a model is a 1D model because it covers one spatial coordinate, height. Although the atmosphere might be vertically well-stirred, it certainly is not homogenous. Thus one compartment will not be sufficient. In addition, absorption of chemical constituents and emission occurs only in the boundary layer due to human activity, wind or natural emissions. Thus this layer is somehow special, making it a likely candidate for a separate compartment. Due to friction wind speeds increase with increasing height and therefore in- and outflows increase with height, too. This also calls for a stack of compartments, in this case with different advection terms. While Fig. 3.7

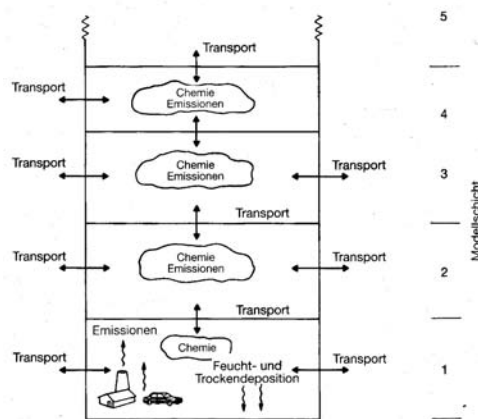


Figure 3.7: 1D atmosphere model [52]

relates to a more local (and also height limited) problem of atmospheric chemistry, a very similar approach is used in climate modeling. In the simplest models, the quantity transported is heat with radiation transfer as the main transport mechanism. Only if transport by convection or the transport of latent heat comes into play, also the transport of matter

has to be considered.

A 2D model results if one horizontal coordinate is added. In a simple 2D climate model this is the latitude because the temperature gradient between equator and pole is the ultimate driver of all transport processes. Thus meridional transport has to be covered in a 2D model. In a chemistry model, such as sketched in Fig. 3.8, also horizontal transport is considered. Here we do not have a ‘natural’ coordinate as in case of a river but are free to choose one. The best choice is the prevailing wind direction because this defines the direction and magnitude of in- and outflow.⁶ Naturally, model results will be useless for entirely different weather patterns. However, summer smog is a typical application for such kind of model. And summer smog also is related to particular weather patterns. Thus the prevailing wind direction is well-defined and consistent – the requirement for the limitation to a model as sketched in Fig. 3.8 instead of a full 3D solution is fulfilled.

Present day climate and atmosphere models still are some kind of compartment models: the simulation volume is too large to be divided accurately to fit in a finite difference scheme. On the other hand, spatial scales are quite large, making such a small-scale mathematical division superfluous. Climate models are 3-D models considering most terms in the transport equation. Nonetheless, the simple models as sketched above are very educational: for instance a 1D-atmosphere allows pretty good estimates on the greenhouse-effect as long as increases in global temperature are concerned. Since it does not contain a horizontal coordinate, it certainly is not able to model regional changes in temperature, wind or precipitation.

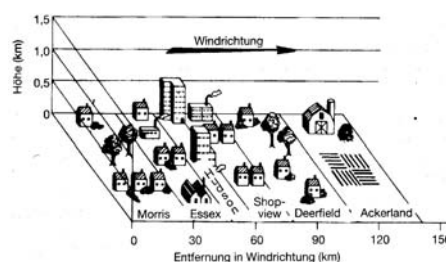


Figure 3.8: 2D atmosphere model [52]

Literature

The use (or better the history) of compartment models in atmospheric chemistry is described in [52]. An entirely different field for compartment models, steady-state or time-dependent, is the material flow management (Stoffstrommanagement) as described, for instance, in Baccini and Brunner [4] or Baccini and Bader [3].

Questions

Frage 10 Sketch the centered difference scheme. Describe its differences to the methods known from the Rechenmethoden lecture, such as Euler, Leapfrog and Runge-Kutta (these methods briefly are recapitulated in sect. D.3).

Frage 11 Explain the differences between the implicit scheme and the Crank-Nicolson scheme.

Frage 12 Can you develop a scheme that does not require matrix inversion? Hint: start with the steady-state problem: the spatial scheme calls for matrix inversion, not the temporal one. If lost, recheck the simple numerical methods in sect. D.3.

⁶Note that this is not necessarily a 2D model. The prevailing wind gives a 1D model. The horizontal direction perpendicular to the prevailing wind can be omitted because turbulence close to the surface of Earth in general is large enough to ensure good mixing – a well stirred atmosphere results. The same is true in the planets boundary layer: this is defined as the lower portion of the atmosphere where friction between the moving atmosphere and the ground leads to turbulence which in turn assures mixing.

Exercises

Aufgabe 7 Insert any numbers for the relevant parameters and compare the analytical and numerical solutions for the steady-state reactor in sect. 3.1. Use different step-sizes for the numerical method. Before starting, recheck the integration constants B_1 and B_2 in the analytical solution.

Aufgabe 8 The rate of change of the concentration of a pollutant in a lake equals the difference between the concentration of the polluted water entering the lake and that leaving the lake. Assume that water containing a constant concentration C of pollutants enters the lake at a rate of $150 \text{ km}^3/\text{year}$. Water leaves the lake at the same rate; the lake's constant volume is 5000 km^3 .

1. formulate the mathematical model to find the rate of change of the pollutants concentration in the lake.
2. find the general mathematical solution.
3. find the solution for an initial condition of a pollutant's concentration of 40 kg/m^3 .
4. the fastest possible clean-up of the lake will occur if the inflow of the pollutant suddenly ceases: $C = 0$. How long will it take to reduce pollution to 50% of its current value?

Aufgabe 9 Apart from inflow and outflow, another method by which mass can enter or leave a reactor is by a chemical reaction. If the chemical decays, the reaction can sometimes be characterized as a first order reaction with $r = -RVc$ with V as the Volume, c as the concentration and R as reaction rate which can be interpreted as the fraction of the chemical removed from the solution per unit time. Substitution of the reaction into the mass balance yields with the flow rate F

$$V \frac{dc}{dt} = Fc_{\text{in}} - Fc - RVc. \quad (3.47)$$

1. Find the steady-state concentration of the reactor in the case where $R = 0.25 \text{ min}^{-1}$, $c_{\text{in}} = 50 \text{ mg/min}^3$, $F = 10 \text{ m}^3/\text{min}$ and $V = 200 \text{ m}^3$.
2. Calculate the transient concentration response for $c_0 = 20 \text{ mg/m}^3$. Validate the results using Euler's numerical method from $t = 0$ to 30 min.

Aufgabe 10 Compare the numerical solutions for the longitudinal tank in sect. 3.2. Implement both algorithms in a programm package or a programming language of your choice. Perform runs with different step sizes; compare accuracy and computing time in both schemes. Note that a comparison to the analytical solution for the steady-state model in sect. 3.1 is possible at late times.

Aufgabe 11 Determine accuracy and stability conditions for the centered difference method.

Aufgabe 12 Determine accuracy and stability conditions for the implicit scheme.

Aufgabe 13 Determine accuracy and stability conditions for the Crank-Nicolson scheme.

Chapter 4

Diffusion and Heat Conduction

Diffusion is the fundamental stochastic transport process. It can be applied to the transport of matter or energy (heat transport). The mathematical description is rather simple and analytical solutions are available for simplified geometries. Thus numerical solutions can be tested against the analytical ones. Nonetheless, in heat transfer even rather simple problems often require more than one spatial coordinate. Numerical schemes thus have to be adapted to accommodate additional spatial coordinates. The introduction of such a scheme in sect. 4.2 will be the numerical focus of this chapter; most other applications only give supportive information on the physical background or straightforward extensions of numerical methods encountered so far.

In addition, in many natural conditions, diffusion is just one of many transport mechanisms. In this chapter, we will also consider directed transport which leads to the diffusion–convection equation already encountered in chap. 3 as well as some basics of transport in porous media and transport including reactions. Simple numerical models will be discussed in this chapter, the application to more complex situations is topic of chapters 5 and 6.

The last section, sect. 4.6.3, introduces the Stefan problem: here the boundary condition changes with time, such as in solidification of a body of a fluid as it cools down. A traffic jam is a practical application for the modeling of such a phase transition.

Goals: after working through this chapter you should be able:

- to develop numerical schemes for diffusive transport (including other processes such as advection/convection and chemical reaction/decay) in 2 or 3D and discuss the special problems arising in the discretization/solution of the spatial transport term.
- to describe the physical basis of diffusion and dispersion for different situations accordingly and to sketch applications of diffusion and diffusion related transport equations under different circumstances.
- to compare a Stefan problem with a boundary value and explain the common features as well as the differences and give examples for Stefan problems in different fields.

4.1 Diffusion – The Basics

Definition 5 Diffusion *is the formal description of a stochastic transport process.*

4.1.1 Examples

If you are asked to explain diffusion to a non-physicist, you probably will resort to examples from daily life. A drop of ink in a glass of water stays put only for a short time. Then thin streaks start to spread out from the drop, wiggling through the water until the ink is evenly distributed in the glass.

If the same process happens in a fast running rivulet, two additional processes happen. First, the ink (and the water volume it fell into) will be advected with the rivulet's flow. Thus the stochastic motion diffusion is superposed by a systematic motion, the convection with the flow. The resulting transport is described in a diffusion–convection model, already encountered in chapter 3. Secondly, eddies present in the rivulet will also spread the ink around its original drop. This dispersion will even work faster than diffusion: diffusion is a property of the ink molecules while dispersion is related to small-scale flows in the surrounding medium. Thus although dispersion is a stochastic process, too, the spatial scales covered within a time interval are larger and thus the process is more efficient.



Side question 18 Is the spread of the ink in the above example really diffusion? What about cold cream in hot coffee?

The diffusive process is not limited to liquids. In air it is also well known: even if the only person smoking a cigarette is banned into a remote corner of the room, with time the smoke will be smelled everywhere in the room: first with a higher intensity close to its source, the smoker, later everywhere.

A smokestack in principle is not very different from the smoker: it injects a marked gas which in time mixes with the atmosphere. But the smokestack also brings a few additions to diffusion to mind. First of all, in calm weather the smoke from a smokestack rises rather straight into the air owing to the upward motion of the heated gas. Thus again a directed motion is superposed on the diffusive process. Another directed motion might be superposed if wind drives the smoke from the chimney almost horizontally. Again, this process can be described by a diffusion–convection model – but, as always in the atmosphere, the process is 3D and cannot be approximated by a 1D model as easily as in a rivulet. Such processes consisting of a diffusive part and a superposed directed motion are described by a diffusion–convection model, sometimes also called diffusion plus advection.



A diffusive process also works in solids. Only here, it is not matter that is transported but momentum. Or if you prefer to think in terms of corpuscular transport, phonons are transported. This process also is called heat conduction. Thus it is a familiar process, although the layman will not necessarily make the connection between diffusion and heat conduction.

Heat conduction in a solid is based on the thermal motion of the atoms: they vibrate around their rest position with an displacement increasing with increasing temperature. Eventually, two neighboring atoms collide and momentum is transferred between them. Although the momentum transfer itself is strongly deterministic, depending only on the relative momenta of the collision partners, the likelihood for such a collision depends on the momentary positions and velocities of the atoms as does the amount and direction of momentum transfer. Consequently, the momentum transfer can be described as a stochastic process.

The situation is exactly the same for the smoke particles or the ink droplet – besides from the fact that the atoms do not stay in the vicinity of some rest position but can move rather freely since coherence is only weak. Owing to this freedom, not only momentum is transported but together with the momentum also matter. Thus diffusion can also be described as stochastic motion of particles under the influence of (stochastic) collisions with the ambient medium.

4.1.2 Formal Description of Diffusive Processes

The formal treatment of stochastic processes can follow two lines of thought:

- matter can be treated as particular, that is we will follow the individual particles and record their fate individually.
- matter can be treated as a continuum which leads to a description in terms of a fluid.

The former approach is used in statistical mechanics and Monte Carlo simulations as discussed in chap. 8. It only makes sense if a sufficiently large number of particles is considered and suitable averages are taken. Otherwise we would never get the description of the fate of an ink droplet but only one particular of the almost infinite number of possible paths of an ink molecule in water. Thus almost each ink molecule has to be simulated and the results for each droplet have to be superposed. Still we would not get the fate of an actual droplet but only a subset of the possible paths of droplets inside the water. But since this subset is representative, the simulated tracks give a representative description of the fate of the ink droplet. And normally we are rather interested in the expected size of the droplet after a certain time than in the actual position of the individual molecules. But since we only get a representative description, we can also resort to the statistical or fluid description. Nonetheless, the particle approach allows for some simple illustration of the basics of the diffusive process.

Spatial Diffusion

Diffusion is the consequence of frequent, stochastically distributed collisions – some general considerations regarding collisions are given in sect. C.4. Thus diffusion is a stochastic process. Therefore, it is not reasonable to discuss the motion of individual particles; instead one has to consider an assembly of particles, described by the distribution function (some general comments on distribution functions are given in sect. C.2).

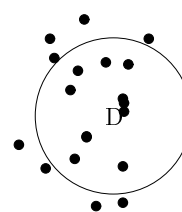
But diffusion is not only spatial diffusion. If we carefully drip a drop of ink into a glass of water, in time the drop will spread and eventually ink and water will be mixed completely: the thermal motion leads to collisions between ink and water molecules, distributing both species uniformly. This is spatial diffusion. If we carry out the same experiment with a good drop of cold cream and a cup of steaming hot tea, we find a second consequence of the collisions: after some time, tea and milk have the same temperature – or more accurate, the distributions of thermal speeds have become undistinguishable. Thus thermal energy is transferred from the faster molecules to the slower ones, leading to diffusion in momentum space.

Let us start with spatial diffusion alone. All particles have the same speed and collisions lead to changes in the direction of motion only. To describe the effect of diffusion, we have to keep track of a larger number of small spatial steps for a large number of particles. Because the stochastic aspect is important, we can borrow some concepts from probability calculus and use simple games with coins as illustrations.

Side question 19 Does “cold” diffusion make any sense from the physical point of view? Does it really happen or is it a mathematical fiction. If it is the latter, why then introduce it?

Tumbling Drunkards and Tossed Coins

Spatial diffusion, or more correctly, the motion of a particle in spatial diffusion, occasionally is called drunkards walk. To get the picture, imagine a couple of drunkards, happily lingering around a distiller. As they hear a police siren in the distance, they start to stagger away, everyone in his own direction. They all make steps of equal length λ but random direction. As a police helicopter arrives at the scene, every drunkard has made N steps. The spatial distribution of the drunkards, as seen from the helicopter, is



shown in the figure. None of the drunkards has covered the maximum possible distance $N\lambda$. Instead, they are still relatively close to the distiller. How close, compared with the maximum distance, can be described by a quantity called the expected distance or, mathematically more correct, the average squared distance. This average displacement $\lambda\sqrt{N}$ is indicated by the circle.

Let us now reduce the problem to the one-dimensional case: the test objects can only move along a straight line, again with constant step length λ . We can simulate the resulting motion by flipping a coin: a head leads to a step in the positive direction, a tail to a step in the negative one. Let us consider one particle only. At first glance one might expect the expected distance to be close to the starting point. In particular, after a large number of tosses, we would expect the number of heads and tails to be roughly equal and therefore the net displacement to be small. This, however, is a faulty reversion of the law of large numbers, which is often observed in people gambling only occasionally: if the coin has shown tails 9 times in succession, the chance of heads in the next toss is exactly the same as in all previous tosses, 50%, because the coin just does not remember the results from the last tosses. Thus in a long series of tosses, there can be quite a large deviation from a deadlock between heads and tails. This has been known since the middle of the seventeenth century when game theory was quite popular, in particular in the Bernoulli family. Thus if for a long time one side of the coin can be dominant, as indicated in Fig. 4.1, then a large net gain for the one and a large loss for the other gambler results. Or, in case of one-dimensional motion, the displacement from the starting position can become quite large.

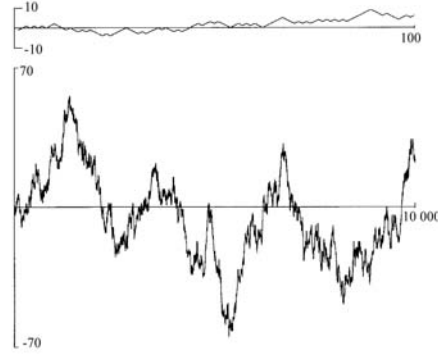


Figure 4.1: Gain and loss chart for 100 tosses (top) and 10 000 tosses of a coin

The average squared distance $\langle \Delta x \rangle^2$, or the expected distance for short, can be determined easily. The total squared displacement of the particle is the sum of the displacements dx_i in each individual step:

$$(\Delta x)^2 = \left(\sum_{i=1}^N dx_i \right)^2 = (dx_1 + dx_2 + \dots + dx_N)^2 = \sum_{i=1}^N \sum_{j=1}^N dx_i dx_j . \quad (4.1)$$

The individual displacements dx_i are either $+\lambda$ or $-\lambda$, both with a probability of 0.5. Thus the product $dx_i dx_j$ is either λ^2 or $-\lambda^2$. For $i \neq j$, dx_i and dx_j are independent and both positive and negative values of the product have the probability 0.5. In the sum (4.1) these terms cancel and only products with $i = j$ remain. They are always $+\lambda^2$ and there are N such products. Equation (4.1) then becomes

$$\langle \Delta x \rangle^2 = N\lambda^2 . \quad (4.2)$$

Thus with increasing number N of steps, the average displacement from the starting point increases as \sqrt{N} .

If the particle has a speed v , the total distance s traveled during a time t is $s = vt$. If N is the number of direction reversals during this time interval, the distance also can be written as $s = N\lambda$. Therefore in (4.2) we can substitute N by vt/λ :

$$\langle \Delta x \rangle^2 = N\lambda^2 = v\lambda t = 2Dt . \quad (4.3)$$

Here D is the diffusion coefficient:

$$D = \frac{1}{2}v\lambda . \quad (4.4)$$

Note that this diffusion coefficient has been defined for one-dimensional motion. For three-dimensional motion, the diffusion coefficient is

$$D = \frac{1}{3}v\lambda . \quad (4.5)$$

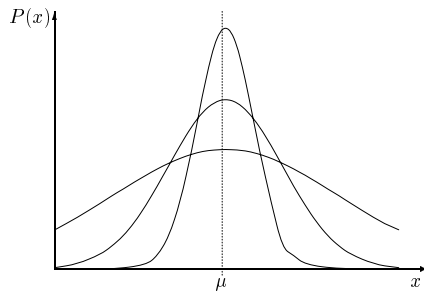


Figure 4.3: Broadening of a Gauß distribution with increasing standard deviation. Physically, this is equivalent to the diffusive broadening of a distribution with time

Galton Board and Bell Curve (Gauß Distribution)

The average distance is a statistical term which refers to a large assembly of particles. The individual particles scatter around the starting point. Their distribution can be described by the bell curve (Gauß distribution).

The Galton board is a graphical way to derive this distribution. It consists of rows of pins, indicated by dots in Fig. 4.2, and models the scattering the particles experience: as a ball hits a pin, it is deflected either to the left or to the right. Then it hits a pin in the next row, which leads to another deflection and so on. The solid line indicates a sample path. Below the lowest row, the particles are collected in slots. The slot in which a ball finally comes to rest, results from a large number (equal to the number of rows) of stochastic interactions of comparable strength. If we use a large number of balls, the distribution in the slots will be a bell curve or Gauß distribution:¹

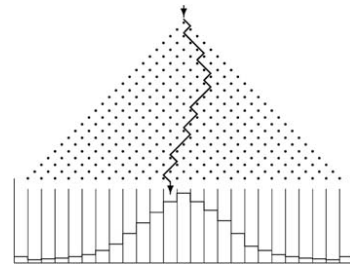


Figure 4.2: Galton board

$$P(x) = \frac{1}{\sqrt{2\pi}\sigma} \exp\left(-\frac{(x-x_0)^2}{2\sigma^2}\right). \quad (4.6)$$

Here x_0 is the average and σ is the standard deviation. $P(x)$ describes the probability of a ball to be found in the slot at position x . The standard deviation σ defines the width of the distribution: 68.3% of all balls will be inside the interval $[x_0 - \sigma, x_0 + \sigma]$ and 95.4% inside $[x_0 - 2\sigma, x_0 + 2\sigma]$. The standard deviation is given as

$$\sigma^2 = \frac{1}{n} \sum (x - x_0)^2 =: \langle \Delta x^2 \rangle, \quad (4.7)$$

and therefore describes the widening of the particle distribution or the expected displacement from the origin.

We can rewrite (4.6) and (4.7) to find an expression depending on the diffusion coefficient. With (4.3) and (4.4) we find for the standard deviation

$$\sigma = \sqrt{\langle \Delta x^2 \rangle} = \sqrt{2Dt} = \sqrt{v\lambda t}, \quad (4.8)$$

and therefore for the bell curve

$$P(x) = \frac{1}{\sqrt{2\pi v\lambda t}} \exp\left(-\frac{(x-x_0)^2}{2v\lambda t}\right). \quad (4.9)$$

Note that the maximum stays fixed while the distribution broadens with time, as described by (4.3) and shown in Fig. 4.3.

¹The number of balls in each slot is proportional to the number of possible paths from the start to that particular slot. The probabilities of all paths are equal. Thus the resulting distribution can be determined from counting the number of good paths to get the ball from the start to the target. This task fits well into the framework of statistical distribution functions and in particular Gauß' distribution.

The Diffusion Equation

If collisions happen in a homogeneous gas enclosed in a fixed volume, the relevant quantity to describe the diffusive process is the mean free path, see also sect. C.4.1 for its definition. It does not make sense to talk about a diffusion coefficient or an expected displacement because, viewed from the outside, the collisions do not change the properties of the gas, only the individual molecules change positions. This could be depicted by something similar to the Galton board: while in the Galton board the pins are arranged to form a triangle with the input only at the tip of the triangle, the modified board would consist of pins arranged in a rectangle with the input all over the top line. For each input slot, the spatial distribution is the same as for a Galton board. But the superposition of all the different input slots leads to the same number of particles in each output slot. For a gas this implies that on average for each particle leaving a volume element another one enters, see also the lower panel in Fig. 4.4.

The situation is different if there is a gradient, as in the top panel in Fig. 4.4. Then there are more particles of the species under study in one part of the volume than in the other. Accordingly, a random walk carries more particles out of the volume with high density than particles are carried in from the lower density region. Thus a net transport results, reducing the gradient and eventually leading to the equalized distribution shown in the bottom panel. The streaming \vec{S} of particles can be described as

$$\vec{S} = -D\nabla U, \quad (4.10)$$

with D being the diffusion tensor for anisotropic diffusion and U the particle density. The gradient is the driving force for the flow, a larger gradient leading to a larger flow. The flow also depends on the mobility of the particles, described by the diffusion tensor. If diffusion is isotropic, the diffusion tensor reduces to the diffusion coefficient and the streaming becomes $\vec{S} = -D\nabla U$. Since the diffusion coefficient depends on particle speed and mean free path, for a given gradient the flow as well as the average displacement are largest for fast particles undergoing only few collisions (having a large mean free path) and smallest for slow particles undergoing many collisions.

The diffusion equation can be derived from the equation of continuity. Equation (2.32) gives for a volume element

$$\frac{\partial N}{\partial t} + \oint_{O(S)} \vec{S} d\vec{\sigma} = 0. \quad (4.11)$$

Here N is the number of particles and \vec{S} is the flux of particles through the surface $\vec{\sigma}$ of the volume element V . If U is the particle density, (4.11) yields

$$\frac{\partial}{\partial t} \int_V U d^3x + \oint_{O(V)} \vec{S} d\vec{\sigma} = 0. \quad (4.12)$$

With Gauß' theorem (A.21) this is

$$\frac{\partial U}{\partial t} + \nabla \cdot \vec{S} = 0. \quad (4.13)$$

With (4.10) we can write the diffusion equation as

$$\frac{\partial U}{\partial t} = \nabla \cdot (D \nabla U). \quad (4.14)$$

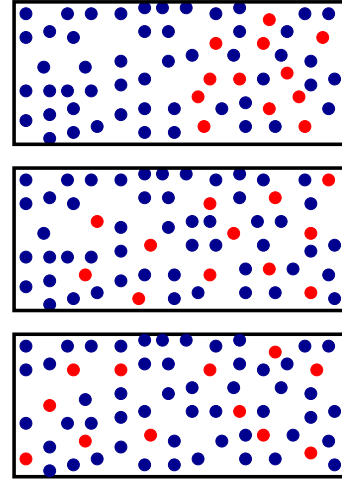


Figure 4.4: Transport by diffusion requires a gradient

If the diffusion is independent of the direction (isotropic diffusion), we can use the diffusion coefficient (4.4) instead of the diffusion tensor and get

$$\frac{\partial U}{\partial t} = \nabla \cdot (D \nabla U) . \quad (4.15)$$

If the diffusion coefficient is also independent of the spatial coordinate, as for example in a homogeneous medium, the equation can be reduced further:

$$\frac{\partial U}{\partial t} = D \Delta U . \quad (4.16)$$

Solutions of the Diffusion Equation.

The solution of the diffusion equation depends on the boundary conditions. In the general case we shall consider propagation from the source at a position r_0 . Thus we have to consider a source Q in the diffusion equation:

$$\frac{\partial U}{\partial t} - D \Delta U = Q(r_0, t) . \quad (4.17)$$

For a spherical symmetric geometry this can be written as

$$\frac{\partial U}{\partial t} - \frac{1}{r^2} \frac{\partial}{\partial r} \left(r^2 D_r \frac{\partial U}{\partial r} \right) = Q(r_0, t) \quad (4.18)$$

with D_r being the radial diffusion coefficient.

The simplest case is a pulse-like injection of N_0 particles at the position $r_0 = 0$ at time $t_0 = 0$; the Galton board and the drunkards are examples for such an initial condition. A typical example is the injection of solar energetic particles (SEPs) into the interplanetary medium, as will be discussed in chapter 5. The solution of the diffusion equation for a radial-symmetric geometry then reads

$$U(r, t) = \frac{N_0}{\sqrt{(4\pi D_r t)^3}} \exp\left(-\frac{r^2}{4D_r t}\right) . \quad (4.19)$$

Two typical diffusive profiles are shown in Fig. 4.5. The intensity rises fast to a maximum and then decays slowly as $t^{-3/2}$. The time of maximum t_m can be determined by setting the first temporal derivative to zero:

$$t_m(r) = \frac{r^2}{6D_r} . \quad (4.20)$$

The time of the maximum decreases with increasing mean free path and increasing particle speed. That is what we expect from our experience with gases and liquids: the diffusion of a minor constituent is faster with increasing temperature (corresponding to a higher particle speed) and decreasing density (corresponding to an increase in particle mean free path). The time of the maximum increases quadratically with increasing distance. This can be understood easily from (4.8): the average distance increases with \sqrt{t} .

Graphically, the time to maximum can be interpreted as follows: if we write (4.20) in the form $t_m = (r/2\lambda)(r/v)$, we have r/v as the direct travel time for the distance r and can interpret $r/2\lambda$ as a measure of the number of mean free paths between the origin and the observer at r . The quantity $r/2\lambda$ therefore characterizes the delay due to diffusion.

Inserting (4.20) into (4.19) gives the density at the time of maximum:

$$U(r, t_m) = \frac{N_0}{\sqrt{(4\pi r^2/6)^3}} \exp\left(-\frac{3}{2}\right) \sim \frac{N_0}{r^3} . \quad (4.21)$$

The intensity at the time of the maximum thus decreases with increasing radial distance but it is independent of the diffusion coefficient.

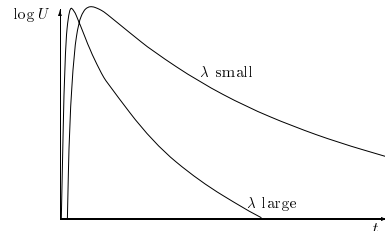


Figure 4.5: Typical diffusive profiles for small and large λ s

Equation (4.20) is used frequently as a simple estimate of the radial mean free path from the time of maximum of a particle profile observed in interplanetary space. Rewriting (4.20) we obtain

$$\lambda_r = \frac{r^2}{2vt_m}. \quad (4.22)$$

Solutions of the diffusion equation so far have been obtained for the spherically symmetric case, assuming that particles propagate radially from one shell at r to the next one at $r + \Delta r$. The mean free path λ_r then refers to the radial mean free path. In interplanetary space, the geometry is different: particles propagate along the magnetic field line, thus it is more reasonable to use a particle mean free path λ_{\parallel} parallel to the magnetic field line. In addition, the field is not radial but Archimedian, as shown in Fig. 5.1. The solution, however, is identical to the radial one as long as the relation

$$\lambda_r = \lambda_{\parallel} \cos^2 \psi \quad \text{or} \quad D_r = D_{\parallel} \cos^2 \psi \quad (4.23)$$

is obeyed. Here ψ is the spiral angle between the radial direction and the Archimedian magnetic field line. Note that here it is assumed that diffusion perpendicular to the magnetic field is negligible.

4.1.3 Diffusion and Dispersion

Sofar, we have described diffusion by its basic property, the particle mean free path λ . The latter is the average distance a particle travels between two successive collisions, see sect. C.4.1. The less graphical but more formal description is the diffusion coefficient D . Diffusion is based on stochastic collisions; the particle path therefore is determined by a large number of small stochastically distributed collisions. These collision frequency is determined by the motion of the individual particles. Diffusion thus works on the molecular level.

Dispersion resembles diffusion in such that transport is a stochastic process: particles are convected with the turbulent motion of the fluid. The stochastic part in this process is the turbulence: eddies, such as indicated in Fig. 4.6 (from http://www.efluids.com/efluids/gallery/gallery_pages/iso_turbulence_page.htm) move particles back and forth through the volume. Dispersion therefore is a process working on the level of the eddies. Consequently, it is also called eddy diffusion.

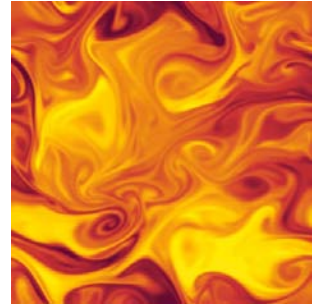


Figure 4.6: Isotropic turbulence

The transport coefficient, the dispersion coefficient, is linked to the properties of the eddies. Thus it is linked not to microscopic but macroscopic properties of the fluid. A standard method to derive the dispersion coefficient is mixing length theory; here the mixing length has a meaning similar to the mean free path in ordinary diffusion. Assume a fluctuating flow speed \vec{u} . The flow can be decomposed into a directed part $\vec{u}_0 = \langle \vec{u} \rangle$ and a fluctuating part \vec{u}' with $\langle \vec{u}' \rangle = 0$: $\vec{u} = \vec{u}_0 + \vec{u}'$. The kinetic energy contained in these fluctuations is proportional to $(u'_x)^2 + (u'_y)^2 + (u'_z)^2$. Turbulent motion can only exist down to a finite scale. Molecular diffusion will eventually wipe out variations in the flow properties.

The transport of a property ε with the turbulent flow, also called the turbulent mixing, is determined by the average flux of this property. For each component we get $\langle u'_i \varepsilon \rangle$ with $i = x, y, z$. Turbulent flux tends to diffuse properties of the medium. Thus as in diffusion it is linked to the spatial gradient of the property ε :

$$\langle u'_i \varepsilon \rangle = K_i \left\langle \frac{\partial \varepsilon}{\partial i} \right\rangle \quad \text{with} \quad i = x, y, z \quad (4.24)$$

with K_i being the turbulent diffusion coefficient, also called eddy diffusion coefficient or dispersion coefficient.

Side question 20 Explain the formal and physical similarities (and differences) between diffusion und dispersion coefficient.

The dispersion coefficient can be derived from a simple scale analysis. The diffusion coefficient is the product of a propagation speed, in that case the particle speed v , and a typical scale length of the motion, the mean free path λ . In analogy, the dispersion coefficient should be the product of a typical speed and a scale length L . For the speed we choose a typical turbulent speed $u_{t,i}$ and obtain

$$K_i \sim u_{t,i} L . \quad (4.25)$$

The lowest limit for the scale length is the Kolmogoroff scale

$$L_k = 2\pi \left(\frac{\nu^3}{\epsilon} \right)^{1/4} \quad (4.26)$$

with ν being the kinematic viscosity and ϵ the rate of turbulent energy dissipation. Below the Kolmogoroff scale, molecular diffusion will wipe out variations in the flow properties and dispersion becomes diffusion. In a slightly circular manner (as in the definition of the mean free path and diffusion coefficient), the rate of energy dissipation is related to the length scale of turbulence and the energy density in the flow by $\epsilon \sim u_i^3/L$.

4.2 Diffusion/Heat Conduction – Simple Cases

As in chapt. 3 we will start with an example that allows for an analytical solution for the stationary case. This allows the introduction to a FDM for 2D as extension of the centered finite difference scheme already encountered.

4.2.1 Stationary Heat Transport in a Plate

Consider a rectangular plate with width a and b . The Temperature at the edges is prescribed by the boundary conditions. We are interested in the temperature distribution in the plate.

The Transport Equation

The general transport equation is the heat conduction equation. Here we are only interested in steady-state conditions, thus the equation is reduced to

$$\frac{\partial^2 T}{\partial x^2} + \frac{\partial^2 T}{\partial y^2} = 0 \quad \text{für } 0 < x < a \quad \text{and} \quad 0 < y < b . \quad (4.27)$$

The boundary conditions require a temperature of zero at three edges. At the fourth edge, the temperature is prescribed by a function $f(x)$:

$$T(x, 0) = T(0, y) = T(a, y) = 0 \quad \text{und} \quad T(x, b) = f(x) . \quad (4.28)$$

As example, we will use a temperature profile

$$f(x) = T_0 x (a - x) . \quad (4.29)$$

The Analytical Solution

An analytical solution of the Laplace equation (4.27) can be obtained by a separation ansatz $T(x, y) = X(x)Y(y)$. Inserting this ansatz yields

$$Y X'' + X Y'' = 0 . \quad (4.30)$$

Rearrangement gives

$$\frac{X''}{X} + \frac{Y''}{Y} = 0 . \quad (4.31)$$

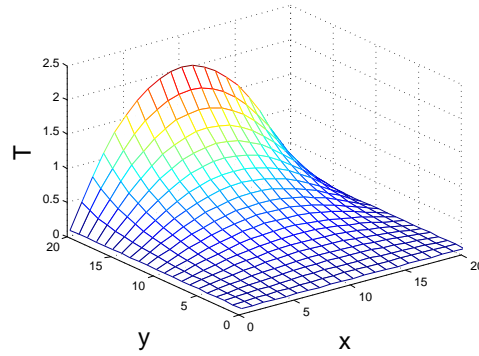


Figure 4.7: Temperature distribution in a rectangular plate

The first term depends on x only, the second on y only. The equation is valid for all values of x and y . Thus both terms must be constant. With the separation constant $-\beta^2$ (4.31) can be rewritten as

$$X'' + \beta^2 X = 0 \quad \text{und} \quad Y'' - \beta^2 Y = 0. \quad (4.32)$$

Both equations are second order ODEs describing an oscillation. Their general solutions are

$$\begin{aligned} X_n(x) &= \gamma_1 \sin\left(\frac{n\pi x}{a}\right) + \gamma_2 \cos\left(\frac{n\pi x}{a}\right), & n = 1, 2, \dots, & \quad \text{und} \\ Y_n(y) &= \gamma_3 \sinh\left(\frac{n\pi y}{a}\right) + \gamma_4 \cosh\left(\frac{n\pi y}{a}\right), & n = 1, 2, \dots. & \end{aligned} \quad (4.33)$$

The boundary conditions (4.28) with $T = 0$ yield $\gamma_2 = \gamma_4 = 0$. Thus a part of the solution of the PDE is

$$T_n(x, y) = \gamma_n \sin\left(\frac{n\pi x}{a}\right) \sinh\left(\frac{n\pi y}{a}\right), \quad n = 1, 2, \dots. \quad (4.34)$$

The entire solution is the superposition of all these partial solutions:²

$$T(x, y) = \sum_{n=1}^{\infty} T_n(x, y) = \sum_{n=0}^{\infty} \gamma_n \sin\left(\frac{n\pi x}{a}\right) \sinh\left(\frac{n\pi y}{a}\right). \quad (4.35)$$

The remaining boundary condition $T(x, b) = f(x)$ yields

$$T(x, b) = f(x) = \sum_{n=0}^{\infty} \gamma_n \sin\left(\frac{n\pi x}{a}\right) \sinh\left(\frac{n\pi b}{a}\right). \quad (4.36)$$

Side question 21 In contrast to the solution of the wave equation, in the heat equation the separation constant β is positive in one spatial coordinate and negative in the other one. Is this an arbitrary choice or has it some mathematical/physical significance?

Since the $\sin(n\pi x/a)$ are orthogonal functions, this can be rewritten as

$$\gamma_n \sinh\left(\frac{n\pi b}{a}\right) = \frac{2}{a} \int_0^a f(x) \sin\left(\frac{n\pi x}{a}\right) dx. \quad (4.37)$$

With $f(x) = T_0 x(a - x)$ we obtain

$$\gamma_n \sinh\left(\frac{n\pi b}{a}\right) = \frac{2}{a} \int_0^a T_0 x(a - x) \sin\left(\frac{n\pi x}{a}\right) dx$$

²This superposition formally is the same as in the solution of the wave equation. A fundamental difference, however, remains: the individual solutions of the wave equation are eigenmodes of the vibrating string and can exist in itself. In case of the heat conduction equation, the solution only is complete if the entire space of eigenfunctions is considered. Thus only the sum over all eigenfunctions yields a valid solution but not one eigenfunction in itself.

$$= 4T_0 a^2 \frac{1 - (-1)^n}{n^3 \pi^3}. \quad (4.38)$$

The entire solution

$$T(x, y) = \frac{8T_0 a^2}{\pi^3} \sum_{n=1}^{\infty} \frac{1 - (-1)^n}{n^3} \frac{\sinh\left(\frac{n\pi y}{a}\right)}{\sinh\left(\frac{n\pi b}{a}\right)} \sin\left(\frac{n\pi x}{a}\right). \quad (4.39)$$

is shown in Fig. 4.7.

The Numerical Solution

The numerical solution is based on the centered finite difference scheme in two dimensions, see Fig. 4.8. As in the analytical solution, the system at hand is a cartesian coordinate system. Discretization of the PDE yields

$$\frac{T_{i+1,k} - 2T_{i,k} + T_{i-1,k}}{(\Delta x)^2} + \frac{T_{i,k+1} - 2T_{i,k} + T_{i,k-1}}{(\Delta y)^2} = -\frac{\dot{Q}(x, y)}{\lambda} \quad (4.40)$$

with \dot{Q} being a heat generation function and λ the thermal conductivity. \dot{Q} is evaluated at (i, k) . The boundary conditions are given by an energy input q at the edges.

For equal spatial step sizes in both directions, $\Delta x = \Delta y$, this can be rewritten as

$$T_{i+1,k} + T_{i-1,k} + T_{i,k+1} + T_{i,k-1} - 4T_{i,k} + \frac{\dot{Q}}{\lambda} (\Delta x)^2 = 0.$$

The temperature at the reference point $T_{i,k}$ thus is determined by the temperatures in the four adjacent grid points.

As in the 1D example, grid points can be interior points, edge points and corner points. The discretization scheme leads also to outer nodes: one for each edge point and two for the corner points. These outer nodes again are eliminated using the boundary conditions.

The problem, including its boundary conditions thus can be formulated as a set of algebraic equations. In matrix form these can be written as

$$\mathbf{A}\vec{T} = \vec{F} \quad (4.41)$$

with \vec{F} containing both the heat generating function \dot{Q} and the boundary conditions q . In contrast to the 1D problem in chap. 3, the resulting matrix is not tridiagonal, thus the inversion of the matrix is more difficult. To explore the structure of the matrix, let us take one step back: how do we write the vector \vec{T} ? Since $T = T(x, y)$, the direct approach would suggest to write T as a matrix instead of a vector. To put T in vector form, we have to define some ordering of the matrix components, for instance³

$$\vec{T} = \begin{bmatrix} T_{1,1} \\ T_{1,2} \\ T_{1,3} \\ \vdots \\ T_{1,k} \\ T_{2,1} \\ \vdots \\ T_{i,j} \\ \vdots \\ T_{i,k} \end{bmatrix}. \quad (4.42)$$

³Such ordering sometimes is termed lexicographical ordering. The matrix elements u_{ij} are ordered as vector components U_k such that $k = iN + j$ with N being the number of the matrix columns.

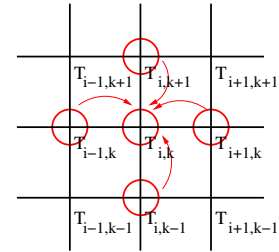


Figure 4.8: Discretization in 2D

The corresponding matrix than has at most five non-zero entries on each line, it is a pentadiagonal matrix. Its structure is a consequence of the mesh used in the discretization of the PDE.

The target quantities \vec{T} can be determined by inversion of the matrix \mathbf{A} :

$$\vec{T} = \mathbf{A}^{-1} \vec{F}. \quad (4.43)$$

Although the matrix is sparse, that is most of its elements are zero, inversion and storage of the entire matrix is very demanding on computer resources. While in the 1D problem the system matrix is a $(n+1) \times (n+1)$ matrix with n being the number of spatial steps, here the target vector \vec{T} has the length $(n+1)^2$ if x and y are divided into the same number of steps or $(n+1) \times (m+1)$ for different numbers of steps in both directions. As a consequence, \mathbf{A} is a $((n+1) \times (m+1))^2$ matrix.

Standard solving tools for systems of linear equations, such as Cramer's rule, are very inefficient. For instance, for an $((n+1) \times (m+1))^2$ matrix, Cramers rule would require $(n+1) \times (m+1) + 1!$ steps – so take a break after starting the program. Gaussian elimination, although faster, still would require about $((n+1) \times (m+1))^3$ operations.

Iterative Methods

Instead of these methods, a number of iterative methods is available, that allow for an efficient solution of the problem. All iterative methods construct a sequence \vec{T}^n that satisfies (4.41) for $n \rightarrow \infty$. For sufficiently large n , the approximation can be considered good enough to terminate the iteration process.

As the iteration proceeds, vector states \vec{T}^n are generated with n iterations out of the arbitrary initial vector \vec{T}^0 . The iteration process is assumed to be low-level: state $n+1$ only depends on state n . The iteration itself is described by a non-singular conditioning matrix \mathbf{H} such that

$$\vec{T}^{n+1} - \vec{T}^n = \mathbf{H}(\mathbf{A}, \vec{T}^n - \vec{F}). \quad (4.44)$$

Note that for $\mathbf{H} = -\mathbf{A}^{-1}$ the exact solution is determined within one single step. Note also that the notation for the iterative step is the same as that for the time step in chap. 3. We will see later, that not only the notation is similar but that there is also a deeper relation between the two.

Iteration of the recurrence formula (4.44) yields

$$\vec{T}^{n+1} = (\mathbf{E} + \mathbf{H}\mathbf{A})^{n+1} \vec{T}^0 - \sum_{m=0}^{\infty} (\mathbf{E} + \mathbf{H}\mathbf{A})^m \mathbf{H}\vec{F}. \quad (4.45)$$

Formally, the last term represents an expansion of $-\mathbf{A}^{-1}$ into a series of matrices, similar to that performed for a scalar quantity:

$$-a^{-1} = -\frac{1}{a} = \frac{h}{1 - (1+ha)} = (1 + (1+ha) + (1+ha)^2 + \dots)h = \sum_{m=0}^{\infty} (1+ha)^m h. \quad (4.46)$$

Let us have a look at the implications of (4.45). To obtain a solution, we require $\vec{T}^n \rightarrow \vec{T}$ for $n \rightarrow \infty$. Since \vec{T}^0 is arbitrary, this requires $(\mathbf{E} + \mathbf{H}\mathbf{A})^{n+1} \rightarrow 0$. It must also be true that

$$\sum_{m=0}^{\infty} (\mathbf{E} + \mathbf{H}\mathbf{A})^m \mathbf{H}\vec{F} \rightarrow \mathbf{A}^{-1} \vec{F} \quad \text{for} \quad n \rightarrow \infty. \quad (4.47)$$

Jacobi Method

To understand the method of Jacobi, let us start from the form

$$\frac{T_{i+1,k}^n - 2T_{i,k}^{n+1} + T_{i-1,k}^n}{(\Delta x)^2} + \frac{T_{i,k+1}^n - 2T_{i,k}^{n+1} + T_{i,k-1}^n}{(\Delta y)^2} = f_{i,k}. \quad (4.48)$$

This equation is valid for all interior nodes, only at the edge and corner nodes, different coefficients arise from the implementation of the boundary conditions.

The new value of the unknown $T_{i,k}^{n+1}$ is obtained from the central terms of the scheme; all other unknowns are kept at their old values. With (4.44) we get

$$\frac{1}{h^2} \left(u_{i,k}^{n+1} - u_{i,k}^n \right) = \frac{T_{i+1,k}^n - 2T_{i,k}^n + T_{i-1,k}^n}{(\Delta x)^2} + \frac{T_{i,k+1}^n - 2T_{i,k}^n + T_{i,k-1}^n}{(\Delta y)^2} - f_{i,k} \quad (4.49)$$

or in matrix form

$$\vec{T}^{n+1} - \vec{T}^n = h^2 \left(\mathbf{A} \vec{T}^n - \vec{F} \right). \quad (4.50)$$

This is true for $\mathbf{H}^{-1} = h^{-2} \mathbf{E}$. Thus the conditioning matrix is $\mathbf{H} = h^2 \mathbf{E}$.

Von Neumann has suggested an approach on this problem which treats the iteration process as an advance in the temporal direction. With the ansatz

$$T_{i,k}^n = g^n e^{i\alpha} e^{ik\beta} \quad (4.51)$$

(4.48) can be rewritten as

$$\frac{g}{h^2} = \frac{1}{(\Delta x)^2} (e^{i\alpha} + e^{-i\alpha}) + \frac{1}{(\Delta y)^2} (e^{i\beta} + e^{-i\beta}). \quad (4.52)$$

Solving for g gives

$$g = \frac{\frac{\cos \alpha}{(\Delta x)^2} + \frac{\cos \beta}{(\Delta y)^2}}{\frac{1}{(\Delta x)^2} + \frac{1}{(\Delta y)^2}}. \quad (4.53)$$

g is real and it is $-1 \leq g \leq 1 \forall \alpha, \beta$.

The speed of convergence for the iteration process is determined by the maximum of g . Since the mesh size determines how many wave modes can be supported (α and β are a multiples of $\pi \Delta x$ and $\pi \Delta y$, respectively), we get an amplification factor

$$|g_{\max}| = 2h^2 \left(\frac{\cos(\pi \Delta x)}{(\Delta x)^2} + \frac{\cos(\pi \Delta y)}{(\Delta y)^2} \right) \approx 1 - 2\pi^2 h^2. \quad (4.54)$$

After n discretization steps, the error is reduced to $|g_{\max}|^n$. Thus for a small $|g_{\max}|$ convergence is faster than for a larger one. For the Jacobi method $|g_{\max}|$ is close to one for fine meshes, thus the method is very slow.

The interpretation of Jacobi's method as an evolution process is rather straight forward from (4.49). If we choose the time step $\Delta t = h^2$, Taylor expansion yields

$$\frac{\partial u}{\partial t} = \frac{\partial^2 T}{\partial x^2} + \frac{\partial^2 T}{\partial y^2} + \mathcal{O}(\Delta t, (\delta x)^2, (\Delta y)^2) \quad (4.55)$$

which is the two-dimensional time-dependent heat equation. The time step $\Delta t = h^2$ is the limit of the stability condition for the heat conduction equation using in explicit centered five-point scheme in space and an advanced scheme in time.

Gauss-Seidel Method

The Gauss-Seidel method starts from a slightly different algorithm as (4.48):

$$\frac{T_{i+1,k}^n - 2T_{i,k}^{n+1} + T_{i-1,k}^{n+1}}{(\Delta x)^2} + \frac{T_{i,k+1}^n - 2T_{i,k}^{n+1} + T_{i,k-1}^{n+1}}{(\Delta y)^2} = f_{i,k}. \quad (4.56)$$

Here the $T_{i-1,k}$ and $T_{i,k-1}$ are new values in the scheme. In spite of these advanced values the scheme is not implicit and thus does not require a simultaneous solution of algebraic equations. Instead, the grid points can be swept with increasing values in i and j , the corresponding values at the grid points than can be calculated from previously computed points. The only unknown variable in the scheme, $T_{i,j}^{n+1}$, can be calculated from

$$-\frac{1}{(\Delta x)^2} \left(T_{i-1,k}^{n+1} - T_{i-1,k}^n \right) - \frac{1}{(\Delta y)^2} \left(T_{i,k-1}^{n+1} - T_{i,k-1}^n \right) + \frac{1}{h^2} \left(T_{i,k}^{n+1} - T_{i,k}^n \right)$$

$$= \frac{T_{i+1,k}^n - 2T_{i,k}^n + T_{i-1,k}^n}{(\Delta x)^2} + \frac{T_{i,k+1}^n - 2T_{i,k}^n + T_{i,k-1}^n}{(\Delta y)^2} - f_{i,k}. \quad (4.57)$$

By identification one finds

$$\mathbf{H}^{-1} = \left[\dots \quad 0 \quad -\frac{1}{(\Delta x)^2} \quad 0 \quad \dots \quad 0 \quad -\frac{1}{(\Delta y)^2} \quad \frac{1}{h^2} \quad 0 \quad 0 \dots \right]. \quad (4.58)$$

\mathbf{H}^{-1} is a lower triangular matrix and its coefficients are the opposite of the corresponding coefficients in \mathbf{A} .

Although the Gauss-Seidel method is more complex to analyze than Jacobi's method, it is simpler to implement in a code and does not require any storage space in addition to the basic areas.

Over-relaxation Method

The Gauss-Seidel method is a particular case of the over-relaxation method. It consists of two steps:

1. compute a provisional value $\tilde{T}_{i,k}$ with the Gauss-Seidel algorithm:

$$\frac{T_{i+1,k}^n - 2\tilde{T}_{i,k} + T_{i-1,k}^{n+1}}{(\Delta x)^2} + \frac{T_{i,k+1}^n - 2\tilde{T}_{i,k} + T_{i,k-1}^{n+1}}{(\Delta y)^2} = f_{i,k}. \quad (4.59)$$

2. Extrapolate the new value using the relation

$$T_{i,k}^{n+1} = T_{i,k}^n + \omega \left(\tilde{T}_{i,k} - T_{i,k}^n \right). \quad (4.60)$$

Here ω is the relaxation factor.

Depending on the value of ω , the method has different properties. For $\omega > 1$ the method is called over-relaxation method. This method is stable in most linear cases, however, for non-linear equations stability might require $0 < \omega < 1$. It is then called under-relaxation method. For $\omega = 1$ the Gauss-Seidel method results.

The two steps (4.59) and (4.60) can be combined into one step by eliminating the provisional value $\tilde{T}_{i,k}$ in (4.59) using (4.60). The resulting iterative process can be expressed as

$$\begin{aligned} & -\frac{1}{(\Delta x)^2} \left(T_{i+1,k}^{n+1} - T_{i-1,k}^n \right) - \frac{1}{(\Delta y)^2} \left(T_{i,k+1}^{n+1} - T_{i,k-1}^n \right) + \frac{1}{\omega h^2} \left(T_{i,k}^{n+1} - T_{i,k}^n \right) \\ & = \frac{T_{i+1,k}^n - 2T_{i,k}^n + T_{i-1,k}^n}{(\Delta x)^2} + \frac{T_{i,k+1}^n - 2T_{i,k}^n + T_{i,k-1}^n}{(\Delta y)^2} - f_{i,k}. \end{aligned} \quad (4.61)$$

The inverse of the conditioning matrix thus can be written as

$$\mathbf{H}^{-1} = \left[\dots \quad -\frac{1}{(\Delta x)^2} \quad 0 \quad \dots \quad 0 \quad -\frac{1}{(\Delta y)^2} \quad \frac{1}{\omega h^2} \quad 0 \dots \right]. \quad (4.62)$$

The stability of the method again can be judged with the von Neumann method with $f = 0$ and the complex wave mode as in (4.51). Some algebra yields

$$\begin{aligned} & \left(\frac{1 - \cos \alpha}{(\Delta x)^2} + \frac{1 - \cos \beta}{(\Delta y)^2} + \frac{1 - \omega}{2\omega h^2} + i \left(\frac{\sin \alpha}{(\Delta x)^2} + \frac{\sin \beta}{(\Delta y)^2} \right) \right) g = \\ & - \left(\frac{1 - \cos \alpha}{(\Delta x)^2} + \frac{1 - \cos \beta}{(\Delta y)^2} - \frac{2 - \omega}{\omega h^2} \right) + i \left(\frac{\sin \alpha}{(\Delta x)^2} + \frac{\sin \beta}{(\Delta y)^2} \right). \end{aligned} \quad (4.63)$$

Stability of the method requires $|g| \leq 1$. Solving the above equation for g shows that this is obtained for $0 < \omega < 2$.

ADI

The alternating direction implicit (ADI) method treats transport by advancing the scheme into the two directions not simultaneously but alternately. The corresponding scheme thus consists of two steps.

The ADI principle is adopted for different schemes. One of them, the Peaseman–Rachford ADI scheme, suggests for the first step

$$u_{i,k}^{n+\frac{1}{2}} = u_{i,k}^n + \rho^n \left(\frac{u_{i+1,k}^{n+\frac{1}{2}} - 2u_{i,k}^{n+\frac{1}{2}} + u_{i-1,k}^{n+\frac{1}{2}}}{(\Delta x)^2} + \frac{u_{i,k+1}^n - 2u_{i,k}^n + u_{i,k-1}^n}{(\Delta y)^2} - f_{i,k} \right) \quad (4.64)$$

and for the second step

$$u_{i,k}^{n+1} = u_{i,k}^{n+\frac{1}{2}} + \rho^n \left(\frac{u_{i+1,k}^{n+\frac{1}{2}} - 2u_{i,k}^{n+\frac{1}{2}} + u_{i-1,k}^{n+\frac{1}{2}}}{(\Delta x)^2} + \frac{u_{i,k+1}^{n+1} - 2u_{i,k}^{n+1} + u_{i,k-1}^{n+1}}{(\Delta y)^2} - f_{i,k} \right). \quad (4.65)$$

The scheme thus advances first by a half-step with an implicit scheme in y at the old grid points and an implicit scheme in x at the new gridpoints. Thus the y -part can be solved directly and only the x -part contains unknowns and requires the simultaneous solution of all algebraic equations. In the half of the step, the scheme is reversed: the solution in x is performed with known quantities while the solution in y is at the new step and requires the simultaneous solution of all algebraic equations. The individual schemes thus correspond to the FTCS method.

The scheme is convergent for solutions of the Laplace equation on a square for any choice of the iteration parameters ρ^n . Nonetheless, maximum computational efficiency requires a proper choice of the ρ^n .

The total amplification factor is the product of the amplification factors of both steps: $g = g_1 g_2$. With the abbreviations $\sigma_x = \rho^n / (\Delta x)^2$ and $\sigma_y = \rho^n / (\Delta y)^2$, the amplification factor for the first step is

$$g_1 = \frac{1 - 2\sigma_y(1 - \cos \beta)}{1 + 2\sigma_x(1 - \cos \alpha)}. \quad (4.66)$$

For the second step we get

$$g_2 = \frac{1 - 2\sigma_x(1 - \cos \alpha)}{1 + 2\sigma_y(1 - \cos \beta)} \quad (4.67)$$

and thus for the total amplification factor

$$g = g_1 g_2 = \frac{(1 - 2\sigma_y(1 - \cos \beta))(1 - 2\sigma_x(1 - \cos \alpha))}{(1 + 2\sigma_x(1 - \cos \alpha))(1 + 2\sigma_y(1 - \cos \beta))}. \quad (4.68)$$

Thus $|g| \leq 1 \forall \alpha, \beta$. The ADI scheme therefore is unconditionally stable.

ADI schemes are used in rather complex problems such as time-dependent solutions for transonic potential flows or solutions to the Euler or Navier–Stokes equations. For time-dependent solutions they are more efficient than the schemes described above. In addition, the ADI has the advantage that in certain simple situations the exact solution can be obtained in a finite number of steps.

4.2.2 The Time-Dependent Problem

The time-dependent problem requires the full solution of the heat conduction equation

$$\frac{\partial T}{\partial t} = \lambda \Delta T. \quad (4.69)$$

Formally, time is added as an additional dimension. This does not pose a new numerical challenge to us. For the 1D case, we have already encountered this equation in chap. 3. The additional variable time was considered in an implicit scheme as well as in the Crank–Nicolson

scheme. In both cases, the spatial dependence was treated similar as in steady-state by some numerical scheme `spatialsolver` and the temporal scheme was wrapped around it:

```
sol(0) = initval
for t=1,tsteps
    spatialsolver(t,sol(t-1))
    sol(t) → sol(t-1)
end
```

The situation is not different in the 2D or 3D-case, although `spatialsolver` is more complex. Thus we do not face any principal problems in moving from the steady-state to the time-dependent solution; our only challenges concern the resources: the required memory is not much larger than in the steady-state model because only the vector `sol(t-1)` for an earlier time must be stored in addition to the other vectors and matrices encountered in that scheme. But computational times rise: for each time-step, the modified steady-state scheme has to be solved, requiring the inversion or expansion of the matrix. Thus the total computing time is more than that for the steady-state scheme multiplied by the number of time steps in the transient solution.

Comment on Climate Modeling

This demand on computational resources in time dependent schemes is the main reason why early climate models, say up to the middle of the 1990s, always showed simulations for a doubling in CO₂ concentration. In this case, only one steady-state simulation was performed, reducing demand on computational resources, in particular time. Although such steady-state simulation gives excellent first hints, it is not really helpful in understanding climate change. First of all, it implies some basic semi-linear behavior of the climate system: with increasing CO₂ concentration, the system behaves consistently and there is no critical concentration or accumulation that might cause one system parameter to change in such a manner that the entire development changes. For instance, a moderate increase in CO₂ concentration might cause the Greenland glaciers to melt. This would supply fresh water to the northern Atlantic and thus the thermohaline circulation might be inhibited. This would drive rapid glaciation of the northern hemisphere and the heating trend would be reversed. Such a process would not necessarily show up in a steady-state simulation because there temperatures would be much higher and again might be associated with a stable thermohaline circulation.

The second problem is concerned with predictability: the time of CO₂ doubling is difficult to predict because atmospheric CO₂ concentrations depend on CO₂ emission (which also implies some basic ideas about global economic development and production of fossil fuels), CO₂ sinks (uptake of the biosphere and chemical reactions binding the CO₂, both also depending on temperature) and CO₂ storage (oceans, but CO₂ solubility also depends on temperature).

And finally, the steady-state model makes tests difficult since all comparisons between model and reality have to be postponed until CO₂ doubling has occurred. It is also difficult to judge whether present day climate change is due to natural or anthropogenic effects or a combination of both. From a transient model, typical patterns of climate change (temporal, spatial, temperature, precipitation, wind systems) can be derived even for moderate changes in CO₂. These fingerprints can be compared to observed changes in the climate system to support or reject the hypothesis of anthropogenic climate change.

Side question 22 So far, we have limited ourselves to the 2D model by adapting the 1D scheme to a second spatial dimension. Could we extend this procedure also into 3D (or even into higher dimension)? How does the demand on computational resources increase with each added dimension?

4.3 Diffusion–Convection Model

A typical extension to a diffusion process is a superposed directed motion. The chemical reactor in sect. 3.1 is such an example; other examples are a spill of chemicals in a river or the propagation of pollutants in the atmosphere. All these processes are governed by the same equation, the one we have already derived as (3.2). Diffusion may be molecular (such as discussed above or in heat conduction) or turbulent (such as the dispersion in the chemical reactor example) or a combination of both (which is most often the case in natural systems). Convection also is called advection, thus a diffusion–convection equation and a dispersion–advection equation are identical.

Side question 23 What happens in a situation in which both dispersion and diffusion are effective? How does the presence of both processes change the transport equation as well as the numerical scheme? And what is the influence on the solution?

4.3.1 The Transport Equation

The streaming in (4.10) has to be supplemented by the convective streaming $\vec{S}_{\text{conv}} = U\vec{u}$, giving $\vec{S} = U\vec{u} - D\nabla U$. Here \vec{u} is the velocity of the convective flow.

As above, the streaming can be inserted into the equation of continuity (2.32), giving the diffusion–convection equation

$$\frac{\partial U}{\partial t} + \nabla(U\vec{u}) = \nabla(D\nabla U). \quad (4.70)$$

If \vec{u} and D are independent of the spatial coordinate, (4.70) reads

$$\frac{\partial U}{\partial t} + \vec{u}\nabla U = D\Delta U. \quad (4.71)$$

4.3.2 Simple Analytical Solution

In the radial-symmetric case, the solution for a δ -injection then is

$$U(r, t) = \frac{N_0}{\sqrt{(4\pi D_r t)^3}} \exp\left\{-\frac{(r - ut)^2}{4D_r t}\right\}. \quad (4.72)$$

The only difference is the ut -term in the exponential. This just gives the offset from the source during the time t . But that is exactly the convective motion. Thus basically the solution for a simple diffusion model results, only the center of the distribution is not stationary at the injection site but shifted with the convective flow.

For small bulk speeds \vec{u} of the medium the transport equation as well as its solution converge towards the simple diffusion equation.

4.3.3 Numerical Solutions

Numerical solution for the 1D diffusion-convection model have been described in detail in chap. 3, only the reaction term $-\gamma c$ has to be omitted from the solution. That does not change the properties of the numerical scheme such as accuracy, stability and convergence.

Before attempting numerical solutions of a diffusion–convection model in more than one spatial dimension, the modeler should ask himself whether a second or even third spatial direction really is required. We should keep in mind that convection is tied to a flow \vec{u} . This flow is prescribed. A natural choice always would be to adjust the coordinates such that one axis points along the flow. Then the problem is a 1D problem. This is also possible for a flow changing direction as is the case for a river. In that case, the spatial coordinate is length along the flow-direction; the same procedure as described for energetic particles in interplanetary space in chap. 5. Turbulence on small-scales is advantageous in such that it ensures mixing perpendicular to the flow on small spatial scales. In that case, the diffusion

coefficient must be replaced by a dispersion coefficient. Turbulence on large scales, that is scales comparable to the length scale covered by the flow, however, is not treated in the framework of a diffusion-convection model. Here the convective part vanishes and all transport is due to turbulence. This has two consequences: (a) no preferred direction exists, the model therefore cannot be limited to one spatial dimension, and (b) all transport is by dispersion and the multi-dimensional diffusion/heat conduction equation has to be solved as discussed in sect. 4.2.

4.4 Diffusion–Reaction Model

Leopards (Fig. 4.9, from <http://www.bergoiata.org/fe/felins/Calculation,SnowLeopard.jpg>) also can be treated as a transport problem. In this text we are neither dealing the the transport problem posed by a living leopard to a smuggler of exotic animals or the oil companies advertisement slogan “put the tiger in your tank”. We will treat the leopard in terms of transport in a diffusion–reaction model. And it is not the leopard that diffuses but chemicals inside the animal coat the diffuse and react, forming typical animal coat patterns. Turing [166] was the first to suggest that these patterns can be described in a diffusion–reaction model.



Figure 4.9: Snow Leopard

We already have encountered a diffusion–reaction model. The diffusion–convection equation is the limiting case of the longitudinal compartment model in chap. 3 for a vanishing loss term. The other limiting cases, the diffusion–reaction model, arises for a vanishing convection term. The diffusion–reaction model in chap. 3 is very simple in such that it only contains a loss term as reaction term:

$$\frac{\partial c}{\partial t} = D \frac{\partial^2 c}{\partial x^2} - \gamma c. \quad (4.73)$$

The general diffusion reaction model might be written in the form

$$\frac{\partial \vec{c}}{\partial t} = \mathbb{D} \Delta \vec{c} + \vec{F}(\vec{c}). \quad (4.74)$$

Here we use a vector \vec{c} of concentrations of different species c_i to allow for reactions between species and track all of them, a diffusion tensor \mathbb{D} to allow for different diffusion coefficients for the different species,⁴ the Laplace operator to allow for three-dimensional transport and a vector function $\vec{F}(\vec{c})$ that contains losses and reactions. This function mathematically couples the different balances because the reactions provide the coupling between the different species: the losses in c_i might be the sources in c_{i+1} or vice versa. The basic equations describing these reactions are summarized in sect. C.1.

The main differences in the numerical treatment compared to the simpler model (4.73) discussed in chap. 3 are: (1) the convection-term is neglected (as already indicated in (4.73)). This does not influence the numerical treatment because the schemes had been chosen to accommodate diffusion but were not optimized for convection. (2) The spatial scheme is not limited to one dimension but can work in up to three dimensions. The consequences for the numerical treatment are the introduction of a five-point scheme (for 2D) or a seven-point scheme (for 3D) instead of the centered scheme. This has already been discussed in connection with the heat conduction equation in sect. 4.2.1. (3) The problem does not consist of just one PDE but a scheme of coupled PDEs. This is the new aspect; it will be discussed in this section.

⁴ \mathbb{D} thus becomes a diagonal tensor – diffusion is assumed to be isotropic for each species, the tensor only is required to allow for different diffusion coefficients for each species.

4.4.1 Turing Patterns

As an example we will discuss here a simple diffusion–reaction model proposed by A. Turing in the early 1950s [166] as a possible mechanism for biological pattern formation.

Turing suggested that pattern development in plants and animals could be understood from the interaction of basic processes. He showed that stable processes could combine to produce an instability. The particular example he took was of diffusion-driven instability. This phenomenon has now been found in chemistry but it is still controversial in biology. However, the model does produce patterns that are intriguingly similar to those observed in animals and has stimulated a number of laboratories to carry out experiments to test the model. A more recent overview is given in [104] and [105].

The model involves a low-range diffusing activator and a wide-range diffusing inhibitor: the activator A stays close to its injection site while the inhibitor H disperses through a much larger volume. Activator production is enhanced by the presence of the activator while it is inhibited by the presence of inhibitors. The inhibitor production is linked to the presence of activators, but it does not depend on the presence of the inhibitor: the inhibitor is not self-enhancing. The temporal change in local activator concentration,

$$\frac{\partial A}{\partial t} = \frac{k_{A,1}A}{H} - k_{A,2} + k_{A,1}k_{A,3} + D_A \frac{\partial^2 A}{\partial x^2}, \quad (4.75)$$

is determined, from left to right, by activator production from existing activator at a production rate $k_{A,1}$, activator decay with a decay rate $k_{A,2}$, basic activator production (does not require the presence of the activator) as described by a production rate $k_{A,3}$, and the diffusion of the activator, described by the diffusion coefficient D_A . Here the production of the activator is a second order process.

The change in concentration of the inhibitor,

$$\frac{\partial H}{\partial t} = k_{H,1}A^2 - k_{H,2}H + k_{H,3} + D_H \frac{\partial^2 H}{\partial x^2}, \quad (4.76)$$

is determined by the second-order production of H regulated by a production rate $k_{H,1}$, inhibitor decay regulated by the decay rate $k_{H,2}$, basic inhibitor production without an activator present regulated by the production rate $k_{H,3}$, and the diffusion of the inhibitor, regulated by the diffusion coefficient D_H .

For this special case, the inhibitor has a wide-range while the activator has a small-range only, thus it is $D_A < D_H$. Stable patterns arise for $k_{A,1} \approx k_{A,2} \approx k_{H,2}$, $k_{H,3} \approx k_{A,1}k_{A,3}$ and $k_{H,1} \ll k_{A,1}$.

Different problems lead to slightly different versions of the two coupled diffusion–reaction equations (4.75) and (4.76). The mathematical treatment, in particular the introduction of dimensionless variables is described and discussed in detail in [180], although the focus of that paper is material sciences rather than animal coats. Here the transition to dimensionless variables has the advantage that the same equations can be scaled for different geometries/reaction constants. The topic of Turing patterns and the mathematical treatment of the resulting equations will not be discussed in detail in this text but is the topic of project 1 as described in sect. 10.2.

4.4.2 Other Application of Diffusion–Reaction Models

Diffusion–reaction equations in biological matter face applications not only in patterns on animal coats but also in neurological imaging. Here the aim is functional imaging, that is a tracer material is transported by the blood stream into the brain. The brain's metabolism strongly depends on its activity. Thus the brain's activity is reflected in the reaction coefficients. Using a tracer that can be detected from the outside (either because they are emitting hard radiation that can be detected at the outside as in PET and SPECT) or strongly modify incident X-rays (such as in CT), the brain's activity patterns can be studied. Examples are given on (<http://www.bocaradiology.com/cases/neuro/>).

A more general introduction to the topic of Turing pattern in biology and to different mathematical methods is given at (http://zool33.uni-graz.at/schmickl/Self-organization/Pattern_formation/Reaction-diffusion/reaction-diffusion.html)

A non-biological application of coupled diffusion–reaction equations are material sciences, in particular the development of low-dimensional layers on surfaces. Papers [105] and [179] give excellent overviews on this topic; [180] a carefully discussed and described example. The BA thesis [138] introduces a slightly different but compact and fast model to solve these equations for nucleation on vicinal layers.

4.5 Diffusion in Porous Media

Diffusion of a substance in a fluid is based on the molecular motion of fluid and chemical and transport parameters can be derived in a rather simple model. Water resources management is interested in this problem, for instance, to determine countermeasures to be taken in the event of an oil spill. But water resources management also is interested in a related problem: the transport of water and/or pollutants through porous media. This process converts surface water to groundwater but also allows pollutants to leak from the surface into the ground water, spoiling valuable resources. The related buzzword is transport through porous media and a wealth of literature and models exists, such as [9, 10, 41, 62, 95, 96].

A porous medium such as sketched in Fig. 4.10 consist of matter in all three phases. The base is the solid phase, such as soil particles or fractured rock. Since this matter is not continuous but particulate, pores build between the particles. These pores can either be filled with a fluid, in general water, or air. The porosity ε is defined as the ratio of the volume of the pore compared to the total volume. Some of these pores, however, are irrelevant for the subsoil flow: some are entirely closed (isolated pores), thus no fluid can penetrate into them. Others are dead-end pores: they are only partially relevant for fluid transport. Thus the efficient porosity, which is relevant for transport, is smaller than the porosity.

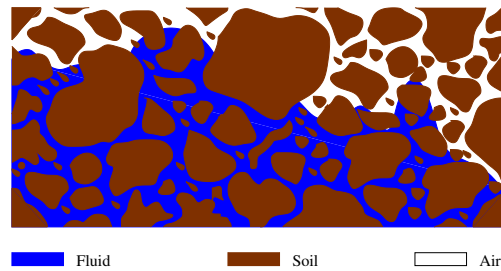


Figure 4.10: Porous medium

Soil is saturated, that is saturation $S = 1$, if the entire pore volume is filled with water: the saturated zone is the realm of groundwater. The zone between the saturated zone and the terrestrial surface is the unsaturated or vadose zone. Here the pores are filled partly with fluid and partly with air.

The flow of water through a porous medium is regulated by the volume flow Q through the surface A :

$$v_{\text{filter}} = \frac{Q}{A}. \quad (4.77)$$

This speed, also called the filtration speed or D'Arcy speed, can be determined from observational studies. It is related to the particle speed u by

$$u = \frac{v_{\text{filter}}}{\varepsilon S} \quad \text{or} \quad v = \frac{Q}{A \varepsilon S} \quad (4.78)$$

because εS describes the efficient surface available for the flow. In case of a saturated medium, the effective surface is εA ; if the medium is partly saturated, it becomes $\varepsilon S A$.

The subsoil flow (Sickerströmung) is described by D'Arcy's law [34]. It is an empirical law, derived from experiments with columns of sand. The filter speed is proportional to the pressure difference Δp at the inflow and outflow of the pipe, the effective permeability K and it is inversely proportional to the vertical length of the pipe (here only the difference in

height is relevant, not a path length along a slanted pipe):

$$v = K \frac{\Delta p}{L} . \quad (4.79)$$

The effective permeability K is related to the viscosity μ and the density ρ of the fluid and the permeability k of the soil:

$$K = \frac{k \rho g}{\mu} \quad (4.80)$$

with g being the acceleration of gravity. D'Arcy's law is valid in a large number of circumstances, however, it fails for high velocities (Reynolds' numbers exceeding 10), large pressure differences and clefted rock. The empirical part is the efficient permeability; the structure of D'Arcy's law also can be derived from the Navier–Stokes equation [62].

The more general form of D'Arcy's law allows for a three dimensional flow. Thus the scalar quantity permeability K has to be substituted by a tensor \mathbf{K} and the fraction $\Delta p/L$ by a gradient

$$\vec{v} = -\mathbf{K} \nabla p . \quad (4.81)$$

In this section we will limit ourselves to a very simple example; we will encounter D'Arcy's law again in a more complex problem in chap. 6.

Side question 24 What are similarities and differences both formally and physically between D'Arcy's law and conventional diffusion?

4.5.1 A Simple Example: Ground Penetration from an Oil Spill

In an oil spill on soil, the main question is concerned with the dependence of penetration depth from time: how much soil has to be removed to remove all oil. In our example, an oil slick of depth h_0 is deposited. It begins to seep into the ground, the vertical distance z is measured from the soil's surface downwards.

In the simplest model, we start from the mass balance in the soil:

$$\begin{array}{rcl} \text{Rate of oil in} & - & \text{Rate of oil out} & = & \text{Rate of change of oil content} \\ \rho v A & - & 0 & = & \varepsilon \rho A \frac{dz}{dt} . \end{array} \quad (4.82)$$

Here ε is the porosity of the soil and v the penetration velocity. A is a surface, ρ the density. The speed can be expressed using D'Arcy's law in the form

$$v = \frac{K}{\mu} \frac{\Delta p}{L} \quad (4.83)$$

with K as the efficient permeability of the soil and μ the viscosity of the oil. Δp is the driving force for the process, which is a pressure difference. It can be expressed as the weight per unit area of the oil column: $\Delta p = \rho g(z + h)$ with h being the variable thickness of the oil column covering the top surface of the soil. L is the depth of the porous medium in contact with the oil and thus corresponds to penetration depth z . D'Arcy's law (4.83) thus can be rewritten as

$$v = \frac{K}{\mu} \rho g \frac{z + h}{z} . \quad (4.84)$$

The penetration depth z appears in both numerator and denominator because v increases with column weight $\rho g(z + h)$ while further seeping is hindered by an increase in the soil column z already filled with oil.

To describe the system completely, a third equation is required, and that is the total oil balance:

$$\begin{array}{rcl} \text{Initial oil amount in layer} & = & \text{Oil left in layer} & + & \text{Oil in soil} \\ h_0 \rho A & = & h \rho A & + & z \rho \varepsilon A \end{array} \quad (4.85)$$

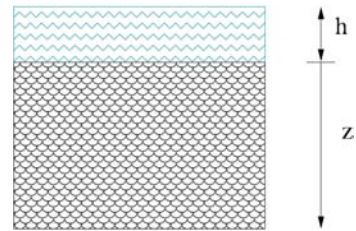


Figure 4.11: Oil layer above soil

or

$$h = (h_0 - \varepsilon z). \quad (4.86)$$

The equations (4.84), (4.82) and (4.86) can be combined into one differential equation

$$\frac{dz}{dt} = \frac{K \varrho g}{\varepsilon \mu} \left[\frac{h_0}{z} + (1 - \varepsilon) \right]. \quad (4.87)$$

This is an ordinary differential equation that can be integrated by separation of variables:

$$t = \frac{\varepsilon \mu}{K \varrho g} \left[\frac{L}{1 - \varepsilon} - \frac{h_0}{(1 - \varepsilon)^2} \ln \left(1 + \frac{L(1 - \varepsilon)}{h_0} \right) \right] \quad (4.88)$$

with L being the penetration depth at time t .

For a simple test we assume an initial height of the oil layer of $h_0 = 6$ cm, a porosity of the ground $\varepsilon = 0.7$, a permeability of the ground $K = 10^{-6}$ cm², an oil viscosity $\mu = 0.02$ Pa s, and an oil density $\varrho = 800$ kg/m³. The time it takes the oil to penetrate 4 cm into the ground then is 210 s, that is a time scale of minutes. This fast penetration into the ground results from the rather high permeability. For dense soils, it can be lower by about 2 orders. In addition, the porosity in dense soil can be as low as 0.1. The time scale then is of the order of hours rather than the minutes derived for the values above.

4.6 Phase Transitions: The Stefan Problem

Heat conduction basically can be linked to a diffusion process. The fundamental difference between heat being transferred in a liquid and a chemical diffusing through that liquid is the energetics: while in diffusion the temperature does not change and thus the process is kept alive through the thermal motion of the molecules, in heat conduction the heat is transported through the medium by collisions. If we consider a container with a liquid (such as chicken soup) and put it into a cooler environment (such as a refrigerator) heat transfer will occur from the container to its surroundings but also inside the container. And as heat is removed from the container, in parts of the liquid the temperature will drop below freezing point and the liquid will solidify. Thus heat transport can invoke a phase transition – which is related to a drastic change in inner energy.

Phase transitions are a topic in many industrial processes (e.g. steel production), in crystal growing or in traffic modeling because a traffic jam also can be viewed as a phase transition from the mobile liquid phase to the solid phase. The reverse process also can be considered, e.g. an evaporating droplet or a burning particle/beam. Oxidative degrading of organic particles in the atmosphere is an environmentally sound example.

4.6.1 The Shrinking Core Model and Quasi-Steady State

To get a first idea, we will start with a simple moving boundary problem. The general aim in modeling such processes is the temporal evolution of the system. For instance, we might be interested in a rate for crystal growth or dissolution or the time needed for a reacting particle to be consumed completely. Since the state variables of such systems in principle are functions of distance and time, normally the system is described by coupled nonlinear PDEs. Occasionally, such a system can be reduced to a set of simple algebraic equations and ODEs. This is possible if the following simplifying concepts can be fulfilled:

- the shrinking (or growing) core refers to the material contained by the moving front. Examples are a burning particle (e.g. coal dust), an evaporating droplet or a growing crystal seed. The core is assumed to have uniform properties and can be treated as an unsteady stirred tank.
- the movement of the front is slow enough to allow the transport rates outside the core to attain a quasi-steady state. This implies that as the core front slowly recedes or grows,

the rate of diffusion or conduction through the external layer quickly adjusts itself to a steady-state value given by Fick's law or Fourier's law.

- the processes involved (phase change, transport, reaction) are dominated by a single rate-controlling step.

Under these assumption, distance and time are no longer independent variables but distance (expressed through the changing size or mass of the core) becomes a dependent variable for the core's unsteady balance but is retained as an independent variable for the external, quasi-steady state balance. Time only appears in the core balance. The model thus is composed of unsteady core balances and quasi-steady-state external balances. When both mass and energy changes are involved, two such balances constitute the complete model. When there is a change in mass only, single equations suffice with the reaction rates entering the system as auxiliary relations.

After these general remarks let us turn to the problem: a solid spherical particle undergoes a reaction according to the scheme



with reaction rates r_A and r_B which are related by the stoichiometry of the reactions as follows

$$r_A = \frac{1}{b} r_B. \quad (4.90)$$

The reaction rate is fast enough to assure that all the reactant arriving at the surface of the particle is consumed instantaneously: $C_A|_{r=r_c} = 0$. The core front, on the other hand, moves slowly enough to permit the external layer of solid products to be in steady-state.

We are now looking for the time dependence of the particle radius r_C . The first task is to collect the relevant equations. The unsteady core balance can be written as

$$\begin{aligned} \text{Rate of B in} & - \text{Rate of B out} = \text{Rate of change of B} \\ 0 & - r_B = 4\pi r_C^2 \rho_B \frac{dr_C}{dt} \end{aligned} \quad (4.91)$$

with the unknown reaction rate r_B and the particle density ρ_B . The second relevant equation is the steady-state mass balance in the product layer:

$$\begin{aligned} \text{Rate of A in at } r & - \text{Rate of A out at } r_C = 0 \\ 4\pi r^2 D_{\text{eff}} \frac{dC_A}{dr} & - r_A = 0. \end{aligned} \quad (4.92)$$

Here D_{eff} is the effective diffusivity of reactant A in the product layer. This equation can be separated and integrated

$$\frac{4\pi D_{\text{eff}}}{r_A} \int_0^{C_{A_0}} dC_A = \int_{r_C}^{r_0} \frac{dr}{r^2} \quad (4.93)$$

giving

$$\frac{4\pi D_{\text{eff}} C_{A_0}}{r_A} = \frac{1}{r_0} - \frac{1}{r_C} \quad (4.94)$$

with r_0 being the initial radius of the particle, see also Fig. 4.12.

Equations (4.90), (4.91) and (4.94) describe the system completely. They can be combined into one ODE for $r_C(t)$:

$$-\frac{4\pi D_{\text{eff}} b C_{A_0}}{1/r_C - 1/r_0} = 4\pi r_C^2 \rho_B \frac{dr_C}{dt}. \quad (4.95)$$

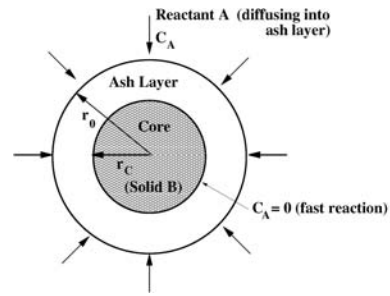


Figure 4.12: Reacting solid particle with external ash layer

Separation of variables and integration yields

$$t = \frac{\varrho_B r_0^2}{6bD_{\text{eff}}C_{A_0}} \left[1 - 3 \left(\frac{r_C}{r_0} \right)^2 + 2 \left(\frac{r_C}{r_0} \right)^3 \right]. \quad (4.96)$$

The time required for the particle to be consumed completely by the reaction then is

$$t_{\text{end}} = \frac{\varrho_b r_0^2}{6bD_{\text{eff}}C_{A_0}}. \quad (4.97)$$

Side question 25 The model is based on some assumptions. Discuss for each of them how the model must be modified if the assumption cannot be met by reality.

4.6.2 Solidification in Heat Transfer

This example attempts to model a Stefan problem for a few specialized geometries. Solidification in heat transfer is one example for a phase change problem. An ordinary heat transfer problem is a boundary-value problem: the equations and conditions on a prescribed fixed boundary are known. In case of solidification/melting the boundary of the problem is not known. Thus we must solve the diffusion or heat equation in an unknown region which has to be determined as part of the solution.

In this case, analytical solutions are possible only for extremely restricted geometries and initial and boundary conditions. Thus modeling requires numerical methods.

Problem 1: Melting in Simple Geometry

A material at its freezing temperature T_f fills the space above the x -plane. It is subject to variable temperatures $T(t, 0)$ at $x = 0$. In this case, the governing equation is

$$\frac{\partial T}{\partial t} = \frac{\partial^2 T}{\partial x^2}; \quad 0 < x < s(t) \quad \text{and} \quad t > 0 \quad (4.98)$$

with the boundary condition

$$T(t, 0) = f(t) \quad \text{and} \quad T(s(t), t) = T_f. \quad (4.99)$$

The latter equation states that at the boundary $s(t)$ between solid and liquid the temperature always is exactly at the freezing temperature. The position $s(t)$ of the moving boundary between solid and liquid phase has to be determined in this problem. The condition for this boundary (which is a second boundary condition to our problem) can be described as

$$\frac{ds}{dt} = -\alpha \left(\frac{\partial T}{\partial x} \right)_{x=s(t)}. \quad (4.100)$$

Here $\alpha = c(T_f - T_{\text{ref}})/L$ is the Stephan number with c being the specific heat capacity, L the latent heat, and T_{ref} some reference temperature. The reference temperature can be selected such that $f(t = 0) = 1$ or $\max_{0 \leq t \leq t_{\text{final}}} |f(t)| = 1$.

Although this geometry is extremely simple, it is also instructive because it allows for simple approximations and is also applies to entirely different situations such as the traffic jam in sect. 4.6.3.

Problem 2: Outward Spherical Solidification

Consider a sphere of a saturated liquid. Temperatures at its boundary are low enough to allow solidification to start. Again the governing equation is (4.98), only now it is given in spherical coordinates:

$$\frac{\partial T}{\partial t} = \frac{1}{r} \frac{\partial^2 (rT)}{\partial r^2} \quad 1 < r < s(t) \quad \text{and} \quad t > 0. \quad (4.101)$$

Boundary conditions also have to be written in spherical coordinates

$$T(r = 1, t) = f(t), \quad T(r = s(t), t) = T_f \quad (4.102)$$

and for the moving boundary

$$\frac{ds}{dt} = \alpha \left(\frac{\partial T}{\partial r} \right)_{r=s(t)}. \quad (4.103)$$

Summary of Methods

To solve one of the above problems, a number of different methods is available:

- the *enthalpy method* is a popular fixed-domain method. An enthalpy function is introduced such that the flux condition is automatically satisfied across the phase front because this can easily be recognized as a jump in enthalpy. Thus the solution is identical to the position of the jump in enthalpy.
- the *boundary immobilization method (BIM)* requires a suitable transformation such that the moving boundary is fixed. The solution then can be obtained by a finite difference method.
- the *perturbation method* only works for problems described by small Stefan numbers.
- the *nodal integration method (NIM)* is a semi-analytical method. The space-time domain is first discretized into space-time nodes. Then space-averaged, time dependent temperatures and time-averaged space-dependent temperatures are defined for each node, reducing the problem to a simple first-order ODE.
- the *heat balance integral method (HBIM)* requires a good guess for a temperature profile to start with. The heat equation then is integrated over limited parts of space to obtain a set of heat balance equations. The main idea is to subdivide the dependent variable and assume a linear profile within each subdivision.

All methods have their pros and cons (and also their limitations). They are discussed in more detail and applied to the two examples given above in [20].

4.6.3 Traffic Jam and Phase Transition

Traffic jams can be modeled in different ways, for a review see e.g. [117]. One possibility is to view a traffic jam as a phase transition. In free flowing traffic, vehicles can overtake or are outrun by others, resembling particle motion in a directed flow. In a traffic jam, however, vehicles are almost equally spaced, resembling a crystal lattice.

Within this lecture we will not dig deeper into this problem, however, one of the end-of-term-projects is concerned with the traffic jam as special form of the Stefan problem, see sect. 10.3.

Literature

The classical introduction to diffusion is Crank [32]; the chapters in Bird et al. [16] also give introductions to diffusion and heat transfer. Both books do not deal with numerical methods but provide large samples for solutions of the relevant equations for limited geometries or boundary/initial conditions. Nonetheless, they allow for a good understanding of the physical basics. Other references, in particular more specialized ones, have been given throughout the text.

A standard journal regarding transport (including theory, experiments, applications and numerics) is *Transport in Porous Media* (Springer), which is available in electronic form at the UB (click your way from the UB homepage through the steps EZB → Geologie und Paläontologie → Transport in Porous Media).

Questions

Frage 13 The diffusion coefficient is given in units of area/time. Explain why (the statement, that is is the product of a mean free path and a speed is not sufficient).

Frage 14 Explain similarities and differences between diffusion and dispersion

Frage 15 How can the diffusion coefficient be derived, how the dispersion coefficient.

Frage 16 What is the relation between diffusion and a bell curve (Gauß distribution)?

Frage 17 Can diffusion and dispersion co-exist?

Frage 18 Is diffusion limited to spatial diffusion? Why not? Give other examples.

Frage 19 Imagine milk in a cup of tea. The tea is well-stirred. Do milk molecules diffuse in this liquid? Do they move at all?

Frage 20 Sketch the derivation of a diffusion equation. What are the relevant ingredients?

Frage 21 Sketch the derivation of a dispersion equation. What are the relevant ingredients?

Frage 22 Sketch the derivation of a diffusion–convection equation. How does this differ from the derivation of a simple diffusion equation?

Frage 23 How do solutions to a diffusion problem and to a diffusion–convection problem differ? What does this tell us about the relation between the two processes.

Frage 24 A common tool for PDEs is the separation ansatz. Sketch the idea of this ansatz. Give physical examples for the application of this principle.

Frage 25 Describe the discretization of a PDE in 2D. Discuss advantages and disadvantages. Compare to methods in 1D.

Frage 26 Sketch the idea of iterative methods in the inversion of large matrices. What is the conditioning matrix?

Frage 27 Briefly sketch the ideas of convergence and amplification factor (either a general discussion or one related to the iterative methods).

Frage 28 Discuss advantages and disadvantages in the conventional approach in climate modeling: calculate atmospheric parameters for CO₂ doubling.

Frage 29 Try to develop a graphical description for the generation of Turing patterns.

Frage 30 Discuss D’Arcy’s law as one example for a phenomenological model. Try to derive it from Navier–Stokes. This basically is a decision on which terms can be neglected.

Frage 31 Discuss porosity and relative porosity.

Frage 32 What is a Stefan problem in general? Give examples. Which challenges offers a Stefan problem in modeling? Or even simpler: which quantity is the target quantity in a Stefan problem?

Focused Transport: Finite Difference Model with Splitting Scheme

This chapter is not easy reading but allows a glimpse on the problems in real world modeling. It starts from a simple one-dimensional diffusion–convection equation as encountered in chapter 4. However, since the transport equation contains additional terms, a time splitting scheme has to be introduced and the terms have to be treated differently according to the type of PDE they represent. The example is focused transport in interplanetary space, that is the equation governing the propagation of energetic charged particles from the Sun to an observer in interplanetary space, for instance Earth. The numerical schemes employed in this solution differ from the ones encountered so far in such that the transport schemes do not require a simultaneous solution of all the difference equations but solutions can advance step by step – although this comes at the expense of accuracy (most schemes are accurate to second-order only), the advantage is a very compact scheme requiring only limited computational resources. The extended version of the transport equation including the shock as a moving source of energetic particles (or formally as a moving boundary condition – a Stefan problem) is also discussed briefly.

Goals: after working through this chapter you should be able:

- to separate a complex transport PDE into subequations and discretize these according to the type of the sub-PDE.
- to explain (and apply) the concept of a splitting scheme.
- to describe the relevant transport processes in interplanetary space and their physical basis.

5.1 The Problem

Energetic charged particles from different sources populate the interplanetary medium. Some sources, such as planetary magnetospheres or the galactic cosmic radiation are continuous. Solar energetic particles (SEPs), on the other hand, are a more or less δ -like particle injection from the Sun. The motion of these particles through interplanetary space is modified by a number of processes, namely pitch angle scattering at magnetic field turbulence, focusing in the diverging interplanetary magnetic field, field parallel propagation, convection with the solar wind and adiabatic deceleration with the expansion of the solar wind. All processes combined lead to a rather complex transport equation – with a correspondingly complex numerical model.

Fits of this transport equation to solar energetic particle events observed in interplanetary space allow us to determine propagation parameters, such as the pitch angle diffusion coefficient. These results, in turn, help to understand the propagation for particles from

the continuous sources and thus allows to estimate their source strength. Therefore solar energetic particles allow us to determine Green's function of the interplanetary medium.

5.2 The Model

Our transport model is concerned with energetic charged particles, namely electrons, protons, and α -particles in interplanetary space. To develop the transport model we have to consider the interactions between particles and the interplanetary medium – thus we must help ourselves to some knowledge about the interplanetary medium. A legendary text, insightful although based on only sparse observations, is Hundhausen's *Solar Wind* [66], a more recent tutorial is given by Russell [145].

The basic features of the interplanetary medium are the solar wind and the interplanetary magnetic field (IMF). The *solar wind* is a continuous plasma flow directed radially outward from the Sun. Its basic characteristics are a density of a few particles per cm^3 at Earth's orbit, an average speed of 400 km/s and a temperature of about 1 Mio K [151, 158].

The interplanetary magnetic field has its origin in the solar magnetic field. In the equatorial plane, the coronal magnetic field is directed radially – the entire solar magnetic field topology more closely resembles a monopole than a dipole. In interplanetary space the field geometry can be described by an Archimedian spiral:¹ the footpoint of the magnetic field line rotates with the Sun at constant angular speed. On the other hand, the magnetic field is frozen-in into the radially expanding solar wind. Thus the field line is deflected from the radial into a spiral, see Fig. 5.1. The figure also might help to reduce some objections against the radial solar magnetic field: it is not a monopole field because the polarity changes – it is just a complex field with a topology that in the equatorial plane is best described as radial.

As a consequence of the Archimedian shape, the field does not decrease as r^{-2} but as

$$B(r) = \frac{B_o r_o^2}{r^2} \sqrt{1 + \left(\frac{\omega_\odot r}{u_r}\right)^2}. \quad (5.1)$$

Here r_o and B_o are distance and magnetic field at the solar surface, u_r is the radial solar wind speed and ω_\odot is the Sun's angular speed.

Fluctuations in the solar wind parameters and the supergranular motion on the Sun's surface create turbulence in interplanetary space. Since the magnetic field is frozen-in into the solar wind, the magnetic field is turbulent, too. This turbulence leads to pitch angle scattering, thus the basic process of interplanetary propagation is a stochastic process.

The magnetic field fluctuations can be described by a power density spectrum

$$f(k_\parallel) = C \cdot k_\parallel^{-q}. \quad (5.2)$$

Here k_\parallel is the wave number parallel to the field, q the slope, and C a constant describing the level of the turbulence.

¹The Archimedian spiral is the superposition of two motions: a mass moves along a rod at constant speed while the rod rotates around its starting point with constant angular speed.

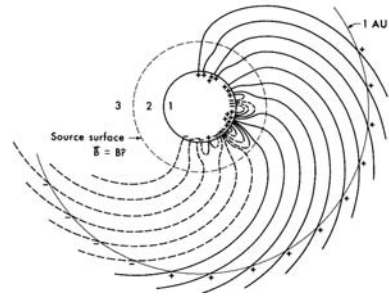


Figure 5.1: Interplanetary magnetic field [147]

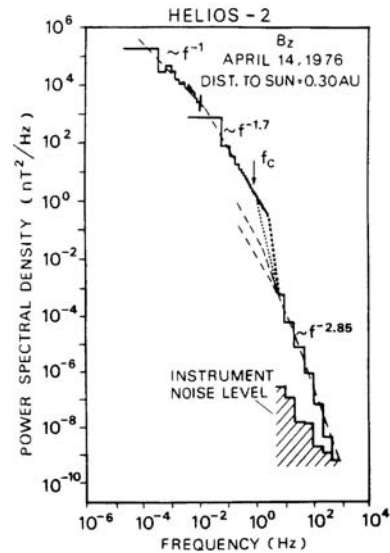


Figure 5.2: Magnetic field power-density spectrum [36]

The power density spectrum in Fig. 5.2 shows magnetic field fluctuations on different scales. Its slope is distinct in different parts of the spectrum, indicating different sources and modes of turbulence. Basically, four regimes can be distinguished: (1) Large-scale structures lasting a few days up to a solar rotation are related to the stream structure of the solar wind and to solar wind expansion. Both processes are the sources of turbulence on smaller scales; the frequencies of the large-scale turbulence are below 5×10^{-6} Hz. (2) Meso-scale fluctuations are associated with the flux-tube structure of the interplanetary medium which originates in the photospheric supergranulation. Frequencies range between 5×10^{-6} and about 10^{-4} Hz. (3) In the inertial range, mainly Alfvén waves with periods between some 20 min and more than 15 h are found, corresponding to frequencies between 10^{-4} and 1 Hz. The slope q varies between -1.5 and -1.9 . Magnetic field fluctuations in the inertial range seem to be responsible for the scattering of protons in interplanetary space. (4) The smallest scales are in the dissipation range above 1 Hz. Here the spectrum is steeper with a slope close to -3 . The observed fluctuations can be attributed to ion cyclotron waves, ion acoustic waves, and Whistlers.

5.2.1 Physical Basis

The propagation of a particle in an electromagnetic field is determined by Lorentz' force

$$\vec{F} = q \left(\vec{E} + \vec{v} \times \vec{B} \right). \quad (5.3)$$

Since the interplanetary plasma is completely ionized and densities are low, electric fields are canceled almost immediately. The Lorentz' force therefore reduces to

$$\vec{F} = q\vec{v} \times \vec{B}. \quad (5.4)$$

In a slowly varying field² the particle motion can be decomposed into two parts: a field parallel motion described by $v_{\parallel} = \mu v = v \cos \alpha$ and a motion perpendicular to the field, described by $v_{\perp} = v \sin \alpha$. Here α is the pitch angle, that is the angle between the particle's direction of motion and the magnetic field line.

The magnetic field thus introduces a special frame of reference into the description of charged particle motion: the direction of the field line. The description of the motion thus will use the length s along the interplanetary magnetic field line as spatial coordinate. The motion of the particle along the field line then is determined by a systematic process, that is focusing in the diverging interplanetary magnetic field, and by a stochastic process, namely resonant pitch angle scattering at superposed magnetic field irregularities.

5.2.2 Focusing in the Large Scale Interplanetary Magnetic Field

Focusing is related to the constancy of the magnetic moment

$$\mu = \frac{E_{\text{kin},\parallel}}{B} = \frac{mv_{\parallel}^2}{2B} = \frac{mv^2 \sin^2 \alpha}{2B} = \text{const} \quad (5.5)$$

or for two different positions and magnetic field strengths

$$\frac{\sin^2 \alpha_1}{B_1} = \frac{\sin^2 \alpha_2}{B_2}. \quad (5.6)$$

²Slowly varying field here means (a) the temporal variation is small compared to the gyration time, (b) the spatial variation perpendicular to the field is small within a Larmor radius, and (c) the spatial variation along the field is small within the field-parallel distance traversed by the particle during one gyration. If these conditions are fulfilled, the particle motion can be described by adiabatic invariants. Most prominent example for such an invariant is the constancy of the magnetic moment. It explains magnetic mirrors and magnetic bottles and thus includes the foundations of plasma confinement. The concept of adiabatic invariants and single particle motion is briefly introduced in [88]; classical texts on this topic are Alfvén and Fälthammar [2] and Northrop [122].

This short form is valid because the Lorentz force acts perpendicular to the particle's velocity. Thus particle acceleration implies a change in direction but not in speed and thus also not in kinetic energy: $E_{\text{kin}} = \text{const} \Rightarrow v = \text{const}$.

From (5.6) we can determine the change of pitch angle along the interplanetary magnetic field line because we know the variation of B with s (see (5.1)).

5.2.3 Pitch Angle Diffusion

Thus far we have not discussed the physical process of scattering. In the graphical description we have tacitly assumed that we are dealing with large-angle interactions: either the particle continues to propagate in its original direction of motion or it is turned around by 180° . Fast particles in a plasma are more likely to encounter small-angle interactions. Thus to turn a particle around, a large number of interactions is required.³

In space plasmas small-angle interactions are not due to Coulomb scattering at the background plasma but due to scattering at plasma waves. The physical processes is briefly sketched in Sect. 5.2.5; the formal description is similar to the one in spatial diffusion.

If the energy density of the magnetized plasma exceeds that of the energetic particles, the latter can be regarded as test particles gyrating around the lines of force. A particle has a pitch angle $\mu = \cos \alpha$. Each interaction leads to a small change in μ , i.e. a diffusion in pitch angle space. We can derive a scattering term strictly analogous to spatial diffusion. Equation (4.14) can be rewritten easily: the driving force for spatial diffusion, the spatial gradient, is replaced by the driving force for pitch angle diffusion, the gradient in pitch angle space. The spatial derivatives have to be replaced by a derivative to μ and the scattering term reads

$$\frac{\partial}{\partial \mu} \left(\kappa(\mu) \frac{\partial f}{\partial \mu} \right), \quad (5.7)$$

with κ as pitch angle diffusion coefficient and f as phase space density. Note that the scattering depends on μ , and thus the scattering can be different for different pitch angles, depending on the waves available for wave-particle interaction. The pitch angle diffusion coefficient can be related to the particle mean free path parallel to the magnetic field

$$\lambda_{\parallel} := \frac{3}{8} v \int_{-1}^{+1} \frac{(1 - \mu^2)^2}{\kappa(\mu)} d\mu. \quad (5.8)$$

Here λ_{\parallel} does not describe the average distance traveled between two consecutive small-angle scattering but the distance traveled before the particle's pitch angle has been changed by 90° , i.e. the direction of motion has been reversed. Thus for the overall motion, λ_{\parallel} has a meaning comparable to the mean free path in ordinary spatial diffusion.

The term (5.7) also can be used to describe spatial diffusion if we also consider the field-parallel motion μv of the particles. Thus as in the diffusion-convection equation we have to consider the streaming of particles with respect to the scattering centers. The transport equation then can be written as

$$\frac{\partial f}{\partial t} + \mu v \frac{\partial f}{\partial s} = \frac{\partial}{\partial \mu} \left(\kappa(\mu) \frac{\partial f}{\partial \mu} \right). \quad (5.9)$$

Here $\partial f / \partial s$ is the spatial gradient along the magnetic field line. This dependence is sufficient, because the motion of the guiding center is one-dimensional along the magnetic field line and the particle gyrates around it. We will encounter this equation again as part of the focused transport equation (5.14) for particles in interplanetary space.

³Collisions and the relative amount of large and small-angle interactions in Coulomb collisions are discussed in sect. C.4.2.

5.2.4 Diffusion in Momentum Space

Collisions not only change a particle's direction of motion but also its energy. This is a basic requirement in the establishment of a thermal distribution. Momentum transfer can happen by collisions between particles as well as by wave-particle interaction. If the energy gain in each interaction is small compared with the particle energy, this can be described as diffusion in momentum space. Instead of particle flow, streaming S_p in momentum results in

$$S_p = -D_{pp} \frac{\partial f}{\partial p} + \frac{dp}{dt} f. \quad (5.10)$$

Here D_{pp} is the diffusion coefficient in momentum space. The second term describes non-diffusive changes in momentum, such as ionization, and corresponds to the convective term in the spatial diffusion equation. It therefore can also be described as convection in momentum space. Again, the physics of the scattering process is hidden in D_{pp} .

5.2.5 Wave-Particle Interactions

Here we shall briefly introduce some of the basic processes of wave-particle interactions which are an example of the non-linearity of plasma physics. While for the linear aspects treated above a well-developed mathematical description is available, in the non-linear theory no general algorithms exist. Only few analytical methods are known, most of them relying on approximations. One of them is the limitation to lowest-order perturbations.

Quasi-Linear Theory

Quasi-linear theory is based on perturbation theory; interactions between waves and particles are considered to first order only. Thus all terms of second order in the disturbance should be small enough to be ignored. Only weakly turbulent wave-particle interactions can be treated this way: the particle distribution is only weakly affected by the self-excited waves in a random-phase uncorrelated way. This requirement not only corresponds to small disturbances but even directly results from it because the waves are described in the framework of perturbation theory. The waves generated by the particles will affect the particles in a way which will tend to reduce the waves. Thus we assume the plasma to be a self-stabilizing system: neither indefinite wave growth happens nor are the particles trapped in a wave well.

The basic equation is the Vlasov equation⁴ (C.39). We split all quantities into a slowly evolving average part, such as f_0 , $\vec{E}_0 = 0$, and \vec{B}_0 , and a fluctuating part f_1 , \vec{E}_1 , and \vec{B}_1 . The long-term averages vanish: $\langle f_1 \rangle = \langle \vec{E}_1 \rangle = \langle \vec{B}_1 \rangle = 0$. Note that here the quantities with index '0' are not constant background quantities but slowly evolving average properties of the system. These are the quantities we are interested in – the fluctuating quantities are of interest only in so far as they give rise to the evolution of the phase space density.

With the above ansatz, the average Vlasov equation reads

$$\frac{\partial f_0}{\partial t} + \vec{v} \cdot \nabla f_0 + \frac{q}{m} \vec{v} \times \vec{B}_0 \cdot \frac{\partial F_0}{\partial \vec{v}} = -\frac{q}{m} \left\langle \left(\vec{E}_1 + \vec{v} \times \vec{B}_1 \right) \cdot \frac{\partial f_1}{\partial \vec{v}} \right\rangle. \quad (5.11)$$

The term on the right-hand side contains the non-vanishing averages of the fluctuations and describes the interactions between the fluctuating fields and the fluctuating part of the particle distribution. These interactions combined with the slowly evolving fields on the left-hand side of (5.11) lead to the phase space evolution of the slowly varying part of the distribution. Note that we have not made any assumptions about the smallness of the fluctuations, the only limitation is a clear separation between the fluctuating part and the average behavior of the plasma.

Equation (5.11) is the fundamental equation in non-linear plasma physics. Solutions, however, are difficult to obtain because they require an a priori knowledge of the fluctuating

⁴As the Boltzmann equation, the Vlasov equation is a transport equation for phase space density in case of collisions. The Vlasov equation is the limitation to electromagnetic forces, see also sect. C.3.

fields to calculate the average term on the right-hand side. This term has the nature of a Boltzmann collision term. Note that these collisions are not particle–particle interactions but result from the non-linear coupling between the particles and the fluctuating wave fields.

If the particles and the fluctuating fields are known, the term on the right-hand side can be calculated. It can then be used to derive an expression for the scattering coefficients mentioned above which depends on particle properties, in general the rigidity,⁵ and the properties of the waves, in particular their power density spectrum as shown in Fig. 5.2.

Resonance Scattering

The scattering of particles by waves can be described as a random walk process if the individual interactions lead to small-angle scattering only. Thus a reversal of the direction of motion requires a large number of these small-angle scatters. If we assume a particle to be in resonance with the wave, the scattering is more efficient because the small-angle changes all work together into one direction instead of trying to cancel each other. Thus pitch angle scattering will mainly occur from interactions with field fluctuations with wavelengths in resonance with the particle motion along the field. Such a resonance interaction can formally be understood from a simple mechanical or electrical analogy, such as a light torsion pendulum in a turbulent gas or a resonant circuit excited by noise.

The idea is sketched in Fig. 5.3. Assume a simple model of magnetic field fluctuations (the slab model): the (relevant) waves propagate only along the magnetic field ($\vec{k} \parallel \vec{B}_0$) and the fluctuating quantities are symmetric around the wave vector. Single out a certain wave number k . A particle is in resonance with this wave if it propagates a wave length λ_{\parallel} along the magnetic field during one gyration: $\lambda_{\parallel} = v_{\parallel} T_c = \mu v T_c$. With $k_{\parallel} = 2\pi/\lambda_{\parallel}$ and $T_c = 2\pi/\omega_c$ the resonance condition can be written as

$$k_{\parallel} = \frac{\omega_c}{v_{\parallel}} = \frac{\omega_c}{\mu v} . \quad (5.12)$$

The amount of scattering a particle with pitch angle α experiences basically depends on the power density $f(k_{\parallel})$ of the waves at the resonance frequency. This dependence clearly shows why the pitch angle diffusion coefficient κ depends on μ : particles with different pitch angles are scattered by different wave numbers with different power densities.

The pitch angle diffusion coefficient is related to the magnetic field power density spectrum in interplanetary space by

$$\kappa(\mu) = A(1 - \mu^2)|\mu|^{q-1} , \quad (5.13)$$

with A being a constant related to the level C of the turbulence. The particle mean free path can then be determined by (5.8). The mean free path depends on particle rigidity as $\lambda_{\parallel} \sim P^{2-q}$, as long as $q < 2$.

An even more graphical example for resonant wave–particle interaction is stochastic acceleration. In contrast to spatial scattering here the interaction leads to scattering in momentum space. The particle interacts with the fluctuating electric field of a wave, in particular if this field rotates around the magnetic field line as in a circularly polarized wave. A particle is in resonance with the wave if its gyration frequency equals the frequency of the wave. In that case, the particle is either accelerated or decelerated continuously. Figure 5.4 shows a particle gyrating

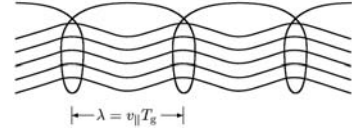


Figure 5.3: Resonance scattering

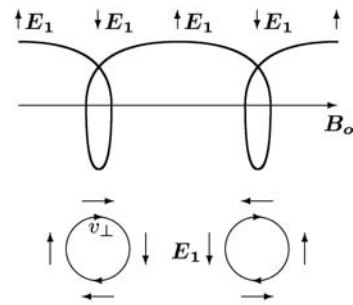


Figure 5.4: Resonant wave–particle interaction

⁵Rigidity is momentum per charge. This quantity is introduced to help in the description of the motion of particles in electromagnetic fields: particles with the same rigidity follow the same path although their momentum/speed/energy might be different. Or in other words: once a solution for the particle trajectory in an electromagnetic field has been obtained, it also describes the motion of all particles with the same rigidity.

around \vec{B}_0 together with the fluctuating electric field. To make the figure readable, the fluctuating magnetic field is not shown. In the lower panel, the two extreme cases are illustrated: depending on the phase between wave and gyro-orbit, the particle either moves parallel or anti-parallel to the electric field. Thus, either deceleration or acceleration results. In the latter case, the wave energy is converted into particle energy, and in the former case the particle energy is converted into wave energy. The resulting acceleration is called stochastic acceleration because the result (acceleration or deceleration) depends on the random phase between wave and particle.

Since the acceleration or deceleration changes the particle speed perpendicular to the average magnetic field, its pitch angle changes too. Stochastic acceleration can be described as diffusion in momentum space if the energy gain is small compared with the particle's energy (see Sect. 5.2.4). Then the accompanying change in pitch angle is small, too.

5.2.6 Solar Wind Effects

Solar wind effects can be divided into two parts: convection with the solar wind and adiabatic deceleration. Convection with the solar wind is slightly different from a conventional diffusion–convection equation for two reasons: first, the diffusion is anisotropic with a preference for the direction of the magnetic field while convection with the expanding solar wind occurs along the radial. With increasing distance from the Sun, the interplanetary magnetic field line becomes more and more oblique with respect to the radial direction. Thus convection leads to a particle transport oblique to its original direction of propagation.

The second difference to a typical diffusion–convection equation regards the relative speeds. In a standard diffusion–convection problem as described in chapter 4 the typical distances traveled per unit time by a particle during the diffusive process are small compared to the ones traveled due to advection. In interplanetary space this is true only for the slowest particles; particles with higher energies travel almost at the speed of light which is pretty fast compared to the 400 km/s average solar wind.

Adiabatic deceleration is related to solar wind expansion: as the solar wind expands, the distance between the scattering centers frozen into the solar wind increases. Thus, the “cosmic ray gas” expands too, and, therefore, cools. Adiabatic deceleration differs from the other transport processes, insofar as it changes particle momentum.

5.2.7 The Transport Equation

The transport equation has developed in two steps. The first model was developed by Roelof [140] under the name of focused transport. It only included the effects of pitch angle scattering, field-parallel motion and focusing. The applicability of the model was limited to high energetic particles: if particles are much faster than the solar wind, convection with the solar wind can be neglected. Based on this approach, Roelof gave the following transport equation:

$$\frac{\partial f}{\partial t} + \mu v \frac{\partial f}{\partial s} + \frac{1 - \mu^2}{2\zeta} v \frac{\partial f}{\partial \mu} - \frac{\partial}{\partial \mu} \left(\kappa(\mu) \frac{\partial f}{\partial \mu} \right) = Q(r, v, t). \quad (5.14)$$

Here s is the length along the magnetic field spiral, and $\zeta = -B(s)/(\partial B/\partial s)$ is the focusing length. The terms from left to right describe the field parallel propagation, focusing in the diverging magnetic field, and pitch angle scattering. The term on the right-hand side describes the particle source.

From solutions of the transport equation we can determine the phase space density as a function of time, location and pitch angle. Thus, for a fixed location not only can we determine the intensity–time profile but also the temporal evolution of the pitch angle distribution. The latter can be described as an anisotropy: if the anisotropy vanishes, particles are streaming isotropically from all directions, while for a large anisotropy particles predominantly come from one direction. An example is given in Fig. 5.5. The time development of the anisotropy can be understood quite easily. If we would look at the spatial distribution of the particles, it would spread in a similar way as suggested in Fig. 4.3. Thus the first

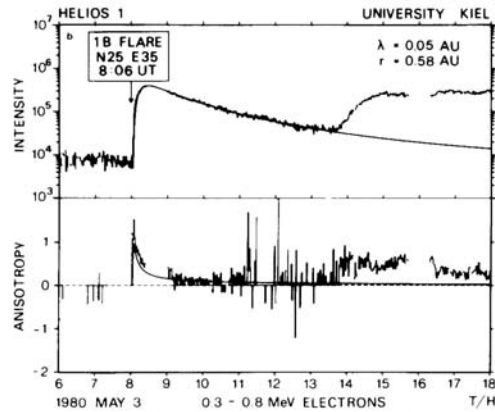


Figure 5.5: Example for a fit with the focused transport model [91]

particles always arrive from solar direction, leading to the high anisotropy early in the event. With time, more particles have reached the observer's site. Since also more particles are already swept behind the observer, the spatial gradient is reduced and therefore also the net streaming away from the Sun ceases. This can be seen as the reduction of the anisotropy with time.

The extended version, including the solar wind effects, was suggested by Ruffolo [144]. In a simplified form this equation reads

$$\begin{aligned}
 \frac{\partial F}{\partial t} &+ \frac{\partial}{\partial s} \left(\left[\mu' v' + \left\{ 1 - \frac{(\mu' v')^2}{c^2} \right\} v_{\text{sowi}} \sec \psi \right] F \right) \\
 &- \frac{\partial}{\partial p'} \left(p' v_{\text{sowi}} \left[\frac{\sec \psi}{2\zeta} (1 - \mu'^2) + \cos \psi \frac{d}{dr} \sec \psi \mu'^2 \right] F \right) \\
 &+ \frac{\partial}{\partial \mu'} \left(v' \frac{1 - \mu'^2}{2\zeta} F - \kappa(s, \mu') \frac{\partial F}{\partial \mu'} \right) = Q(t, s, \mu', p'). \quad (5.15)
 \end{aligned}$$

The distribution function $F(t, s, \mu', p')$ depends on time t , distance s along the field line, pitch angle μ' and momentum p' . The primes indicate that the latter two quantities are measured in the solar wind frame. Note that F is not the phase space density but a distribution function: in contrast to phase space density, it depends on momentum but not energy.

Equation (5.15) considers, in addition to the terms already covered in (5.14), the convection with the solar wind (the additional term in the first set of parentheses) and adiabatic deceleration (the $\partial/\partial p'$ term). This term makes numerical solutions to the transport equation even more complex since momentum is added as an additional dimension [85, 144].

5.2.8 Boundary and Initial Conditions

The model attempts to describe particle transport along the interplanetary magnetic field line, thus the model is essentially 1D: the relevant coordinate is the distance s along the field line. Spatial boundary conditions thus are relevant only for the inner and outer ends of the field line. At the inner end, that is the fieldline's footpoint on the Sun, reflection is a reasonable assumption for the boundary condition: particles propagating towards the Sun encounter a converging magnetic field and thus are likely to be reflected. Alternative assumptions could include absorption or partial reflection. Once the numerical code is running, different assumptions can be tested and compared to each other. For the outer boundary, we can either assume free escape or partial reflection. If the outer boundary is far beyond the observer's position, almost no particles come back to the observer once encountering the outer boundary. Therefore, the choice of the outer boundary's properties is almost irrelevant. To save memory and computing time, however, an outer boundary closer to the observer might be useful: in that case, a partial reflecting boundary is a reasonable choice with its reflectivity adjusted such that it roughly reflects the relative amount of particles scattered back by turbulence.

The initial conditions at time $t = 0$ are $f = 0 \forall r \neq r_{inj}$: space is empty except at the injection site. Note that the injection $Q(t, s, \mu', p')$ can be extended in time or move through interplanetary space to reflect the continuous particle injection from a propagating shock.

5.3 The Numerical Scheme

Both focused transport equations are solved by finite difference schemes. We will discuss here the numerical scheme for (5.15); a numerical scheme for (5.14) can be derived from it by neglecting the additional terms in (5.15) and their discretization. The important part of the numerical solution is the splitting scheme.

5.3.1 The Splitting Scheme

Equation (5.15) is solved with a numerical scheme based on an enhanced fractional time step and time splitting method (e.g. [107]). The basic idea of such a splitting scheme can be understood for the simplified example consisting of only spatial and pitch-angle transport. The arbitrary decision to transport first in s and then in μ' or vice versa gives two different numerical solutions, see Fig. 5.6. Obviously, transporting first in s and then in μ (triangles in Fig. 5.6) should yield different results than transporting first in μ and then in s (squares in Fig. 5.6). The differences are small for the omnidirectional intensity and more pronounced in the anisotropies. In general such an approximation is only of first order in Δt . A better result can be achieved by alternating the order of fractional time steps and hence get an approximation of second order in Δt :

$$L(t, s, \mu', p') = \frac{1}{2}L(s) + \frac{1}{2}L(\mu') + \frac{1}{2}L(p') + \frac{1}{2}L(p') + \frac{1}{2}L(\mu') + \frac{1}{2}L(s) + O((\Delta t)^2). \quad (5.16)$$

The steps of the transport therefore are

- (1) the spatial transport is advanced by half a step
- (2) the pitch-angle transport is advanced by half a step
- (3) momentum transport happens in two half steps
- (4) the pitch-angle transport is advanced by the second half step
- (5) the spatial transport is advanced by the second half step.

5.3.2 The Spatial Transport $L(s)$

The spatial transport is described by a hyperbolic differential equation:

$$\frac{\partial F}{\partial t} + \frac{\partial}{\partial s}(a(s)F) = 0 \quad \text{where} \quad a(s) = \mu'v' + \left(1 - \frac{(\mu'v')^2}{c^2}\right)v_{sw} \sec\psi. \quad (5.17)$$

In case of $v_{sw} = 0$ the equation is a well known model problem with a large variety of numerical schemes solving it. Here it is discretized by a flux limiter method, which is under optimal circumstances (low spatial gradient) of second order in space. Both a detailed discussion and a comparison to other methods can be found in [56, 57]. The advantage to other methods (e.g. [144]) is the good accuracy combined with a low computational effort.

5.3.3 The Pitch-Angle Transport $L(\mu')$

The transport in pitch angle is described by a parabolic convection-diffusion equation. The difficulty in solving numerically this equation comes from the two pitch-cosine terms which can be relative to each other of different magnitude. Close to the sun the focusing term dominates while far away the pitch-angle diffusion becomes dominant. The same problem occurs when cases with large and small scattering or a pitch-angle diffusion coefficient $D(\mu')$ with a pronounced shape shall be calculated. Usually in literature this is called a singular perturbed problem which needs special numerical treatment (e.g. [142]). A scheme constructed

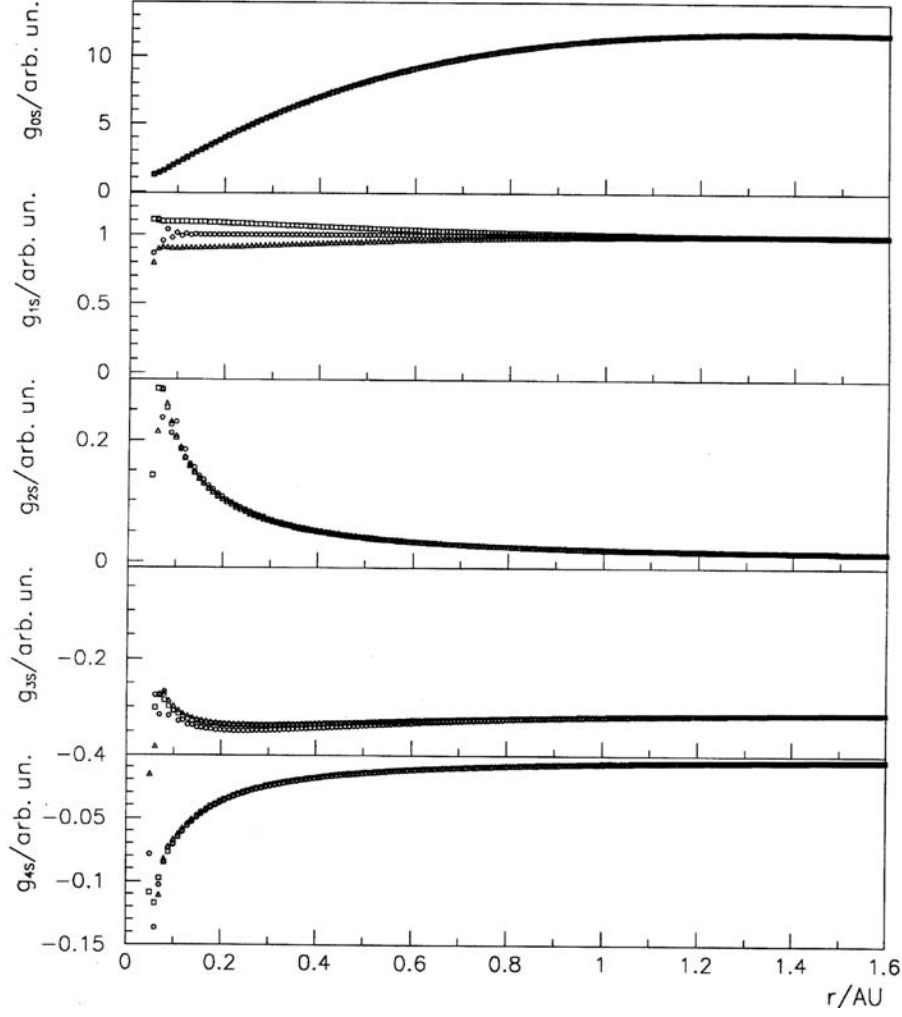


Figure 5.6: Time splitting, simplified example considering only s and μ transport. From top to bottom: omnidirectional intensity, and anisotropies of orders 1 to 4. Squares: μ transport first, then s transport; triangles: s - μ transport; circles: half step s , two half steps μ , second half step s [56]

for this type of problem is the Iljin scheme. Here the following implicit scheme, which is under optimal circumstances of second order in pitch-cosine, is used:

$$L_{\Delta\mu'} F_i = \frac{a_{i+1/2}(F_{i+1} - F_i) - a_{i-1/2}(F_i + F_{i-1})}{\Delta\mu'} - \frac{1}{(\Delta\mu')^2} [\chi_{i+1/2} b_{i+1/2}(F_{i+1} - F_i) - \chi_{i-1/2} b_{i-1/2}(F_i - F_{i-1})] \quad (5.18)$$

with the abbreviations

$$a_{i+1/2} = 1 - \mu'_{i+1/2}{}^2 \tilde{a}, \quad \tilde{a} = \frac{v'}{2L(s)}, \quad \chi_{i+1/2} = \frac{\tilde{a}\Delta\mu'}{2\tilde{b}_{i+1/2}} \coth\left(\frac{\tilde{a}\Delta\mu'}{2\tilde{b}_{i+1/2}}\right)$$

and

$$b_{i+1/2} = 1 - \mu'_{i+1/2}{}^2 \tilde{b}, \quad \tilde{b}_{i+1/2} = \left(\frac{1}{\Delta\mu'} \int_{\mu'_i}^{\mu'_{i+1}} \frac{d\mu'}{\tilde{\kappa}(\mu')} \right)^{-1} \quad \text{and} \quad \kappa_{i+1/2} = 1 - \mu'_{i+1/2}{}^2 \tilde{\kappa}(\mu').$$

If an isotropic pitch angle coefficient $\kappa(\mu') = A(1 - \mu'^2)$ is considered, the scheme is a pure Ijijn scheme. In case of a pronounced shape of $\kappa(\mu')$, a so called resonance gap around $\mu' = 0$, the averaging of $\tilde{\kappa}(\mu')^{-1}$ per $\Delta\mu'$ -interval gives better results. It is motivated by an integro-interpolation scheme (e.g. [146]), which leads to the definition of $\tilde{b}_{i+1/2}$. For a very pronounced $\kappa(\mu')$ the following choice, where the focus is on the integro-interpolation scheme, gives even better results:

$$\chi_{i+1/2} = \frac{a_{i+1/2}\Delta\mu'}{2b_{i+1/2}} \coth\left(\frac{a_{i+1/2}\Delta\mu'}{2b_{i+1/2}}\right) \quad \text{and} \quad b_{i+1/2} = \left(\frac{1}{\Delta\mu'} \int_{\mu'_i}^{\mu'_{i+1}} \frac{d\mu'}{\kappa(\mu')}\right)^{-1}$$

5.3.4 The Momentum Transport $L(p')$

The momentum transport also is described by a hyperbolic differential equation:

$$\frac{\partial F}{\partial t} - \frac{1}{\tau_D} \frac{\partial}{\partial p'} (p' F) = 0 \quad (5.19)$$

with

$$\frac{1}{\tau_D} = v_{\text{sw}} \left[\frac{\sec\psi}{2L(s)} (1 - \mu'^2) + \cos\psi \frac{d}{dr} (\sec\psi) \mu'^2 \right]. \quad (5.20)$$

As the spatial transport it is discretized by a flux limiter method. The step size in $\Delta p'$ is chosen to be constant on a logarithmic scale of momentum p' . Compared to the geometric interpolation used by Ruffolo [144], the flux limiter method has the advantage of particle number conservation even if the momentum spectrum cannot be described by a power law – which will be the case during the course of a particle event, even if the initial spectrum is a power-law, cf. Fig. 5.8.

5.4 Closure

Model tests take place in two parts. The numerical scheme can be tested for each transport mode separately by comparison to analytical solutions or established numerical codes. The combined transport modes also can be tested in such that the different transport modes are compared to each other. In the extreme case of one or two vanishing transport modes the scheme should arrive at the analytical/numerical solution of the remaining mode.

The mathematical model itself, that is the transport equation, is more difficult to test. Two aspects should be considered: (a) the reproduction of observations for reasonable parameters, such as shown for the simple model in Fig. 5.5; and (b) does the relative importance of the effects meets our expectations. Since part (a) already has been performed in connection with Fig. 5.5, we will focus on the latter part. Basically, this implies a comparison of the numerical solutions of (5.14), that is focused transport without solar wind effects, to the solution of (5.15).

Figure 5.7 demonstrates the influence of solar wind effects at different energies (20 KeV, 66 KeV, 220 keV, 730 KeV, 2.4 MeV, 8 MeV, 26 MeV, 85 MeV, 260 MeV, 711 MeV, 1.7 GeV). The observer is located at 1 AU, the radial mean free path λ_r is 0.1 AU. Two effects can be separated:

- if solar wind effects are considered (solid lines), the intensities rise earlier and consequently show an earlier maximum. This becomes most obvious in the lowest energy bands where the average particle speed is comparable to the solar wind speed. The effect can be understood as mainly due to convection with the solar wind, adiabatic deceleration contributes only a small part to this because of the energy spectrum.
- the intensity decays faster because of adiabatic deceleration which, owing to the energy spectrum, adds a rather small number of particles from the higher energies while removing a larger number to lower energies. In the lower energy ranges, convection with the solar wind also contributes to the faster removal of particles from the observer's position. Because

Figure 5.7: Intensity time profiles with (solid) and without (dashed) solar wind effects for different energies (20, 66, 220, and 730 keV, 2.4, 8, 26, 85, 260, and 711 MeV, and 1.7 GeV; the highest energies rise first, the lowest last), a δ -injection at $t = 0$, and a radial mean free path $\lambda_r = 0.1$ AU [58]

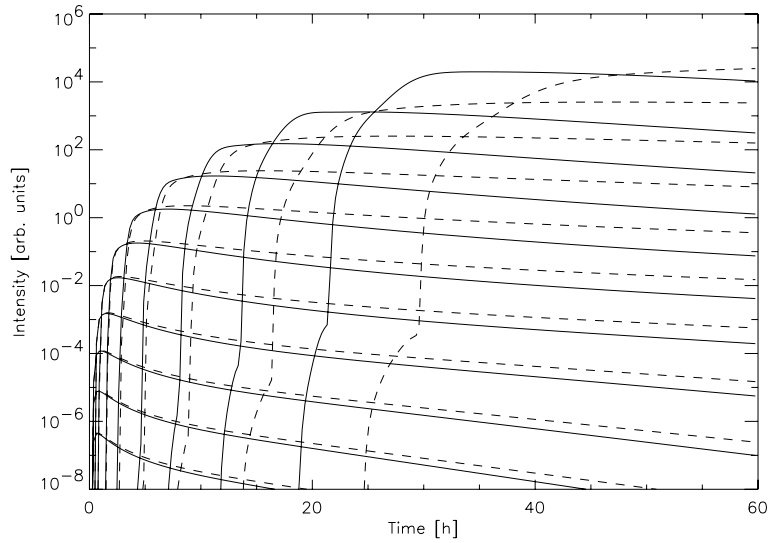
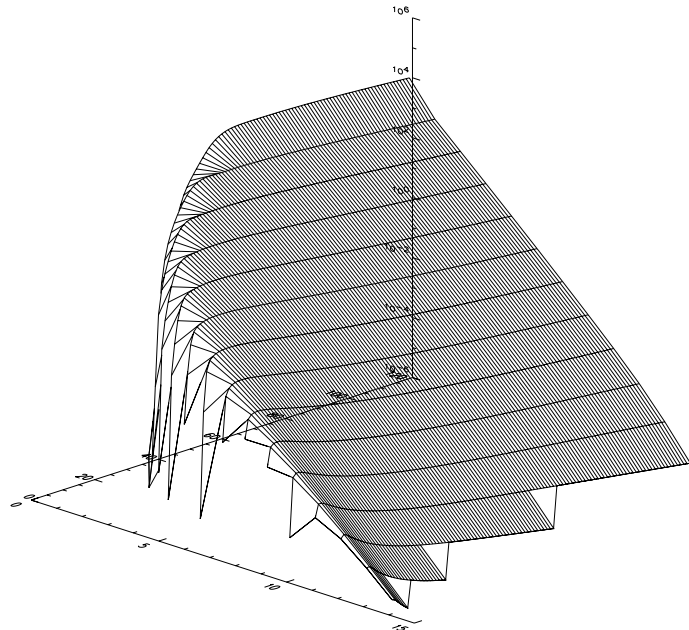


Figure 5.8: Temporal evolution from $t=0$ h to $t=60$ h of the energy spectrum in the range 20 keV to 1.7 GeV after a solar injection at $t=0$ [58]



low energetic particles acquire maximum intensity at rather late times, this removal also leads to a lower maximum intensity.

In the anisotropies (not shown in the figure) consequently a faster decay towards isotropy can be seen, at late times anisotropies even can become negative as the – in the solar wind frame isotropic – particle distribution is convected across the observer, leading to an inward directed intensity gradient and thus a streaming of particles towards the Sun.

Figure 5.8 shows the temporal evolution of the energy spectrum $I(E) = I_0(E/E_0)^{-\gamma}$ at the observer's site. The injection spectrum has a power-law index $\gamma = 2.5$ in energy. At early times, due to the late arrival of slow particles, the spectrum turns over at lower energies. Only with the arrival of the bulk of the slow particles, the spectrum turns to roughly a power-law, however, its slope is much steeper than the slope of the injection spectrum, even bending to a steeper slope at late times and high energies. Thus for most of the time of the event the description of the spectrum in interplanetary space by a power-law would be a crude simplification. Note that a similar behavior would be observed if solar wind effects were neglected, in particular the turn-over of the spectrum at low energies would be observed

up to much later times, owing to the later arrival of the low energies. If a decreasing slope has been established it would even be steeper than under consideration of solar wind effects.

5.5 Extensions

The above transport equation has been modified to accommodate interplanetary shocks. Basically, the inclusion of the shock does not change the transport equation and its numerical solution but introduces an additional boundary condition: for the shock as source of particles, the source term has been modified accordingly. To accommodate the modified focusing related to the passage of the shock and the magnetic cloud driving it, the focusing length cannot be kept constant in time but becomes time-dependent.

5.5.1 The Shock as a Moving Source of Particles

The transport equation (5.15) contains a source term on its right hand side. Normally, this source is assumed to be fixed on the Sun, extending only in time. Observations show that interplanetary shocks are efficient particle accelerators and thus also inject energetic particles. Such extensions have been proposed for Roelof's simple transport equation (5.14) for instance in [90] and tested in a multi-spacecraft study [82] as well as in a statistical study [83].

A similar extension also has been applied to Ruffolo's transport equation (5.15) for instance in [89, 85]. The idea is quite simple: just modify the source term such that it emulates the properties of a shock as particle accelerator. It should be noted, that this leads only to a black box model: the details of the acceleration process are not simulated. Instead, some acceleration and injection efficiency of the shock is assumed.

Specifying the Source

For modeling, the following details of the shock have to be specified in the model:

- (1) the shock is spherical symmetric and expands at a constant speed. Although this is physically incorrect, in particular as the shock speed decreases towards the flanks and with increasing radial distance, the results are not strongly influenced by this assumption, see also Fig. 6 in [90]. However, if we attempt to relate the inferred injection from the shock front to shock speed, this assumption has to be dropped and replaced by a more realistic motion of the cob-point (footpoint of the observer's magnetic field line on the shock front) along the shock front.
- (2) the acceleration efficiency depends on radial distance r and angular distance $\phi_{\text{con}}(t)$ from the nose of the shock and is described by a separation ansatz

$$Q = Q_o \cdot \left(\frac{r}{r_o}\right)^\alpha \cdot \exp\left\{-\frac{\phi_{\text{con}}(t)}{\phi_c}\right\}, \quad (5.21)$$

with ϕ_c being the e-folding angle of the intensity along the shock front. The injection is isotropic at the shock front, that is particles are injected into the upstream and downstream medium. In addition, a separate solar injection can be assumed, if necessary.

- (3) additional upstream turbulence (self generated turbulence) can be included (but not self-consistently).

- (4) the background magnetic field is assumed to be Archimedian. Obviously, this is not valid in the downstream medium. However, variations with downstream focusing and downstream scattering show that the assumptions about the downstream medium do not strongly influence the results of the model, see also Fig. 3 in [90].

The relevant parameters to be specified in the model then are (1) the radial particle mean free path λ_r (in a more advanced version this depends on particle rigidity: $\lambda \sim P^{0.3}$), (2) the injection $S(r, \phi)$ from the shock front, and (3) a solar injection S_\odot , if required.

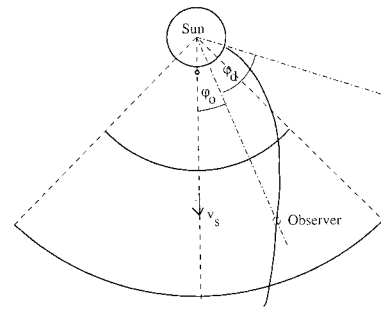


Figure 5.9: Geometry shock [85]

Figure 5.10: Intensity time profiles with (solid) and without (dashed) solar wind effects for different energies (20, 66, 220, and 730 keV, 2.4, 8, 26, 85, 260, and 711 MeV), a radial mean free path $\lambda_r = 0.1$ AU, a shock speed of 800 km/s, and constant acceleration efficiency along the observer's magnetic field line. The shock passes the observer at $t = 48$ h [89]

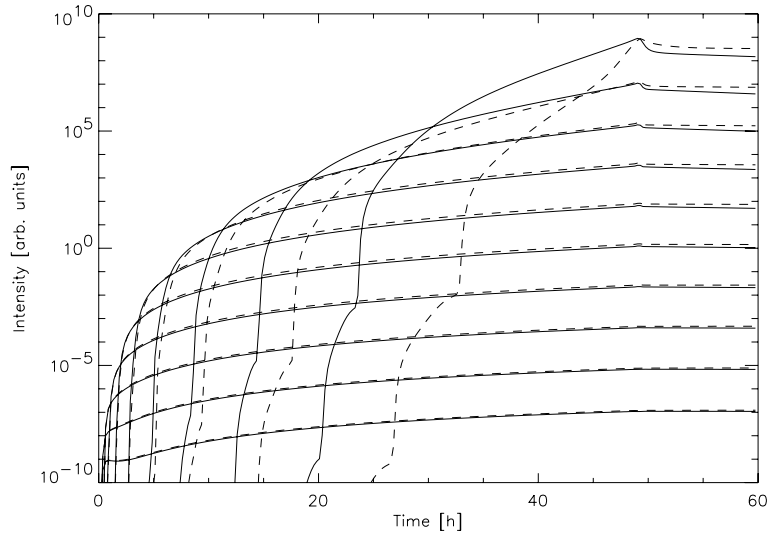
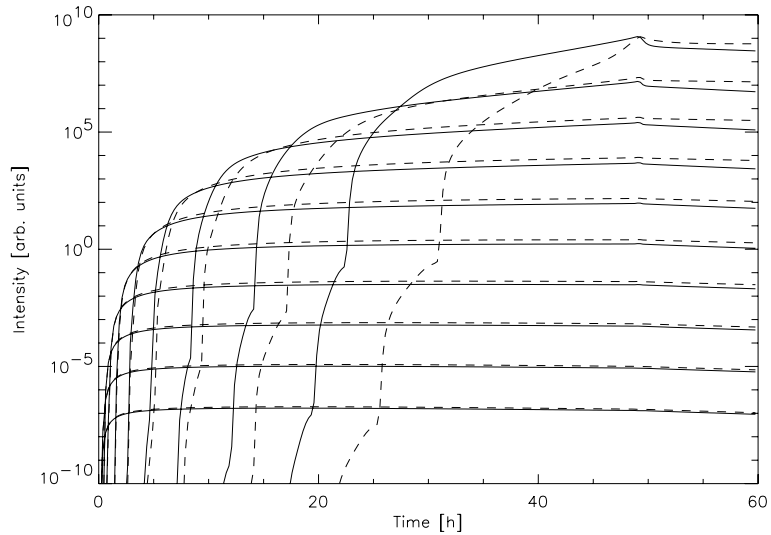


Figure 5.11: Same as Fig. 5.10 but the shock efficiency decreases as r^{-2} along the observer's magnetic field line [89].



Results

Figure 5.10 shows a comparison of the results for the standard shock of [90] (shock speed 800 km/s, observer at a radial distance of 1 AU, particle mean free path $\lambda_r = 0.1$ AU independent of particle speed, no turbulent upstream region, particle energies from 20 keV to 700 MeV, the injection from the shock is constant along the entire field line, its spectral index γ is 3.5) under consideration of solar wind effects (solid lines) and neglecting solar wind effects (dashed). The shock arrives after 48 h, the small peak in the lowest energy channel marks its arrival.

As in the case of a solar injection, the consideration of solar wind effects leads to an earlier onset. This is most obvious in the lower energies where average particle speeds are comparable to the solar wind speed. Correspondingly, the intensity increase upstream of the shock is much flatter than without consideration of solar wind effects. The typical faster decay of the intensity, however, is much less pronounced than in case of a solar injection (see also Fig. 5.7): in particular in the higher energies this decay is predominately due to adiabatic deceleration. To become effective, this process takes time, the characteristic time constant at 1 AU is a few days. In case of the continuous injection of particles from the shock, always a fresh supply of particles is added on top of the previous injections. These later injections therefore suffer less from adiabatic deceleration. As a consequence, solar wind effects are of

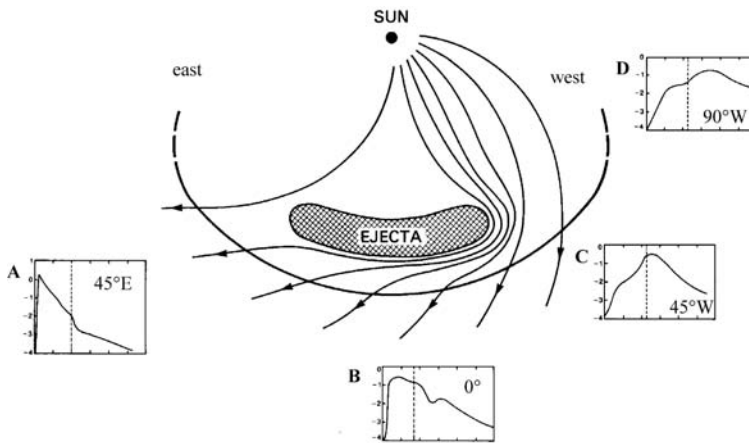


Figure 5.12: Spatial variation of particle events at shocks [23]

minor importance for energies in the MeV range or higher. This belatedly justifies the use of the more simple model by [90] for fitting particle events observed in the MeV range [82, 83].

However, we should be aware that the above statement is made for a shock with constant acceleration efficiency along the observer's magnetic field line. If the acceleration efficiency increases, the same reasoning is true. In case of a decreasing acceleration efficiency, the situation is in between the solar injection and the situation depicted in Fig. 5.10, that is although solar wind effects become more prominent they still are less pronounced than for a solar injection, as can be seen from Fig. 5.11. Note that an increase in scattering conditions leads to more pronounced solar wind effects mainly for a shock acceleration efficiency decreasing along the observer's field line but does not enhance the differences in case of constant or increasing shock efficiency. In addition, solar wind effects will increase with increasing radial distances because of the longer time scales.

Figure 5.13 shows 4 sets of intensity profiles for different locations of the observer relative to the nose of the shock. Again, shock speed is 800 km/s, the shock efficiency is assumed to not depend on radius ($\alpha = 0$) but only on azimuthal distance from the nose of the shock with a characteristic e-folding angle of 15° . These profiles reproduce the basic relations known from the observations: at the eastern flank of the shock, the intensity rises to an early maximum with the time of maximum decreasing with increasing particle energy and decreases towards the approaching shock while at the western flank the intensity continues to rise towards the shock, even in the higher energies; see also Fig. 5.12. The differences between the different locations would be more pronounced if a smaller e-folding angle is chosen (as e.g. the 10° suggested in [90]). Note that in this model the profiles further to the east/west are similar to the E80/W80 profiles except for the absolute intensity. This is a direct consequence of the separation ansatz.

5.5.2 Magnetic Cloud and Modified Focusing

A magnetic cloud is a closed magnetic blob that is ejected from the Sun. If its speed exceeds the signal speed of the medium, a shock develops. While not all magnetic clouds are fast enough to drive an interplanetary shock, all shocks are driven by magnetic clouds.

These closed magnetic structures squeeze somehow through the average interplanetary magnetic field, leading to its deformation and thus to local changes in focusing length. The focusing length enters into the pitch-angle transport term of the transport equation. In standard solutions, the focusing length ζ is determined under the assumption of an Archimedian interplanetary magnetic field. Thus ζ depends on the spatial coordinate, in this case the length s along the magnetic field line: $\zeta = \zeta(s)$. But ζ does not depend on time. This changes if we allow a shock to propagate through the interplanetary medium. Then $\zeta(s, t)$ is different from the local value in an undisturbed interplanetary medium and also depends on time.

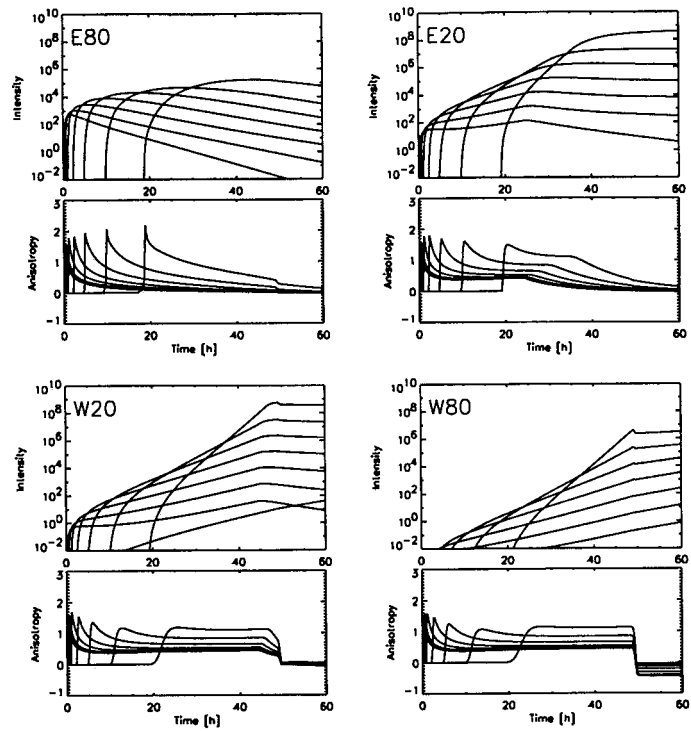


Figure 5.13: Intensity time profiles for observer at different locations with respect to the nose of the shock: for an observer on the eastern flank of the shock, the intensity rises to an early maximum and decreases towards the shock while an observer on the western flank sees a continuous intensity increase towards the shock [85]

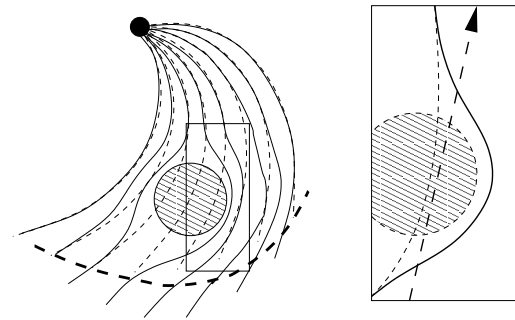


Figure 5.14: Geometry of the interplanetary magnetic field around a magnetic cloud [86]

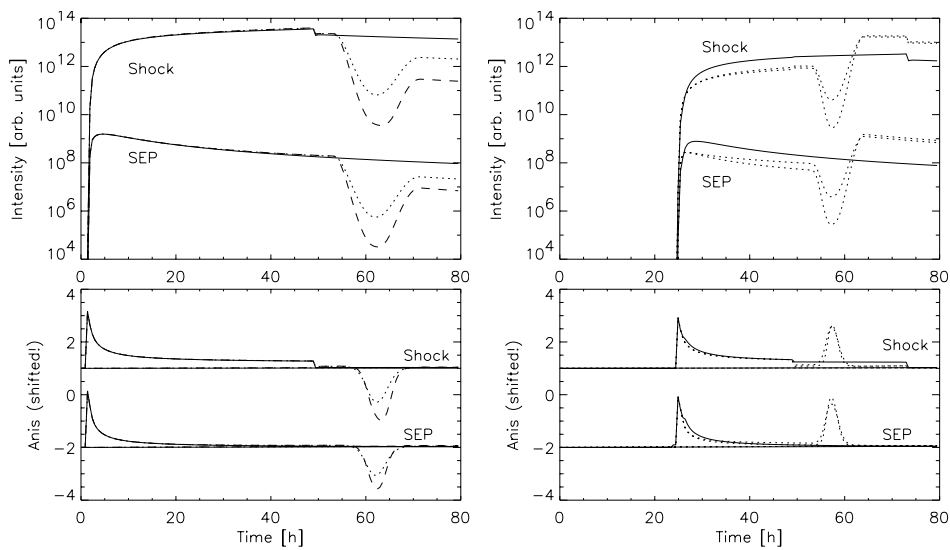


Figure 5.15: Modification of intensity time profiles by magnetic clouds [86]

Results of the numerical simulation indicate that the magnetic cloud acts as a barrier for the propagation of energetic particles, partly decoupling the media upstream and downstream of the cloud. These results have consequences for our interpretation of energetic particle events as well as our understanding of particle acceleration and interplanetary shocks and in particular the generation of extremely large events between converging magnetic clouds.

The left hand side of Fig. 5.15 shows the simulation for a standard situation: solar energetic particles (SEPs) and a magnetic cloud are injected from the Sun simultaneously. The cloud is fast enough to drive an interplanetary shock. If the deformation of the interplanetary medium by the magnetic cloud is not considered, intensity profiles as in Fig. 5.10 are expected. This is the case for the solid profiles. For the dashed profiles, the modified focusing was considered; the two profiles represent different modifications in focusing length. As a consequence, particle intensities show a depression as the cloud passes by. Downstream of the cloud, intensities are markedly reduced compared to the solid profile: particles with very small pitch angles are able to pass the cloud into the solar direction, the others are reflected back outwards. The the magnetic cloud partly decouples both parts of the medium.

The idea of the magnetic cloud as a barrier to particle propagation is employed further in the right panel of Fig. 5.15. A magnetic cloud has started at $t = 0$ from the Sun and propagates through interplanetary space. As a slow cloud it does not drive a shock: the cloud has just the barrier function but is not combined with the shock as a particle source. A day later, a conventional particle event as in the left panel starts at the Sun. The solid line gives the resulting intensity profiles if no cloud were present in the medium. These solid profiles are the same as the solid ones in the left panel. The dashed profiles are obtained under consideration of the cloud: again its barrier function is obvious: before the arrival of the cloud intensities are reduced while after cloud passage they are increased because particles are stored in the medium behind the cloud.

5.5.3 The Numerics behind the Shock

In both schemes the numerical solution of the transport equation is retained. The shock as source of energetic particles is considered in the source term on the right-hand side of the transport equation as described in the separation ansatz (5.21). This method has one general disadvantage: it can create large gradients at the injection site. For the numerical scheme presented here, large gradients do not pose a problem because the difference equations all contain a flux limiter. In addition, the stability conditions have been taken to extremes. Thus any numerical diffusion that might arise from the steep gradient is counter-balanced by small step-sizes and a flux-limiter.

An alternative scheme could treat the shock as a moving inner boundary. Formally, this corresponds to the Stefan problem. Such a solution is numerically more elegant and poses less challenge to the numerical code. But that scheme has the disadvantage that the downstream medium between shock and Sun vanishes completely. In consequence, no particles can pass through the shock and their motion has to be accounted for by introducing some arbitrary partial reflection off the shock. Thus the more consistent numerical scheme would not meet the physics. And since the downstream medium is ignored completely, such a scheme also would not be able to cover the magnetic cloud behind the shock. Its inclusion is simple, because one of the constants of the transport equation, the focusing length ζ , has to be varied in a prescribed manner in each time step of the scheme. This poses no problems to a numerical scheme as long as stability conditions are not violated. Thus again a sensible choice of the step sizes of the scheme is important.

5.5.4 Extension: Perpendicular Diffusion

One main objection against the transport equation (5.14 is the limitation in the scattering term: particle scattering is described as pitch angle scattering and thus leads, combined with the field parallel motion, to spatial diffusion along the magnetic field line only. No transport perpendicular to the field line is considered. This assumption is true as long as the only

scattering process in interplanetary space is resonant wave particle interaction as described in sects. 5.2.3 and 5.2.5.

If we also allow for conventional scattering due to (Coulomb) collisions between the particles (see also sect. C.4), transport perpendicular to the magnetic field line arises. To test the influence of such a perpendicular transport, a very simple 2D approach is made, allowing for perpendicular transport inside the plane of ecliptic only [99]. The resulting transport equation is

$$\frac{\partial f}{\partial t} + \mu v \frac{\partial f}{\partial s} + \frac{1 - \mu^2}{2\zeta} v \frac{\partial f}{\partial \mu} - \frac{\partial}{\partial \mu} \left(\kappa_{\parallel}(\mu) \frac{\partial f}{\partial \mu} \right) - \frac{\partial}{\partial z} \left(\kappa_{\perp} \frac{\partial f}{\partial z} \right) = Q(r, v, t) \quad (5.22)$$

with the additional term describing the perpendicular diffusion along coordinate z .

Although the transport equation not considers diffusion in two dimensions, this is not isotropic diffusion as for instance in a lake or in heat transport. Instead, the diffusion is anisotropic with different mechanisms and strength in the different spatial coordinates. Consequently, it is not necessary to solve transport in both directions simultaneously as discussed in sect. 4.2 but we can resort to the ADI scheme, solving transport in both spatial coordinates separately. This method has the advantage that the perpendicular transport is solved in a separate implicit scheme which later can be transported easily from the simple focused transport model (5.14) to the more advanced model (5.15) considering also the solar wind effects.

5.6 Particle Motion going Extreme

The transport of energetic charged particles through interplanetary space certainly is a very special transport problem. Is it worth to work in this field, can I sell my diploma thesis or PhD thesis to a prospective employer? Probably not under the name of interplanetary transport. But most of the numerics is not specific to interplanetary transport, only the actual numbers are taken for interplanetary transport. Instead, the process of focusing is relevant in any spatially varying magnetic field as the process of pitch angle scattering is relevant in any turbulent plasma. Thus in fact the thesis was concerned with charged particle in complex and variable electromagnetic fields rather than with interplanetary transport. This topic also interests all people working with the confinement of a plasma, for instance in chemical reactions or even more ambitious in plasma fusion. Roman Hatzky, who coded the numerical solution of (5.15), went on to a permanent position with the MPI for Plasma Physics to work on particle trajectories in the German fusion project Wendelstein (see Fig. 5.16). If a beam of energetic particles is required, such calculations also are helpful. Applications here range from plasma welding and cutting to radiation therapy with particles (see also project 5 in sect. 10.5).

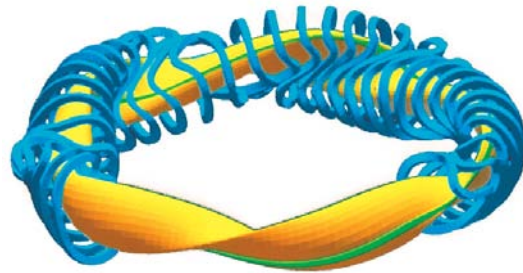


Figure 5.16: Wendelstein

Literature

This chapter is not meant as an introductory course into interplanetary propagation. Instead, it shall show that even rather simple transport equations can become more complex than described in the earlier chapters and introduce some additional topics related to PDEs. Good introductory texts to PDEs and their numerics are Pinchover and Rubinstein [128] with an approach strongly based on examples and application; a bit more formal is Knabner and Angermann [94]. More classic texts are Rubinstein and Rubinstein [143] which formerly was some kind of bible for PDE-addicts. A simpler, but also classical text is Großmann [53]; a

more modern version is Tveito and Winther [164]. The topic of flux corrected transport is discussed in detail in Kuzmin et al. [98]. The physical background to the model described here is summarized in Kallenrode [88].

Questions

Frage 33 Explain the idea behind a splitting scheme.

Frage 34 Is a splitting scheme useful in a diffusion–convection equation? What about a diffusion–convection model including decay?

Frage 35 Explain the idea of a flux-limiter.

Frage 36 Is diffusion in pitch angle space always related to spatial diffusion?

Frage 37 Explain and illustrate diffusion in momentum space.

Frage 38 Explain and illustrate wave–particle interaction.

Frage 39 Explain and illustrate the concept of resonance interaction.

Chapter 6

Dikes: Finite Element Modeling

From the viewpoint of physics, this chapter is concerned with dikes at rivers. Here high water levels can be sustained for a rather long time period. Thus the dike soaks with water (an application of transport in porous media) and eventually might become unstable. In addition, the water often is contaminated by pollutants resolved in flooded upstream areas.

Formally, this problem becomes more complex than the previous ones: we are not only concerned with losses. Thus the transport model is not limited to one equation but consists of a set of equations. This set of equations will be solved simultaneously by a finite element method instead of finite differences because finite elements provide a better approach to rather complex geometries. Most computational fluid problems (see chap. 7) also are solved by finite element methods (FEM). Since FEMs rely more strongly on software packages rather than just on a programming language, we will only sketch the principle of FEM modeling but will not go into too much detail. However, one of the projects (see sect. 10.4) also is concerned with this method. And since it is used in many interesting problems (see also chap. 7), at least you should be aware of the existence of this method.

Goals: after working through this chapter you should be able:

- to sketch the basic ideas of finite element methods and compare them to finite difference methods.

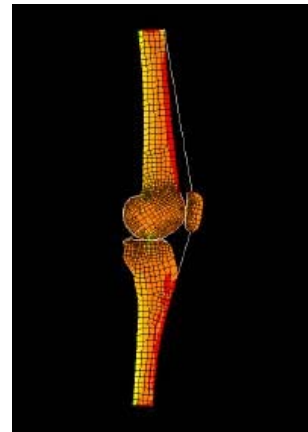
6.1 Finite Elements

Sofar, we have solved PDEs by the method of finite differences: the simulation volume is divided into steps of equal length in the relevant spatial coordinate (e.g. the three cartesian coordinates or the distance along the interplanetary magnetic field line in chap. 5). In a time-dependent solution, time also is divided into a grid of equal-sized time steps. This approach has two disadvantages:

- realistic geometries are difficult to describe,
- the equal-sized steps can be a hinderance in case of strongly varying gradients: while small step sizes are required in the presence of a strong gradient, large ones will suffice for small gradients. Thus if regions of large/small gradients fixed in space exist, a change in grid size might be desirable.¹

¹The desire for different grid sizes also can be stimulated by the geometry: in modeling ocean currents, large cells will suffice in the middle of the ocean while the terrain becomes more variable closer to the shore and thus requires simulation on a finer grid. In chap. 5 we have encountered a rather simple geometry and solved the problem with a finite difference method. However, stability dictates small spatial steps of the scheme because focusing is very strong close to the Sun. But it is weak at larger distances; stability there could be obtained with much larger step sizes. Thus either an adaptive grid or a finite element method could be chosen instead. Another example is weather prediction: an accurate prediction is required of land while

The finite element method FEM is much more suitable in cases which call for variable and non-rectangular grids. Basically, FEM divides the simulation volume into many finite elements of variable shape and size. Thus these elements can be adapted such that the relevant physical processes in this particular geometry can be described most accurately. A bending knee, such as shown to the right, involves not only a relative complex structure of finite elements. Its motion also requires, that the finite elements belonging to different parts of the simulation volume can be shifted with respect to each other. An animated version of the figure to the right can be found at http://fam.uni-paderborn.de/Forschung/Biomechanik/FE-Simulation_des_menschlichen_Bewegungsapparates.html



FEM thus often is applied in situations in which geometry calls for flexibility:

- structural design and stability, for instance bridges, crane booms or artificial hips;
- flows in realistic geometries, such as
 - heat conduction in any 2D geometry more complicated than a rectangle (and in 3D of course), for instance the temperature distribution in a building or a motor block;
 - diffusion in complex geometries such as naturally arising in aquifers,
 - computational fluid dynamics (CFD), see also chap. 7, that is all solutions to the Navier–Stokes equation in realistic geometries. This includes engineering problems (flows around an obstacle, drag on a moving body, spread of smoke from a fire in a buildings) as well as applications to natural systems (all motion in oceans and the atmosphere).
- Maxwell's equations in electrodynamics and even more complex in magnetohydrodynamics.

6.1.1 Introductory Example

Let us have a look at a rather simple daily problem related to the heat conduction equation. Assume a room with a window and a radiator beneath, such as sketched in 2D in the figure to the right. Basically we are talking about heat conduction in a rectangular plate, such as discussed earlier in sect. 4.2.1. The main differences are the assumptions about the boundaries: D_1 is an (infinitely thin) window that allows for heat escape, D_2 an infinitely thin radiator that provides heat, N_1 are partially isolated walls and N_2 is the totally isolated floor. The room is the total simulation volume Ω , the relevant variables are the temperature $T = T(x_1, x_2)$ and the heat flow \vec{j} . Both are connected by the heat transport equation

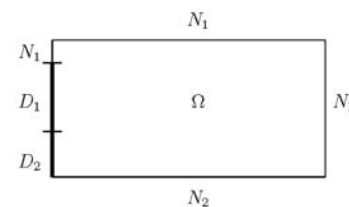


Figure 6.1: FEM: Room with boundaries [80]

$$\nabla \vec{j} = \frac{\partial j_1}{\partial x_1} + \frac{\partial j_2}{\partial x_2} \quad \text{in } \Omega, \quad t > 0. \quad (6.1)$$

This equation allows for any heat flow \vec{j} due to conduction, convection or radiation transfer. If we limited ourselves to heat conduction, the heat flow becomes $\vec{j} = \nabla T$. If we further limit ourselves to stationary conditions, $dT/dt = 0$, (6.1) is reduced to the elliptical PDE

$$\Delta T = 0 \quad \text{in } \Omega. \quad (6.2)$$

The boundary conditions verbally can be summarized as

- the temperature of the window T_w is assumed to be constant: if the room temperature T exceeds T_w , heat is lost through the window.

the prediction over the oceans can be less accurate. Thus the grid size must be much smaller over land than over the oceans. This is more easily be incorporated in a FEM than in a FDM.

- the radiator has a constant temperature T_r .
- the floor is totally isolating. Thus any heat flow through the floor vanishes. Or more formally: the normal component of the heat flow $\nabla T \cdot \vec{n}$ vanishes, with \vec{n} being the normal vector on the floor.
- the walls are partially isolated, thus heat loss is possible.

Formally, these conditions read

$$\begin{aligned} T &= T_w && \text{on } D_1, \\ T &= T_r && \text{on } D_2, \\ 0 &= \nabla T \cdot \vec{n} && \text{on } N_2, \\ 0 &= \nabla T \cdot \vec{n} + \alpha(T - T_w) && \text{on } N_1. \end{aligned} \tag{6.3}$$

Equations (6.2) and (6.3) describe an elliptical bc

This boundary system has a simple solution for $T_r = T_w$: in that case, the result is $T = T_w = \text{const.}$ in Ω . More realistic boundary conditions, such as $T_w = 10^\circ\text{C}$, $T_r = 70^\circ\text{C}$ and $\alpha = 0.05$ lead to a solution like the one shown at the right – the resulting room temperature of 20° in the right part of the room also is a reasonable result.

Note an artefact in the figure: the patterning from the FEM still is visible (at least at certain combinations of screen/printer and enlargement).

This example is meant to illustrate the principle and to introduce the boundary conditions (see below). We will not go into deeper detail here, but project 3 (see sect. 10.4) also is concerned with this problem.

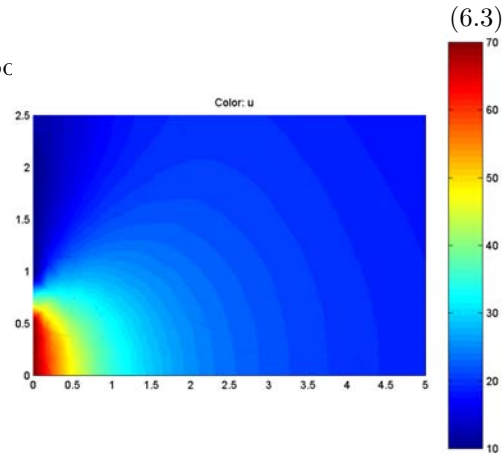


Figure 6.2: Temperature distribution in room from Fig. 6.1 [80]

Boundary Value Problem

Before we dig deeper into the details of FEM, let us briefly have a look at the boundary conditions. As mentioned above, FEM has the advantage that it can accommodate rather complex geometries and thus also complex boundary conditions. Even in the simple example, we have allowed for two different types of boundary conditions: (a) the prescribed value of the temperature at the window and at the radiator) and (b) the normal component of the heat flow through the walls.

With u being the unknown quantity and Ω being the simulation volume, the boundary conditions can be classified as

- Dirichlet boundary condition: the value of the unknown is prescribed on the boundary $\partial\Omega$: $u = g(x)$ on $\partial\Omega$;
- Neumann boundary condition: the flow of the unknown normal to the boundary is prescribed: $\nabla u \cdot \vec{n} = g(x)$ on $\partial\Omega$;
- Robin boundary condition: $\nabla u \cdot \vec{n} + \alpha(x)u = g(x)$ on $\partial\Omega$.

Boundary conditions also can be combined. For instance, in the above example we have mixed Dirichlet–Neumann boundary conditions with $u = g_1(x)$ on Γ_1 and $\nabla u \cdot \vec{n} = g_2(x)$ on Γ_2 under the condition $\delta\Omega = \Gamma_1 \cup \Gamma_2$ and $\Gamma_1 \cap \Gamma_2 = \emptyset$.

6.1.2 FEM – The Idea

Divide the simulation volume (or the region of interest) Ω into n elements Ω_e :

$$\Omega = \bigcup_{e=1}^n \Omega_e. \tag{6.4}$$

Within Ω_e an ansatz of m functions is made. These functions are different from zero only in a finite number of Ω_e . A linear combination of the ansatz functions within the element fixes the possible solutions of the numerical approximation:

$$y|_{\Omega_e} \approx \sum_{i=1}^m c_{e,n} \psi_{e,n}. \quad (6.5)$$

Both, the differential equation and the boundary conditions, are multiplied by weighting functions and integrated in Ω . The integral now can be substituted as a sum of integrals over the individual finite elements Ω_e ; the integration often will be approximated by numerical integration. Since the ansatz function often vanishes in most of the elements, the result is a large sparse system of linear equations with unknown coefficients. Such a system in principle could be solved by Gaussian elimination. However, as discussed in sect. 4.2.1, Gaussian elimination is too slow and iterative methods such as the Jacobi method or the Gauss-Seidel algorithm should be used instead.

6.1.3 FEM – The Scheme

To derive a solution with FEM, the following scheme is helpful:

- find a weak form of the differential equation under study. Little to no computerization is usually required for this step, the transformation is done by hand on paper.
- fractionalize/discretize the weak form over the simulation volume and determine size and shape of the basic elements. This can be done by hand in a simple 1D problem (as will be described below) but requires computational aid in a more complex problem. The result is a large but finite dimensional linear problem.
- Solve it – basically you encounter the same techniques of matrix inversion as already discussed for the finite difference methods.

Weak Form and Weak Solution

Most PDEs involve the Laplace operator Δ , that is we are looking for a function that has to be differentiated twice. The weak form of such a problem implies the reduction of the original PDE to a form in which the unknown function has to be differentiated only once. Let us start from the elliptical boundary problem

$$\Delta u = f \quad \text{in } \Omega \quad \text{with} \quad u = 0 \quad \text{on } \partial\Omega. \quad (6.6)$$

Let us now multiply this equation with a function v with $v = 0$ on $\partial\Omega$. Application of Gauss' divergence theorem then yields

$$\begin{aligned} \int_{\Omega} f v \, dx &= \int_{\Omega} \nabla(\nabla u) v \, dx = \int_{\Omega} \nabla(v \nabla u) \, dx - \int_{\Omega} \nabla u \cdot \nabla v \, dx \\ &= \int_{\partial\Omega} v \nabla u \cdot \nu \, dx - \int_{\Omega} \nabla u \cdot \nabla v \, dx = - \int_{\Omega} \nabla u \cdot \nabla v \, dx = -\Phi(u, v). \end{aligned} \quad (6.7)$$

Thus we are looking for a function u that vanishes on the boundary $\partial\Omega$ such that for any function v that vanishes on $\partial\Omega$ the relation

$$\int_{\Omega} \nabla u \cdot \nabla v \, dx = - \int_{\Omega} f v \, dx. \quad (6.8)$$

is fulfilled. Since now we use the ∇ -operator instead of the Laplace operator Δ , our solution has to be differentiated once and not twice. This is called the weak form of the PDE.

Thus one aspect of FEM is the reduction of the problem: the solution approach is based on either eliminating the differential equation completely (steady-state problems) or rendering the PDE into an equivalent ODE which then can be solved using standard techniques such as finite differences.

Figure 6.3:
Discretization in 1D
FEM (left) and basis
functions (right)

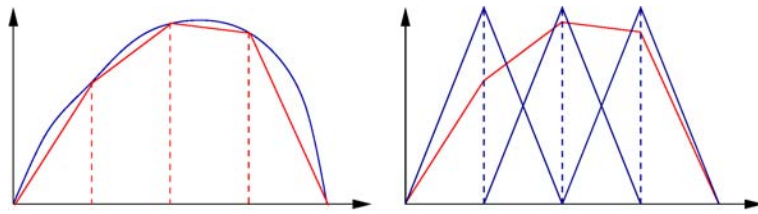


Figure 6.4: Tessellation according to Escher: although the irregular shape and the different sizes of the individual elements in FEM is possible, such an elaborate tessellation in general is not required



Fractionalization/Discretization

Fractionalization is concerned with the division of the space Ω in which the equation is defined into a number of subsets. It is essentially the same process as the discretization in FDM; consequently, the terms fractionalization and discretization can be used interchangeably.

The simplest approach is the use of piecewise linear subspaces. Figure 6.3 shows this approach for a 1D problem. The function (blue) vanishes at the boundaries of the interval $[0,1]$: $u(0) = u(1) = 0$. It is approximated in the interval $[0,1]$ by a function (red) that is piecewise linear between the nodes (vertical dashed lines). A similar method of piecewise linear approximation also can be applied to higher dimensional problems: an area, for instance, can be divided into triangles (triangulation).²

The discretization in the 1D case on the left hand side in Fig. 6.3 is quite similar to the discretization known from FDM. Formally, this discretization creates a finite dimensional subspace V with n x values such that the interval is covered continuously and that the function is linear between adjacent nodes. Note that this requirement implies that the function is not differentiable in the nodes.

To complete the discretization, we must select a basis of V . In this 1D case we chose a piecewise linear function (Zeltfunktion in German) that is 1 at the corresponding node and decreases to 0 at the two adjacent nodes. Thus this function is a unique function in V in such that is 1 at one node and 0 at all other nodes.³

Owing to this choice of the basis functions, their inner products

$$\langle v_j, v_k \rangle = \int_0^1 v_j v_k \, dx \quad \text{and} \quad \Phi(v_j, v_k) = \int_0^1 v_j' v_k' \, dx \quad (6.9)$$

²Note that the linear in piecewise linear is not necessarily required: elements also can have a curved shape. But for the understanding of the method, the assumption of piecewise linear elements is sufficient. And it is really not necessary to try tessellations like the ones typically associated with M.C. Escher, see also Fig. 6.4

³The term finite element in FEM is used not unambiguously: some authors refer with element just to the element obtained from the discretization while others refer to the basis functions and a third group refers to the combination of element and basis functions.

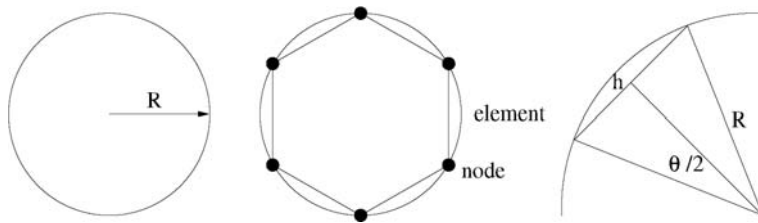


Figure 6.5: Finite element method to determine π

vanishes for almost all j, k . In the 1D case, the support of v_k is in the interval $[x_{k-1}, x_{k+1}]$. Thus the integrands of $\langle v_j, v_k \rangle$ and $\Phi(v_j, v_k)$ are identical to zero whenever $|j - k| > 1$.

The Linear System of Equations

With the series

$$u(x) = \sum_{k=1}^n u_k v_k(x) \quad \text{and} \quad f(x) = \sum_{k=1}^n f_k v_k(x) \quad (6.10)$$

we can rewrite (6.8) as

$$-\sum_{k=1}^n u_k \Phi(v_k, v_j) = \sum_{k=1}^n f_k \int v_k v_j \quad \text{for } j = 1, \dots, n. \quad (6.11)$$

The linear set of equations can be written as

$$-\mathcal{L}\vec{u} = \mathcal{M}\vec{f} \quad (6.12)$$

with \mathcal{L} being the stiffness matrix (Steifigkeitsmatrix) and \mathcal{M} being the mass matrix (Ladevektor). $\vec{f} = (f_1, \dots, f_n)^T$ and $\vec{u} = (u_1, \dots, u_n)^T$ are column vectors and \mathcal{L} and \mathcal{M} are matrices with

$$\mathcal{L} = (L_{ij}) = (\Phi(v_i, v_j)) \quad \text{and} \quad \mathcal{M} = (M_{ij}) = \left(\int v_i v_j \right). \quad (6.13)$$

6.2 Simple 1D Examples

In this section two 1D examples are presented as introduction to FEM. Since a 1D geometry is very simple, our attention is not absorbed by the geometrical definition of the finite elements but by the method how these elements are connected and thus how the equation is solved.

6.2.1 First Encounter with π

π is defined by the relation between the perimeter or the area of a circle and its radius. Thus to determine π we need a measure for these quantities. While the method using the area is used as illustration for a Monte Carlo simulation in sect. 8.1.1, we will use the perimeter as an illustration for the finite element method.

The method is illustrated in Fig. 6.5. To calculate the perimeter of the circle with radius R , follow these steps:

1. Finite element discretization: discretize (or fractionalize) the circle into a mesh with n nodes and n elements; in the middle panel in Fig. 6.5 n is chosen to be 6.
2. Determine a local approximation on the solution: since we are interested in the length of the arc of each element, the length of the chord

$$h = 2R \sin \frac{\theta}{2} \quad (6.14)$$

is a reasonable approximations.

3. Assemble the finite element equations: we have to collect all elements to get a representation of the whole system:

$$P_n = \sum_{i=1}^n h_i = \sum_{i=1}^n 2R \sin \frac{\theta_i}{2} = \sum_{i=1}^n 2R \sin \frac{\pi}{n} = 2nR \sin \frac{\pi}{n}. \quad (6.15)$$

4. Obtain the solution: inserting $n = 6$ gives $P_6 = 6R$.
 5. Test/analyse the solution: since we know the expected result, an increase in n might be the most reliable test: $P_{10} = 6.1803$, $P_{50} = 6.2791$, $P_{100} = 6.2822$ und $P_{1000} = 6.2832$. For the limiting case $n \rightarrow \infty$ we will obtain

$$\lim_{n \rightarrow \infty} P_n = 2\pi R. \quad (6.16)$$

6.2.2 Longitudinal Tank

The longitudinal tank has been discussed in detail in chap. 3, its steady-state solution in sect. 3.2. We can solve this example also with a finite element method.

With $p = -u/D$ and $q = -\gamma/D$ we obtain for the standard form of ODE (3.2)

$$c'' + pc' + qc = 0 \quad (6.17)$$

with the boundary conditions

$$c_{\text{in}} = c(0) - \frac{D}{u} c'(0) \quad \text{or} \quad c'(0) = -p(c(0) - c_{\text{in}}) \quad (6.18)$$

and

$$c'(L) = 0. \quad (6.19)$$

Since the tank is well mixed vertically and laterally, the relevant coordinate again is length along the axis of the tank. This extension is divided into n steps of length h . As in the finite difference scheme, the resulting system consists of n elements and $n+1$ -nodes from x_0 to x_n .

We now multiply the ODE (6.17) with a smooth function ν and integrate over the simulation interval $[0, L]$:

$$\begin{aligned} 0 &= \int_0^L (c''pc' + qc) \nu \, dx = [c'\nu]_0^L - \int_0^L c'\nu' \, dx + \int_0^L pc'\nu \, dx + \int_0^L qcv \, dx \\ &= c'(L)\nu(L) - c'(0)\nu(0) - \int_0^L c'\nu' \, dx + \int_0^L pc'\nu \, dx + \int_0^L qcv \, dx. \end{aligned} \quad (6.20)$$

Let us now write $c(x)$ as a series with

$$c(x) = \sum_{k=0}^N \alpha_k \Phi_k(x) \quad \text{and} \quad \nu(x) = \Phi_i(x) \quad (6.21)$$

with

$$\Phi_i(x_k) = \begin{cases} 0 & \text{for } i \neq k \\ 1 & \text{for } i = j \end{cases} \quad \text{and} \quad c_i \approx c(x_i). \quad (6.22)$$

This series is defined at all nodes; the smooth function $\nu(x)$ just serves in a similar fashion as the Kronecker- δ : it defines which term in an integrand vanishes for a certain node and which not.

Inserting the series into (6.20) yields

$$-\sum_{k=0}^n \alpha_k \Phi'_k(0) \Phi_i(0) - \sum_{k=0}^n \alpha_k \int_0^L \Phi'_i \Phi'_k \, dx + p \sum_{k=0}^n \alpha_k \int_0^L \Phi_i \Phi'_k \, dx + q \sum_{k=0}^n \alpha_k \int_0^L \Phi_i \Phi_k \, dx = 0.$$

The first term can be evaluated directly, giving

$$p(c(0) - c_{\text{in}})\Phi_i(0) - \sum_{k=0}^n \alpha_k \int_0^L \Phi_i' \Phi_k' dx + p \sum_{k=0}^n \alpha_k \int_0^L \Phi_i \Phi_k' dx + q \sum_{k=0}^n \alpha_k \int_0^L \Phi_i \Phi_k dx = 0 .$$

Rearrangement of the terms gives

$$p\alpha_0 \Phi_i(0) + \sum_{k=0}^n \alpha_k \left(- \int_0^L \Phi_i' \Phi_k' dx + p \int_0^L \Phi_i \Phi_k' dx + q \int_0^L \Phi_i \Phi_k dx \right) = p c_{\text{in}} \Phi_i(0) . \quad (6.23)$$

The terms Φ_k and Φ_k' directly are related to the elements of the FEM:

$$\begin{aligned} \Phi_k &= \begin{cases} (x - x_{k-1})/h & x \in (x_{k-1}, x_k) \\ (x_{k+1} - x)/h & x \in (x_k, x_{k+1}) \end{cases} \\ \Phi_k' &= \begin{cases} 1/h & x \in (x_{k-1}, x_k) \\ -1/h & x \in (x_k, x_{k+1}) \end{cases} \quad k = 1, 2, \dots, n-1 . \end{aligned} \quad (6.24)$$

Thus (6.23) can be rewritten as a system of $n+1$ algebraic equations which again can be written in the form of a tridiagonal matrix

$$\begin{bmatrix} a_{0,0} & a_{0,1} & 0 & 0 & \dots & 0 \\ a_{1,0} & a_{1,1} & a_{1,2} & 0 & \dots & 0 \\ \vdots & \ddots & \ddots & \ddots & \dots & \vdots \\ 0 & 0 & 0 & \dots & a_{n,n-1} & a_{n,n} \end{bmatrix} \begin{bmatrix} c_0 \\ c_1 \\ \vdots \\ c_n \end{bmatrix} = \begin{bmatrix} p c_{\text{in}} \\ 0 \\ \vdots \\ 0 \end{bmatrix} \quad (6.25)$$

with

$$\begin{aligned} a_{0,0} &= a_{n,n} = -\frac{1}{h} + \frac{p}{2} + \frac{qh}{3} , \\ a_{k,k} &= -\frac{2}{4} + \frac{2qh}{3} & k = 1, 2, \dots, n-1 \\ a_{k,k-1} &= \frac{1}{h} - \frac{p}{2} + \frac{qh}{6} & k = 1, 2, \dots, n-1 \\ a_{k,k+1} &= \frac{1}{h} + \frac{p}{2} + \frac{qh}{6} & k = 0, 1, \dots, n-2 . \end{aligned} \quad (6.26)$$

Again, the problem of solving the ODE is reduced to the inversion of a matrix.

Note that all numerical methods for the longitudinal tank problem become inaccurate if dispersion is decreased. The stability criterion again is

$$h \leq \frac{2D}{u} . \quad (6.27)$$

Side question 26 Is it surprising that this is the same stability criterion as in FEM? Substantiate your answer.

6.3 Application: Dikes

FEM has its advantage in geometries deviating from equidistant rectangular grids. In this section we will discuss dikes as an application for FEM because (a) most of the physics is already known from previous chapters and (b) although not rectangular, the dike still has a rather simple shape and consequently does not require very complex shapes for its elements. In addition, we still limit our analysis to a prescribed flow and are not forced to solve the Navier–Stokes equation selfconsistently.

6.3.1 The Problem

For most people, a dike simply is a hill made of sand. Dikes exist at the coast (in particular the German and Dutch tidelands) and at rivers. These applications require different kinds of dikes because the forces applied to the dikes are different. A coastal dike is subject to occasional strong forces during storm tides with a high water level lasting on the dike for

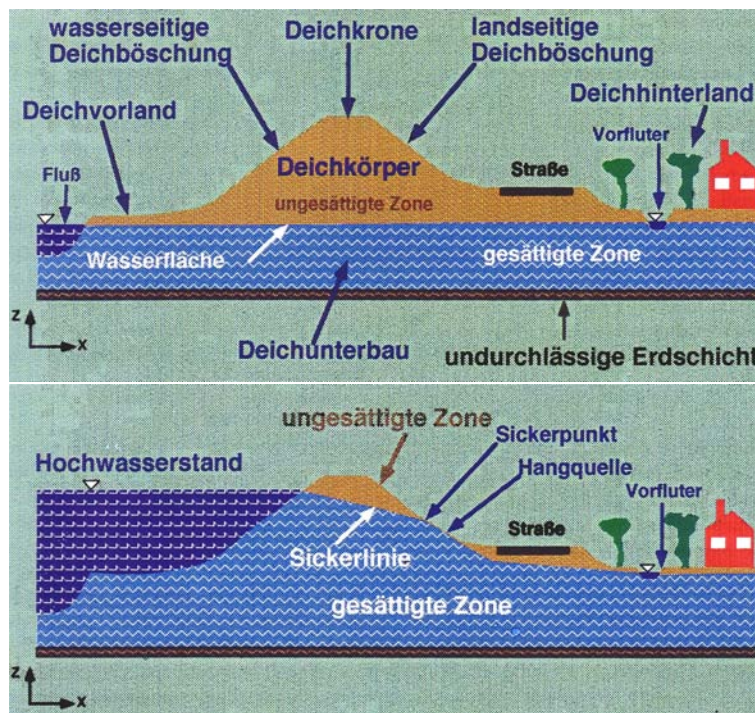


Figure 6.6: Dike during normal and high water levels [37]

some hours. Here the main risk is mechanical damage due to surges that sweep over the dikes top and might wash out its steeper back slope.

The situation is entirely different at a river. Here the flood lasts for days to weeks, e.g. due to heavy precipitation as in the Oderflut in 1997, the Weichselflut in 2001 or the Elbeflut in 2002 – all consequences of a particular weather pattern called Vb which also caused the flooding in Switzerland in 2005 – or due to heavy spring snow melt. The flood is not accompanied by high waves, thus mechanical damage as in coastal dikes is not expected. Instead, the main problem is soaking of the dike, that is the intrusion of water into the pores of the dike. Consequences are twofold: the short term problem is a weakening of the mechanical structure which eventually might lead to a total failure of the dike. The long term consequence regards pollutants: with the water also pollutants infiltrate the dike which in turn might be absorbed by the dikes grass cover and then enter the human food chain via sheep grazing on the dike to keep the grass short and thick to protect the dike.

Figure 6.6 illustrates the problem: under normal conditions (upper panel) the dike is not saturated while the soil below it is saturated up to water level. Open water (which defines this level) is the river and the flow in the run-off ditch (Vorfluter). During a flood, however, open water levels on the water side are much higher than usual. As the dike gets soaked with water, the saturation line (Sickerlinie) moves upwards, still connecting the water levels in the river and in the run-off ditch. When the saturation line intersects the landwards embankment, water leaks out of the dike at the Sickerpunkt, eventually forming an embankment spring (Hangquelle).

6.3.2 The Model

The model is constructed such that both questions can be answered: (a) dike stability against mechanical failure and (b) concentrations of toxic matter in different layers of the dike – a toxic in the dikes very core would not be harmful because it would not be absorbed by vegetation and just stay there. Both questions are interrelated because they depend on how fast and how far water infiltrates the dike.

The Problem: Processes of Dike Failure

To answer these questions, we also must be aware of the factors that might cause dike failure. This is a rather large number of processes; the most important ones include:

- breaking or sliding of the embankment (Böschungsbruch, Böschungsrutschen): this is of particular importance as water retreats. Soaked sand loses its stability because the grains no longer interlock – the water serves as some kind of lubricant. As long as the water level is high, the pressure exerted by the water guarantees the dike's stability. As the pressure is reduced, the embankment follows the pull of gravity and just slides down the dike's slope. The consequences for the remaining dike (and the chance that this process occurs) increase with increasing infiltration depth and decreasing water pressure from the outside. Thus both quantities must be known to evaluate this effect.
- surface erosion of the embankment: as the water infiltrates larger and larger parts of the dike, it might seep through the entire dike and leave it on the land side in an embankment spring (Hangquelle). Since the water is moving fast, erosion is strong and might lead to mechanical failure. In particular, since water leaks from the dike in its lower portion, erosion might lead to a failure of the entire landside embankment which reduces dike stability strongly.
- suffosion in the dike's body and underground: sand and soil are a collection of grains of very different sizes. If only large grains were present, large cavities would form between the grains. In reality, such cavities do not exist but are filled to a large part with smaller grains. But smaller grains are mobile and can be carried away by a strong subsoil flow (Sickerströmung). Thus unstable cavities might form which in time collapse and weaken the mechanical structure of the dike.
- contact erosion at the boundary of layers with different grain sizes: a subsoil flow parallel to such a boundary might wash out fine grains from the cavities of the coarse-grained soil. In consequence, coarse-grained soil might collapse into the fine-grained part, leading to a mechanical instability. Again, to describe this effect, the subsoil flow must be known.
- shear failure due to erosion, hydraulic base failure (Erosionsgrundbruch, hydraulischer Grundbruch): if flow speeds below the dike are large, in particular close to the run-off ditch (Vorfluter) erosion sets in. In time, a layer underneath the dike will be washed out and collapse, leading to a complete mechanical failure of the dike.
- buoyancy (artesian pressure): in certain dike geometries (see Fig. 6.7) a layer of Klei⁴ lies underneath the dike. Since water cannot penetrate through this layer, in time a high pressure might build up below this layer just lifting the dike. Don't lean on it – you might push it a few meters away from its original side (in particular in case of closed Klei-layers as in geometry 4).
- overpressure of water: this again is a problem related to retreading water levels: while the high water level persists, in time the water pressure in the dike rises as it is soaked with water. When the water retreats, the outer water pressure drops down while the water pressure inside the dike still is high, eventually lifting the embankment from below and allowing it to slide down the dikes side.

Note that a successful model must be able to cover all these possible mechanisms of failure in such a way that it returns the relevant parameters such as pressure heights and speed of the subsurface currents that are required to assess the risk for a certain failure.

Dike Geometries

Dikes are not manufactured at a plant and then placed in nature. Instead, they are built from material locally available and suitable for dikes. Thus albeit from the outside dikes all look the same, their internal structures can be quite different. This holds in particular for the distribution of water blocking layers, such as Klei. Figure 6.7 shows different internal

⁴Sorry, I did not find an English word for this. But you can check LEO's discussion forum on this topic: <http://dict.leo.org/cgi-bin/dict/urlexp/20050427151856>.

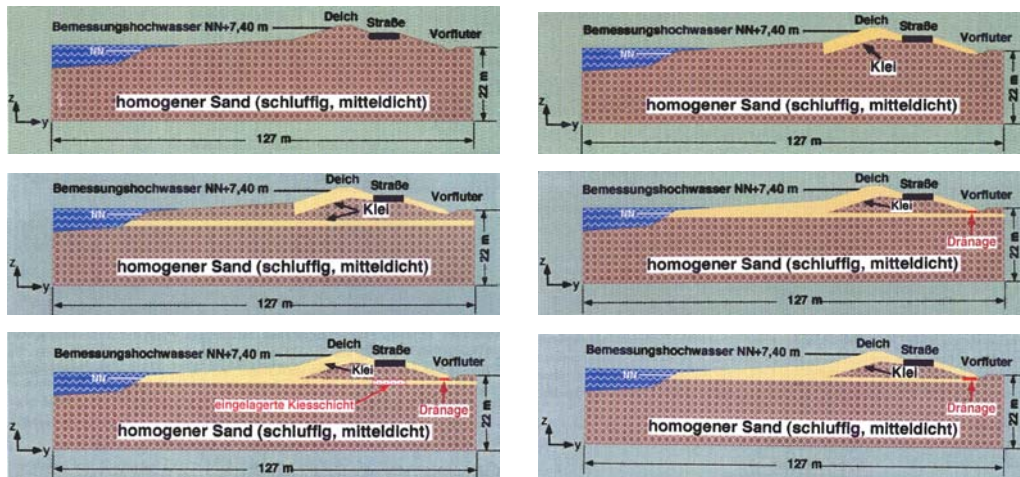


Figure 6.7: Different dikes, for explanation see text [37]

structures of dikes. Note that the external geometry always is the same, only the usage of building material has been different.

1. the topmost dike is a simple hill of homogeneous sand with the typical street (Deichverteidigungstraße) on its landside. The sand hill is covered with grass (except for the street, of course).
2. the second dike is covered by a Klei-layer which reduces water transfer into the dike and thus prevents the dike from soaking during heavy rain. It also prevents soaking during high water levels.
3. owing to the topography of that particular region, in the third case the dike geometry is essentially the same as in the second one – besides from a continuous natural layer of Klei below the entire dike – and also below NN. Note that the Klei layers do not form a closed envelope but the natural layer below and the artificial layer on top of the dike are separate layers.
4. similar geometry as in case 3 but the natural bottom Klei-layer and the top Klei-layer form a closed envelope around the dike. Thus basically no water will be able to enter the dike – doesn't that sound good?
5. again a similar geometry but below the street the bottom Klei-layer is removed and substituted by coarse gravel (just for the sake of the street's stability in case it is required to defend the dike).
6. the last dike again has a closed Klei-envelope – only here the bottom Klei-layer does not extend beyond the run-off ditch (Vorfluter).

Physical Basis

To account for the different possible mechanisms of dike failure as discussed above, the physical model of the dike must keep track of the following quantities

- the total pressure level in- and outside the dike,
- the water pressure level in- and outside the dike,
- the subsoil flow speeds,
- the relative amount of water inside the dike,
- as well as concentrations and flow speeds of pollutants.

The Model Equations

- the equations of continuity for

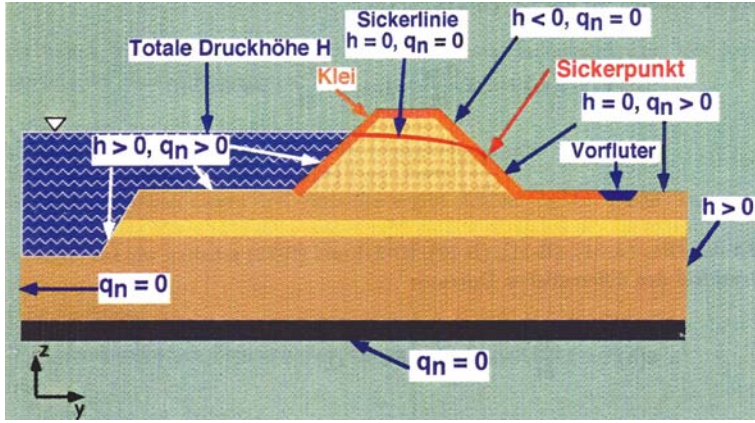


Figure 6.8: Boundary conditions at the dike [37]

– water:

$$\frac{\partial}{\partial t} (S n_e \rho_w) + \nabla (S n_e \rho_w \vec{v}_s) + \nabla (\rho_w \vec{v}_{rs}) = 0 \quad (6.28)$$

with S being the saturation, n_e the effective porosity, ρ_w the density of water, \vec{v}_{rs} the fluid speed relative to the soil matrix and \vec{v}_s the speed of the deformable granular structure of the soil.

– soil:

$$\frac{\partial}{\partial t} n_e - \nabla \vec{v}_s + \nabla (n_e \vec{v}_s) = 0 \quad (6.29)$$

- the equation for the velocity field \vec{v}_{rs} , that is the D'Arcy speed (4.79):

$$\vec{v}_{rs} = \vec{v}_D = -\frac{\rho_w g}{\mu_w} \mathbf{k} \nabla H = -\mathbf{k} \nabla (h + z) \quad (6.30)$$

with μ_{rmw} as the viscosity of water, \mathbf{k} as the permeability and ∇H as hydraulic gradient.

- Constituting equations:

– density of water ρ_w and fluid pressure height h :

$$h = \frac{1}{\rho_w g} (p - p_0) = \frac{1}{\rho_w g} \sigma \quad (6.31)$$

with p_0 as a reference pressure (normally $p_0 = 0$) and σ as an incremental fluid pressure (tension).

– velocity v_s of the soil:

$$\nabla \vec{v}_s = \frac{\partial e}{\partial t} = \alpha \frac{\partial \sigma}{\partial t} = \alpha \rho_w g \frac{\partial h}{\partial t} \quad (6.32)$$

with α_s as coefficient for the consolidation of the soil and e as volume dilation.

– effective porosity, saturation and moisture content (Feuchtigkeitsgehalt):

$$\Theta = n_e \sigma = \Theta(h) \quad (6.33)$$

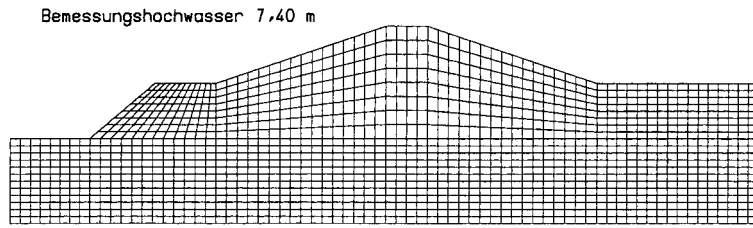
with $\Theta(h)$ describing the specific properties of the porous soil.

Equations (6.28)–(6.33) are a set of 6 equations for the 6 variables h , ρ_w , S , n_e , \vec{v}_D and \vec{v}_s .

Note that the pressure field is not included as separate equation in the above set of equations but can be derived from the equation of continuity for the water.

A similar set of equations has to be considered for the infiltration with pollutants, assuming that the substances are advected with the flow, are allowed to diffuse into the surrounding medium and also are allowed to decay. The latter is not meant in the sense of radioactive decay but to allow for losses due to chemical reactions without involving a self-consistent chemistry module. This assumption can be validated easily: normally, all potential reaction partners in the soil have much higher concentrations than the toxic advected with the flow. Thus the removal depends only on the rate of the toxic and the reaction rate – as discussed already as one possible aspect for simplification.

Figure 6.9:
Discretization of a dike with 1376 finite elements and 1469 nodes [37]



Boundary Conditions

The boundary conditions on the dike certainly cannot be the same all over the simulation volume: on the river side, for instance, water pressure will be exerted which is not the case on the land side. In fact, all three kinds of boundary conditions mentioned above will be encountered with the dike, see also Fig. 6.8.

On the water side, the total pressure height is the relevant parameter. This leads to a Dirichlet boundary condition:

$$H = H_D(y_b), z_b, t. \quad (6.34)$$

For stationary high water levels, the total pressure height on the waters surface is constant while it is variable in case of a rising tide.

Cauchy boundary conditions, on the other hand, are relevant at all points where a flow normal to the simulation surface might occur. In this particular problem, they can be written as

$$-\vec{n}(\mathbf{K}\nabla h + \mathbf{K}\nabla z) = q_c(y_b, z_b, t). \quad (6.35)$$

Special attention must be paid to the boundary conditions at the land side, in particular in places where an embankment spring might form. Thus the intersection of the saturation line with the embankment leads to a shift in boundary conditions from Dirichlet to Neumann.

6.3.3 Finite Elements Applied

As usual, the finite element approach requires the discretization or fractionalization of the simulation volume and the formulation as a weak problem.

Figure 6.9 shows the discretization of the dike with 1376 finite elements and 1469 nodes. For the actual simulation an even finer grid with 5504 finite elements and 5689 nodes was chosen, however, the actual layout of the elements is the same. Note that the elements in this model still have a quite regular shape and do not differ too much in size.

Extensive tests with this grid, and also smaller grids, have been performed: for lower resolution grids, numerical artefacts in the sense of a discontinues patterning become visible: between the high fluid pressure on the embankment and a region of high fluid pressure inside the dike, for instance, regions with reduced fluid pressure exist (for details see [37]). Since such a result does not make any sense physically, the model is not useful. However, since the problem vanishes with increasing number of nodes, the un-physical result just reflects the inappropriate size of the finite elements. Or suggests to use a different kind of weighting function, which does not force the linear relation between adjacent nodes. Nonetheless, the grid mentioned above leads to physical sound results without numerical artefacts and thus appears to be a reasonable (and managable) choice.

The interpolation inside the finite elements is described by the following weighting functions:

$$\begin{aligned} N_1(r, s) &= \frac{1}{4}(1+r)(1+s), \\ N_2(r, s) &= \frac{1}{4}(1-r)(1+s), \\ N_3(r, s) &= \frac{1}{4}(1-r)(1-s), \end{aligned}$$

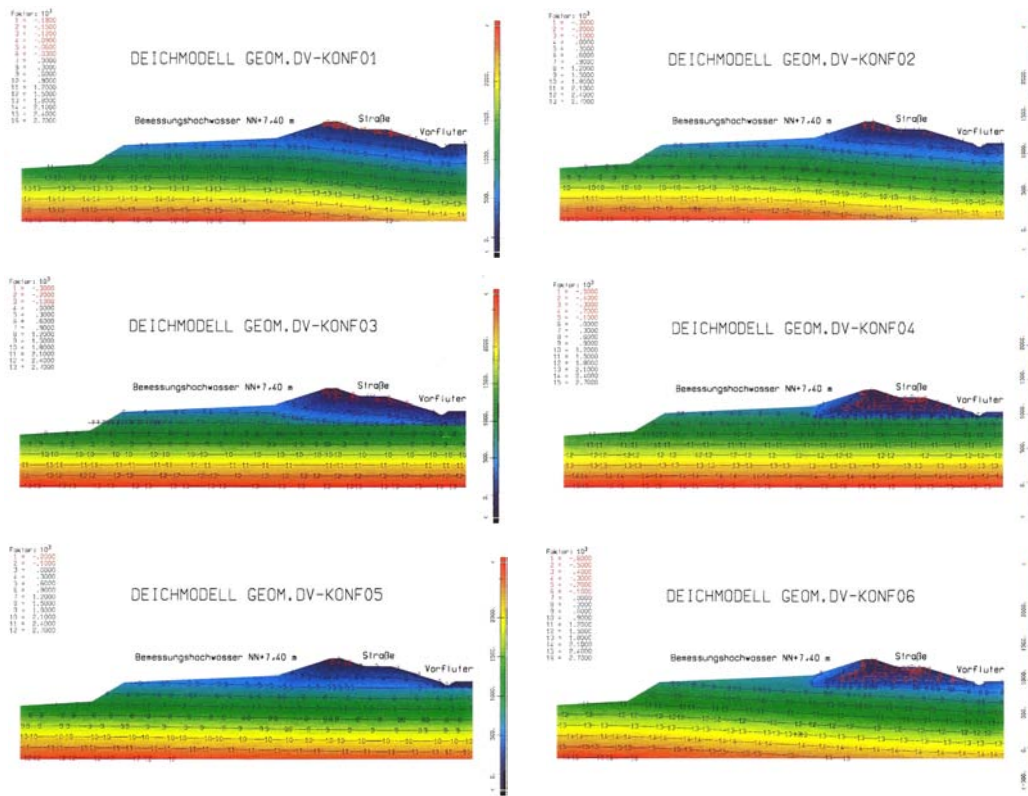


Figure 6.10: Fluid height levels for the dike geometries of Fig. 6.7 for stationary conditions [37]

$$N_4(r, s) = \frac{1}{4}(1+r)(1-s), \quad (6.36)$$

with r and s ($(r, s) \in \{(1, 1), (-1, 1), (-1, -1), (1, -1)\}$) being the local coordinates in each finite element.

The next step is to find the weak form of the problem. As mentioned in the general description of the problem, this does not require the usage of a computer but can be done by hand. Nonetheless, we do not want to repeat all this calculation here, the interested reader is referred to [37].

6.3.4 Results

As mentioned in connection with the discretization (and also mentioned frequently in the first chapters), tests of the results are relevant. Thus in the following we will briefly scan through the results for the stationary simulation for all six dike geometries of Fig. 6.7. While individual results sometimes appear to be a little bit far fetched, the comparison between the different geometries aids the interpretation of the results. Thus more confidence into the model can be gained.

Fluid Pressure Height

The first set of results (see Fig. 6.10; dike geometries in the same order as in Fig. 6.7) is concerned with the fluid pressure height for stationary conditions. Fluid pressure height informs us about

- saturation: which regions are saturated, which still are unsaturated,
- the free water surface,

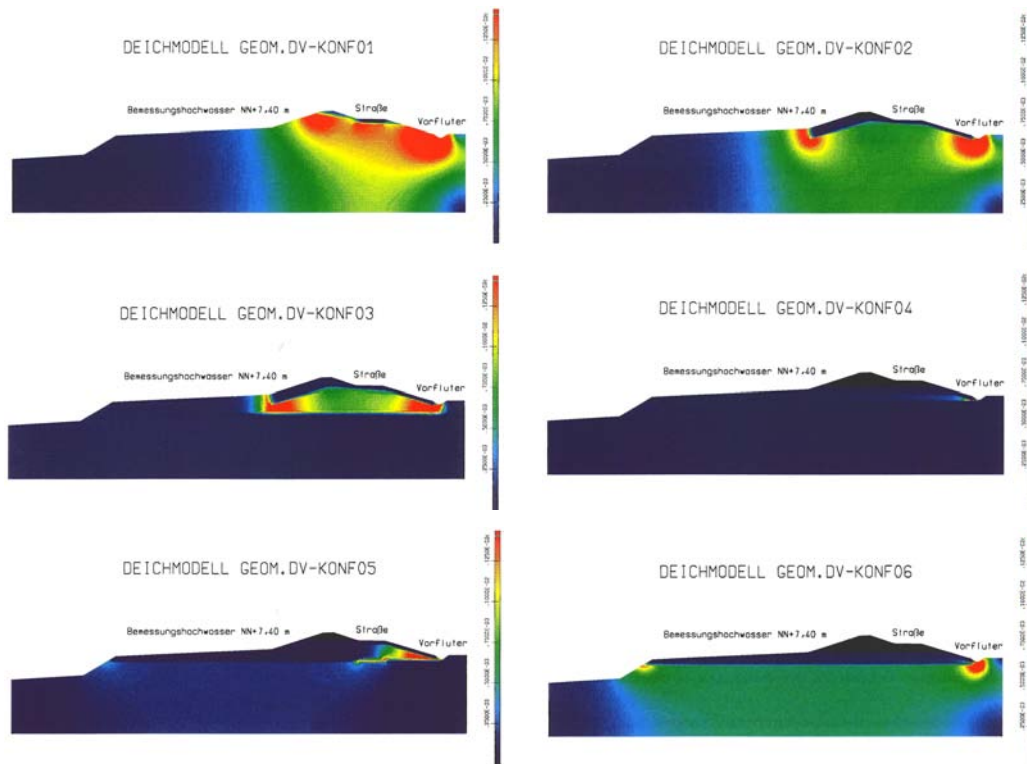


Figure 6.11: Subsoil flow speeds for the dike geometries of Fig. 6.7 for stationary conditions [37]

- the location of the embankment spring,
- the distribution of pore pressure in the different layers.

The overall picture of total fluid pressure is quite similar in all geometries: fluid pressure is highest close to the bottom and decreases with increasing height (not really a surprise). Independent of the dike geometry, fluid pressure is largest below the river bed (that is to the left in each figure). Water pressure decreases towards the right in geometries 1 and 2 (top row) while it stays constant in geometries 3 and 4 (middle row). In geometry 5 the decrease to the land side is rather small, while it is again well pronounced in geometry 6. The reason is quite simple: pressure is isotropic. In the saturated zone below the dike pressure is everywhere the same as the pressure on top stays constant. That is the case in geometries 3 and 4 where the Klei-layer beneath the dike continues through the entire simulation volume. It acts as a mechanical barrier, keeping the pressure below at constant level. On top of the Klei-layer, pressure decreases towards the right, that is towards the land side, as in the other figures. This unloading basically is due to the run-off ditch. A similar effect happens in geometries 5 and 6. Although in both cases a bottom Klei-layer exists, it is not a closed boundary: in geometry 5 pressure is released by water flowing through the gravel stretch into the dike. And in geometry 6 pressure release occurs at the land side because the Klei-layer does not continue beyond the run-off ditch.

Embankment springs form at 2.5 m above the base of the run-off ditch in geometry 1 and at 1.5 m in geometry 2. In geometry 3, no embankment spring forms but the pressure on the bottom of the Klei-layer exceeds the pressure due to the soil on top of it: in principle, this might lead to a fountain discharging into the run-off ditch – which might have more serious consequences than just a small embankment spring. The situation in geometry 4 is quite similar. In geometry 5, pressure release occurs through the gravel stretch in the Klei-layer: since this water is pushed up like a fountain, almost the entire dike soaks. Nonetheless,

underneath the run-off ditch, the risk for a failure in the Klei-layer, although smaller than in geometries 3 and 4, still persists. Since pressure is released in geometry 6, this risk does not persist there.

Subsoil Flow Speed

Fluid pressure heights are concerned with mechanical loads on the system. Erosion, however, is a consequence of running water. Thus a look at the subsoil flow speeds should help to appreciate other aspects of dike stability. Figure 6.11 shows the results for stationary conditions for all three geometries.

In contrast to the fluid pressure heights in Fig. 6.10, the subsoil flow speeds show a much stronger variation with geometry. In addition, the effects of the Klei-layer (and also its location) are easily to be identified.

Geometry 1 basically is the sand hill. Subsoil flow speeds increase from left to right: they are almost vanishing in the river bed and in the dike's foreland (Deichvorland) and show a small increase below the dike. However, the highest flow speeds are observed at and just below the saturation line at the regions of water entry (embankment on the river side), below the street and in particular around the run-off ditch. Thus such a dike is vulnerable to erosion in particular at its back where the rather strong flow easily might wash out large parts of the embankment close to the Deichfuß. The resulting instability might lead to a collapse of the entire structure. In addition, the high flow speeds and the resulting erosion below the street are a source of concern: in case of high water levels, this street will be filled with trucks and people trying to support the dike with sandbags. Such a mechanical load on a street with vanishing support certainly is not a good idea.

A Klei-layer on the dike, such as in geometry 2, leads to a different flow pattern. Since water does not path through the Klei, all the flow squeezes through the sand just at the ends of the Klei layers leading to strong local erosion. Again, at the land side, the erosion occurs at the run-off ditch, however, there is no erosion below the street. The regions of high flow speed extend well below the dike.

Geometry 3 is quite similar except for the Klei-layer below the dike. As a consequence, a small flow channel between the bottom Klei-layer and the Klei-layer on top of the dike forms with relative high subsoil flow speeds in large parts of the dike. Such a construction is most suitable to lead to an shear failure (hydraulic base failure, Erosionsgrundbruch, hydraulischer Grundbruch). Thus this kind of design might not be regarded as a clever design. The problem is that this is a rather common design. Not because it has been designed like this but because a natural Klei-layer exists at the bottom and the dike has been covered with Klei to reduce soaking. The risk of this problem in existing dikes is difficult to evaluate because normally no information about the extend, location and thickness of the natural Klei-layer exists.

And the location and consistency of the natural Klei-layer matters, as can be seen from the flow speeds in the remaining three geometries. If no flow channels forms, as in geometry 4, there is no significant flow and erosion is not a concern. But before suggesting to build all dikes in this geometry keep in mind that the pressure is pretty high below the Klei-layer – in fact, it might be high enough to lift the entire dike.⁵ And since the bottom Klei-layer is a natural layer, nobody can be sure whether it is a continuous layer or not. If it is not, such as in geometry 5, water will seep with pretty high velocity through this gap and again create an erosion channel. And if the bottom Klei-layer does not extend beyond the run-off ditch, a nice flow will form along it, again leading to erosion at the run-off ditch.

⁵While presenting his results to a group of engineers and dike reeves from the port and dike authorities in Hamburg, the modeler tried to apologize for this in his opinion obvious nonsense only to learn that his results could be explain one never understood observation from a few years earlier: a harbor dike, which is basically a sand core in a closed concrete envelope had been offset ba a couple of meters landward during a strong flood.

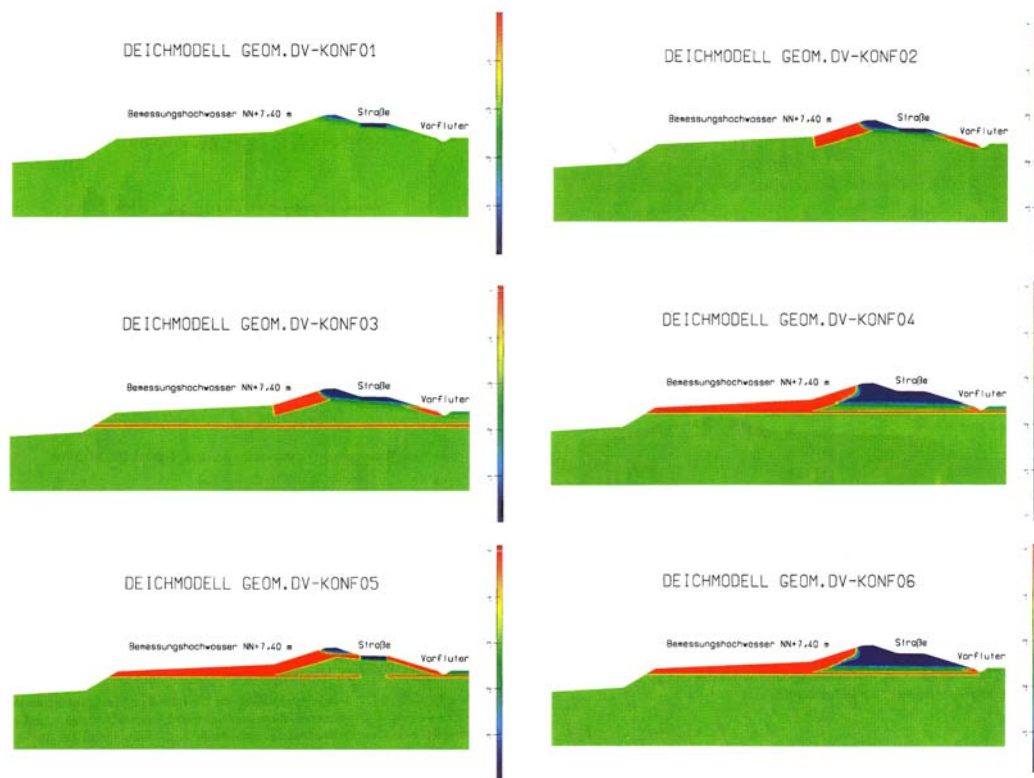


Figure 6.12: Moisture content for the dike geometries of Fig. 6.7 for stationary conditions [37]

Moisture content

Figure 6.12 shows the moisture content for the different geometries under study. In the sand hill of geometry 1 almost all of the dike is saturated, only a small region at the crown and around the street stays unsaturated. If the dike is covered with an additional Klei-layer as in geometry 2, the unsaturated region is larger, basically because the Klei soaks with water but does not transport it. This result is independent on whether there is a natural layer below the dike (as in geometry 3) or not (as in geometry 2). If the Klei-layer is closed around the dike as in geometry 4, however, most of the dike is in the unsaturated zone. This is the case for a bottom Klei-layer extending through the entire simulation volume (geometry 4) as well as a shorter layer that terminates at the run-off ditch (geometry 6). But this holds only as long as the bottom Klei-layer is closed: if water is passes through it (as in geometry 5), again almost the entire dike will be in the saturated zone, except for the crown.

Pollutants

Figure 6.13 shows relative toxic concentrations (left) for geometries 1 (top) and 2 (bottom) and the flux of pollutants (right). The concentrations are relative to the ones in the water. In both geometries the relative concentrations are 1 in the river side region of the dike and decrease down to 0.5 at the land side surface. The distribution follows the total pressure height. In both models flow speeds of pollutants are highest close to the run-off ditch. Note that this distribution basically reflects the flow speeds already shown in Fig. 6.11.

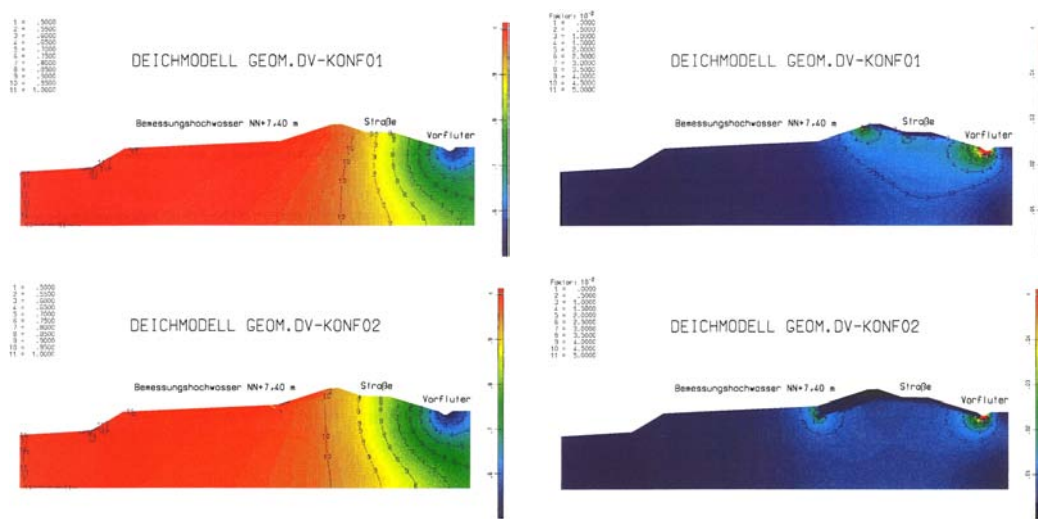


Figure 6.13: Concentrations and flow speeds for pollutants for the dike geometries 1 and 2 for stationary conditions [37]

Literature

Simple introductions into FEM are given in Jüngel [80] and Baumann and Stein [7]. FEM also is covered in many books on numerical mathematics or numerical physics. There is also a wealth of special books devoted to FEM, such as [6].

A popular tool for FEM is z88, distributed for instance with the SUSE-Linux versions or available from the www under <http://www.z88.org/> for both Linux and Windows. CAMMPUS (<http://www.haw-hamburg.de/rzbt/dnksoft/cammpus/cammpus.html>) is a free tool (for educational purposes only) for DOS machines. MatLab itself does not provide the tools for FEM, however, two of the solvers in MatLab are based on FEM: `fem1ode` and `fem2ode`; for further information consult the MatLab help. The PDE toolbox for Matlab includes tools for FEM, however, it is not contained in the standard distributions of MatLab.

Questions

Frage 40 Describe the principle of FEM

Frage 41 What is the weak form of a problem? What is the advantage of introducing a weak form?

Frage 42 What is the meaning of the basis functions/weight function?

Panta Rei: Computational Fluid Dynamics (CFD)

In this text we have frequently encountered a flow: in the compartment models in chapter 3 the flow was prescribed, in the diffusion–convection model in sect 4.3 the flow was added to the diffusive process but also in a prescribed way. Not even in the temperature distribution in sect. 4.2 we have solved the equation for the flow but have limited us to a stationary situation. And the flowing river soaking the dike in sect. 6.3 was not even a prescribed flow but only a prescribed level of water pressure/height. In this chapter, some aspects related to the modeling of a flow will be briefly introduced.

The fundamental equation in computational fluid dynamics (CFD) is the Navier–Stokes equation. It will be introduced in detail in sect. 7.1. For most applications, a set of additional equations is required, for instance the equation of continuity or reaction equations. In sect. 7.3 we will introduce a few sets of equations for typical CFD problems such as fire and smoke modeling and magnetohydrodynamics. Most sets of equations are, at least for realistic geometries, easier solved in a finite element scheme than with a finite difference method. However, the treatment of the numerics of these problems is well beyond the scope of this paper.

A careful numerical treatment in this chapter is limited to a rather simple boundary layer problem, that is the motion of fluid layers as discussed in sect. 7.2.

Goals: after working through this chapter you should be able:

- to describe the equations relevant for CFD and to explain the special physical and numerical difficulties in CFD problems.
- to model simple physical problems occurring at boundaries/interfaces.

7.1 The Physics of the Flow: Navier–Stokes Equation

The motion of a fluid element in hydrodynamics can be described by Euler’s equation or the Navier–Stokes equation. All these different *equations of motion* or *momentum balances* have one basic ingredient, the pressure-gradient force. In single-body motions, only external forces act on the body. In a fluid, on the other hand, regions of different pressure, for instance related to temperature differences, can exist, exerting forces on fluid elements. Thus, before inserting the external forces into the equation of motion, let us have a look at this internal force, the pressure-gradient force.

7.1.1 Pressure-Gradient Force

Regions of different pressure in a gas exert forces: particles move from the high pressure towards the low one. This force is proportional to the pressure gradient $-\nabla p$ and is called the pressure-gradient force. Here we give its derivation, closely following Chen [30].

Pressure is related to the thermal motion of particles. The pressure-gradient force leads to a transport in momentum resulting from the motion of particles in and out of a fluid element $V|_{x_0} = \Delta x \Delta y \Delta z$ at position x_0 (see Fig. 7.1). If the random thermal motion is limited to the x -axis, particles enter and leave the volume through surfaces A and B only. The fluid particles are characterized by their mass m , their speed \vec{v} and their number density n . During a time interval

$$\Delta n = \Delta n_v v_x \Delta y \Delta z \quad (7.1)$$

particles with speed v_x pass through surface A with area $A = \Delta y \Delta z$ into the positive x -direction. Here

$$\Delta n_v = \Delta v_x \int \int f(v_x, v_y, v_z) dv_y dv_z \quad (7.2)$$

is the number density of particles with speed v_x , with f being the distribution function (see sect. C.2.1).

Each particle carries a momentum mv_x . The total momentum P_A^+ transported through A into the positive x -direction is

$$P_A^+ = \sum \Delta n_v m v_x^2 \Delta y \Delta z = \Delta y \Delta z \left[\frac{1}{2} m \langle v_x^2 \rangle n \right]_{x_0 - \Delta x} . \quad (7.3)$$

Here the sum over Δn_v is expressed by the average $\langle v_x^2 \rangle$ of the distribution times the particle number density. The factor 1/2 indicates that only half of the particles in the adjacent volume element $V|_{x_0 - \Delta x}$ at $x_0 - \Delta x$ have a speed in the positive x -direction and transport momentum through A into $V|_{x_0}$. But particles inside $V|_{x_0}$ also have a momentum in the positive x -direction which is carried out of the volume through the surface B. Their number is given as

$$P_B^+ = \Delta y \Delta z \left[\frac{1}{2} m \langle v_x^2 \rangle n \right]_{x_0} . \quad (7.4)$$

Therefore, the net gain of the positive x -momentum in $V|_{x_0}$ is

$$P_A^+ - P_B^+ = \Delta y \Delta z \frac{1}{2} m (-\Delta x) \frac{\partial n \langle v_x^2 \rangle}{\partial x} . \quad (7.5)$$

Particles moving into the negative x -direction double the momentum gain in (7.5) because the negative x -momentum is transported into the negative x -direction:

$$\frac{\partial}{\partial t} (nmv_x) \Delta x \Delta y \Delta z = -m \frac{\partial}{\partial x} (n \langle v_x^2 \rangle) \Delta x \Delta y \Delta z . \quad (7.6)$$

The particle speed $v_x = u_x + v_{x_{th}}$ consists of two parts, the bulk speed u_x of the fluid element with $u_x = \langle v_x \rangle$ and the superimposed thermal speed $v_{x_{th}}$ with $\langle v_{x_{th}} \rangle = 0$. The latter is described by a one-dimensional Maxwell distribution (see sect. C.2.3). The relationship between average thermal speed and temperature is:

$$\frac{1}{2} m \langle v_{x_{th}}^2 \rangle = \frac{1}{2} k_B T . \quad (7.7)$$

With (7.6) we obtain

$$\frac{\partial}{\partial t} (nm u_x) = -m \frac{\partial}{\partial x} \left[n (\langle u_x^2 \rangle + 2 \langle u_x v_{x_{th}} \rangle + \langle v_{x_{th}}^2 \rangle) \right] . \quad (7.8)$$

The last term on the right-hand side can be substituted by (7.7). The term in the middle is zero because u_x is constant and thus $\langle u_x v_{x_{th}} \rangle = u_x \langle v_{x_{th}} \rangle = 0$:

$$\frac{\partial}{\partial t} (nm u_x) = -m \frac{\partial}{\partial x} \left(n u_x^2 + \frac{n k_B T}{m} \right) . \quad (7.9)$$

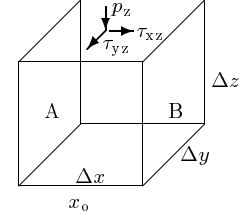


Figure 7.1: Normal forces p and shear stresses τ

The partial differentiation on the right-hand side with $nu_x^2 = nu_x u_x$ gives

$$mn \frac{\partial u_x}{\partial t} + mu_x \frac{\partial n}{\partial t} = -mu_x \frac{\partial(nu_x)}{\partial x} - mn u_x \frac{\partial u_x}{\partial x} - \frac{\partial(nkT)}{\partial x}. \quad (7.10)$$

The second term on the left-hand side and the first term on the right-hand side cancel (see the equation of continuity (2.29)). With the pressure p defined as $p = nk_B T$ rearrangement leads to

$$mn \left(\frac{\partial u_x}{\partial t} + u_x \frac{\partial u_x}{\partial x} \right) = mn \frac{du_x}{dt} = - \frac{\partial p}{\partial x}. \quad (7.11)$$

Generalization to three dimensions gives the pressure-gradient force density

$$mn \left(\frac{\partial \vec{u}}{\partial t} + \vec{u}(\nabla \cdot \vec{u}) \right) = mn \frac{d\vec{u}}{dt} = -\nabla p. \quad (7.12)$$

Since n is a number density (unit m^{-3}), the product nm gives the density ρ and we can write alternatively for the acceleration due to the pressure gradient force

$$\frac{d\vec{u}}{dt} = -\frac{1}{\rho} \nabla p. \quad (7.13)$$

7.1.2 Equation of Motion: Euler and Navier–Stokes

The simplest equation of motion for a fluid considers the acceleration due to the pressure-gradient force and gravitation

$$\frac{d\vec{u}}{dt} = -\frac{1}{\rho} \nabla p + \vec{g}. \quad (7.14)$$

This equation is known as Euler's equation and often is used for simple estimates in atmospheric or oceanic motion. Euler's equation can be applied to ideal fluids only. In a real fluid, viscous forces have to be considered too. Here the Navier–Stokes equation is useful:

$$\frac{d\vec{u}}{dt} = -\frac{1}{\rho} \nabla p + \nu \nabla^2 \vec{u} \quad (7.15)$$

with ν being the kinematic viscosity. Often, other forces, depending on the situation under study, are added to this equation. Some of these forces will be discussed below where we also shall have a closer look at the viscous forces.

7.1.3 Stress Tensor and Viscosity

In the generalization of (7.11) we tacitly assumed that x_i -momentum is transported in x_i -direction only and that the fluid is isotropic. This is true in an ideal gas or fluid but not in a viscous one, where momentum can be transported in directions perpendicular to the particle motion, and momentum transport is not necessarily isotropic. Then the scalar property p has to be replaced by a tensor \mathbf{P} , and the pressure-gradient force ∇p has to be replaced by $\nabla \mathbf{P}$. \mathbf{P} not only considers the pressure, which is orthogonal to the surface of a volume element, but also shear stresses, which are forces parallel to the element's surface (see Fig. 7.1). The stress tensor \mathbf{P} has the dimensions of a pressure or an energy density. It is symmetric with six independent components P_{ij} for each point: $P_{ij} = mn v_i v_j$; i being the direction of the momentum transport and j the component of the momentum involved. A more compact method to write the stress tensor is

$$\mathbf{P} = mn \langle \vec{v}_{\text{th}} \vec{v}_{\text{th}} \rangle. \quad (7.16)$$

Here $\vec{v}_{\text{th}} \vec{v}_{\text{th}}$ is not a shorthand for a scalar product but the tensor product (dyad) of two vectors: such tensor products $\vec{a} \vec{b}$ of two vectors are tensors \mathbf{T} with

$$\mathbf{T} = \vec{a} \vec{b} = \begin{pmatrix} a_x \\ a_y \\ a_z \end{pmatrix} \begin{pmatrix} b_x \\ b_y \\ b_z \end{pmatrix} = \begin{pmatrix} a_x b_x & a_x b_y & a_x b_z \\ a_y b_x & a_y b_y & a_y b_z \\ a_z b_x & a_z b_y & a_z b_z \end{pmatrix}. \quad (7.17)$$

Its obvious from its definition (7.16) that this tensor is symmetric with six independent components.

In the simplest case, the particle distribution is an isotropic Maxwellian and the stress tensor \mathbf{P} can be written as

$$\mathbf{P} = \begin{pmatrix} p & 0 & 0 \\ 0 & p & 0 \\ 0 & 0 & p \end{pmatrix} = p\mathbf{E}, \quad (7.18)$$

where \mathbf{E} is the unit tensor. Here $\nabla\mathbf{P}$ equals ∇p . In the presence of a magnetic field, a plasma can have two different temperatures T_{\parallel} and T_{\perp} parallel and perpendicular to the magnetic field, leading to different pressures $p_{\parallel} = nk_{\text{B}}T_{\parallel}$ and $p_{\perp} = nk_{\text{B}}T_{\perp}$. In a coordinate system oriented with its z -axis parallel to B , the stress tensor can be written as

$$\mathbf{P} = \begin{pmatrix} p_{\perp} & 0 & 0 \\ 0 & p_{\perp} & 0 \\ 0 & 0 & p_{\parallel} \end{pmatrix}. \quad (7.19)$$

This tensor is diagonal and it is isotropic in a plane perpendicular to \vec{B} .

The off-diagonal elements of the stress tensor in an ordinary fluid are associated with viscosity. Viscosity results from collisions between particles and tends to make the flow more uniform. Quantitatively, the effect of viscosity is described by a kinematic viscosity coefficient $\nu = v_{\text{th}}\lambda$ where v_{th} is the thermal speed and λ the mean free path between collisions. Alternatively, a viscosity coefficient $\eta = \nu\rho$ can be used. In a fluid, friction is described by

$$\vec{f}_{\text{frict}} = \eta\nabla^2\vec{u} + \frac{1}{3}\eta\nabla(\nabla \times \vec{u}). \quad (7.20)$$

In an incompressible fluid, the second term on the right-hand side vanishes:

$$\vec{f}_{\text{frict}} = \eta\nabla^2\vec{u} = \nu\rho\nabla^2\vec{u}. \quad (7.21)$$

This can be interpreted as the collisional part of $\nabla\mathbf{P} - \nabla p$. Note that the inclusion of viscosity into the momentum balance has two consequences: (a) in agreement with the irreversible character of the transport process, the transport equation is no longer time-reversible: if $\vec{u}(\vec{r}, t)$ is a solution of the transport equation, then $\vec{u}(\vec{r}, -t)$ is not. (b) Viscosity increases the order of the partial differential equation. Therefore, to determine solutions we need more boundary conditions than in the case of a non-viscous fluid.

In a plasma, off-diagonal elements can arise without collisions: gyration brings particles into different parts of the plasma, a process which tends to equalize the fluid speeds. The scale of this collisionless viscosity is given by the Larmor radius rather than by the particle mean free path.

7.1.4 Fictitious Forces in Rotating Systems

The forces discussed so far are sufficient to give the equation of motion for a plasma in the laboratory setting. In large-scale natural plasmas, such as the ionosphere or stellar atmospheres, additional forces act: the Coriolis force and the centrifugal force.

Consider two frames of reference C and C' , with C rotating with an angular velocity $\vec{\Omega}$ with respect to C' . A vector \vec{r} fixed in C , in C' moves with a speed $\vec{\Omega} \times \vec{r}$. The temporal derivative of \vec{r} in C' is

$$\left(\frac{d\vec{r}}{dt}\right)_{C'} = \left(\frac{d\vec{r}}{dt}\right)_C + \vec{\Omega} \times \vec{r} \quad \text{or} \quad \vec{v}' = \vec{v} + \vec{\Omega} \times \vec{r}. \quad (7.22)$$

The temporal derivative gives the acceleration in the rotating frame:

$$\vec{a}' = \left(\frac{d\vec{v}'}{dt}\right)_{C'} = \frac{d'\vec{v}'}{dt} = \frac{d\vec{v}'}{dt} + \vec{\Omega} \times \vec{v}' = \frac{d\vec{v}}{dt} + 2\vec{\Omega} \times \vec{v} + \vec{\Omega} \times (\vec{\Omega} \times \vec{r}). \quad (7.23)$$

Thus the density of the fictitious forces in a rotating frame of reference is

$$\vec{f}_{\text{rot}} = -\rho 2 \vec{\Omega} \times \vec{v} - \rho \vec{\Omega} \times (\vec{\Omega} \times \vec{r}) \quad (7.24)$$

with the first term on the right-hand side describing the Coriolis force and the second term the centrifugal force.

In the near-Earth environment the Coriolis force has to be considered in the atmospheric motion and in the ionospheric and magnetospheric current systems; it is of vital importance in the dynamo process inside the Sun and the planets. The influence of the Coriolis force can be illustrated by its effect on the atmospheric motion. In the northern hemisphere, wind is deflected towards the right. On a global scale, this deflection leads to the break-up of the Hadley cell driven by the temperature gradient between the equator and the pole into three separate cells, which determine the global atmospheric circulation and govern the energy transport from equator to pole. The Coriolis force, and therefore the size of the deflection, depends on the wind speed: with increasing speed, the distance travelled by a volume of air during a time interval increases. A longer trajectory also means a larger displacement. The Coriolis force becomes effective only if the scales of the system are large enough. Contrary to popular belief, the eddy at the outflow of a bath-tub is not due to the Coriolis force: its direction depends on residual motions in the water or the motion induced by pulling the plug.

7.1.5 Electromagnetic Forces

A charged particle in an electromagnetic field experiences the Lorentz force. With n being the number density, the force on a volume element can then be written as

$$mn \frac{d\vec{u}}{dt} = mn \left[\frac{\partial \vec{u}}{\partial t} + (\vec{u} \cdot \nabla) \vec{u} \right] = qn \left(\vec{E} + \vec{u} \times \vec{B} \right) . \quad (7.25)$$

The dimension of n is m^{-3} , thus (7.25) can also be written as a force density

$$\vec{f}_{\text{elmag}} = \rho \frac{d\vec{u}}{dt} = \rho \left[\frac{\partial \vec{u}}{\partial t} + (\vec{u} \cdot \nabla) \vec{u} \right] = \rho_c \vec{E} + \vec{j} \times \vec{B} , \quad (7.26)$$

with $\rho = mn$ being the density, $\rho_c = qn$ the charge density, and $\vec{j} = nq\vec{u}$ the current density. Equation (7.26) gives the force density of the electromagnetic field. For infinite conductivity, the charges immediately rearrange and cancel out the electric field. The force density then reduces to

$$\vec{f}_{\text{elmag}} = \vec{j} \times \vec{B} . \quad (7.27)$$

7.1.6 Putting it all Together

Adding these forces gives the equation of motion or momentum balance:

$$\begin{aligned} \rho \frac{d\vec{u}}{dt} &= \rho \left(\frac{\partial \vec{u}}{\partial t} + (\vec{u} \cdot \nabla) \vec{u} \right) \\ &= -\nabla P + \rho \vec{E} + \vec{j} \times \vec{B} + \rho \vec{g} - 2\rho \vec{\Omega} \times \vec{u} - \rho \vec{\Omega} \times (\vec{\Omega} \times \vec{r}) . \end{aligned} \quad (7.28)$$

If we neglect the electric field and the fictitious forces and split the stress tensor into the pressure-gradient force and friction, (7.28) can be written as

$$\rho \frac{d\vec{u}}{dt} = \rho \left[\frac{\partial \vec{u}}{\partial t} + (\vec{u} \cdot \nabla) \vec{u} \right] = -\nabla p + \rho \nu \nabla^2 \vec{u} + \vec{j} \times \vec{B} + \rho \vec{g} . \quad (7.29)$$

This equation is the Navier–Stokes equation used in hydrodynamics complemented by the forces exerted by the electromagnetic field.

The momentum balance (7.28) still is relatively simple: (a) it does not consider sources and sinks, e.g. due to ionization or recombination, which might involve a net gain or loss of momentum; (b) it does not consider momentum transport due to Coulomb collisions between

charged particles; and (c) it does not consider momentum transport arising from the forces exerted by a particle component of opposite charge inside the plasma. The latter will be discussed briefly in the two-fluid description of a plasma (see sect. 7.3.3).

7.2 Boundary Layer Problem: Motion of Fluid Layers

This example is a very simple problem from CFD – basically it is defined by a prescribed boundary condition and there is not much adjustment required from the flow. Nonetheless, it is numerically simple (thus we can obtain a complete solution) and it is also instructive from the viewpoint of physics because it describes a boundary layer problem. Such boundary layers occur frequently in natural systems and are the very layers in which transport between two distinct media, such as atmosphere and ocean, atmosphere and ground, or ocean and bottom topology occur.

Imagine a layer of oil on a body of water. Wind acts on the oil's surface, driving it into the wind direction. The wind only acts on the boundary between air and oil. The moving upper layer of the oil film exerts a stress on the oil layer underneath. Thus inside the oil film a vertical velocity gradient develops, its steepness determined by the oil's viscosity. This gradient does not continue to the bottom of the water but only to the boundary between oil and water. Physically, at this interface the same things happen as at the air–oil interface and a vertical velocity gradient develops in the water, too. Its steepness depends on the water's viscosity. The aim is to determine the vertical velocity profiles for different times.

7.2.1 The Model

The physical problem can be described by a layer of oil and one of water sandwiched between two parallel horizontal plates. The top plate is moving at constant speed v_d . The governing equations are the equation of motion including only the stresses:

$$\frac{\partial u_o}{\partial t} = \mu_o \frac{\partial^2 u_o}{\partial x^2} \quad \text{and} \quad \frac{\partial u_w}{\partial t} = \mu_{\text{water}} \frac{\partial^2 u_w}{\partial x^2} \quad (7.30)$$

with the index 'o' indicating oil and 'w' indicating water. As the fluid layers both equations are coupled at the oil–water interface:

$$u_o = u_w \quad \text{and} \quad \mu_o \frac{\partial u_o}{\partial x} = \mu_w \frac{\partial u_w}{\partial x}. \quad (7.31)$$

The first equation describes the positional continuity of the velocities of the two fluids at the interface. The second refers to the tangent at the interface: if both viscosities are the same, this equation again confirms the tangential continuity of the velocities at the interface. With different viscosities, the ratio of the tangents is described by the inverse of the ratio of the viscosities.

Mathematically, we have two parabolic PDE boundary value problems involving the velocities of the two fluids. For the water we have

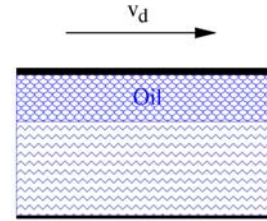
$$\frac{\partial v_w}{\partial t} = \mu_w \frac{\partial^2 v_w}{\partial x^2}, \quad 0 \leq x \leq x_i \quad (7.32)$$

with the boundary conditions

$$v_w(x, 0) = 0, \quad v_w(0, t) = 0, \quad v_w(x_i, t) = v_o(x_i, t) \quad \text{and} \quad \mu_o \frac{\partial v_o}{\partial x} \Big|_{x=x_i} = \mu_w \frac{\partial v_w}{\partial x} \Big|_{x=x_i}. \quad (7.33)$$

For the oil we get

$$\frac{\partial v_o}{\partial t} = \mu_o \frac{\partial^2 v_o}{\partial x^2}, \quad x_i \leq x \leq x_t \quad (7.34)$$



with the boundary conditions

$$v_o(x, 0) = 0, \quad v_o(x_t, t) = v_d, \quad v_o(x_i, t) = v_w(x_i, t) \text{ and } \mu_o \left. \frac{\partial v_o}{\partial x} \right|_{x=x_i} = \mu_w \left. \frac{\partial v_w}{\partial x} \right|_{x=x_i}. \quad (7.35)$$

Here we have chosen our frame of reference such that $x = 0$ is at the bottom plate, x_i is the height of the oil–water interface and x_t is the top of the oil layer.

Equations 7.32 and 7.34 are simple parabolic PDEs. However, we cannot solve them separately. Instead, these equations are coupled by the boundary conditions at their interface, given in red in (7.33) and (7.35).

7.2.2 Numerical Solution: Finite Centered Differences in Time and Space

For this example the numerical scheme again will be implicit but this time with finite centered differences in both space and time. The entire height x is divided into n equidistant steps Δx . The first m nodes are within the water layer, the remaining nodes in the oil-layer. Node m is at the interface. The difference equations then read

$$\frac{v_{w,k}^{l+1} - v_{w,k}^l}{\Delta t} = \mu_w \frac{v_{w,k+1}^{l+1} - 2v_{w,k}^{l+1} + v_{w,k-1}^{l+1}}{(\Delta x)^2}, \quad k = 1, 2, \dots, m \quad (7.36)$$

and

$$\frac{v_{o,k}^{l+1} - v_{o,k}^l}{\Delta t} = \mu_o \frac{v_{o,k+1}^{l+1} - 2v_{o,k}^{l+1} + v_{o,k-1}^{l+1}}{(\Delta x)^2}, \quad k = m, m+1, \dots, n. \quad (7.37)$$

Rearrangement yields

$$\frac{\mu_w}{(\Delta x)^2} v_{w,k-1}^{l+1} - \left(\frac{2\mu_w}{(\Delta x)^2} + \frac{1}{\Delta t} \right) v_{w,k}^{l+1} + \frac{\mu_w}{(\Delta x)^2} v_{w,k+1}^{l+1} = -\frac{1}{\Delta t} v_{w,k}^l, \quad k = 1, 2, \dots, m \quad (7.38)$$

and

$$\frac{\mu_o}{(\Delta x)^2} v_{o,k-1}^{l+1} - \left(\frac{2\mu_o}{(\Delta x)^2} + \frac{1}{\Delta t} \right) v_{o,k}^{l+1} + \frac{\mu_o}{(\Delta x)^2} v_{o,k+1}^{l+1} = -\frac{1}{\Delta t} v_{o,k}^l, \quad k = m, m+1, \dots, n. \quad (7.39)$$

Since we have centered differences, nodes outside the simulation volume are introduced. Again, these nodes can be expressed by using the boundary conditions. At node $k = 1$ at the bottom the difference equation

$$-\left(\frac{2\mu_w}{(\Delta x)^2} + \frac{1}{\Delta t} \right) v_{w,1}^{l+1} + \frac{\mu_w}{(\Delta x)^2} v_{w,2}^{l+1} = -\frac{1}{\Delta t} v_{w,1}^l - \frac{\mu_w}{(\Delta x)^2} v_{w,0}^{l+1} \quad (7.40)$$

the last term on the right hand side vanishes because $v_w(0, t) = v_{w,0}^{l+1} = 0$. At the top plate a similar manipulation of the difference equation using the boundary condition $v_{o,n}^{l+1} = v_d$ gives the difference equation

$$\frac{\mu_o}{(\Delta x)^2} v_{o,n-2}^{l+1} - \left(\frac{2\mu_o}{(\Delta x)^2} + \frac{1}{\Delta t} \right) v_{o,n-1}^{l+1} = -\frac{1}{\Delta t} v_{o,m+1}^{l+1} - \frac{v_d \mu_o}{(\Delta x)^2}. \quad (7.41)$$

At the interface, the original difference equations are

$$\frac{\mu_w}{(\Delta x)^2} v_{w,m-1}^{l+1} - \left(\frac{2\mu_w}{(\Delta x)^2} + \frac{1}{\Delta t} \right) v_{w,m}^{l+1} + \frac{\mu_w}{(\Delta x)^2} v_{w,m+1}^{l+1} = -\frac{1}{\Delta t} v_{w,m}^l \quad (7.42)$$

and

$$\frac{\mu_o}{(\Delta x)^2} v_{o,m-1}^{l+1} - \left(\frac{2\mu_o}{(\Delta x)^2} + \frac{1}{\Delta t} \right) v_{o,m}^{l+1} + \frac{\mu_o}{(\Delta x)^2} v_{o,m+1}^{l+1} = -\frac{1}{\Delta t} v_{o,m}^l. \quad (7.43)$$

The outside nodes $v_{w,m+1}^{l+1}$ and $v_{o,m-1}^{l+1}$ can be removed using the second boundary condition. Since this is still written with differentials, we first have to rewrite it as a difference equation

$$\mu_w = \frac{v_{w,m+1}^{l+1} - v_{w,m-1}^{l+1}}{2\Delta x} = \mu_o \frac{v_{o,m+1}^{l+1} - v_{o,m-1}^{l+1}}{2\Delta x} \quad (7.44)$$

the water is not moving at all. With increasing time, momentum is transferred to the lower part of the oil layer. As the interface starts to move, momentum also is transported into the water layer. With increasing time, gradients become linear and approach steady-state (indicated by the crosses).

7.3 Typical Examples from CFD

CFD (<http://www.cfd-online.com/>) has its strength in complex situations. The above introductory example was rather simple, the more applied cases all rely on a much larger set of equations. These equations somehow have to be combined into a numerical scheme. This section does not attempt to train you to solve such a problem,. Instead, it will allow a brief glance on a few current problems in CFD.

7.3.1 Flow around a Body

One rather simple application of CFD is the flow around a body. This application is simple in such that only a limited set of equations is required. In addition, it faces a broad range of applications: all design problems in transport are concerned with the relative motion between a solid body and a fluid. CFD for these problems leads to nice figures which are frequently presented in the mass media, the internet or in advertising (see also the linke below).

The governing equations for such a problem are the Navier–Stokes equation and the equation of continuity; reaction equation or thermal balances are normally not required. Thus the mathematical problem is rather simple. The main question to be answered is: how and where do eddies develop that lead to frictional forces?¹ In earlier times, such problems have been solved in a flow channel. This is still true for present day problems, for the example of an airplane see e.g. [136]. Nonetheless, a flow channel simulation under realistic conditions (pressure and temperature at flight level, changes in these parameters during take-off and landing, reactions to potentially lethal shear winds) are difficult and extremely expensive.

CFD provides a much less expensive and more flexible environment for such kind of design studies. Some first impressions on industrial advertisement and CFD can be found at the following links: <http://www-berkeley.ansys.com/testimonials/ICEM-TESTIMONIAL-AIRBUS.pdf>, http://www-berkeley.ansys.com/optimesh/examples/747_examples/747_solution.html, <http://www.cerfacs.fr/cfd/REPORT-0001/cfd00-1010.html>, or, last but not least, http://www.hypercomp.net/Technologies/CFD/cfd_low.html. Non-airplane related examples can be found, for instance, under <http://www.cmis.csiro.au/cfd/fem/index.htm>, <http://www.fluent.com/solutions/examples/x179.htm>, <http://www.modelbasin.com/CFD.htm> or <http://www.eng.uab.edu/me/CSLab/research.html>.

Accident investigation (oh no, catastrophe again) for airplanes under certain circumstances also strongly relies on CFD: if a flight became fatally instable due to eddies produced by an earlier plane, it is difficult to simulate the situation in a flow channel or to test this hypothesis experimentally. Instead, a CFD might be the solution, see for example www.nts.gov/events/2001/AA587/presentations/02.airplane_perf.ppt. The flow speeds (and resulting temperatures) in the region of wing damage at the space shuttle Columbia also have been subject to CFD simulations (see e.g. investigation report at

¹In the discussion of this problem we should be aware of the fact the friction in fluid motion has two sources: the viscous forces lead to friction on a molecular level. Thats similar to friction between the soles of your shoes and the pavement. But for a car, the friction between tire and pavement cannot be reduced any further (how would you accelerate?); here the drag comes from the different pressure levels in front and behind the car: air piles up in front of the car, corresponding to a high pressure. On the other hand, eddies at the car's rear end reduce pressure at that side. This pressure difference is what cases drag. And note, the drag can be reduced by increasing the viscous forces. The best example is the golf ball. All the dents on its surface increase he drag by viscous forces. Bat the increased drag slows down the air flowing around the ball. Thus the flow sticks to the ball for a longer time and the eddies behind the ball are smaller. As a consequence, the pressure difference between the ball's front and rear side is reduced and therefore also drag is reduced.

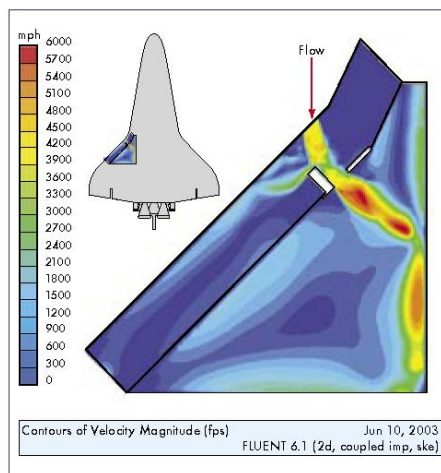


Figure 7.3: CFD simulations also helped to understand the break-up of the shuttle Columbia during re-entry into the atmosphere after some foam insulation had damaged the heat shield at the left wing. The resulting hole permitted flow speeds of almost 6000 mph, corresponding to temperatures in the order of 5000 K. This highly effective welding torch led to fast structural desintegration (from caib report (see text))

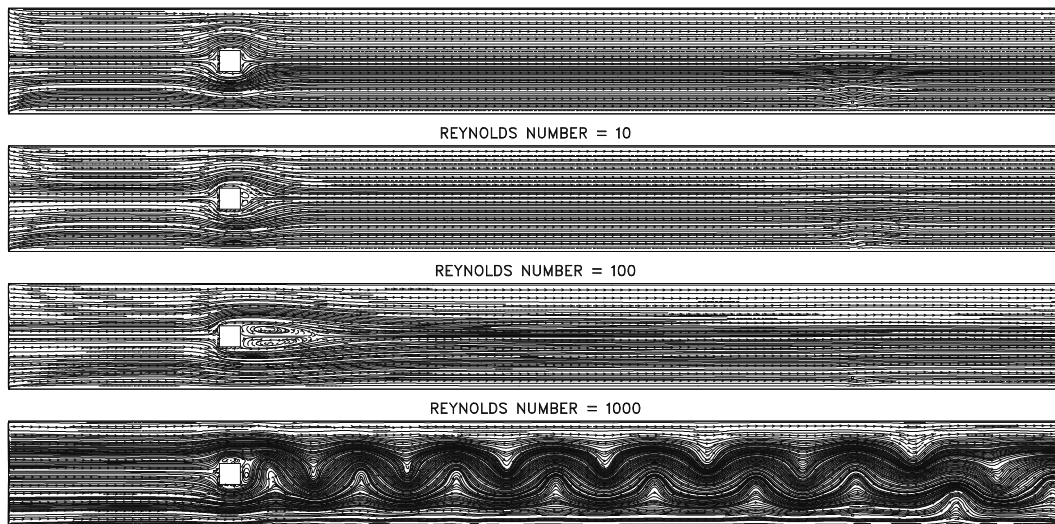


Figure 7.4: Flow around an obstacle for different Reynolds' numbers [110]

<http://usgovinfo.about.com/gi/dynamic/offsite.htm?site=http://www.caib.us/> or Fig.

Although all these links shows the colorful side of CFD (and require a large computer and, in most cases, expensive commercial software), we should not forget, that even with CFD we can save time by first reducing the problem to dimensionless variables, as briefly discussed in sect. 2.2.3. The Reynolds' number describe the basic properties of the flow as a relation between the viscous and the inertial forces. Thus it depends on a characteristic length scale, a characteristic flow speed and viscosity but not on actual length and flow speed. A solution obtained for one geometry thus also is valid for a different geometry – as long as the other parameters are adjusted such that the Reynolds' number is the same. Figure 7.4 should serve as an example for the variation of the properties of a flow around an obstacle with the Reynolds' number.

7.3.2 Fire and Smoke Modeling

Fire and smoke modeling is an extended version of the above problem. It contains the above problem because the propagation of smoke (and heat) are typical flow problems. But it also contains many more equations, in particular all the reaction equations related to the burning

process: for instance, a fire in a sealed room would keep on smoldering for some time but would eventually die out because it lacks oxygen. If oxygen supply to the same room was large, the fire would burn brightly and spread rather fast. But what if a fire is smoldering in an (almost) sealed room and somebody suddenly opens the door: the sudden supply of oxygen certainly would fuel the fire. But how much depends strongly on how long the fire has smoldered before. If time was sufficiently long, pyrolysis would have supplied a lot of easily inflammable substances to the air which suddenly ignite in a flash-over, posing a serious risk to the person that opened the door.

But fire often is not the main hazard in a fire – it is the smoke instead.² Thus in the design of escape routes, in evacuation plans as well as in accident investigation smoke plays an important role. Thus the generation and spread of smoke often are a more serious question in fire modeling than the spread of the fire itself.

On the web there are quite a lot resources on fire modeling. A very mathematical introduction is given in [110] (http://fire.nist.gov/fds/docs/fds_class_notes.pdf). A little less black and white (and also less mathematical) and a bit more animated is the introduction by the University of Maryland Department of Fire Protection Engineering (www.fpe.umd.edu/department/modeling/index.html). Also an university page is <http://fseg.gre.ac.uk> from the Fire Safety Engineering Group at the University of Greenwich which is concerned with quite famous accidents such as 9-11 or the burning Swiss MD before New Foundland. An overview regarding fire simulation models with all relevant links also is given at www.fire.nist.gov/ and www.firetactics.com/FIRE-MODELING.htm. A fire and smoke simulator is provided by <http://fire.nist.gov/fds/refs/readme.html>; a collection of fire modeling software can be found at <http://www.bfrl.nist.gov/866/fmabbs.html>. It is interesting to just browse through this list because different models focus on very different topics. And understanding and appreciating these differences explains very much regarding the underlying physical processes. and if you want to dig into an example for an accident investigation, you might try <http://www.firetactics.com/3120.pdf>.

As the thermal balance of a building in sect. 2.3.4, fire and smoke modeling is also applied during the design phase of a building. A very illustrative example is the simulation of smoke distribution and extraction in Terminal 2 of Munich Airport by P. Vogel (available at <http://www.fluent.co.jp>). Here even rather small details such as the influence of open or closed doors or latches on fire and smoke propagation are considered to validate the design of the building and its escape routes.

7.3.3 Magnetohydrodynamics

After all these catastrophe, let us now turn to an entirely different topic in CFD, that is magnetohydrodynamics (MHD). MHD is concerned with a plasma.

A plasma differs from a neutral gas in so far as it (also) contains charged particles. The number of charged particles is large enough to allow for electromagnetic interactions. In addition, the number of positive and negative charges is nearly equal, a property which is called quasi-neutrality: viewed from the outside the plasma appears to be electrically neutral. The reason for this quasi-neutrality can be understood from the electrostatic forces between charged particles. For instance, in a gas discharge a typical length scale is $L = 0.01$ m and a typical number density number density of the electron gas is $n_e = 10^{20}$ m⁻³. The electric field on the surface of a sphere with $r = L$ containing only the electron gas but no ions is then $E \approx 10^{10}$ V/m. Such a strong field will immediately cause a rearrangement of charges and quasi-neutrality will be restored. In the rarefied plasmas in space, number densities are smaller by many orders of magnitude; however, since the spatial scales are measured in kilometers or even thousands of kilometers, the same argument can be applied: on the relevant spatial scales the plasma is quasi-neutral even in the rarefied plasmas in space,

²In a fire accident, most fatalities are by smoke poisoning rather than by direct contact with the flames. Or in other wordings: most burnt corpses found after a fire have died from smoke inhalation before the fire reached them.

although this is not necessarily the case on the centimeter scale.

Because a plasma (partly) consists of free charges, it is a conductor. Moving electric charges are currents. These currents induce magnetic fields which in turn influence the motion of the very particles forming the field-generating currents. Thus the particle motion in a plasma is not only controlled by external electric and magnetic fields, but also creates fields which add to the external ones and modify the motion of the particles: a plasma can interact with itself. Consequently, dynamics in a plasma are more complex than in a neutral gas. This is most obvious in the large number of different types of plasma waves.

Side question 27 Can a similar problem of self-interaction also be found in the neutral flow as described e.g. by the Navier–Stokes equation? In that case, the ∇p causes motion which in turn modifies ∇p which in turn modifies the motion. Is that already sufficient for self-interaction?

In apparently simple situations, a plasma can behave counter-intuitively. Pouring milk into our coffee, we expect the milk to heat up and mix with the coffee. A sunspot is a sharply bordered volume of cool gas embedded in the hot solar photosphere; but it stays stable for several months prevented by strong magnetic fields from warming or mixing with its environment. A cold and dense volume of gas or liquid in a hot environment sinks. A solar filament is cold and dense compared with the ambient corona but it is held in position against gravity by strong magnetic fields. Such discrepancies between our daily experience and the behavior of ionized gases clearly show that plasmas do not form a significant part of our environment. Why then do we study such exotic phenomena? Are there applications for plasmas?

First, plasmas are not exotic but quite common. The interplanetary and interstellar medium and the stars are made of ionized gases. Thus about 99% of matter in the universe is plasma. Nearest regions dominated by plasmas are the magnetosphere with its radiation belts, the ionosphere, lightning bolts in the atmosphere, and, in a wider sense, the Earth's core; thus even in the system Earth plasmas are not uncommon. Plasma physics, therefore, contributes to the understanding of our environment. In turn, the natural plasma laboratories, i.e. the ionosphere, the magnetosphere, and interplanetary space, help to test the concepts of plasma physics on spatial scales and at densities unattainable in a laboratory.

Even some everyday materials can be described as plasmas because they show similarities to the free-electron plasma described above: the conduction electrons in metals and electron–hole pairs in semiconductors are charges which can move quasi-freely and lead to a behavior of the matter which can be described in the same way as for a plasma.

Second, plasmas can be used for quite worldly applications. One of the most ambitious projects is nuclear fusion: to merge hydrogen atoms to helium, imitating the processes inside the Sun and the stars, in order to create a clean and long-lasting power source. The main aspects of this project are the production of a plasma with suitable properties (density, temperature, losses) and its confinement inside a magnetic field.

There are also less spectacular applications of plasma physics. Chemistry utilizes the different chemical reactions in plasmas and neutral gases: for instance, cyan gas can be synthesized by burning coal dust in a nitrogen electric arc plasma. Plasma beams are used for ion implantation in microchip production. Plasma burners and pistols are used to cut, weld, or clean metals. Other technical applications of plasmas are as diverse as lasers, capacitors, oscillators, and particle accelerators.

Another interesting application of MHD is the magnetohydrodynamic dynamo. Such a dynamo is the source of the geomagnetic field (and also of other planetary magnetic fields as well as the Sun's magnetic field). These dynamos convert rotational energy (that of the Earth's or planet's rotation) into electromagnetic energy.

Formally, we need to assemble a set of equations that allows us to describe a plasma in hydrodynamical terms – that the reason to talk about magnetohydrodynamics.

One-Fluid Description

We shall start with the one-fluid description of a plasma, i.e. the fluid consists of one particle species only. This is entirely sufficient to introduce the basic concepts. In a real plasma, quasi-neutrality suggests the existence of two fluids with positive and negative charges, respectively. For certain phenomena, such as ion waves, a description in the framework of a two-fluid theory will be required.

In magnetohydrodynamics some assumptions about the properties of the system are made: (a) The medium can be neither polarized nor magnetized: $\varepsilon = \mu = 0$. (b) Flow speeds and speeds of changes in field properties are small compared with the speed of light: $u/c \ll 1$ and $v_{\text{ph}}/c \ll 1$. As a consequence, electromagnetic waves cannot be treated in the framework of MHD theory. (c) Conductivity is high, thus strong electric fields are immediately canceled out: $E/B \ll 1$. As a consequence, the displacement current $\partial E/\partial t$ can be ignored compared with the induction current. MHD is a theory linear in u/c , v_{ph}/c , and E/B and ignores all terms of higher order in these quantities. MHD considers the conservation laws of fluid mechanics which are concerned with mass, momentum, energy, and magnetic flux. The formal description is then based on the following set of equations:

- Maxwell's equations:

$$\nabla \cdot \vec{E} = \rho_c/\varepsilon_0, \quad (7.49)$$

$$\nabla \cdot \vec{B} = 0, \quad (7.50)$$

$$\nabla \times \vec{E} = -\frac{\partial \vec{B}}{\partial t}, \quad (7.51)$$

$$\nabla \times \vec{B} = \mu_0 \vec{j}; \quad (7.52)$$

- Ohm's law:

$$\vec{j} = \sigma \left(\vec{E} + \vec{u} \times \vec{B} \right); \quad (7.53)$$

- equation of continuity:

$$\frac{\partial \rho_c}{\partial t} + \nabla \cdot (\vec{u} \rho_c) = 0; \quad (7.54)$$

- equation of motion (momentum balance):

$$\rho \frac{\partial \vec{u}}{\partial t} + \rho(\vec{u} \cdot \nabla) \vec{u} = -\nabla p + \vec{j} \times \vec{B} + \rho \vec{g} + \rho \nu \nabla^2 \vec{u}; \quad (7.55)$$

- equation of state:

$$\frac{d}{dt} \left(\frac{p}{\rho^{\gamma_a}} \right) = 0. \quad (7.56)$$

This set of partial non-linear differential equations can be solved for given boundary conditions. For certain applications only a part of the equations is required, or some equations can be used in a simplified form: in magnetohydrostatics the left-hand side of the momentum balance vanishes while in magnetohydrokinematics an external velocity field is prescribed and therefore the momentum balance can be ignored completely.

The momentum balance gives us hints on the kind of motion: in certain slow motions the inertial term $\rho \vec{u}$ can be ignored while in weak magnetic fields the Lorentz force can be ignored. The relative strength of these two forces is determined by the ratio

$$S = \frac{B^2/2\mu_0}{\rho u^2/2} = \frac{\text{magnetic field energy density}}{\text{kinetic energy density}}. \quad (7.57)$$

For $S \gg 1$ the magnetic field determines the motion of the particles and the single-particle approach can be used. For $S \ll 1$, the magnetic field is swept away by the plasma motion, in

accordance with the concept of the frozen-in field. S is another expression for the plasma- β , giving the ratio between the gas dynamic pressure and the magnetic pressure: $\beta = 2\mu_0 p/B^2$.

It should be noted that these two definitions are useful only for an isotropic plasma. If the plasma is anisotropic, frequently a parallel and a perpendicular plasma- β are defined as

$$\beta_{\parallel} = \frac{2\mu_0 p_{\parallel}}{B^2} \quad \text{and} \quad \beta_{\perp} = \frac{2\mu_0 p_{\perp}}{B^2}. \quad (7.58)$$

In a low- β plasma ($\beta \ll 1$), the energy density in the thermal motion is much larger than in the magnetic field, while in a high- β plasma ($\beta \gg 1$) the opposite is true.

Two-Fluid Description

So far, we have treated the plasma as a fluid consisting of one kind of charged particles only. A real plasma, however, contains electrons, ions, and possibly also neutral particles. Each particle component has its own speed, temperature, and partial pressure.

Since a plasma is expected to be quasi-neutral, the number of positive and negative charges has to be equal. The charge density is $\varrho_c = n_i q_i + n_e q_e = \varrho_i + \varrho_e$ with n_i and n_e being the number densities of ions and electrons with charges q_i and q_e . The current density is $\vec{j} = n_i q_i \vec{u}_i + n_e q_e \vec{u}_e = \vec{j}_i + \vec{j}_e$. If we limit ourselves to a two-fluid plasma, we have to deal with an electron and an ion component; the neutral component is ignored. In addition to the assumptions made in the one-fluid description we assume: (a) the fluid is in thermal equilibrium ($T_i = T_e$), and (b) the plasma is quasi-neutral ($\varrho_i = \varrho_e$). The basic equations in two-fluid MHD are

- Maxwell's equations

$$\nabla \cdot \vec{E} = (\varrho_i + \varrho_e)/\varepsilon_0, \quad (7.59)$$

$$\nabla \cdot \vec{B} = 0, \quad (7.60)$$

$$\nabla \times \vec{E} = -\frac{\partial \vec{B}}{\partial t}, \quad (7.61)$$

$$\nabla \times \vec{B} = \mu_0(\vec{j}_i + \vec{j}_e) + \varepsilon_0 \mu_0 \frac{\partial \vec{E}}{\partial t}; \quad (7.62)$$

- Ohm's law

$$\frac{m_e}{e^2 n} \frac{\partial \vec{j}}{\partial t} = \vec{E} + \vec{u} \times \vec{B} - \frac{\vec{j} \times \vec{B}}{en} + \frac{\nabla p_e}{en} - \frac{\vec{j}}{\sigma}; \quad (7.63)$$

- equation of continuity

$$\frac{\partial n_j}{\partial t} + \nabla \cdot (n_j \vec{u}_j) = 0, \quad j = i, e; \quad (7.64)$$

- momentum balance (equation of motion)

$$m_j n_j \frac{d\vec{u}_j}{dt} = q_j n_j (\vec{E} + \vec{u}_j \times \vec{B}) - \nabla p_j \pm \beta(\vec{u}_i - \vec{u}_e), \quad j = i, e; \quad (7.65)$$

- equation of state

$$p_j = p_j(\varrho_j, T_j), \quad j = i, e. \quad (7.66)$$

Compared with the equations in one-fluid MHD we find the following differences: (a) The equations of state, motion and continuity are given for each component separately. (b) The equation of motion contains an additional term coupling the two components to consider momentum transfer arising from Coulomb collisions. The force between the two components depends on their relative speed, therefore $\vec{f}_i = -\vec{f}_e = \beta(\vec{u}_i - \vec{u}_e)$. (c) Gauss's law for the electric field contains both charge densities as Ampère's law contains both current densities. (d) Ohm's law has become unrecognizable. The left-hand side gives the current acceleration. The first, second and last terms on the right-hand side are expressions already known from

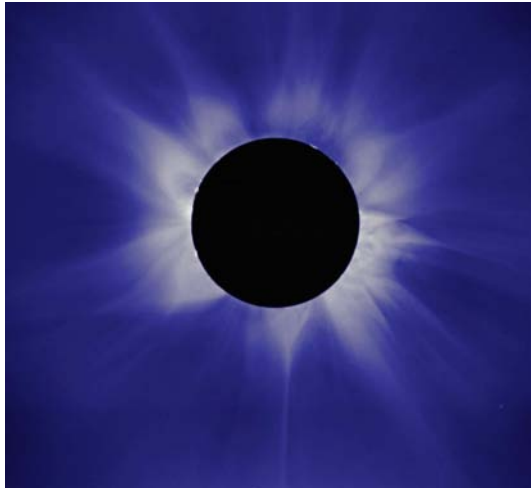


Figure 7.5: Structure of the corona during a solar eclipse. The loop-like structures indicate closed magnetic field lines inside the corona where plasma is trapped while the streamer like structures indicate plasma (and magnetic field) streaming into interplanetary space

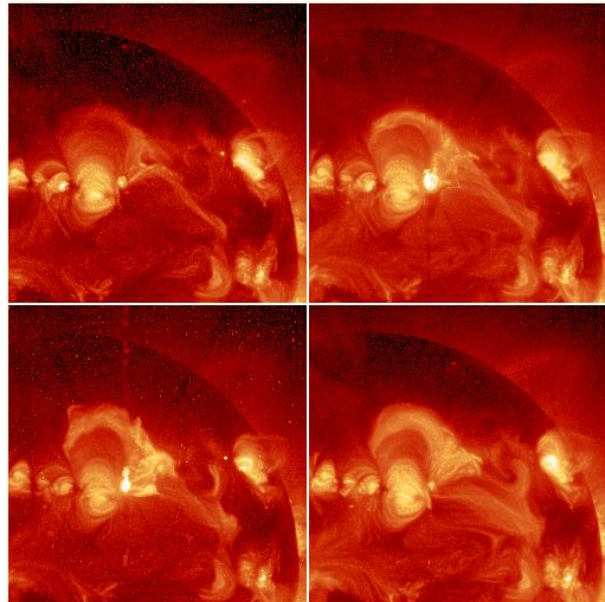


Figure 7.6: Sequence of four soft X-ray images of the Sun indicating the restructuring of coronal magnetic fields during flares and coronal mass ejections [101]

Ohm's law in one-fluid MHD. The $\vec{j} \times \vec{B}$ term is called the Hall term and describes the Hall effect: in a magnetic field the current created by the moving charges is deflected by the Lorentz force, resulting in an additional electric field perpendicular to both \vec{j} and \vec{B} . The fourth term on the right-hand side gives the pressure diffusion: in the presence of a pressure gradient, both particle species diffuse with respect to each other, creating a current along ∇p .

Simple Application of MHD in Space

Many important concepts of magnetohydrodynamics such as magnetic pressure or the concept of frozen in magnetic fields already encountered in the description of the interplanetary spiral field can be derived from the basic set of equations without touching the core of fluid dynamics: magnetic pressure and tension do not even require a motion but are a static problem, frozen in magnetic fields can be derived assuming a prescribed flow.

Although these concepts are quite valuable to understand the basics of MHD and can be applied to quite a large number of simple phenomena, their use is limited by some assumptions. For instance, in a frozen in flow the energy density must exceed that of the magnetic field by orders of magnitude. This is the case in free interplanetary space, but the assump-

tion is violated at boundaries. In the lower corona, for instance, the energy density of the magnetic field exceeds the one in the plasma flow by orders of magnitude, see also Fig. 7.5. And here all the interesting phenomena such as flares and coronal mass ejections happen when magnetic field energy is converted to plasma motion and heating, such as indicated in the sequence in Fig. 7.6. Modeling of these processes requires the simultaneous solution of the full set of MHD equations.

A similar dynamical situation arises at the front of the terrestrial magnetosphere in the interaction between the geomagnetic field and the solar wind. Although the general shape of the magnetosphere can be described in a static model based on a pressure equilibrium between the interplanetary plasma and the plasma in geospace, a dynamical approach requires the solution of the full set of MHD equations.

Graphical Description of the MHD Dynamo

Some aspects of the MHD dynamo can be derived analytically, see e.g. [88]. A few ideas are sketched below (taken from [88]).

In principle, a dynamo consists of a permanent magnet and a rotating circuit loop in which the current is induced. In the hot interior of the Sun and the planets, permanent magnets cannot exist. Thus the static magnetic field must be created by a current, too. Part of the current induced into the circuit loop than is fed back into the system to support the static field. Without such a feedback, the MHD dynamo would not work.

In the core of the Sun or the planets such well-defined parts as coils or rotating wires do not exist. Instead, we find a homogeneous and highly conductive fluid, rotating with the star or planet. Thus the dynamo also is called a homogeneous dynamo. Since the matter inside the core is liquid, the question of how to create a magnetic field can be reduced to a simpler form: What is the nature of the plasma flow that allows to support the required currents?

Since we want to apply the dynamo to planets and stars, the model has to explain the most important features of their magnetic fields, such as: (a) the magnetic flux density increases with increasing rotation speed, (b) to first-order, the field is dipole like, (c) the dipole axis and the axis of rotation are nearly parallel, (d) the dynamo should allow for fluctuations in the magnetic field direction and flux density, and (e) polarity reversals with quasi-periodic but nonetheless stochastic character should be allowed. This latter point means that the reversal period can be identified (for instance 11 years for the Sun and about 500 000 years for the Earth), but that the individual cycle lengths are distributed stochastically around this average.

Since the fields are axial-symmetric, a configuration as the uni-polar inductor in tempting. There a metal cylinder rotates parallel to a homogeneous magnetic field, leading to a potential difference between the center and the mantle of the cylinder. But in the uni-polar inductor the field cannot be amplified. For astrophysical plasmas this is expressed by Cowling's theorem, dating back to 1934: there is no finite velocity field that can maintain a stationary axial-symmetric magnetic field. The proof of this theorem is based on the induction equation which, under the conditions cited in Cowling's theorem, would allow for decaying magnetic fields only.

The situation is different in a statistical magnetic field: on the Sun, for instance, the turbulent motion in the convection zone modifies the field. The average field $\vec{B}_0 = \langle \vec{B} \rangle$ still is axial-symmetric but it is modified by fluctuations \vec{B}_1 with $\langle \vec{B}_1 \rangle = 0$ – we have encountered a similar approach already in the discussion of quasi-linear theory in sect. 5.2.5. Thus the magnetic field is $\vec{B} = \vec{B}_0 + \vec{B}_1$ and the velocity field is $\vec{u} = \vec{u}_0 + \vec{u}_1$. The cross product of the speed and the magnetic field reads

$$\langle \vec{u} \times \vec{B} \rangle = \vec{u}_0 \times \vec{B}_0 + \langle \vec{u}_1 \times \vec{B}_1 \rangle. \quad (7.67)$$

The products $\langle \vec{u}_1 \times \vec{B}_0 \rangle$ and $\langle \vec{u}_0 \times \vec{B}_1 \rangle$ vanish because the quantities with index 'o' are constant and the average of the other quantity equals zero. The product $\langle \vec{u}_1 \times \vec{B}_1 \rangle$, which is the correlation function, does not vanish because the fluctuations are not independent:

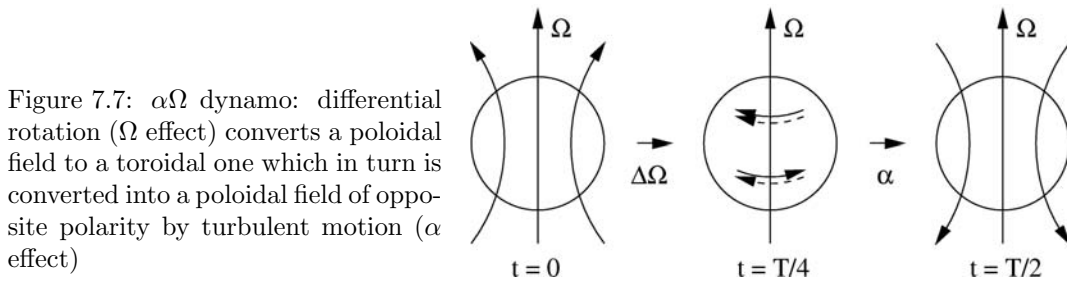


Figure 7.7: $\alpha\Omega$ dynamo: differential rotation (Ω effect) converts a poloidal field to a toroidal one which in turn is converted into a poloidal field of opposite polarity by turbulent motion (α effect)

because the matter has a high conductivity, the magnetic field is frozen-into the plasma, and a change in the velocity field leads to a corresponding change in the magnetic field. To first order, the correlation function can be approximated as

$$\langle \vec{u}_1 \times \vec{B}_1 \rangle = \alpha \vec{B}_0 - \beta \nabla \times \vec{B}_0. \quad (7.68)$$

The basic idea of the MHD dynamo can be applied to different geometries and to stationary as well as periodically varying magnetic fields. Because we are interested in axially symmetric fields, it is reasonable to describe the magnetic field as consisting of a toroidal and a poloidal part:

$$\langle \vec{B} \rangle = \langle \vec{B}_{\text{tor}} \rangle + \langle \vec{B}_{\text{pol}} \rangle = B \vec{e}_\phi + \nabla \times A \vec{e}_\phi, \quad (7.69)$$

where \vec{e}_ϕ is the unit vector in the toroidal direction. Thus two scalar quantities, A and B , determine the three field components. With this ansatz, the induction equation gives two equations: one describing the ohmic dissipation of B and the generation of B out of A due to the α -effect and the differential rotation $\nabla\Omega$, the other describing the ohmic dissipation of A combined with the generation of A out of B .

Differential rotation can occur for various reasons. The Sun, for instance, has a higher angular speed at the equator than at higher latitudes, and thus the rotation depends on latitude. The differential rotation inside the Earth is due to the differences in angular speed between the faster inner and the slower outer core. In both cases, because the field is frozen into the plasma, a deformation of the field line arises from the differential rotation.

The α -effect, on the other hand, is associated with the turbulent motion of the plasma, in particular the upward and downward motions associated with convection. Although this motion is stochastic, its combination with the Coriolis force leads to a turbulent motion which introduces a systematic twist into an originally toroidal field. The resulting magnetic field coil allows a current parallel to the undisturbed toroidal field.

The combination of the effects of α and Ω allows us to describe the MHD dynamo. We start with a poloidal field in the Sun at $t = 0$. The differential rotation deforms the magnetic field, leading to a toroidal field ($t = T/4$). The α -effect leads to electromagnetic forces parallel to the field, and thus a toroidal current flows (dashed lines). Although the magnetic field directions are opposite in the two hemispheres, the asymmetry of the Coriolis force leads to an asymmetric α -effect and therefore parallel currents in both hemispheres. This current leads to a magnetic field directed opposite to the original field ($t = T/2$). Half a cycle is now finished. This dynamo is called the $\alpha\Omega$ dynamo because both the α -effect and the differential rotation contribute to the dynamo process. The dynamos inside the Sun and the Earth are based on this principle.

If the α -effect was not at work, the differential rotation would still transform the poloidal magnetic field into a toroidal one. However, no polarity reversal would occur and, in time, the entire field would dissipate. The differential rotation, on the other hand, is not essential to the MHD dynamo. The α -effect can also work with turbulent motions which, for some reason, have a preferred direction of motion; this is often an upwelling of magnetic flux combined with a particular direction of rotation of the flux tubes.

The MHD dynamo requires an initial magnetic field which is amplified by a suitable feedback mechanism. Thus at first glance the MHD dynamo violates Lenz's rule which states

that all fields, currents and forces are directed so as to hinder the process that leads to their induction. For instance, an increase in the magnetic field leads to currents which create a magnetic field opposite to the original one. Lenz's rule thus stabilizes the system; it does not allow for the positive feedback required in the MHD dynamo. Were we to build such a dynamo on the basis of one process only, Lenz's rule would be violated. But the MHD dynamo has the remarkable feature that although all individual processes obey Lenz's rule, their sum allows for positive feedback.

CFD

Analytical approaches allow us to describe the main aspects of the MHD dynamo – and thus to identify its principle ingredients and to understand the basic processes. However, all analytical approaches do not allow to model a dynamo self-consistently. A particular problem are the details of the polarity reversal: it is easy to model (and to understand) the build-up of magnetic flux but the reversal process, that is basically the break down of the flux and the start with opposite sign, are difficult to model.

A full CFD model of the relevant MHD equations (7.49)–(7.57), leads to promising results. Some examples can be found on the web. A Japanese group gives a report on the FEM implementation of the problem on http://geofem.tokyo.rist.or.jp/report_common/GeoFEM02_004.pdf and a second report on the optimization of the code for the Earth Simulator on http://geofem.tokyo.rist.or.jp/report_common/GeoFEM02_009.pdf. The preference for ES might explain why we do not do MHD dynamos as end-of-term projects. Results from the simulations can be found in a picture gallery on <http://www.tcsc.nifs.ac.jp/kage/gallery/gallery-dynamo.html>. Glatzmeier's famous dynamo makes its appearance on <http://www.es.ucsc.edu/~glatz/geodynamo.html>; at this page, also links to other dynamo projects are given. From the German side, the AIP dynamo could be mentioned (<http://www.aip.de/groups/mhd/index.engl.html>) – these are rather simple descriptions that do not go into technical details.

7.4 Literature

A very good introduction into the basics of fluid dynamics and also into some technical aspects of the equations is given in Faber's book [42]; a classical text on the same topic is Pedlow's [127], an interesting side aspect is added to the physics in Massel [109]. A very readable and concise text on the basics of CFD is Chattot [29]. That text also gives a good introduction into the different types of PDEs.

Since the atmosphere and the oceans are fluids and play an important role in the meridional energy transport, CFD also plays an important role in oceanography and atmospheric science, in particular also in climate modeling.

Exercises

Aufgabe 14 Use a different algorithm for the numerical solution of the problem in sect. 7.2. Compare solutions regarding accuracies and runtime for different step of the numerical schemes.

Energetic Particles in the Atmosphere: Monte Carlo Simulation

The Monte Carlo method is a statistical method. The first encounter with Monte Carlo simulations often is numerical integration. Here a Monte Carlo method is the modern version of the old method of weighting a graph of the function to be integrated. Since the solution of a differential equation also invokes integration (as can be seen best in the method of separation of variables), Monte Carlo methods also can be applied to the solution of differential equations.

Monte Carlo aspects also enter into transport problems if transport parameters cannot be determined reliably. Here a solution of the transport equation might invoke statistical variations in the relevant parameter, according to its observed distribution.

Goals: after working through this chapter you should be able:

- to explain the basic ideas of Monte Carlo simulations and compare the method to the more conventional approaches of FDM and FEM.
- to develop and run Monte Carlo models for simple problems.

8.1 Monte Carlo – A first Encounter

As mentioned in the introduction, the first encounter with Monte Carlo methods often is numerical integration.

8.1.1 Numerical Integration

π is not a rational number. So how can π be determined? While the Euler number e can be introduced (and calculated) as a series, π is defined by the circle in such that it described the relation between the circumference of or the area inside a circle and its radius. Consequently, π only can be determined by comparison between the radius and other properties of a circle (ok, Archimedes introduced a series that led to π , thus a definition of π by a series also is possible).

A simple approach could start with drawing a large circle on a sheet of graph paper. If we than count the number of squares inside the circle, we get some approach on the circle's area and by relating this to its radius also on π . A different 'hands on' version relies on drawing a circle on a plank with known area, weighting the plank, sawing out the circle and weighting it. The relative weight of the circle compared to the weight of the plank yields the area of the circle relative to that of the plank. Thus π can be determined.

The Monte Carlo approach is quite similar, although neither paper nor plank is required. Take a square in number space, for instance $[-1 \leq x \leq 1, -1 \leq y \leq 1]$. This square occupies

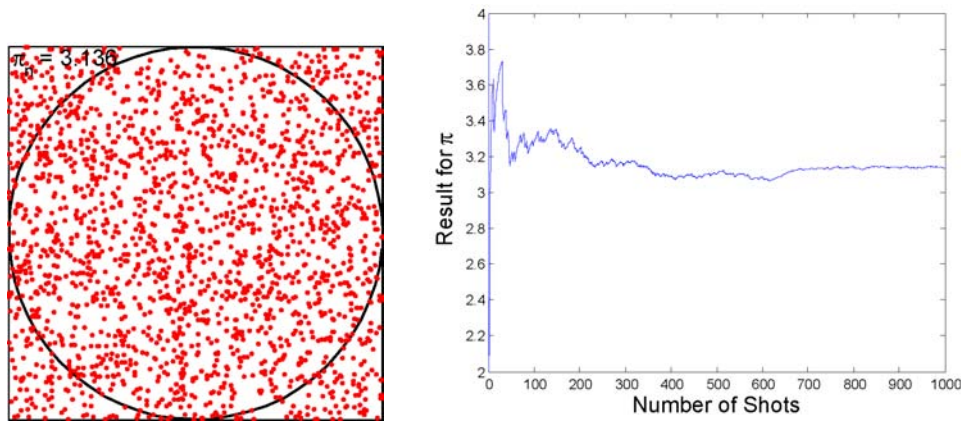


Figure 8.1: Monte Carlo method to determine π : (left) points picked out arbitrarily; (right) development of the result as the number of points increases

on area of 4 AU.¹ All points inside this space either belong to a circle of unit radius around the origin or do not belong to it: for $\sqrt{x^2 + y^2} \leq 1$, the point (x, y) belongs to the circle, for $\sqrt{x^2 + y^2} > 1$ it does not belong to it. We know select arbitrarily points (x, y) in the number space and check whether they belong to the circle or not. If they do, the counter `incircle` is incremented; for each selection, the counter `number` is incremented. This gives as π :

$$\frac{\text{incircle}}{\text{number}} = \frac{\pi}{4} \quad \Rightarrow \quad \pi = 4 \frac{\text{incircle}}{\text{number}} . \quad (8.1)$$

A less formal description of this method (may be even suitable for a Terminator) might be such: draw a circle on a large square of plywood. Take a machine gun with broad scatter. Fire. Count the impacts inside the circle and the number of impacts on the board. Ask somebody to evaluate the ratio between the two to compute π .

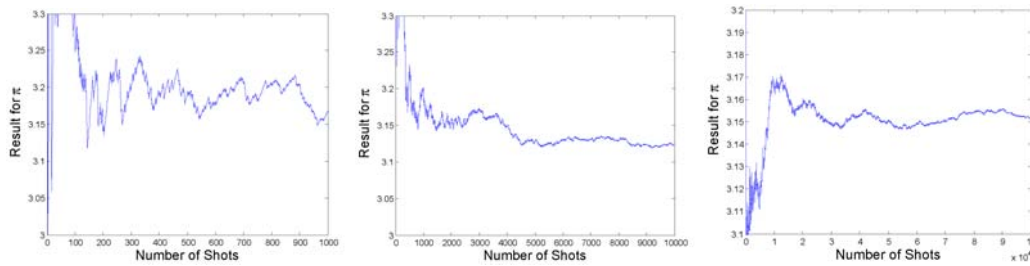
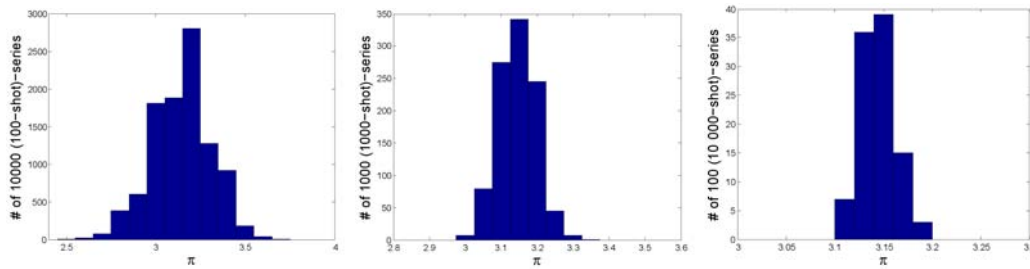
The left part of Fig. 8.1 shows a sample result for such an experiment with 1000 shots fired, although this particular experiment was performed with the computer. The right panel shows how the result evolves towards π . For small numbers of shots, the deviation from π can be quite large: with one shot, the result is either hit or miss. Or in numbers: 0 or 4. With the second shot, we might have two hits, one hit or zero hits. Or in numbers 0, 2 or 4. And so on. For the sample in the figure, the initial shot was a hit on the circle, the next a miss and all 8 following shots were hits. Thus the first ten results on π read

1	2	3	4	5	6	7	8	9	10
4.	2.	2.6667	3.	3.2	3.3333	3.4286	3.5	3.5556	3.6

As expected from this series and also visible in the right panel in Fig. 8.1, the accuracy of the result increases as the number of shots becomes larger. However, accuracy does not increase linearly with number of shots. Instead, there can be deviations from the true value into one direction for an extended number of shots in a row. Similarly, sustained deviation into the other direction might arise. We have encountered this behavior of random processes already in connection with the drunkards walk, see in particular Fig. 4.1.

The situation does not improve too much if the number of shots is increased. Figure 8.2 shows the development of the result with the number of shots for 1000 (left), 10 000 (middle) and 100 000 (right) shots. The 1000-shot panel (left) is a good example for the strong variability of the result. Note that the right panel in Fig. 8.1 also has been obtained for 1000 shots: here the scatter is much smaller and after about 400 shots the result does not change very much. With the 1000 shot panel in Fig. 8.2 the situation is different: the result at shot 880 would be larger by 0.5 than the result at shot 960 – and even that is larger than the target number π . Thus one round with 1000 shots apparently does not necessarily give a reliable result.

¹AU here is not meant as astronomical unit but as area unit (or as arbitrary unit for the area).

Figure 8.2: Variation in the result for π depending on the number of shotsFigure 8.3: Variation in the result for π depending on the number of shots

Strategies to improve the results obviously rely on strategies improving the statistics. One might suspect, that a larger number of shots yields better results. A comparison of the 1000 shot and the 10 000-shot panels in Fig. 8.2 suggests scattering to be reduced as the number of shots increases, however, the results still deviates from the target and it also shows varying trends that allow for rather large deviations from the target value. The result only becomes slightly better when we look at the 100 000-shot panel. Nonetheless, even its variation allows for sustained deviations from the target result – although the number of shots and thus the computing time has been increased by a factor of 100 compared to the 1000-shot panel.

A different approach on improving statistics is the repetition of the shooting process and subsequent averaging of the results. To get some feeling for the process, we can analyze a 10^6 -shooting package in different ways. First, the points are broken into 10 000 parcels with 100 points each. The distribution of results for π is shown in the left panel of Fig. 8.3. The distribution is rather broad; simulated values for π can be as low as 2.5 and as large as 3.7. Thus one might be tempted to argue that 100-shot series are too inaccurate to be useful. However, a closer look at the distribution shows that about 46% of the 100-shot runs yield values in the interval (3.1, 3.2) and thus are relatively close to the target value of 3.1416. The average value of π from this shooting is 3.1446.

For the middle panel in Fig. 8.3 the same vector of 10^6 points is broken into 1000 parcels with 1000 shots each. The distribution is narrowed down to values between 3.0 and 3.35; again, about 85% of the values lie in the interval (3.1, 3.2). The lack of values with strong deviation from the target value, such as observed in the left panel, is partly caused by the higher accuracy and partly by the lower total number of trials.

In the right panel of Fig. 8.3 the distribution of 100 parcels with 10 000 shots each is shown. All values lie within the interval 3.1 to 3.2.

It should not come as a surprise to you that the average values of π in all three versions is 3.1446. Assume a vector of n elements. Its average is

$$\langle x \rangle = \frac{1}{n} \sum_{i=1}^n x_i . \quad (8.2)$$

Let us now break the vector into k subvectors of length n_k with $n = k n_k$. The average of

each part then is

$$\langle x_{n_k} \rangle = \frac{1}{n_k} \sum_{i=1}^{n_k} x_i . \quad (8.3)$$

Since all n_k are equal, the average of the subvectors then is

$$\langle x_{\text{subs}} \rangle = \frac{1}{k} \sum_{i=0}^k \langle x_{n_k} \rangle = \frac{1}{k} \sum_{i=0}^k \left(\frac{1}{n_k} \sum_{i=1}^{n_k} x_i \right) = \frac{1}{k} \frac{1}{n_k} \sum_{i=0}^k \left(\sum_{i=1}^{n_k} x_i \right) = \frac{1}{n} \sum_{i=0}^n x_i = \langle x \rangle .$$

8.1.2 Accuracy of a Monte Carlo Result

Tossing a coin is a statistical process. Here we are interested in the number X of hits (e.g. heads) in n tosses with X_i being the result in the n th toss. The variate (or random variable) X_i obeys a Bernoulli distribution with parameter (probability for a positive result) p . In this case, we get for the expected value $\mu = p$ and for the standard deviation $\sigma^2 = p(1-p)$. The difference between the Monte Carlo approximation Y and the parameter μ to be determined is according to the 3σ -rule

$$P\left(-3\frac{\sigma}{\sqrt{n}} < Y - \mu < 3\frac{\sigma}{\sqrt{n}}\right) \approx 0.997 . \quad (8.4)$$

This equation can be used to determine the number n of trials required to obtain with a probability of 99.7% an approximation on μ with a given accuracy ε .

The ansatz

$$\varepsilon = 3\frac{\sigma}{\sqrt{n}} \quad \Leftrightarrow \quad n = \left(3\frac{\sigma}{\varepsilon}\right)^2 \quad (8.5)$$

yields the approximation

$$n \geq 9\frac{\sigma^2}{\varepsilon^2} . \quad (8.6)$$

8.1.3 How Random are Random Numbers?

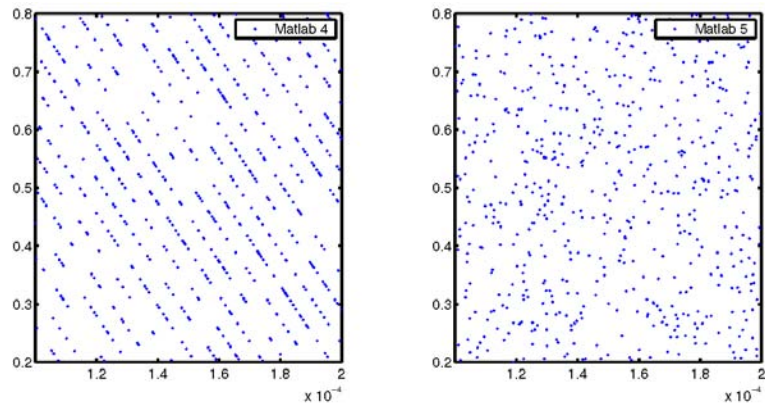
Compared to rolling a dice or tossing a coin, a random number generator never is random. Instead, it is based on an algorithm. Normally, this is a simple algorithm: a seed number is multiplied by a large number, another large number is added and everything is normalized to the maximum possible number that can be handled during the process. The new un-normalized number serves as seed for the next random number and so on. The seed is either a fixed variable or can be taken e.g. from the system clock. If the seed is a fixed variable, the same sequence of random numbers is generated when the random number generator is started. If a different number is taken as seed, either provided by the user or some system variable, each initialization of the random generator creates a different series of random numbers.

In MatLab, the state of the random number generator is set at the start of MatLab. If not provided with a seed, the random number generator always yields the same sequence of random numbers. However, if `rand` is called repeatedly during one MatLab session, the individual series will show different sequences because the last value of the first series is the seed for the second series and so on. However, the total sequence of numbers will be the same.

The process is supposed to generate equally distributed numbers in the range $[0,1]$ (if normalized) or in some other prescribed range.² Even simple random generators tend to fulfill this requirement of yielding equally distributed numbers. A more serious problem arising from the algorithm is repetition: once the random generator yields a number that (during

²In Matlab, the range is not exactly $[0,1]$ but instead $[\text{eps}, 1-\text{eps}]$ with eps being 2^{-53} . If you think it is relevant to correct the code for this deviation, please feel free to do it.

Figure 8.4: Test of a random number generator [159]



this run) already has been used as a seed number, the entire sequence from that seed to its first repetition will be repeated endlessly – the random number generator will never deviate from the sequence but stick to it. If that happens, random numbers no longer are statistically independent. A simple way to check for this dependence is to generate two vectors of random numbers and plot one versus the other. If the numbers are statistically independent, the points are distributed stochastically, as can be seen for a small part of the number space in the right panel of Fig. 8.4.

MatLab provides three different modes for the random number generator (see `rand.m` in the Matlab directory `.\toolbox\matlab\elmat`). The right panel of Fig. 8.4 has been obtained from the standard version of the random number generator, for the left panel the older version implemented in Matlab 4 and earlier has been used. Here the patterns indicate that the random numbers are not statistically independent – the random number generator starts to repeat itself.

8.2 Monte Carlo Simulation – First Steps

A Monte Carlo simulation tracks the fate of individual particles (or volume elements) during the simulation. Thus as in numerical integration, the accuracy of the result depends on the number of particles under study – as does the computing time. To illustrate the process of a Monte Carlo simulation let us start with some simple physical problems that are suitable for such a simulation.

8.2.1 Radioactive Decay

Radioactive decay obviously is a problem most suitable for Monte Carlo simulation. We are interested in the number $N(t)$ of particles left at time t . Formally, this process can be described by a simple ODE

$$\dot{N} = -\lambda N \quad (8.7)$$

with λ being the decay probability. Thus the process is stochastic. As in a finite difference solution, the simplest approach divides time in steps Δt . For each particle we now follow the time line: after each time step Δt , we throw a dice/coin and decide whether the particle decays or not. If it decays, the particle cannot be tracked any longer.

The main challenge in this procedure is the tracking of the large number of particles. Depending on the problem under study, we can try different approaches:

- if we are interested in the number of remaining particles at a certain time t_{end} , we can simulate each particle along the time line: either it arrives at t_{end} or not. The number of particles arriving at t_{end} then gives the desired result.

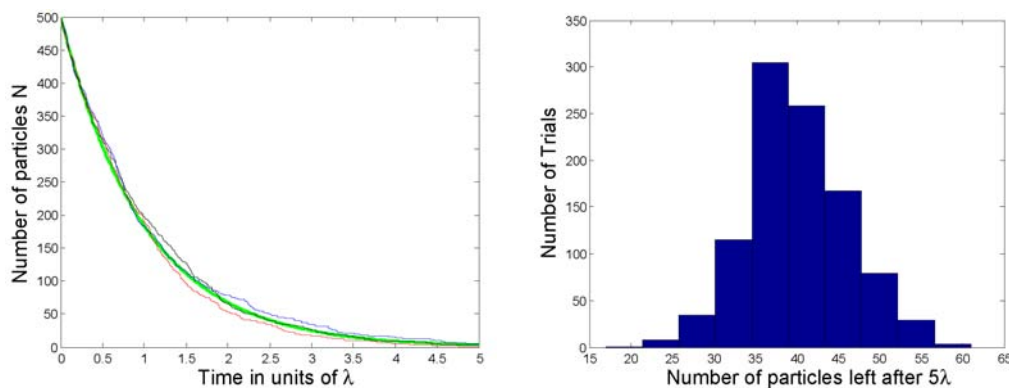


Figure 8.5: Comparison of three Monte Carlo simulations and the analytical solution (green) for the radioactive decay (left). In the right panel, the distribution of results at $t = 2.5$ is shown for a set of 1000 different Monte Carlo runs; the expected value is 41

- if we are interested in the development of $N(t)$, a different approach might be successful. Create a vector of ones with its length corresponding to the number of particles considered in the simulation. At the end of each time step, a stochastic vector is created, containing a zero if the particle decays or a one if it survives. Pointwise multiplication gives the fate of the particles at the end of the interval, the number of ones in this new vector gives the desired $N(t)$.

Of course, both methods also can be applied to the other problem. The first method is fast in such that it does not consider a particle any longer ones it has decayed. However, it requires to keep track of the fates of all particles. The second method is simple in the tracking of the fate of all particles, however, with increasing time the number of zeros in the particle vector increases and the subsequent mathematical manipulation is not required.³

The result of such a Monte Carlo simulation can be compared to the analytical solution for the decay. But what is the advantage of the Monte Carlo simulation? Its disadvantage is obvious: the Monte Carlo simulation is time consuming because a large number of particles must be tracked through a rather large number of time steps. And the result of an individual run does not even give the exact analytical solution as can be seen from the left hand side of Fig. 8.5. Thus as in numerical integration a number of Monte Carlo simulations is required to obtain a stable result. So what is the advantage of this numerical effort? The deviation of the Monte Carlo simulation from the analytical solution reflects the underlying physical process better than the analytical solution: the analytical solution gives the average value of a large number of different possible versions of reality. Each Monte Carlo simulation gives one of these possible realities. Thus the combined results from a number of Monte Carlo simulations gives an approximation on the average result (which also is the analytical result) and on the distribution of results around this average as shown on the right hand side in Fig. 8.5. Thus we do not only get the expected result but also some information about the likelihood and size of deviations from this result. In consequence, the additional numerical efforts in the Monte Carlo simulation also give additional information.

As sideeffect of this reasoning we should realize that a Monte Carlo simulation consumes too many computational resources to be useful for the simulation of a deterministic process but provides additional information in case of a stochastic process.

Side question 28 Is this true? Discuss pros and cons of Monte Carlo simulations in deterministic processes.

³One might modify this approach in such that only the ones in the vector are tracked: thus the length of the vector (as the length of the vector with the random numbers indicating decay or survival) decreases with increasing time.

8.2.2 Convection and Decay

Let us now expand our model from an ODE to a PDE, that is we will introduce a spatial coordinate in addition to time. To describe the idea, we will simply assume that the particle population is advected with speed v along the x -axis.

The details of the model depend on our problem, for instance whether we are concerned with a δ -injection or a continuous injection. Let us start with a δ -injection. Again, we divide time in steps of size Δt . During each time step, two things happen: (a) the particle is advected a distance $\Delta s = v \Delta t$ and (b) at the end of the time step the particle might decay or not (as in the previous section). Since space and time are directly coupled, we can recycle the results from the simple decay model by just scaling the time axis on $N(t)$ by v : in that case, we get $N(s)$ not as a dependence of particle number on spatial coordinate at a fixed time but as particle number that would be observed at position s at time $t = s/v$ as the particle peak is advected across the observer.

Is the situation of a continuous particle injection really different from the δ -injection? Physically, the situation is different because at a fixed distance we will not observe a pulse of particles propagated over the observer but instead a roughly constant intensity: on average the number of particles advected from the upstream medium is the same as the sum of the decaying particles and the particles advected into the downstream cell.

How would we simulate this? Basically we can adopt the $N(t)$ -method from the simple decay: define a matrix $N(s)$ of particles with each column i containing the existence-index of particles at the position x_i . At the end of each time step Δt a random decay matrix is determined and multiplied pointwise with $N(s)$. Then the columns are advanced from x_i to x_{i+1} and the fresh injection is added at x_0 . Thus for each time step $N(s)$ is determined. An approximation on the steady-state solution is acquired as soon as the first particle pulse arrives at the end of the simulation volume.

Side question 29 Is this true? Does this depend on the properties of the boundary? What in case of a (partially) reflecting boundary?

As in case of the radioactive decay, this is an approximation only: while the steady-state obtained from the analytical solution represents some expected state, the individual realizations of the particle distribution can be quite different. Thus again, the Monte Carlo simulation gives not only an approximation on the analytical solution but has the added benefit of providing information about the variations.

8.2.3 Longitudinal Tank

The above model becomes more interesting (and more realistic) if we allow for dispersion in addition to the advection. Physically, we have the same situation as discussed in detail in chap. 3. The Monte Carlo simulation differs from the one described above in such that a second stochastic process is added, the dispersion. Thus at the end of each time interval, the particle is advected (systematic process), it is determined whether it decays or not (stochastic, see above) and a coin is thrown to determine whether it is transported backwards or forwards by dispersion. The development of an implementation of this simulation and its test is the goal of project 4 as described in sect. ??.

Side question 30 Re-evaluate all physical examples discussed in this text for their suitability in Monte Carlo simulations.

8.3 Energetic Charged Particles in the Atmosphere

Within in the framework of the two DFG-Special Programs ‘Geomagnetic Variations’ (http://www.geophys.tu-bs.de/spp/index_en.html) and ‘CAWSES’ (<http://www.iap-kborn.de>).

⁴In consequence, spatial and temporal step size are coupled. This is also the case in FDMs.

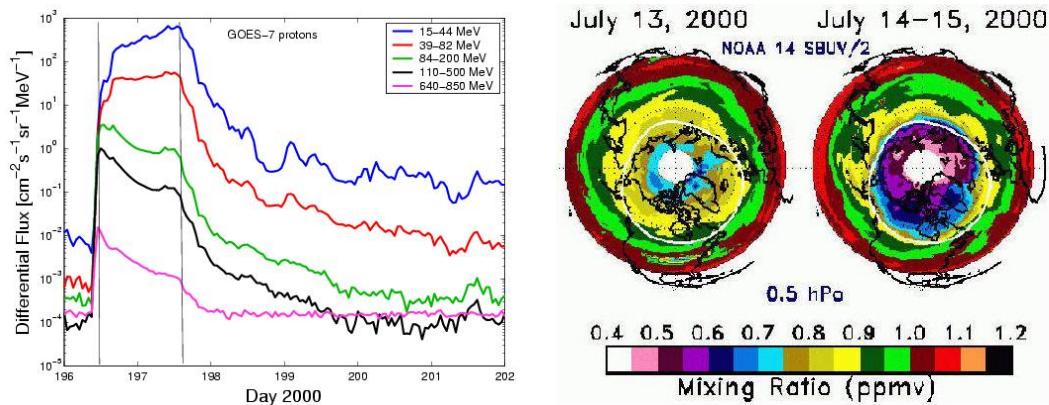


Figure 8.6: Right: Intensity–time profiles for the Bastille Day event (July 14, 2000); Left: variation in ozone concentration on the northern hemisphere [75]

de/causes/index.e.htm) our group studies the consequences of precipitating energetic particles in the atmosphere. Sources of these particles are the magnetosphere and the Sun. The primary consequence of their precipitation is ionization of the atmosphere at heights between about 15 km and 100 km where the atmosphere under normal conditions is neutral. The secondary consequence of such ionization is a change in atmospheric chemistry, in particular the depletion of ozone.

The left panel in Fig. 8.6 shows the intensity time profiles for the July 14, 2000, solar energetic particle (SEP) event (Bastille Day event) as observed in geostationary orbit. The profiles correspond to different proton energy range with the topmost profile (blue) representing the lowest energy (15–44 MeV) and the lowermost profile (magenta) representing the highest energies (640–850 MeV). The points at the left boundary represent background intensities. Thus during the event an increase in the lower energetic protons lasts for more than 1 day and amounts to more than 5 orders of magnitude. Thus a solar energetic particle (SEP) event is a strong forcing signal onto the atmosphere.

The right panel in Fig. 8.6 shows ozone concentrations above 0.5 hPa, that is above about 45 km, in the northern hemisphere. The left part is observed on July 13 prior to the event. The normal latitudinal pattern with higher concentrations at low latitudes (ozone production regions) and lower concentrations at high latitudes is apparent. Observations directly over the pole are not available due to the inclination of the satellite orbit. The thin white ring marks the polar cap: here SEPs are not deflected by the geomagnetic field and can precipitate down into the atmosphere.

The right part of the right panel of Fig. 8.6 shows the result of such particle precipitation: ozone concentrations inside the polar cap drop by 30–40% while they stay at constant level at lower latitudes.

Our interest in energetic particles and ozone lies in three domains, see also the more detailed description in sect. 8.3.3:

- individual events: they are required for calibration of the model because the signal is large (see left panel in Fig. 8.6) and thus atmospheric responses are well defined and can be identified easily in the observational record. Therefore these events can be used to validate the model.
- atmospheric consequences in case of a weakening geomagnetic field or even a field reversal. In this case, particle precipitation would not be limited to the polar cap but would occur over a more extended spatial region. Would this also cause a stronger depletion in ozone? The question is not as far fetched as it appears because polarity reversals often also are accompanied by climate change and the extinction of species. This question is topic of our project ‘Numerical simulation of the atmospheric ionization and the generation of cosmogenic nuclides for different topologies of the geomagnetic field’ within the framework

of the DFG Schwerpunktprogramm ‘Geomagnetic Variations’.

- climate consequences: ozone has radiative properties. Thus ozone concentrations determine the local absorption and emission coefficients of the atmosphere. In consequence, thermal patterns in the atmosphere can be modified which in turn influences the circulation. This question is topic of a common project with the Max-Planck Institute for Meteorology (Hamburg) ‘The atmospheric response to solar variability: simulations with a general circulation and chemistry model for the entire atmosphere’ within the framework of the DFG Schwerpunktprogramm ‘CAWSES – Climate and Weather in the Sun–Earth System’.

While the latter two projects are the more ambiguous ones, the first is the most important one: only if that model sequence works correctly, also the more interesting questions can be tackled. Thus we will here briefly discuss its main steps.

8.3.1 Modeling Individual Events

First observations of SEP event related ozone decreases date back to the 1970s, in particular to the large event in August 1972. Paul Crutzen and coworkers [33] were the first to identify the reactions involved in this effect: basically, the ionization by precipitating charged particles leads to the formation of NO_x and HO_x . Both species are highly reactive. In particular, both destroy ozone. These observations led Crutzen conclude that nitrite oxides play an important role in ozone chemistry – this discovery earned him 1/3 of the nobel prize in 1995.

While the qualitative description of the process is well established, its quantitative description suffers some problems. The observed quantities are, as indicated in Fig. 8.6, the energetic particle flux outside the atmosphere and magnetosphere on the one hand and the temporal/spatial variation of ozone in the atmosphere. The quantitative description of this process requires a sequence of three models:

- a model to understand the particle transfer through the geomagnetic field: SEPs are precipitating almost homogeneously onto the magnetosphere and then are either deflected by the magnetic field or allowed to precipitate down to the atmosphere. In a static magnetosphere, particle orbits can be calculated by integration of the equation of motion. In a dynamic magnetosphere, the same approach can be used, although it is pretty time consuming and requires an additional, time-dependent CFD-model of the dynamical magnetosphere, such as briefly mentioned in sect. 7.3.3.
The result of this model is a spatial pattern of precipitating particles on top of the atmosphere.
- a model to describe the ionization of the atmosphere by precipitating charged particles. This will be described in detail below.
The result of such a model is an ion–pair production rate in the atmosphere, depending on the horizontal coordinate (as inferred from the model magnetosphere above) and the vertical coordinate (depending on the energy spectrum of the precipitating particles).
- a model to describe the chemistry of the atmosphere. Such a model includes a large number of chemical reactions as well as some prescribed (or even self-consistently solved) transport and needs the ion–pair production rates as input.
The result is a 2D or 3D (depending on the dimensionality of the model atmosphere) ozone concentration that can be compared to the observations.

Thus the chain from observation 1 (SEPs in space) to observation 2 (ozone) leads through 3 models.

For the present day magnetosphere, the horizontal pattern of precipitation and therefore also ion–pair production is simple: SEPs precipitate inside the polar cap but not outside. Here the instruments on polar orbiting satellites can be used to derive a detailed description of the precipitating particles and the (variable) size of the polar cap.

The vertical pattern of ion–pair production is regulated by the spectrum of the incident particles. The primary energy loss mechanism for charged protons in the energy range under

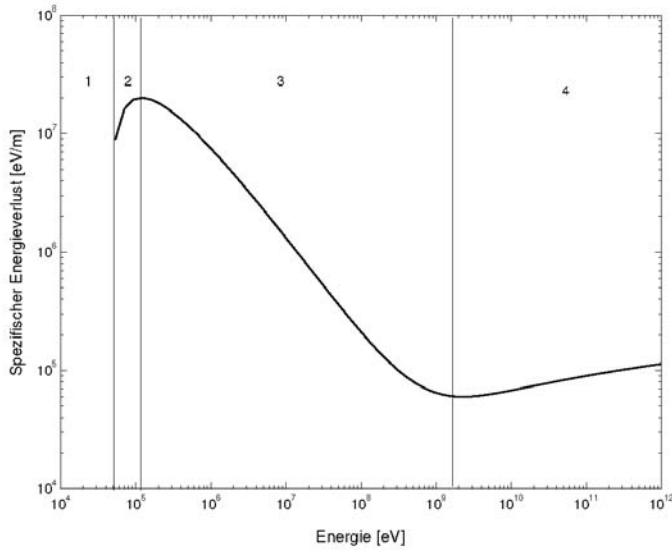


Figure 8.7: Specific energy loss according to the Bethe–Bloch equation for protons [134]

study is ionization. Formally, this process is described by the Bethe–Bloch equation

$$\frac{dE}{dx} = -\frac{e^4}{4\pi\epsilon_0^2 m_e} \frac{Z^2}{v^2} n_e \left[\ln \frac{2m_e v^2}{\langle E_B \rangle} - \ln(1 - \beta^2) - \beta^2 \right]. \quad (8.8)$$

The specific energy loss dE/dx is the energy dE deposited per unit path length dx along the particle track. It depends on (1) a number of constants (first fraction; the elementary charge e , the electron mass m_e and the absolute permeability ϵ_0), (2) the parameters of the incident particle (second fraction: charge Z and speed v), and (3) the electron density n_e of the absorber. The first term in the bracket contain the relative kinetic energy compared to the average bond energy $\langle E_B \rangle$ in the target material. The remaining terms are relativistic corrections with $\beta = v/c$.

Figure 8.7 shows the specific energy loss depending on the particle energy for protons. The specific energy loss decreases with increasing particle energy (interval 3) because the time for interaction decreases with increasing speed. dE/dx becomes minimum around the particles rest energy, afterwards it increases slightly due to relativistic effects (interval 4). Since this is a general behavior, Fig. 8.7 also can be applied to other particle species as long as the horizontal axis is scaled in units of the particle’s rest energy (938 MeV in case of the proton) instead of its energy.

The specific energy loss is maximum at low energies (interval 2). In consequence, the specific energy loss becomes largest close to the end of the particle’s range. Thus the deposited energy as well as the resulting ion–pair production becomes maximum at the end of the range, the so-called Bragg peak. For very low energies (interval 1), the Bethe–Bloch equation is no longer valid: here the main physical processes are collisions between thermal particles and attachment of the electron to an ion. Both processes are not described by the Bethe–Bloch equation.

The energy loss of a particle along its track can be calculated by numerical integration of (8.8). Figure 8.8 shows in its right panel the calculated ion–pair production rates (that is specific energy loss divided by average ionization energy) for three subsequent 12 h intervals, the first one starting at the time marked by the left horizontal line in the left panel. During this interval (blue curve), ion–pair production occurs down to about 15 km because particle energies are rather high (the magenta curve has already acquired its maximum while the blue curve still is rising). With increasing time (going from blue to red to green), the ion–pair production rate shifts to higher altitudes because the intensities at higher energies already are decreasing. In addition, ion–pair production at altitudes around 70 km is increased because the intensities in the lower proton energies (blue curve in the left panel) still are increasing.

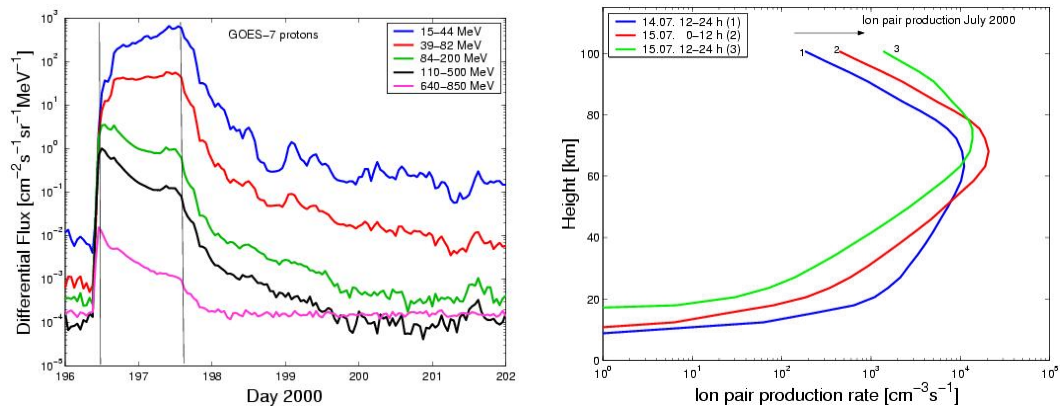


Figure 8.8: Bastille Day event: Particle intensities (left) and ionization rates (right) [134]

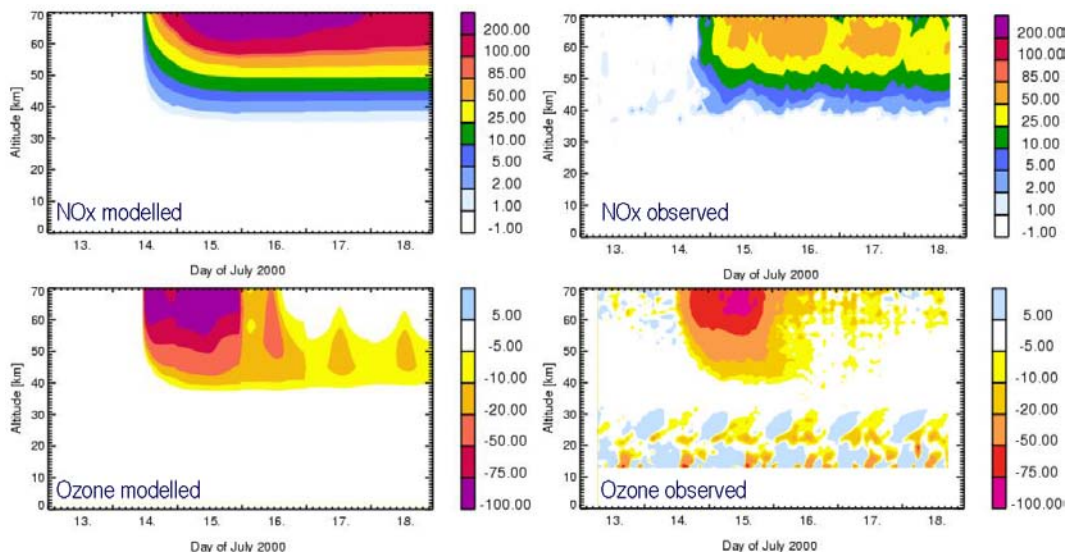


Figure 8.9: Bastille Day event: observed (right) and modeled (left) NO_x (top) production and ozone (bottom) depletion (M. Sinnhuber, U. Bremen, priv. comm.)

For the total model chain, these data now are fed into the model atmosphere. Figure 8.9 shows the modeled (left) and observed (right) NO_x production (top) and ozone depletion (bottom). Although the modeled results tend to overestimate both the NO_x production and the ozone depletion, the overall temporal and spatial pattern is reproduced quite well.

8.3.2 Monte Carlo Simulation of Atmospheric Ionization

Sofar, we have used a direct numerical integration of (8.8). But that approach has two disadvantages. First of all, the Bethe–Bloch equation is an empirical law derived from observations at the ground, that is in a standard atmosphere. And secondly, it neither allows to track the secondary electrons correctly nor to calculate ionization rates for incident electrons. The reason is simple: if a proton ionizes an atom, the collision is between a heavy incident particle and the electron. Thus the primary particle is not deflected as it knocks the electron out of its orbit. In case of an incident electron, however, the collision partners have equal mass and the primary electron will be deflected from its path, too. As a consequence, it does not travel a straight line through matter but is subject to multiple scattering. While the Bethe–Bloch equation still gives a reasonable approach on the specific energy loss along the particle track,

it does not allow to calculate the energy loss within a certain slab of target material. The same problem also holds for the secondary electron.

To model the total inventory of precipitating particles, which in addition to protons also contains electrons and heavier nuclei, a different approach is required. Since the very nature of the ionization process is stochastic, a Monte Carlo simulation is a reasonable approach. Here we need a list of all physical processes and their relevant cross sections/probabilities and then follow the particle along its track in small steps. At the end of each step, the particle either experiences an interaction with the ambient medium or not. The probability for such an interaction directly depends on the interaction cross section. Such an approach allows the consideration of all possible interaction processes, as long as the energy-dependent cross sections are known. This allows also the tracking of electrons: in each interaction not only the energy loss is taken from an energy loss distribution function but also the angle of deflection can be taken from some distribution. And in addition to the simple process of ionization, we also can allow for processes such as the generation of bremsstrahlung and, provided the energy of the incident particle is large enough, pair production.

The Problem

Before digging into too much detail, let us formulate the problem: the particle motion involves the following steps:

- during each time step, the particle is transported by a spatial step $\Delta s = v \Delta t$ with v being the particle speed. This almost corresponds to the advective term in sect. 8.2.2 – it does not correspond to it exactly because in particular for electrons deviations from the direct travel path of the incident particle occur.
- at the end of each time step, a dice is thrown to decide whether the particle interacts with the matter or not. The likelihood of this process is determined by the total interaction cross section. If an interaction happens, a second throw of the dice determines the kind of interaction (for instance, ionization, hadronic interaction, production of Bremsstrahlung) depending on the relative interaction cross sections. If no interaction occurs, the next time step starts. If an interaction happens, we have to throw the dice again to determine the energy loss from the energy loss distribution. The particle properties (energy, eventually also direction of motion) will be updated and the particle's energy loss is added as an energy gain to the volume. Alternatively, it is also possible to just count the ionization processes in each volume element (or along each line element of the travel path). If fast secondaries are produced, they are treated as additional particles and also have to be tracked by a Monte Carlo simulation.

The Model

Our model atmosphere is plane-parallel because the height of the atmosphere is small compared to Earth' radius. Up to a height of 100 km it is divided into 29 equidistant layers; its remaining mass is condensed into a 30th layer, 10 km thick: thus details of the energy deposit above 100 km are lost.

The composition of the atmosphere is homogeneous with 23.3 wt% O₂, 75.5 wt% N₂ and 1.3 wt% Ar. For numerical studies, pressure, density and temperature height profiles are taken from the equatorial June atmosphere in the SLIMCAT/TOMCAT model [31]. This approach ignores the pronounced seasonal variability of the polar atmosphere and gives an average ionization profile instead [135]. For individual SEP events the corresponding polar atmosphere is used.

During a SEP event protons, electrons, and α -particles are accelerated (for a recent summary see e.g. [87]). Electron to proton ratios as well as energy spectra depend on the parent flare, in particular whether it is impulsive or gradual, the properties of the coronal mass ejection, and the geometrical relation between observer and solar activity.

Particle precipitation is assumed to be isotropic from the upper hemisphere: particle distributions in interplanetary space tend to be isotropic for electrons (see e.g. Fig. 5.5) and

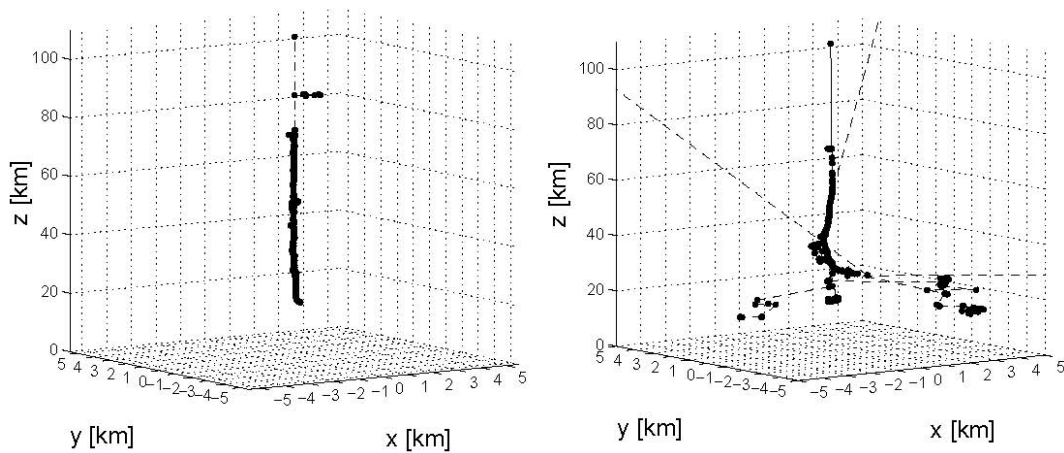


Figure 8.10: Monte Carlo simulation: Tracks of a 50 MeV electron (right) and a 300 MeV proton (left) in a model atmosphere [149]

become isotropic for protons during the time course of the event (e.g. examples in [82]). Observations by the MEPED (Medium Energy Proton and Electron Detector) instrument on board POES (Polar Orbiting Environmental Satellite) even suggest a slight preference for larger pitch angles inside the polar cap at altitudes of 900 km (Bornebusch, priv. comm.).

Energy spectra of precipitating SEPs can be described by a broken power law [51, 44, 78]: $I(E) = I_0 \cdot (E/E_0)^{-\gamma}$ with I_0 being the differential intensity at a reference energy E_0 , E the energy, and γ the spectral index. Around some 100 MeV the spectrum flattens and intensities increase due to the background of galactic cosmic rays [50]. Observed spectra are fitted simultaneously by up to three power-laws; the breaks between the power laws are not at fixed energies but are determined such that the best fit over the entire spectrum results.

Monte Carlo Simulation

The Monte Carlo simulation is performed using the GEANT 4 toolbox developed at CERN. GEANT 4 [1, 47] allows for a multitude of interactions between the precipitating particle and the absorber atmosphere. Our model considers as subset of particles protons, electrons, positrons, α s, and photons. Interactions are limited to electromagnetic ones: multiple scattering, Compton-scattering, ionization, photo electric effect, gamma conversion, annihilation, pair production, and production of bremsstrahlung. Secondaries produced in such interactions are tracked up to a cut-off length for particle propagation of 1 m. If particle energies are lower, the model switches to continuous energy loss.

Precipitating particles have an angular distribution and an energy spectrum. The Monte-Carlo simulation itself is performed for mono-energetic pencil-beams of 100 particles; angles of incidence vary between 0° and 80° in steps of 10° . The energies range from 1 MeV to 500 MeV in 109 logarithmic equidistant steps for protons and 1 MeV to 50 MeV in 340 steps for electrons. Statistics are tested by increasing the number of incident particles by a factor of 10 – the results are essentially the same.

The total energy input into each layer is the sum of the energy depositions of the individual particles; a division by the layer's thickness yields the linear energy transfer (LET) dE/dx . Thus the primary result of the simulation is the LET as function of altitude, initial kinetic energy and impact angle.

Ion pair production rates for individual particle events are obtained by folding the LETs with the observed particle spectrum and angular distribution and assuming an average ionization energy of 35 eV per ion pair [131].

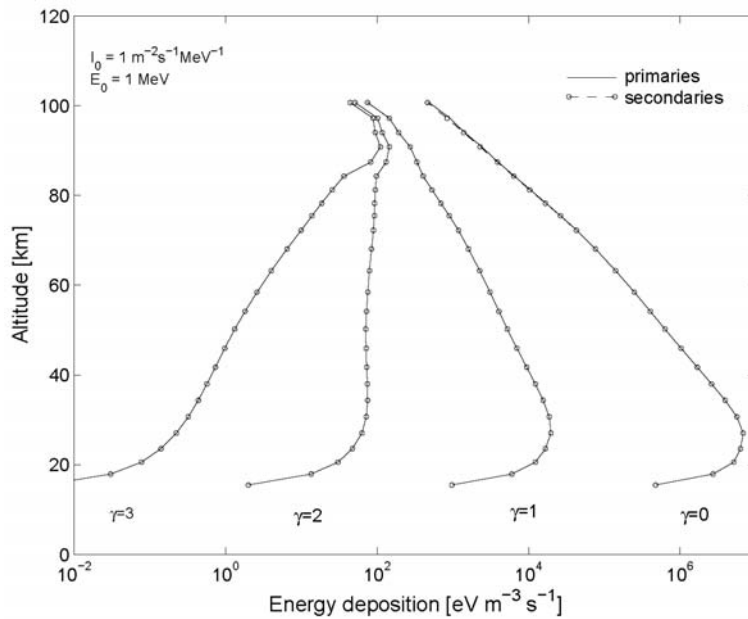


Figure 8.11: Energy losses of 1–500 MeV protons calculated with a Monte Carlo simulation (circles) and Bethe–Bloch (solid line) [149]

Results

Figure 8.10 shows sample tracks for a 300 MeV proton (left) and a 50 MeV electron (right). Production of secondaries is marked by dots, at the lines continuous energy losses occur with the line styles dashed, solid and dashed-dotted indicating neutral, negatively or positively charged particles, respectively.

The proton trajectory basically is a straight line. Only in the extremely rarefied upper atmosphere a trace of a secondary electron with significant path length is visible. Such long tracks occasionally occur in the upper atmosphere, because a low density implies a small interaction probability between the secondary and the atmosphere, leading to a long track. At lower altitudes secondary electrons are quickly stopped by the dense atmosphere and do not show up as separate tracks.

The straight path of the primary proton combined with the short range of the secondaries yields energy loss distributions comparable to those acquired in the conventional way without consideration of secondaries: Fig. 8.11 shows energy losses for proton spectra with four different power law indices γ with (dots) and without (line) consideration of the secondaries. With increasing γ the spectrum steepens and the ion production rate at lower altitudes decreases. Note that $\gamma = 0$ implies that the particle intensity is independent of energy while $\gamma = 2$ represents a SEP spectrum fairly well.

The situation is quite different for electrons, see left hand side of Fig. 8.10: instead of a straight line the path is randomly twisted because the primary's mass is the same as that of the shell electron and thus deflection occurs during interaction. This multiple scattering is not considered in a continuous loss model based on the Bethe–Bloch equation; thus such models underestimate the LET and consequently overestimates penetration depth. In addition, not all secondaries keep close to the track of the primary: aside from the secondary electrons produced during ionization, a primary electron also produces bremsstrahlung (dashed lines). These X-rays propagate large distances before depositing their energy due to Compton scattering and photoionization in denser layers of the atmosphere. Ionization thus can be shifted by several kilometers below the end of the primary track. The resulting energy transmission to altitudes less than 20 km with (dots) and without (lines) consideration of the secondaries is shown in Fig. 8.12, again for four different power law spectra and $\gamma = 2$ being a fair representative for SEP spectra.

To demonstrate the implications of the Monte Carlo simulation for ion–pair production, two different events are analyzed: one prominent event (October 22, 1989) and for compari-

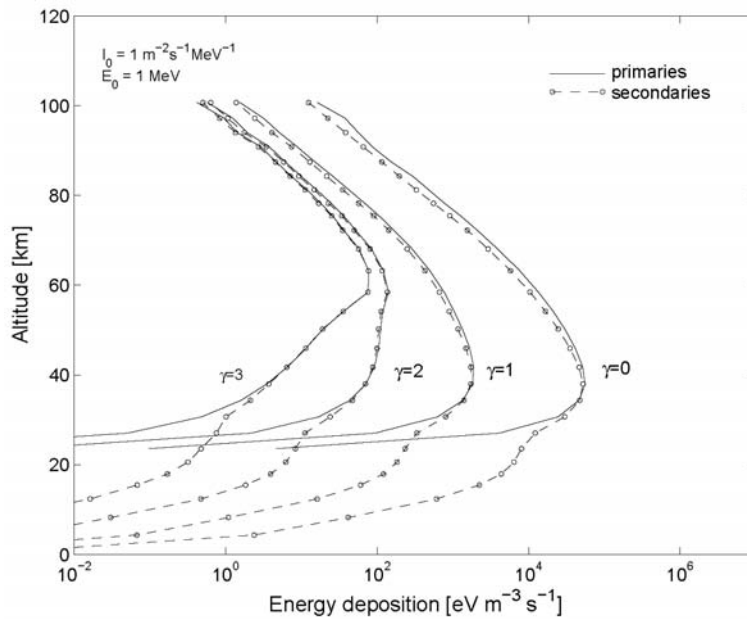


Figure 8.12: Energy losses of 1–50 MeV electrons calculated with a Monte Carlo simulation (circles) and Bethe–Bloch (solid line) [149]

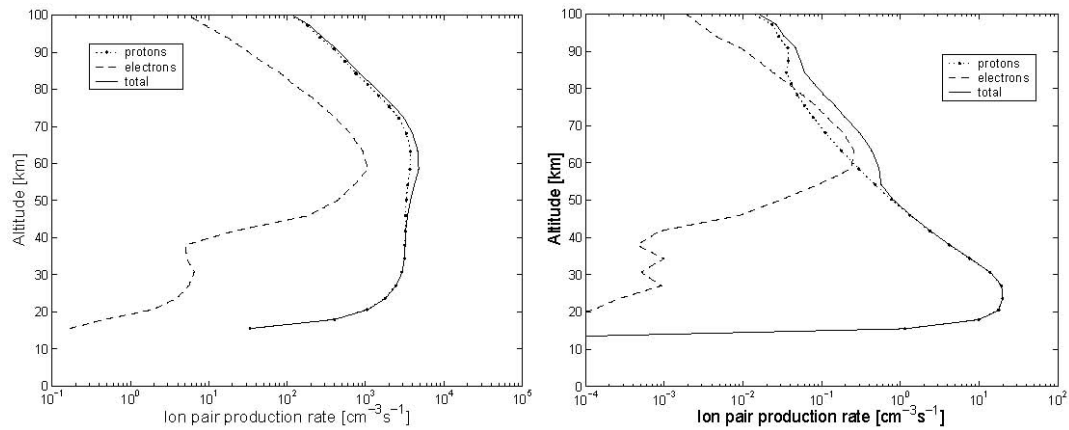


Figure 8.13: Ionization rates of electrons and protons combined for a gradual solar energetic particle event (left) and an impulsive one (right) [149]

son a large impulsive event (June 14, 1989). Electron spectra in the range 0.5 to 2.5 MeV are obtained from the CPME (Charged Particle Measurement Experiment) on board IMP (Interplanetary Monitoring Platform). Comparison with the higher energy electron instrument on IMP shows that in both events the electron spectrum can be extended down to at least 5 MeV. For the June event, proton spectra in the range 0.29 MeV to 440 MeV are obtained from the same instrument; for the October event proton spectra in the range 0.8 MeV to 500 MeV were taken from GOES (Geostationary Operations Environmental Satellite) because IMP measurements are less reliable due to failure of the anticoincidence scintillator.

The left hand side of Fig. 8.13 shows the modeled ion pair production rates for protons (dotted), electrons (dashed) and the sum of both (solid line) in the 4 October event for 6 hours containing the high energy maximum; at later times the instrument is saturated. Ionization of the electrons can amount to up to about 1/3 of that of protons in the height range 50 to 70 km, at lower altitudes electron contribution is insignificant – which is partly due to our abrupt cut off of the electron spectrum at 5 MeV.

The ion pair production rates for the main phase (1 day) of the impulsive June event are shown on the right hand side of Fig. 8.13. Again the contribution of electrons is visible only

above 50 km, however, around 70 km the ion pair production by electrons even exceeds that of the protons.

Conclusions

The main results of the Monte Carlo simulation are:

R1 for 1 MeV to 500 MeV protons ionization rates are essentially the same in the Monte Carlo simulation and in a continuous energy loss model.

R2 for 1 MeV to 50 MeV electrons the consideration of bremsstrahlung shifts the ionization well beyond the Bragg peak to lower altitudes.

R3 electrons in SEP events contribute to ion pair production rates in the height range 50 to 70 km; the amount depends on whether the particle event originated in an impulsive or a gradual flare.

As a consequence of **R1**, the consideration of secondaries in the Monte Carlo simulation cannot explain the difference between the observed and modeled electron densities in the October 1989 event as suggested by Verronen et al. [172]. Instead, **R3** suggests that the inclusion of electrons in the analysis of SEP events might explain such differences. It should be noted that implications of **R3** depend on the focus of research: in the very large events electron contributions are more or less a 10% effect and thus might be neglected as suggested in [74]. For long term studies such as variations over the solar cycle or possible climate impacts, however, also the much larger number of electron-rich impulsive SEPs has to be considered and thus ionization rates (and atmospheric consequences of precipitating particles) can be evaluated only if also electrons are considered.

R2 also has implications for modeling atmospheric effects of precipitating electrons. So far, magnetospheric electrons have been considered as a source of NO_x which, owing its long life-time, sinks down from the mesosphere into the stratosphere and affects ozone chemistry [21, 22]. Our results suggest a modification to their model in such that part of the ionization is directly transferred downwards by Bremsstrahlung. However, consequences are difficult to access since the produced NO_x and HO_x have different life times at different heights and thus implications for chemistry only can be evaluated in combination with a chemistry model.

8.3.3 Applications of the Model

In this section some results of our work on the consequences of solar energetic particles for atmospheric ionization and ozone depletion will be presented. The work is done in collaboration with Miriam Sinnhuber and Holger Winkler from the Institute of Environmental Physics at the University of Bremen.

Modeling of Atmospheric Consequences – Principle

The question under study already is demonstrated in Fig. 8.6: what is the relation between solar energetic particles (left) and ozone depletion (right). Basically, the two figures present the information available: intensity–time profiles for different particle species and energies measured outside the atmosphere and ozone mixing ratios measured in the atmosphere above a certain height. Modeling consists of three modules:

- where do the particles precipitate? The geomagnetic field regulates the spatial pattern of particle precipitation such that it is limited to the polar cap (white ring in the left panel of Fig. 8.6 in the present day atmosphere). For a modified geomagnetic field such as during a field reversal, however, the spatial precipitation pattern has to be modeled.
- primary interaction: ionization. From the particle intensity–time profiles energy spectra are calculated and from them the vertical profile of energy losses in the atmosphere, such as shown in Fig. 8.8.
- from these ion–pair–production rates the generation of the chemically reactive components NO_x and HO_x is determined. From a chemistry model such as the one used at the Uni-

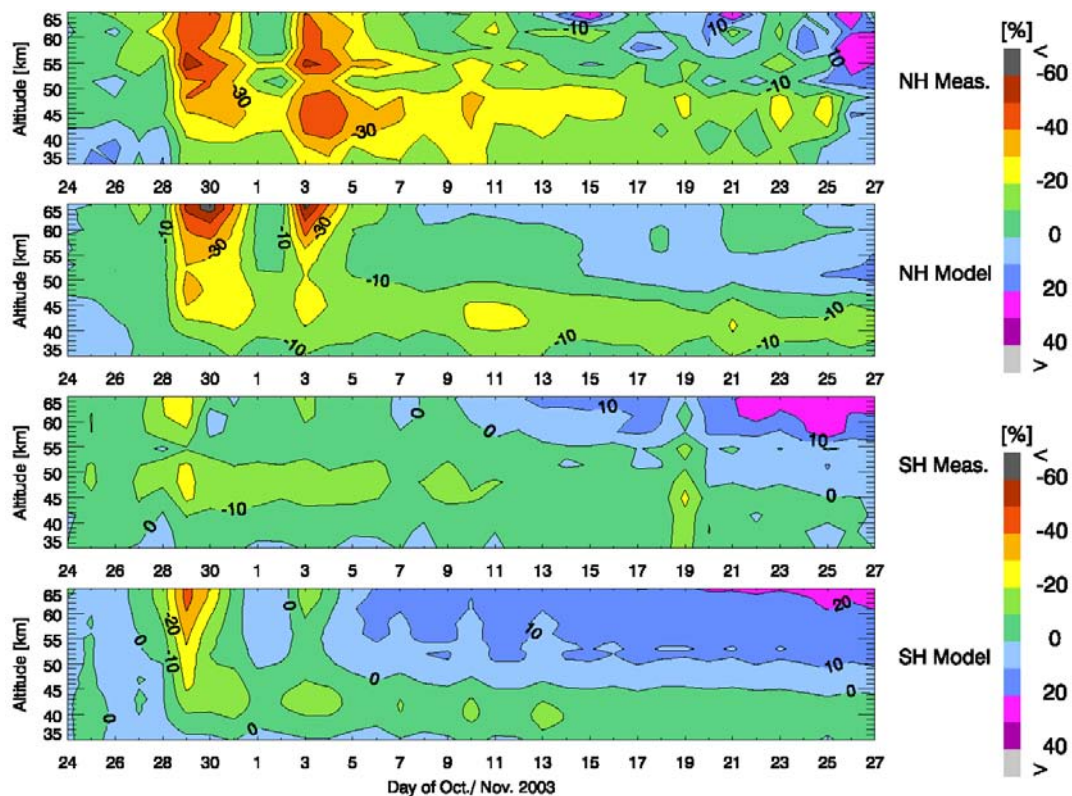


Figure 8.14: Ozone depletion following the series of large events in October/November 2003: modeled and observed ozone variations in the northern and southern hemisphere [141]

versity of Bremen, then ozone depletions can be calculated as shown and compared to the observations in Fig. 8.9.

Since three models stand between the observations, each model must be quite elaborate to avoid a sum-up of the unavoidable errors.

Individual Events

Although modeling is performed with care, errors cannot be excluded. Thus extensive testing is required. However, atmospheric ozone is not only influenced by solar energetic particles but also by other factors such as the Sun's hard electromagnetic radiation and atmospheric temperature and circulation patterns. Thus any variation in ozone at the time of a particle event can have many different sources – the particle event might not even contribute to ozone variation.

Thus the first task is to show the causal relation between ozone depletion and solar energetic particles and then to model it qualitatively. A reasonable approach might follow this line of thought: if solar energetic particles have any non-vanishing influence on the atmosphere, this should be most obvious in the largest events. This is also observed.

In addition, the largest events provide the best test case for modeling: if the effect is large, its dilution due to natural variability is small. Thus a large solar particle event provides some kind of δ -stimulus for the atmosphere and its response can be analyzed despite all the natural noise underlying it. And solar energetic particle events can become quite large: in the Bastille day event in Fig. 8.6, particle intensities increase by up to 6 orders of magnitude above background thus providing a strong stimulus.

As a consequence, large solar energetic particle events can be used to calibrate the model chain mentioned above before we attempt to derive more subtle effects from our models.

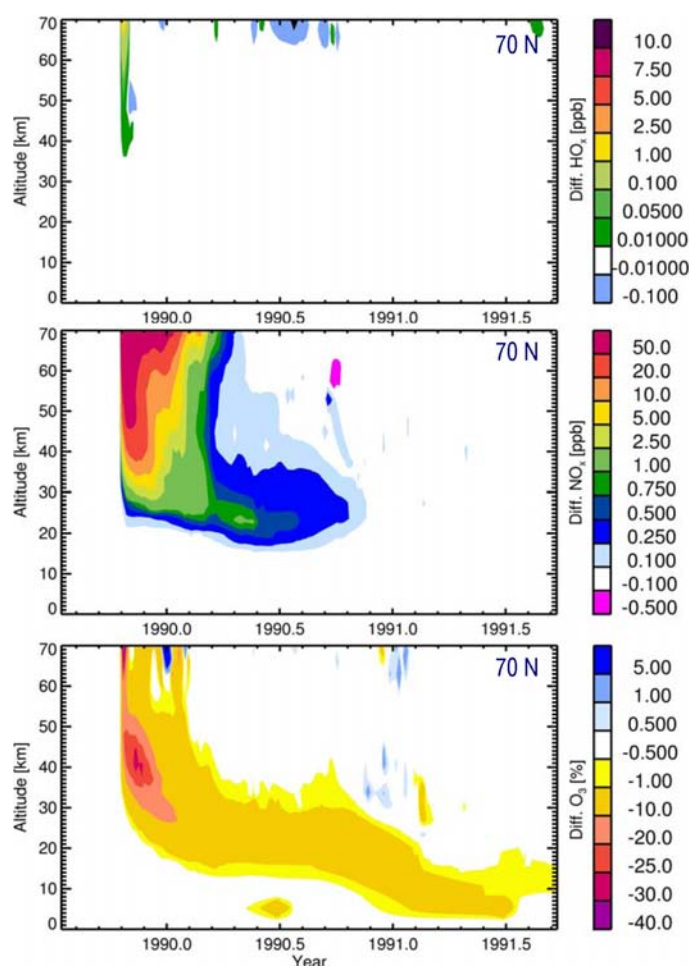


Figure 8.15: Consequences of the large October 1989 event in the atmosphere at N75: HO_x production (top), NO_x production (middle) and ozone depletion (bottom) (courtesy M. Sinnhuber, U. Bremen)

To demonstrate the validity of the model chain, Fig. 8.14 shows comparisons between measurements by SCIAMACHY (top and third panel) and modeled (second and fourth panel) depletions in ozone following the large events in October/November 2003 for the northern (top panels) and southern (bottom panels) hemisphere. Spatial and temporal patterns in both hemispheres are reproduced quite reasonably, although as discussed before ozone depletion in the mesosphere is overrated while it is underestimated for late times in the stratosphere. However, these deviations between observations and model are small compared to the asymmetry between the two hemispheres: while both model and observations indicate a strong ozone depletion in the northern hemisphere, ozone variations in the southern hemisphere are almost negligible. Reasons for this asymmetry will be discussed below.

Long-Term Effects of Solar Energetic Particle Events

While the modeling of the influence of individual particle events on ozone is a goal in itself, our interest is concerned more with longer times scales, in particular time scales related to magnetic field reversals, variations of the terrestrial climate and variations of the atmosphere, in particular its composition.

These long-term questions can be analyzed with different scopes. For instance, we can perform a single event analysis as described above but for modified boundary conditions. This would be a suitable approach to understand ozone depletion in individual events during, for instance, a magnetic field reversal or in a changing atmosphere. However, since magnetic field reversals also are accompanied by climate change and mass extinction, we also might ask whether ozone depletion might lead to climate change. Since large solar energetic particle

events are rather rare (a few per solar cycle), such speculation only can be reasonable if a single event has a sufficiently long influence on the atmosphere and thus the effects from events might overlap and amplify in time.

Figure 8.15 shows atmospheric consequences following the large solar energetic particle event in October 1989. The top panel shows vertical profiles of the HO_x generation at 70 N, the middle panel the same for NO_x. Both species are highly reactive and lead to ozone destruction. HO_x is produced mainly at altitudes above 40 km. It is a short lived species and is easily destroyed by photochemical reactions and during the ozone depletion reaction. Thus HO_x production during a solar energetic particle event certainly will not cause any long-term effects. The situation is different in case of NO_x: it is produced over a much broader height range from about 20 km to the mesosphere, although the maximum production occurs above about 40 km. The fundamental difference compared to HO_x is the live-time: particle precipitation is limited to a few days while high NO_x levels persist for weeks to months. With time, NO_x is depleted in the mesosphere by photochemical reactions – its life time in the stratosphere is much longer and with time it sinks slowly to lower altitudes with its maximum around the height of the ozone layer.

Ozone depletion (bottom panel in Fig. 8.15) is regulated by both species: initially in the event there is a strong depletion in the mesosphere above 60 km due to the combined effects of HO_x and NO_x. The pronounced depletion around 40 km, on the other hand, is due to NO_x as can be inferred from the long time scales. Owing to different temperatures, the NO_x-induced ozone depletion is larger in the stratosphere than in the mesosphere. The most remarkable effect, however, is the persistent ozone depletion by a few percent right in the middle of the ozone layer around 25 km lasting for more than a year. Such a persistent anomaly bears the seed for possible cumulative effects of solar energetic particle events – in particular during magnetic field reversals where the effects of individual events will be even larger than in the present day atmosphere.

Ionization through the Solar Cycle

The first approach on long-term studies is a view on the solar cycle. Figure 8.16 shows ion-pair production rates from 1988 to 2005, that is almost 2 solar cycles. Times of high solar activity are clearly visible as times with increased ion-pair production rates between 1989 and 1992 and again between 2000 and 2005. Solar minimum is around 1996. The sharp drop in ionization rate at 20 km is ‘instrumental’: the highest energies observed by the GOES particle detector are 800 MeV protons which stop at that height. At lower altitudes, ionization expected from higher energies is ignored in this figure – this does not pose a problem for modeling because the subsequent atmospheric chemistry model is limited to the stratosphere and mesosphere and thus is not influenced by neglect of tropospheric ionization.⁵

Figure 8.17 shows the variation in total ozone from 1989 to the middle of 2001, that is one solar cycle. The figure shows a couple of remarkable features:

- the general temporal behavior of the ozone depletion reflects the variation of ion pair production rates with the solar cycle as shown in Fig. 8.16: pronounced ozone depletion is observed between 1989 and 1992 and after 1999; the minimum of the solar cycle (and also the ionization) occurs around 1996.
- to the left, at the end of 1989, a strong decrease in ozone of some percent is visible in the northern hemisphere. This is related to the large solar energetic particle of October 1989 as discussed in connection with Fig. 8.15. As mentioned there, the effect lasts for some month.
- the ozone depletion on the right (middle of 2000) is related to the Bastille day event discussed in connection with Fig. 8.6.

⁵Such a limitation for a chemistry module is validated by the fact that the tropopause is a boundary which strongly inhibits transport of matter and thus almost completely decouples the troposphere from the atmosphere above.

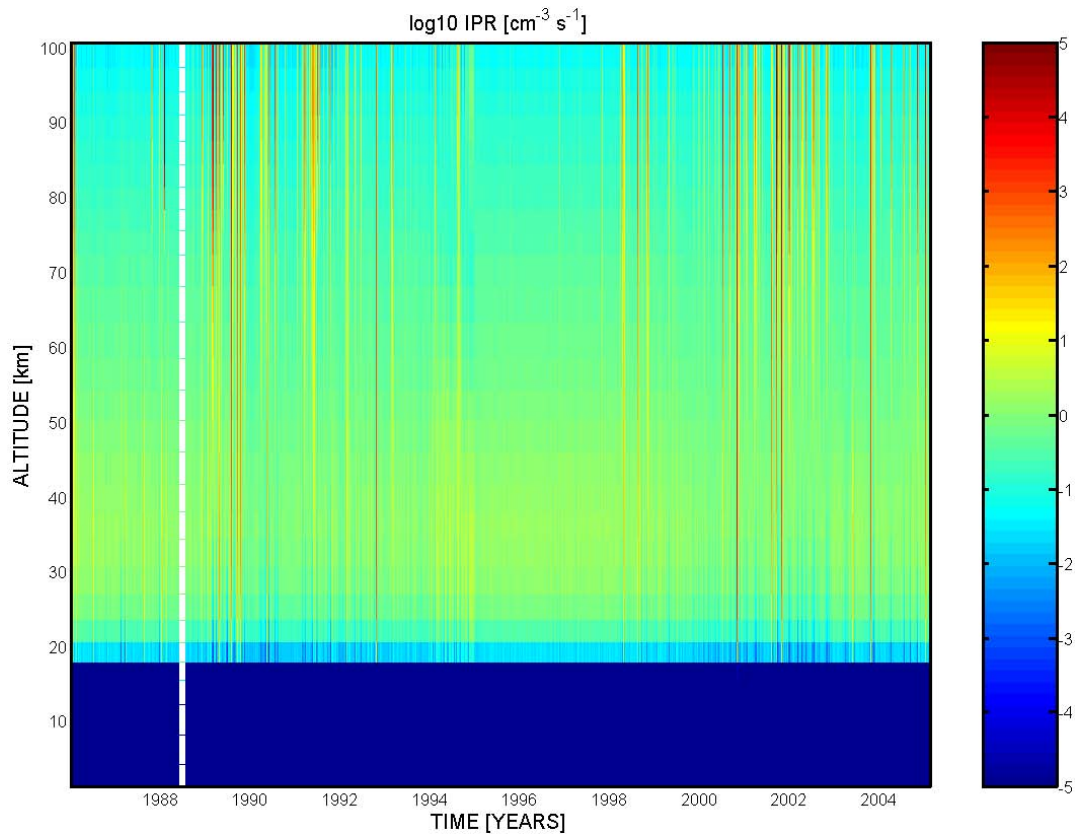


Figure 8.16: Ion-pair production due to energetic charged particles during the solar cycle

- in particular for the October 1989 event a strong hemispherical asymmetry is visible: the ozone depletion is much more pronounced on the northern hemisphere than on the southern one. In contrast, late in 1991 a solar energetic particle event causes an ozone depletion in the southern hemisphere but has almost no influence on the northern hemisphere. This hemispheric asymmetry basically is caused by two effects: (a) HO_x and NO_x life-times are influenced by photochemical processes as are many other chemical processes in the atmosphere. Thus even if all other conditions are equal, both hemispheres might exhibit different patterns of ozone depletion because one is more strongly illuminated than the other one. In the most extreme case, one hemisphere might be in polar night while the other is in polar day. (b) Circulation patterns are very different in both hemispheres: while in the northern hemisphere meridional transport happens all the year, in the southern hemisphere a strong closed vortex persists in the stratosphere that inhibits meridional transport, in particular in winter. In consequence, stratospheric temperatures can be extremely low which influences ozone chemistry. This vortex also explains why an ozone hole is observed at the southern pole while the northern hemisphere ozone hole is rather rudimentary.
- the spatial pattern of ozone depletion varies with the solar cycle: while during solar maximum ozone depletion due to precipitating particles occurs almost down to the equator, during solar minimum ozone depletion is limited to latitudes poleward of about 60° .
- ozone depletion occurs at latitudes where no particles precipitate: owing to the shape of the geomagnetic field, particle precipitation is limited to the polar cap, that is to geographic latitudes well polewards of 60° . Ozone depletion is not limited to these high latitudes but occurs also close to the equator. This shift reflects the atmospheric circulation patterns and the spatial variation in ozone production: the main ozone production is at low altitudes, leading to high ozone concentrations at low altitudes, see also the right panel in Fig. 8.6. The ozone-rich air then is transported polewards at high altitudes. At high latitudes

Figure 8.17: Changes total ozone due to precipitating solar energetic particles during the solar cycle (courtesy M. Sinnhuber, U. Bremen)

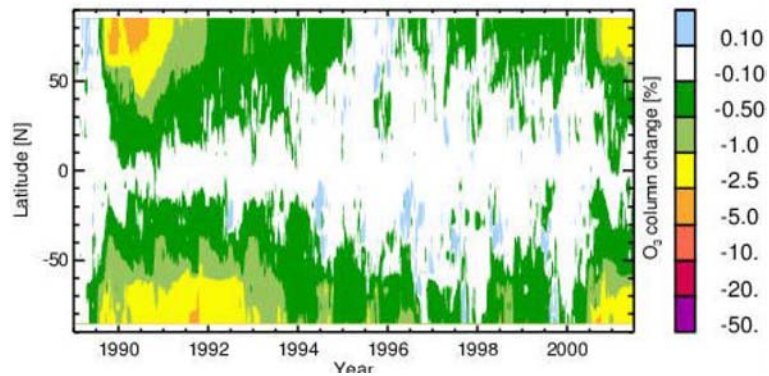
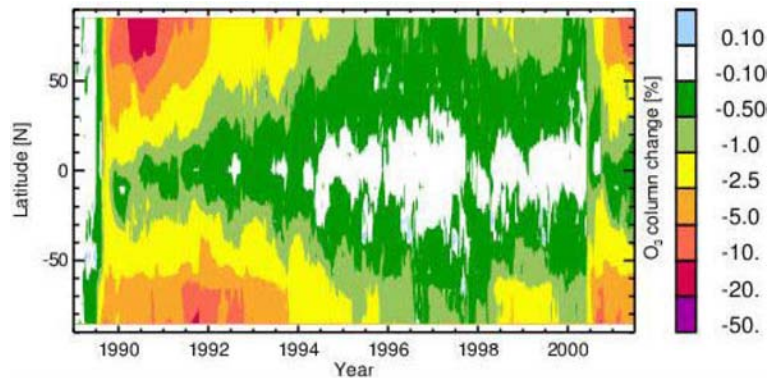


Figure 8.18: Variation in total ozone during the solar cycle without geomagnetic field (courtesy M. Sinnhuber, U Bremen)



ozone is destroyed by photochemical reactions as well as energetic particles. The equation of continuity requires also transport from the pole to low latitudes. This advects ozone depleted air to equatorial latitudes and thus explains the reduction in equatorial ozone.

- in mid-latitudes (around 50°) the solar-cycle variation in ozone due to precipitating energetic particles is comparable to the observed variation – and it is opposite in sign to the variation expected from the solar-cycle variation of the UV radiation.

Vanishing Geomagnetic Field

A worst case estimate for the ozone balance during a magnetic field reversal is obtained in case of a vanishing geomagnetic field. Then particles precipitate into the atmosphere at all latitudes and not only at high latitudes. Figure 8.18 shows model calculations for this case. The results are quite similar to the ones obtained for the present day geomagnetic field in Fig. 8.17:

- total ozone depletion is higher during solar maximum than during solar minimum,
- the effects of individual events are visible,
- ozone depletion in individual events shows a hemispheric asymmetry,
- the spatial pattern of ozone depletion varies with the solar cycle.

Despite all these similarities (in fact, there is one similarity too much) there is also a fundamental and surprising difference between the two figures: ozone depletion in high latitudes is much more pronounced in case of a vanishing geomagnetic field although the number of particles precipitating at high latitudes does not change! On the other hand, the difference in particle precipitation between the present-day field and the vanishing field occurs at low- and mid-latitudes: here the difference in ozone depletion between the two runs is less pronounced than at polar latitudes where no difference would be expected. This again reflects the complex relation between photochemical processes and atmospheric circulation.

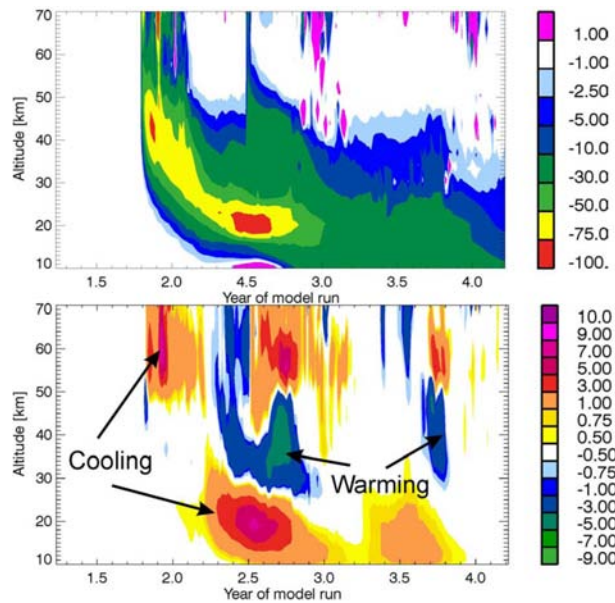


Figure 8.19: variation in ozone (top) and temperature (bottom) at 75N following a large solar energetic particle event during a magnetic field reversal (based on [154])

A closer inspection of Fig. 8.18 suggests ozone depletion by 10–20% at high latitudes lasting for a few month. Ozone has radiative properties, in particular, it absorbs UV radiation and is also a greenhouse gas, that is, it affects the terrestrial long-wave emission. In consequence, a local change in ozone concentration can cause a local change in temperature. Since pressure gradients resulting from temperature gradients are the driving forces for atmospheric motion, a change in ozone concentration might cause a change in atmospheric velocity fields and thus modify climate.

Consequences for Climate?

A first indication for such a process is given in Fig. 8.19: in the top panel ozone depletion at 75N is shown for a large solar energetic particle event at the time of polarity reversal, that is for a vanishing geomagnetic field. Ozone depletion can amount to more than 50% in the stratosphere and stay at such high levels for almost a year. The lower panel in Fig. 8.19 shows the resulting changes in temperature (sorry for the color-coding – differences are differences, but somehow its better to think about the reference point before calculating differences). Although temperature changes are rather small (rarely larger than 5 K), temperature gradients can become quite large. In consequence, wind fields change. And once the wind fields are modified, the entire temperature distribution in the atmosphere is modified, which certainly will affect climate.

The simulation in Fig. 8.19 can be regarded as a first indication for a solar energetic particle induced modification of the climate. The model atmosphere used to obtain that result has been build primarily for the study of atmospheric chemistry. The model is a 2D model only, that is it considers the vertical coordinate and latitude as horizontal coordinate because the relevant transport processes in the atmosphere are meridional. In consequence, atmospheric circulation can not be treated self-consistently. Instead, it is parameterized such that only the meridional component is allowed to vary while the azimuthal transport is fixed. Such a model cannot adjust completely to a different temperature pattern driving the circulation systems. Thus the results in Fig. 8.19 give an indication only.

Within the framework of CAWSES it is planned to use the MPI Hamburg model HAMMONIA (<http://www.mpimet.mpg.de/en/depts/dep1/uma/hammonia/>) to model possible consequences of precipitating solar energetic particles for climate in more detail. It should be noted that this implies a large amount of computational resources. Thus the simple first estimate in Fig. 8.19 has been relevant in such that it has confirmed that the process under

study is possible and worth further investigation. Without such a preliminary study it would have been irresponsible to start the study with the full climate model.

8.4 Some other Examples

8.4.1 Nuclear Physics: GEANT 4

Processes in nuclear physics go down to the sub-atomic level and thus always are stochastic. Therefore, Monte Carlo simulations face a broad range of applications in nuclear physics. The GEANT 4 software from CERN [28] used in the Monte Carlo simulation described above is a widely used tool in nuclear physics. It covers all aspects of particle propagation and interaction, including tracking of secondary particles and particle propagation in electromagnetic fields.

All aspects of the simulation process have been included in the toolkit:

- the geometry of the system,
- the materials involved,
- the fundamental particles of interest,
- the generation of primary events,
- the tracking of particles through materials and electromagnetic fields,
- the physics processes governing particle interactions,
- the response of sensitive detector components,
- the generation of event data,
- the storage of events and tracks,
- the visualization of the detector and particle trajectories,
- and the capture and analysis of simulation data at different levels of detail and refinement.

Applications of the program include all aspects of high-energy and nuclear physics. Some examples include

- design and performance of particle detectors: detectors for energetic radiation often work as stand-alone instruments on satellites or in supervision in nuclear industry. These instruments must be reliable and accurate, extensive testing and calibration in a well-defined radiation field often is not possible. In addition, the detector elements show slight production tolerances: thus despite the same design and use of the same elements, two particle detectors might differ in performance parameters such as detected energy range, detection threshold, or response. Here a Monte Carlo simulation is an extremely helpful tool: since the geometries and materials of detector elements can be specified in detail, production tolerances can be taken into account and each instrument can be simulated as individual instrument. In addition, the incoming radiation field is well-defined and can be varied to almost unlimited numbers. Thus the response of the detector can be defined quite well. In addition, at least known aging effects can be taken into account in the simulation. This is of particular importance for long-term surveillance because here it is important to identify whether a change in counting rates corresponds to a change in the radiation environment (for instance a small leak in the nuclear plant) or whether it does not result from a modified environment but from the aging of the detector alone.
- collisions of high energetic particles: interactions of high energetic particles are not the simple ionization process described in the above example but can include hadronic interactions or lead to the generation of cascades (simple examples for both processes follow below). Thus out of the collision of two sufficiently large and energetic particles a large number of secondaries can be produced which in turn might interact or decay. Such processes also can be modeled with a Monte Carlo simulation.
- simulation of air showers: galactic cosmic rays with very high energies can cause an air shower in the atmosphere, that is a chain reactions where the secondary particles produced by the incident particle again interact with atmosphere and produce tertiaries which

again interact with the atmosphere and so on. For instance, a fast electron might create bremsstrahlung as it interacts with the denser atmosphere in the stratosphere. If the bremsstrahlung photon has a sufficiently high energy, it will lead to pair production, giving an electron and a positron. The electron might create bremsstrahlung which in turn might lead to pair production which in turn ... and so on. The positron, on the other hand, eventually will interact with some atmospheric particle causing decay radiation which in turn might ionize which in turn ... and so on. Thus an avalanche of electrons and photons, called an electromagnetic cascade, propagates downwards through the atmosphere. The photons can be detected at the ground by Cerenkov detectors. Such an array exists, for instance, at the Forschungszentrum Karlsruhe (Kaskade, <http://www-ik.fzk.de/KASCADE/>). The number and spatial distribution of the photons is determined by the energy and direction of the incident particle. Monte Carlo simulations of such cascades are used to infer from the observation the properties of the incident particle.

- production of cosmogenic nuclides is an example for hadronic interactions. It is another aspect of the interaction of energetic particles, here galactic cosmic rays with the atmosphere. Examples for cosmogenic nuclides are radiocarbon (capture of thermal neutrons by atmospheric nitrogen: $^{14}\text{N}(\text{n,p})^{14}\text{C}$) or ^{10}Be (spallation of nitrogen or oxygen due to the capture of fast protons or neutrons). These cosmogenic nuclides are stored in terrestrial archives: ^{14}C is accumulated in all living matter, for instance in tree trunks. ^{10}Be is easily washed out from the atmosphere by precipitation. Storage occurs in the arctic and antarctic ice sheets. Thus the time history of both substance provides information about variations in the precipitation of galactic cosmic rays into the atmosphere, for instance due to modified solar activity, a changing geomagnetic field or a variation in galactic cosmic radiation. While the time history for the stable ^{10}Be can be obtained directly from the measurements, the ^{14}C series has to be corrected for its decay (half life of about 5400 a), for instance by matching tree ring patterns for independent dating.

A word of caution: a Monte Carlo simulation is a powerful tool in nuclear physics, but it is also a tool which relies heavily on a large number of (accurate) observations and on theory. Each Monte Carlo simulation is only as good as the underlying distributions (interaction cross sections, energy loss statistics, etc.).

8.4.2 Medical Applications

A special subtopic is the application of the nuclear physics problem of particle interaction with matter to medicine. This topic includes both diagnosis and therapy.

Diagnostics: CT, PET, SPECT

Modern diagnostic tools heavily rely on the interaction of energetic radiation with matter. This holds not only for the simple X-ray but also for its more advanced 3D version of CT (computer tomography). Also the 3D aspect of CT should not be underrated, it is simple in such that it only gives a still live: it represents the topological features well but it does not tell anything about their functionality.

Functional medical imaging is more interesting. For instance, it can show which parts of the brain are active during reading, listening or writing. It also can show which parts of the brain (or other body tissue) are inactive. Unusual levels of (in)activity often are pathologic and thus a combination of CT and functional imaging might help in diagnostics. And a more refined spatial diagnostics is the basis of modern therapy approaches, see the example of radiation therapy below and in project 5.

But functional imaging is also of interest for a better understanding of the working of the brain, see e.g. [25, 125].

Monte Carlo simulation comes in in two ways:

- The diagnostics relies on the interaction of the radiation with the tissue: if no absorption occurs in an X-ray, no information is obtained. If total absorption occurs, also no informa-

tion is obtained. Thus the energy and intensity of the beam has to be adjusted such that part of its energy is absorbed and part of it passes to the screen. But the absorbed energy is absorbed by the tissue – and thus the tissue is ionized, radiation damage has happened. Basically the same is true for all other methods based on such interactions. Monte Carlo simulation here comes in in tailoring the diagnostic beam: the required amount of energy has to be inflicted onto the tissue but not more than that.

- In addition to tailoring the beam, the energy deposition (and the location of maximum energy deposition) can be determined with such a simulation and alternative diagnostic schemes can be suggested, for instance to move energy deposition from highly sensitive (or important) tissue to less sensitive one.

As in case of detector design and simulation in nuclear physics, here the Monte Carlo simulation has the advantage that the beam can be tailored individually because as in detector elements also in human body parts production tolerances can be quite large and should taken into account: for instance, a lean 80 kg and 190 cm marathon runner might prefer a slightly smaller dose for a chest X-ray than the one used for the previous client, a 150 kg and 160 cm couch potato.

Radiation Therapy

Basically, radiation therapy is optimization of the interaction between the energetic radiation and the tissue in a direction opposite to that in diagnostics: it requires the delivery of a high (or more correct a lethal) dose to the target volume (the tumor) while simultaneously an almost vanishing (or at least only minimally damaging) dose should be delivered to the surrounding tissue. While early approaches in radiation therapy heavily relied on electromagnetic radiation, presently also radiation therapy with protons or heavier nuclei is offered, in particular for brain tumors where damage to the surrounding tissue should be kept as low as possible. As in diagnostics, beam tailoring is an important aspect in therapy planning; further information is given in connection with project 5 in sect. 10.5.

8.4.3 Complex Environments: Stochastic Differential Equations

In the natural environment, such as in the physics of atmospheres and/or oceans or in coastal dynamics, not only some of the transport processes are stochastic but also the spatial/temporal distribution of some transport parameters can be described by distributions rather than by constants or functional dependence. In addition, boundary conditions (such as prescribed flows or properties of the sea bed) often show spatially and temporally fluctuating patterns.

Here a stochastic model often is not used to account for the stochastic processes: diffusion and dispersion are universal transport processes of stochastic nature and are quite difficult to avoid but within all the noise in a natural system the use of the expected values derived from the transport equation often is sufficient. Instead, the stochastic aspects enter at the transport parameters or boundary conditions.

In principle, such variations can be treated in the framework of Monte Carlo simulations. For instance, variable parameters or boundary conditions can be varied according to their respective distributions during the individual runs. However, in an extremely complex model, such an approach is of limited use only because the model is complex and time consuming and, as discussed above, Monte Carlo simulations require a rather large number of runs to give representative results.

Instead of Monte Carlo simulations often Monte Carlo differential equations or stochastic differential equations are used. Both approaches are not to be confused. Stochastic differential equations are an important topic for instance in climate modeling, see e.g. [173]. The climate system comprises the atmosphere, oceans and the cryosphere. In recent times also components such as chemo-physical processes in the atmosphere, land surface processes, influences from the biosphere or even socio-economic processes have been included. For part of

these processes well worked out physical theories exist which in mathematical language lead to parameterized partial differential equations, many of them nonlinear.

But even if all processes were clad in rather simple mathematical descriptions, a fundamental problem still would exist: the fluctuation of physical quantities in the climate system's different components takes place on tremendously different time scales. For instance, the basic set of equations (equation of motion, equation of state, equation of continuity) in the atmosphere accommodates sound waves with time scales in the ms-range as well as the thermohaline circulation with a time scale of order of thousand years. Weather patterns, on the other hand, have time scales of days; the Southern Oscillation, of which El Nino is a part, has time scales of years. How to model? The situation is quite simple, if only very short time scales are concerned, such in weather forecast. Here we can prescribe the thermohaline circulation, make a few different runs for different states of El Nino Southern Oscillation (ENSO) and treatment of weather patterns. The only remaining problem is a careful judgement whether patterns of sound waves might influence the results in such that enough energy is redistributed to modify weather patterns – a simulation of such sub-second phenomena is not reasonable if even the entire time span to be simulated is only some days. The problem of the smaller time scales becomes more visible if we look at the next higher time scale, that is the simulation of ENSO. Again, owing to its much longer time scales, the thermohaline circulation or different states of it will be prescribed. But what about the weather patterns. Persistent weather patterns might be a result of ENSO but also might influence ENSO. Thus weather patterns should not be neglected. But a simulation of some years ENSO with a temporal resolution suitable for weather simulation is not feasible – thus a description of the weather patterns is required that allows to model their average influence on ENSO without going into the details required for weather forecast. The keyword here is *average*. Remember, we did a similar thing in QLT in sect. 5.2.5

If phenomena on very different scales appear in systems described by the same set of nonlinear differential equations, averaging is a useful tool: long time averages over the fast variables gives differential equations for the slow variables in which the influence of the fast variables appears as a stochastic term. The coupling between slow and fast variables then can be regarded as a form of forcing by a stochastic process with Gaussian fluctuations. The general rule of the game is described as

Definition 6 *Averaging transforms multi scale deterministic partial differential equations into stochastic partial differential equations.*

The averaging process is reasonable because the good mixing properties of the fast components are guaranteed by the nonlinearities of the equations.

The most advanced type of climate models, the general circulation model (GCM) is limited not only in temporal but also in spatial resolution. As in the time domain, the performance of these models also can be improved in the spatial domain by stochastic representations of sub-grid scale variability. In terms of modeling and understanding of the physical basis, the introduction of stochastic terms also reduces the complexity of a model – and it is much easier to learn from a simple model than from a complex one. At least in climate models introducing stochasticity constitutes one of the key techniques in model reduction.

The physical laws governing the climate system are derived from conservations laws. They constitute a set of coupled partial differential equations, boundary conditions and initial conditions of the form

$$\frac{\partial}{\partial t} \mathcal{B}\varphi + \mathcal{L}\varphi + \mathcal{N}[\varphi, \varphi] = \Sigma . \quad (8.9)$$

The state of the system is described by $\varphi(\vec{r}, t)$ which generally is a vector function. Linear and nonlinear differential operators \mathcal{B} , \mathcal{L} and \mathcal{N} act on the spatial dependence of φ . Sources and sinks of φ are denoted by Σ . Externally prescribed forces and coefficients also may enter into \mathcal{B} , \mathcal{L} and \mathcal{N} . Nonlinearity, which is an essential property of the climate system, enters through the \mathcal{N} -term. It mostly arises from the advection of φ with the fluid motion: the advection of heat with the atmospheric and oceanic currents is driven by the temperature

distribution and also changes it. Nonlinearity introduces a coupling in the broad range of scales and may lead to multiple equilibria and chaotic behavior.

The averaging (or filtering) mentioned above disregards the high-frequency wave-number part of the spectrum of motions to describe the evolution of the slow manifold. If (8.9) is considered the result of such averaging, φ is an averaged, slowly varying state. The source term Σ then contains the contributions from the field φ' representing the subrange of scales which can be treated as some generalized form of turbulence. In addition, Σ contains terms that couple the resolved component φ to the filtered variables χ which represent the fast manifold:

$$\Sigma = -\overline{\mathcal{N}[\varphi', \varphi']} - \mathcal{N}_1[\chi, \varphi] - \mathcal{N}_2[\chi, \chi] + F \quad (8.10)$$

with F as external source and $\overline{\mathcal{N}[\varphi', \varphi']}$ as the averaged fluctuating quantities. The latter can be described by some parameterization relating the mean turbulent source to the resolved field:

$$\overline{\mathcal{N}[\varphi', \varphi']} = \mathcal{P}[\gamma, \varphi]. \quad (8.11)$$

In most cases the parameterization operator \mathcal{P} is a simple local and linear relation with a constant parameter γ . For instance, the divergence of turbulent fluxes of heat frequently is described by Fick's law.

Stochastic elements enter the problem (8.9), (8.10) and (8.11) where variables or coefficients appear that are not well known and should be considered as members of some random ensemble.

8.5 Summary

The above examples should have illustrated the strength of a Monte Carlo simulation: it is able to treat stochastic processes in such a way that not only the average or expected solution is determined but also the distribution of possible outcomes around this expected value is determined. Thus although making higher demands on computational resources, a Monte Carlo simulation offers an advantage compared to the analytical (or FDM or FEM) solution of the problem.

Literature

A very similar model also is used in conformal radiation therapy planning, see e.g. the textbook by Webb [178].

The literature on Monte Carlo methods often focuses on specific topics. Since Monte Carlo implies something statistical, the most frequent application of Monte Carlo methods is in statistical physics. Two relative recent textbooks on this topic are Landau and Binder [100] and Newman and Barkema [120]. More general applications of Monte Carlo methods in numerical physics are discussed in Milstein und Tretyakov [112]. As described in chapter 4 diffusion and heat transfer also can be understood as stochastic processes. Such applications for Monte Carlo methods are described in Lapeyre et al. [102]. The application of stochastic modeling to climate is discussed in Imkeller and von Storch [68]; stochastic differential equations are discussed in [97] and [102].

Questions

Frage 43 Describe the similarities and differences between Monte Carlo Simulations and Monte Carlo differential equations.

Frage 44 Describe advantages/disadvantages of Monte Carlo simulations compared to more conventional numerical schemes such as FDM or FEM.

Unconventional Transport Processes

Sofar, the text was concerned mainly with problems from physics or geophysics. All transport processes treated so far are conventional in such that they can be described as continuous transport in a continuous medium. But as soon as transport uses living carriers, such as humans (e.g., SARS, money, rumors, even the WWW) or (migrating) species (such as bird's flu, immigrant populations such as rabbits in Australia or certain kind of mussels in the North Sea), spread suddenly is regulated by a rather complex net of pathways (for instance air travel routes, underlying grid of the WWW) as well as the interaction of different individuals and/or subspecies of the transporting population.

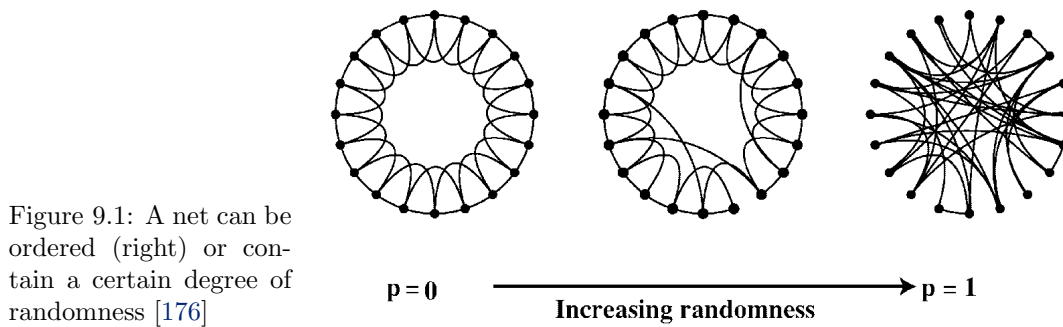
In fact, although at first glance these processes seem to be just transport processes, they are more closely associated with buzzwords such as graph theory, dynamical systems, self-organization and emergence. Consequently, they require a different description and are well beyond the scope of this text. Nonetheless, we will discuss some simple examples. All examples are related to networks and small-world problems, thus some basics in graph theory (e.g. the Wikipedia entry at http://en.wikipedia.org/wiki/Graph_theory, Caldwell's tutorial at <http://www.utm.edu/departments/math/graph/>, for readers with an ample supply of time and a strong interest in basic and clean definitions/explanations Mawata's lessons on <http://oneweb.utc.edu/~Christopher-Mawata/petersen/> or the electronic edition of Diestel's Graph theory at <http://www.math.uni-hamburg.de/home/diestel/books/graph.theory/>) complexity (e.g. the Wikipedia¹ entries at <http://en.wikipedia.org/wiki/Complexity> and http://en.wikipedia.org/wiki/Complex_system, <http://www.calresco.org/themes.htm> with a large number of subtopics including automata, chaos etc., <http://necsi.org/education/onlineproj.html> with some tutorials and interactive examples, and <http://informatics.indiana.edu/rocha/complex/csm.html> on complex system modeling) and the familiarity with the concept of a small world (http://en.wikipedia.org/wiki/Small_world_phenomenon) might be helpful. Or for short: the following will be pretty **Goals:** after working through this chapter you should be able:

- to sketch the basics of self-organizing systems,
- to explain some of the buzzwords like ... to the layman,
- to apply a mathematical model to some simple problems.

9.1 Small Networks

The small-world phenomenon describes the world as a coincidence of high local clustering and short global separation. It has been suggested in the late 1960s by the sociologist S. Milgram to describe the rather amazing experience of meeting a complete stranger with

¹Note that Wikipedia itself is an example for a complex phenomenon – and a rather large number of studies on the development of this complex system exists.



whom we have apparently little in common and finding unexpectedly that we share a mutual acquaintance is one with which most of us are familiar. The phenomenon gained broad public attention as ‘six degrees of separation’: any two individuals from the world population are connected by a chain of no more than six intermediate acquaintances. At first glance, this effect appears to be rather anecdotal, however, after closer examination it turns out that it has wide application. In particular, this small-world phenomenon appears to be a general feature of sparse, decentralized networks that are neither completely ordered nor completely random as discussed in detail in a simple formalization of the small-world concept by [175], a more advanced formalization is given in [176].

Watts [175] gives a very graphical description of the small world such that it has to fulfill four criteria:

1. The network is numerically large in the sense that the world contains $n \gg 1$ people. In the real world, n is on the order of billions.
2. The network is sparse in the sense that each person is connected to an average of only k other people, which is, at most, on the order of thousands – hundreds of thousands of times smaller than the population of the planet.
3. The network is decentralized in that there is no dominant central vertex to which most other vertices are directly connected. This implies a stronger condition than sparseness: not only must the average degree k be much less than n , but the maximal degree k_{\max} over all vertices must also be much less than n .²
4. The network is highly clustered, in that most friendship circles are strongly overlapping. That is, we expect that many of our friends are friends also of each other.

It is probably not difficult to recognize our world as a small world fulfilling the above criteria.

In a simple model, the network is represented as connected graph, consisting solely of undifferentiated vertices and unweighted, undirected edges.³ In addition, the above condition for sparseness must be satisfied. The relevant parameters in the description of the graph are

- the characteristic path length L , defined here as the average number of edges that must be traversed in the shortest path between any two pairs of vertices in the graph.
- the clustering coefficient C is a measure of the local graph structure: it can be regarded as the probability that two vertices will be connected, given that each is also connected to a mutual friend.

Obviously, both parameters are of statistical nature and depend on the portion of the graph under study as well as on n and k .

²In a more advanced version of the scale-free net (http://en.wikipedia.org/wiki/Scale-free_network) this assumption is modified and some nodes act as highly connected hubs (high degree), although most nodes are of low degree. Flight routes, for instance, are described more adequately in such a scale-free net because some airports such as Frankfurt, Amsterdam or London are such highly connected hubs while most airports show a much smaller connectivity.

³A vertex is the fundamental unit of a network, also called a site (physics), a node (computer science), or an actor (sociology). An edge is the line connecting two vertices, also called a bond (physics), a link (computer science), or a tie (sociology) [119].

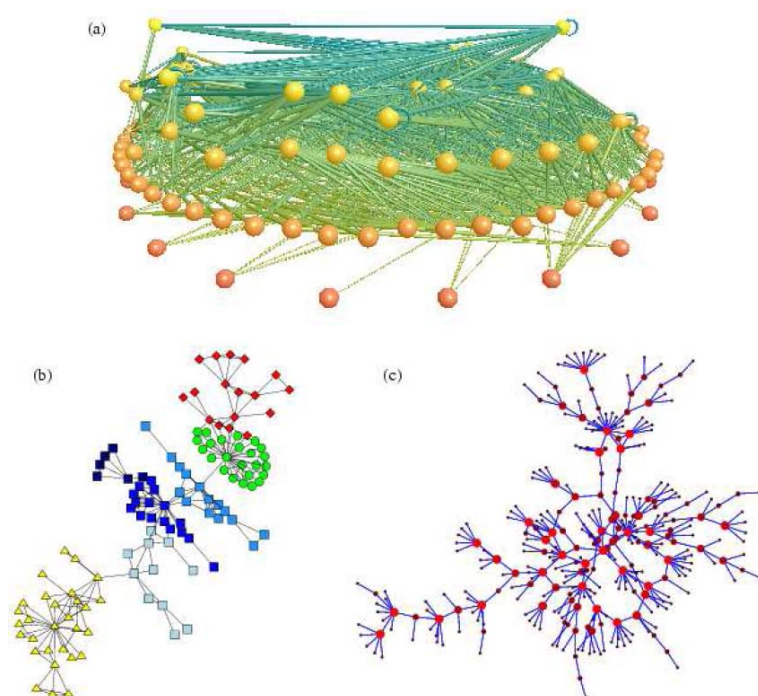


Figure 9.2: (a) A food web of predator-prey interactions between species in a freshwater lake. (b) The network of collaborations between scientists at a private research institution. (c) A network of sexual contacts between individuals infected with HIV (from the aix-server version of [119])

Both parameters also depend on whether a net is ordered or completely random. The left hand panel in Fig. 9.1 shows an ordered net. It consists of a certain number of vertices. Each vertex is connected to its two direct neighbors (along the circumference of the circle) and to the two neighbors over-next (arcs). In the figure, the number of nodes is $n = 20$, the number of connections is $k = 4$ for all vertices. To the remaining 15 vertices no direct contact is possible.

People are mobile and move or the break-up friendships and create new ones. Thus a certain aspect of randomness must be included into such a net. This can be done in two ways: in the middle panel of Fig. 9.1 a few points are randomly chosen and transferred to a different position on the circumference retaining the edges to their former neighbors. In the right panel, edges are shuffled around arbitrarily, leading to an almost complete random net. The quantification of this randomness and its consequences is discussed in more detail in [176].

Note that such a graph is a snapshot of the net. How existing connections determine new ones is a big part of the mystery. One might imagine a world in which people only become acquainted through introduction by one or more mutual friends. It is easy to see that a mechanism such as this leads inevitably to a locally ordered world (in the sense of $C \gg k/n$), the extreme case being the caveman world. At the other extreme, one might also imagine a world in which new friendships are made autonomously and at random, without regard for current friendships. The end product of this tie formation process is a random graph. Of course, the real world lies somewhere between these two extremes.

More realistic (and thus also more complex) examples for such nets are shown in Fig. 9.2. All three nets show distinct patterns. The predator-prey net shows a very high degree of connectivity and appears to be rather homogenous. The collaborating scientists in part (b), on the other hand, form distinct subgroups as indicated by the different colors. The degree of connectivity between different researches within each subgroup is variable, in particular there are always some ‘outsiders’ which are connected to one other scientist only while on the other hand there are a few rather central figures which collaborate with a large number of colleagues – and which often also are the ones that also ensure the collaboration between the subgroups. Note that this structure leads to quite long path length and a low clustering coefficient. The subfigure (c) again represents a different world. It cannot be decomposed into interacting

subgroups but consists of some kind of backbone of interconnected individuals which interact with more than one partner and branching away from this backbone connections to persons that does interact with one partner (the one from the backbone) only.

9.1.1 Why do we need the Small World Concept?

If the world is organized as a small world (or in a more refined version as a scale-free net), all properties transported by humans are regulated by this net. Part (c) in Fig 9.2 is such an example: the spread of a disease certainly depends on the connectivity between individuals. The same is true for rumors.

Disease and Rumor in the Old World

Prior to small worlds, modeling of the spread of a disease was quite simple – as are the assumptions underlying such a model. The transmission of the disease requires a direct contact. It is regulated by some transmission probability (a healthy individual transforms into an infected individual). In addition, immune individuals must be considered: they might be immune from the onset on (e.g. due to vaccination) or after they have recovered from the disease.

In the old world, people stayed close to their ‘rest position’ (home) and had a limited operating range from about 20 km at most. Thus they live in a population that can be regarded as well mixed (again a well-stirred tank concept).

If we now inject a small seed of initiators into the homogenous, well-stirred population, the disease basically spreads like in a diffusion (or diffusion–convection) model. The diffusion coefficient then must be replaced by some coefficient that includes the transmission probability and spatial and temporal scales relevant for transmission such as the average distance between two subsequent interactions of an infected individual with healthy individuals and the time between these interactions.

Rapoport [137] was the first one to suggest that rumors might spread in the same way as disease – albeit with a different ‘diffusion coefficient’. But Rapoport also realized that the spread of a rumor is influenced by something else: the existence of a tight-knit small community.

Disease and Rumor in the Small World

And such substructures exist in small world. Although the mechanisms of the transmission of the disease from one individual to the other are exactly the same, the disease does not spread homogeneously as in the old world but its spread is regulated by the graph of small world – or as Watts [176] puts it: dynamics becomes a function of structure.

Watts and Strogatz [177] simulated the spread of an infectious disease on a simple small-world network model. At time $t = 0$ a single infective is introduced into an otherwise healthy population. After one unit of time, the infective is removed (either because it dies or becomes immune) but in that interval it can infect (with some probability) each of its healthy neighbors. The process is then repeated until it reaches a steady state.

Their findings show three distinct regimes of behavior. In the first (for diseases with low infectiousness), the disease infects little of the population before dying out. In the second, a highly infectious disease infects the entire population regardless of its connective topology, but the time taken to reach this steady state varies dramatically as a function of characteristic path length of the network. (Shorter path length implies faster spreading of the disease.) For intermediate levels of infectiousness, there is some complicated relationship between structure and dynamics, which has not yet been completely characterized. Nevertheless, there is a clear correlation between critical infectiousness—the point at which the disease infects a macroscopic fraction of the population—and the amount of randomness in the network. Beyond those conclusions, not much more can be said. However, it is clear that

for this dynamical system the attractor for the global dynamics does depend on the coupling topology.

In epidemiological terms, small-world networks imply that the level of infectiousness required for a disease to grow to epidemic proportions can be highly sensitive to the connective topology of the population. This may change our way of looking at social diseases, which are often perceived as confined to isolated subgroups of a population. The highly clustered nature of small-world graphs can lead one to believe that a given disease is "far away" when in fact it is very close. In other words, when looked at on a local level, the change in structure that causes the disease to spread much further and faster may not be observable by an individual who has access only to local information.

As Wikipedia (<http://en.wikipedia.org/wiki/Rumor>) notes (although indirectly), the same change in approaches also has happened for rumors:

A rumor or rumour (see spelling differences) is a piece of purportedly true information that circulates without substantiating evidence. The information content/payload of rumors can range from simple gossip to advanced propaganda techniques.

Classically, rumors spread from person to person by word of mouth, as in gossip. Cheap postage rates and then telephone services fomented the pace and range of the swirling of rumors. With the advent of the Internet many rumors have started to spread via email and more recently through blogging, as also occurs with various hoaxes and urban legends.

While many rumors begin or continue to spread as a part of natural human communication that occurs when people discuss something they find funny or interesting, some are started in an intentional attempt to disseminate specific information. Viral marketing campaigns often depend on rumors, as do many political endeavors. Some people in very public positions find rumors very troublesome, annoying or embarrassing, when real or imaginary details about the personal lives they would prefer to keep private start to spread among people who are interested in them. Rumors can have a powerful motivational aspect on those who believe in them – among stock traders, for example, hearing a rumor from a trusted source can lead one to believe that one now has inside information. As rumors spread without corroborating evidence, it's not unusual for those who have heard the rumor to look for some on their own – a rumor about a celebrity's sexual preferences, for example, may cause those who hear it to start judging the celebrity's behavior against known stereotypes.

9.1.2 From Small World to Scale-Free Nets

The results from the Watts and Strogatz approach are a little bit disappointing because they do not allow a simple risk assessment. The problem is not the approach, but – since dynamics becomes a function of structure – the structure of the network. Their underlying random network is quite similar to the network in panel (c) in Fig. 9.2. But such a network does not reflect the world on a global scale – it does not even reflect the structure of the network in a single country or city.

A more realistic approach is a scale-free network (http://en.wikipedia.org/wiki/Scale-free_network) – a concept which is not only a good description for the WWW but instead was born from the analysis of connectivity inside the WWW. The scale free-net allows for hubs as highly connected vertices in an ocean of vertices with low connectivity, such as sketched in Fig. 9.3. Such hubs can be easily identified in a map of the world wide web such as shown in Fig. 9.4 – a natural neural net in the sense of a net composed of neurons looks quite similar. A nice figure of the connections during a denial of service attack can be found at <http://www.prolexic.com/zr/zombiereportq12.edit.png>

In such a scale-free net a disease spreads differently, see Fig. 9.5: in the random small world there is a well defined outbreak at a certain infectiousness. The situation is different in a scale-free network. Here the slope in the graph of the fraction of infected individuals is

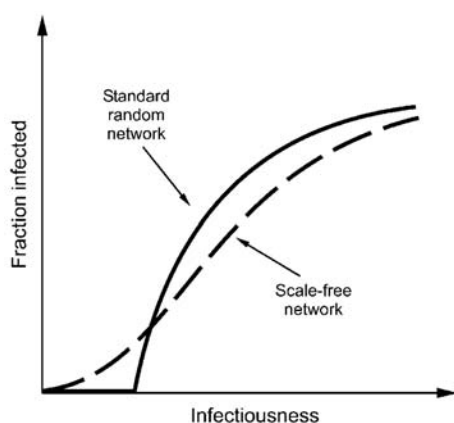


Figure 9.5: Spread of a disease in random and scale-free networks [176]

almost constant. Consequently, no outbreak of the disease shows up but rather an increase in the number of infected people with increasing infectiousness.

And what about the spread of the disease in space? To quote Watts [176]:

The correlation length regulates how far from its source a contagious influence must spread before it feels the effect of the shortcuts. Hence an outbreak of disease can be divided naturally into two stages: (a) a local growth phase in which its spread is slowed by the redundancy present in the local topology of the network; and (b) a global growth phase, in which it can spread exponentially throughout the network via the random shortcuts. Because the correlation length governs the transition from local to global growth, these models suggest that to be effective, strategies for preventing epidemics should focus on eliminating even very rare shortcuts, thus prolonging local growth for as long as possible. The correlation length of networks may also be important from an evolutionary perspective. Boots and Sasaki (1999) have observed that vector-borne diseases such as malaria and cholera tend to be more virulent (that is, they kill off their hosts rapidly) than infectious diseases spread by direct contact. Their explanation was that vector-borne diseases have historically been able to spread via long-range connections—transported by mosquitoes or flowing water, for example—whereas human-to human infections have been more constrained by geographical proximity and hence must survive a local growth phase before they can reach epidemic status. Diseases that rely on direct contact will therefore evolve lower virulence, they argued, in order not to burn themselves out before they reach the correlation length, whereas diseases that are not constrained by an initial local growth phase will evolve to be highly virulent. Boots and Sasaki then suggested that as the correlation length of a network shrinks on account of the introduction of random shortcuts—as the world becomes smaller—one might expect the evolution of more virulent human-to-human diseases.

9.1.3 Not a Test: Disease and Money

A very simple connection in the spread of apparently different things such as viruses and money has been published in January 2006: since both are transported by humans, their travel patterns follow each other closely [19]. Or as the first sentence of their abstract states: “The dynamic spatial redistribution of individuals is a key driving force of various spatiotemporal phenomena on geographical scales.”

The authors study the statistics of human traveling by analysing the circulation of bank notes in the United States, see also Fig. 9.6. The dispersal of bank note is found to be anomalous in two ways: (a) First, the distribution of traveling distances decays as a power law, indicating that trajectories of bank notes are reminiscent of scale free random walks known as Levy flights (http://en.wikipedia.org/wiki/L%C3%A9vy_walk). (b) the probability of

Figure 9.6: Spread of money: since money is transported by the same mechanisms as viruses, a modern virus such as SARS probably will spread in a similar fashion (MPI press release to [19])



remaining in a small, spatially confined region for a time is dominated by algebraically long tails that attenuate the superdiffusive spread.

Although their results confirm that the approaches made in graph theory as described above are valid, the authors deal with these findings in a different way. Instead of resorting to graph theory to model the spread of money (and disease), the authors use a two-parameter continuous-time random walk model: that the dispersal of bank notes and human travel behavior can be described by a continuous time random-walk process that incorporates scale-free jumps as well as long waiting times between displacements. Unfortunately, the authors compare their method only to standard diffusive models for the spread of a disease as used for the old world but not to small world or scale-free networks.

Chapter 10

Projects: Some Interesting Remaining Problems

This chapter is not meant as a lecture. Instead, it contains some examples for end-term student projects related to this course.

You can obtain an ECTS-Grade for the course ‘Modeling Transport’ by working on one of the following projects:

1. Turing patterns in biology and material sciences;
2. Traffic jam as phase transition;
3. Finite element method: temperature distribution in an irregular shaped plate;
4. Monte Carlo simulation of the interaction between energetic charged particles and matter with application in radiation therapy.

If you have ideas on your own, such as modeling along Rapoport's lines for the spread of rumors/disease, you can also suggest such a topic as project and we will discuss the details.

10.1 Rules of the Road

Projects can be worked in groups of two (except you really want to do it all by yourself). In all projects, the following topics should be addressed:

- physical basics,
- mathematical formulation of the problem,
- numerical method (explain your choice and compare to methods not considered in your project),
- coding of the numerical solution (programming language/programm package of your choice; please explain your choice),
- test of the solution,
- closure,
- literature and other aids.

Section 2.3 or chap. 5 can serve as a guidance for the formal structure of your project paper – you should certainly not meet the extend of chap. 5. More detailed hints are given with the individual projects.

Assessment of the projects/relative levels of the projects: the difficulties encountered in the projects are different. For instance, although the objective difficulties in project 3 are pretty low, subjective difficulties will be high because the method has been explained only very briefly in chap. 6. Thus you will spend more time on technical basics than on interesting science or coding. Thus I expect a more accurate and detailed description of these

fundamentals than I would expect in project 1 where all basics has been explained throughout chap. 3–4. The challenge in this project is the application and thus more emphasis should be paid on the description of the physical basics and the test/application of the solution.

Projects have to be handed in at the beginning of the summer term (April 2007). In addition to the elaboration the program files (including a brief documentation) should be handed in.

10.2 Project 1: Turing Patterns in Biology

The aim of the project is the development of a numerical method for the solution of two coupled diffusion–reaction equations. Examples for application are patters in animal skins and structures of surfaces.

10.2.1 Idea

The patterns in animal skins on the one hand are highly deterministic (a tiger shows a different pattern than a leopard or a trout). On the other hand, they are also accidental: two leopards show distinct patterns which allow for identification (like a fingerprint). A formal description of this problem goes back to Turing [166], see also sect. 4.4. He suggested a system of coupled diffusion–reaction equations with one equation describing the development of an activator, the other one that of an inhibitor. The coupling between the two is responsible for pattern formation.

In recent times, Turing’s ansatz has found many applications; to name a few: biomathematics studies pattern in the tidelands [8], chemistry is concerned with reactions [179]. Engineering [180] and surface science [14] also are interested in Turing patterns. The review article by Wollkind and Stephenson [179] gives a good introduction into the topic and shows many comparisons between theory and experiment. The relevant chapters in the dissertation by Leppänen [104] also provide a good introduction to the topic.

10.2.2 Definition of the Project

Within the framework of this project you should be able to describe the basics of Turing patterns, to develop a simple mathematical and numerical model, and to test it. In addition to the general hints given above, you should consider the following:

- give some examples for applications (Google will be helpful).
- describe briefly the ‘geniality’ of Turing’s idea for the description of animal skin patterns.
- the coupled partial differential equations somehow have to be written in a form that is easily transferable into a numerical scheme. You can use, for instance, the method detailed in [180]. If you do so, please explain the method in detail and why it can be done so. If you want, you can also chose a different numerical treatment. If so, please explain your method in detail.
- your numerical scheme should start from discretized equations similar to (16) in [180]. Explain some numerical methods for the solution of such a scheme based on your knowledge from chaps. 3 and 4.
- apply your code to an example. For testing, you can use for instance Fig. 1 in [180] (well, it is not exactly a test, it rather allows some approximation on a test. Why? How can you modify the figure or its results for a test?). Apply your code also to an animal skin pattern: again, Google will help you to find relevant parameters for that problem.

10.2.3 Details

A reader of your project paper will certainly have some question when thinking about Turing patterns. Your paper at least should provide him with the information relevant to answer the following questions:

- is a Turing pattern deterministic or stochastic?
- is a time dependent solution required or will a stationary solution be sufficient? Remember: animal patterns can be used for the identification of individual animals.
- what kind of algorithms allow an efficient treatment of 2D problems? May be, you should consult Google or a book on PDEs.
- is it possible to create Turing-like patterns along one line? Or more general: is there a 1D version of the Turing pattern?
- does the initial distribution of the enzymes matter? Or more specifically: does it matter for the exact pattern? Does it matter for the general rules of the pattern?

10.3 Project 2: Traffic Jam as Phase Transition

The intention of this project is to stimulate thinking about mathematical and numerical basics of a Stefan problem. One example for an application is a traffic jam described as a phase transition.

10.3.1 Idea

The solution of a PDE requires the consideration of both boundary and initial conditions. In the examples discussed throughout the text, boundary conditions are given at a fixed, prescribed boundary. In a Stefan problem, on the other hand, the boundary is moving. Typical examples are, as already described in sect. 4.6, the evaporation or growth of a droplet, the burning of a dust particle or crystal growth. While they share the moving boundary, the models differ in the underlying PDE: in evaporation or solidification this is a heat conduction equation, for the burning particle we encounter a reaction– or diffusion–reaction equation.

A comparison of different problems, albeit on a relatively high level, is given in [171]; different numerical models are compared in [77]. The application of a Stefan problem to a diffusion equation containing evaporation is discussed in detail in [169]. A less obvious Stefan problem is the treatment of a traffic jam as a phase transition [117]. Detailed descriptions of this particular problem are given in [79, 93, 116]; a connection between a traffic jam and emergent phenomena is discussed in [170].

10.3.2 Definition of the Project

Within the framework of this project, the traffic jam should be discussed as one example for a Stefan problem. In addition, a simple numerical solution of the problem should be developed. In addition to the general hints for the projects, the following points should be considered:

- give an overview over Stefan problems, examples and the underlying formal classification (based on the underlying PDE). You can use the literature above as starting point, other literature or Google might also be helpful. Identify the kind of equation relevant for the description of the traffic jam.
- give an overview about principal methods to solve a Stefan problem and in particular the problem of a traffic jam. Sketch the methods briefly.
- develop a simple mathematical model for the description of a traffic jam as a phase transition. Use the papers mentioned above (or other papers or Google information) as a guide line.
- develop a suitable discretization for the problem. Develop also a suitable numerical scheme. Since your previous knowledge from the lecture is focused on finite difference schemes, it might be plausible to develop the numerical solution based on one of them. The simple example in sect. 4.6.1 might guide you through the process. If you have read a little bit on Stefan problems and have encountered different solution methods, feel free to use one of them instead.
- test your numerical solution (comparison with observations, plausibility consideration).

10.3.3 Details

A reader of your project paper will certainly have some question when thinking about Stefan problems and traffic jams. Your paper at least should provide him with the information relevant to answer the following questions:

- Give a graphical description of the relation between a phase transition and a traffic jam.
- Common solutions to Stefan problems use finite element schemes or cellular automata instead of finite difference methods. Please explain why? By the way, what are cellular automata?
- Traffic flow on a highway basically is a 1D directed flow (frame of reference along the highway). How would you describe such a flow formally? Is Euler's or Bernoulli's equation sufficient? Is it possible to create a traffic jam in such a description?
- Does the formation of a traffic jam require an impediment of the flow, such as an obstacle or an accident? Why?
- A Stefan problem describes the evolution of a certain quantity. Which quantity exactly is this?

10.4 Project 3: Finite Element Method: Temperature Distribution in an Irregularly Shaped Plate

Finite element methods (FEM) are used in many 2- or 3D engineering questions, in particular in mechanics and fluid dynamics. However, in contrast to FDM, FEM requires extensive use of computer resources and is complicated by the fractionalization of the simulation space. The aim of this project is to perform a simple FEM simulation using some freely available FEM software such as z88 (<http://www.z88.org/>, available for both Linux and Windows) or CAMMPUS (<http://www.haw-hamburg.de/rzbt/dnksoft/cammpus/cammpus.html>, DOS machines only). Thus this project is more concerned with learning how to handle new software and apply it to a relatively well-defined problem than with the physical background as in some of the other projects.

10.4.1 Definition of the Project

FEM allows to model standard problems from physics (such as heat transport or fluid motion) in complex geometries that are difficult to accommodate in a standard FDM because FEM allows a subdivision of any arbitrarily shaped space in finite elements and does not require fixed step sizes. In FDM the accuracy of the result depends on the discretization, in FEM it depends on the fractionalization. Thus one aspect of the project is to estimate the accuracy depending on fractionalization.

In the lecture, FEM has not been treated in as much detail as the other two methods. In addition, its approach with the weighting functions is less obvious than FDM or Monte Carlo simulations are. Thus other aspects of the project include your familiarization with the fundamental of the method (as described e.g. in [80] or many other books on numerical physics), with its technical aspects (as described e.g. in [7] and many books on numerical physics) and with a standard tool in FEM, such as z88.

The standard tool of your choice than should be applied to some well-defined physical problems. The description of the underlying physics in these problems is not part of the project, thus this is more a mathematical and computational project.

The project thus should consider the following points:

- familiarize yourself with FEM; demonstrate your knowledge by writing a chapter describing the mathematical basis of FEM.
- familiarize yourself with the most important technical aspect of FEM, that is the fractionalization; again demonstrate your knowledge by writing a chapter describing it.

- choose any FEM tool; two are mentioned above with z88 being the more popular one. However, you are free to use any other tool. Familiarize yourself with this by working through its manual, in particular to examples given there. Feel free to write a short section about one of the examples performed during this process.
- apply the FEM tool to the following physical questions:
 - simulate the temperature distribution in a rectangular plate for different boundary conditions. One example, which also can be used to test the result, is given in sect. 4.2. Run your model with different shapes in the fractionalization and different sizes of the elements and discuss the accuracy of your results depending on this choice.
 - as a special case of the above problem simulate the temperature distribution in a room as sketched in Figs. 6.1 and 6.2. The latter figure again can serve for validation.
 - derive a solution for the time-dependent problem of room-temperatures by allowing a temperature variation of the radiator between 20 and 70° for night and day-times respectively.
 - take a square plate and cut out a quarter of an circle from the lower right quadrant of the plate. Again simulate the temperature distribution as in the first application. Vary the boundary conditions at the side with $T \neq 0$.
 - as an add-on (not required): try to simulate the flow in a 2D-tube (river) with a bar blocking half of the tubes diameter (for instance a long pier in the river). What kind of flow forms, what are the properties of the eddies behind the obstacle depending on flow speed, viscosity and obstacle size? You can get some ideas on this question (or formulate yourself a similar problem) by looking into fire-modeling pages, such as www.fpe.umd.edu/departement/modeling/index.html, <http://fseg.gre.ac.uk> or <http://fire.nist.gov/fds/refs/readme.html>; an overview regarding fire simulation models with all relevant links also is given at www.fire.nist.gov/ and www.firetactics.com/FIRE-MODELING.htm.

10.4.2 Details

A reader of your project paper will certainly have some question when thinking about FEM. Your paper at least should provide him with the information relevant to answer the following questions:

- are there any constraints on the shape, number or area of the elements chosen in fractionalization? In particular, must all elements have the same kind of shape or can different shapes be combined?
- explain the meaning of the weight function. Why is it necessary to introduce such functions?
- For the 1D case: is there any difference between FEM and FDM? If yes, explain which and why. If no, explain why.
- The analytical solution for the temperature distribution (4.33) contains an infinite sum (which can be terminated after a few terms). Why does such a solution necessarily lead to a sum? Does such a sum also occur in the FEM solution?

10.5 Project 4: Monte Carlo Simulation of the Interaction between Energetic Charged Particles and Matter with Application in Radiation Therapy

Within the framework of this project you should (a) study the physical basis of the interaction of charged energetic particles with matter, (b) derive a simple Monte Carlo simulation for such an interaction, and (c) apply it to a simplified geometry suitable for the development of a radiation therapy plan.

10.5.1 Idea

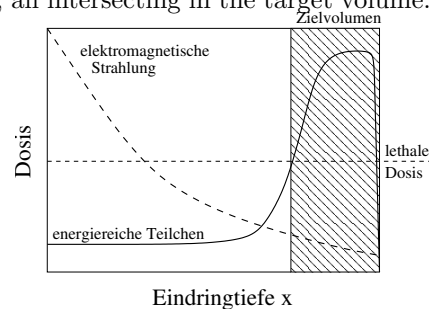
The goal of radiation therapy can be described in rather simple words: determine the properties of a beam of charged particles (or hard electromagnetic radiation) such that most of the dose is delivered to the target to deliver a lethal dose to the tumor cells while the dose in the ambient medium should be extremely low to reduce radiation damage.

Conventional radiation therapy uses hard electromagnetic radiation. This method has the advantage that the radiation is readily available in the form of Bremsstrahlung from an accelerator or γ emitters. Its disadvantage is the spatial distribution of the radiation in the tissue: its intensity I (and thus the deposited dose) decreases with increasing penetration depth x as an exponential (Bouger–Lambert–Beer law): $I(x) = I_0 e^{-\mu x}$ with μ being the absorption coefficient. In radiation therapy the target volume normally lies within the body. Thus before reaching the target, the beam passes through healthy tissue, delivering a higher doses to it than to the target. To avoid complete destruction of all tissue between body surface and target, a number of different beams is used, all intersecting in the target volume.

The situation is different in case of charged energetic particles. The geometry of their interaction with matter is governed by a different rule: energy loss (and thus deposited dose) is largest close to the end of the particles range (Bragg peak). Thus a high dose can be delivered directly to the target volume without destroying the tissue between skin and target.

The specific energy loss of charged particles in matter is described by the Bethe–Bloch equation (8.8) from which one can derive that the energy loss increases with decreasing particle energy (see also Fig. 8.7 and sect. 8.3.1). The aim of this project is a solution of this equation with the help of a Monte Carlo simulation for a suitable geometry. The required information on energy losses and other relevant papers should be found in [24, 28, 126].

The basics of radiation therapy and the simulation of the radiation field are given in an overview [55]; information also is provided in [73] and [178]. Applications of the ansatz described in [55] and links to further sources can be found at <http://www.llnl.gov/peregrine/montecarlo.html>. Links to scientific publications regarding Monte Carlo simulations and radiation therapy planning can be found at <http://gray.mgh.harvard.edu/new/research/Simulation/montecarlo.htm>. A method for the verification of Monte Carlo simulations for radiation therapy planning is described in [11]. A slightly more complex method for the fast optimization of radiation therapy planning is given in [43]. An introduction to Monte Carlo simulations in medical treatment also can be found in the relevant chapters in [40], although that thesis is concerned with photon therapy rather than energetic particles.



10.5.2 Definition of the Project

Within this project you should develop a Monte Carlo simulation that allows to determine the energy loss and thus the deposited dose of energetic charged particles during their interaction with matter. Radiation therapy should serve as an example for the application. In addition to the general hints you should consider the following questions/hints:

- develop a sketch for a Monte Carlo simulation of the energy loss (dose distribution) of energetic charged particles in matter. Develop the model in such a way, that you can add later other physical processes in addition to the continuous energy loss due to ionization. One example for such additional processes is the consideration of the secondary electrons. Tutorials and other information regarding such a simulation can be found at the GEANT 4 homepage at CERN (<http://wwwasd.web.cern.ch/wwwasd/geant4/geant4.html>). Please also describe which parameters (for instance material constants or interaction cross sections) are required to run that kind of simulation.

- begin with a simple simulation: the ionization due to protons in a homogenous medium, for instance water because that is a good proxy for the human body. Take the stochastic nature of the interaction process into account: do not calculate energy losses with the Bethe–Bloch formalism but start from the interaction cross sections/probabilities. The GEANT physics manual [28] might provide useful additional information. Compare the results of your simulation with results obtained from the solution of the Bethe–Bloch equation. How many particles are required to get a reasonable approximation on the analytical solution?
- study the spatial distribution of the energy losses at the end of the particle range. To do this, compare the results of the Monte Carlo simulation with the analytical solution. Use this subproblem to discuss the fundamental differences between the Monte Carlo simulation and Bethe–Bloch.
- expand your simulation to a more realistic geometry. Divide the matter into compartments, corresponding to the healthy tissue (water) and the target volume (water). Structure your simulation such that you are able to insert a third compartment, for instance a bone, into the path of the particle beam.
- Run your simulation with a geometry corresponding to 3 cm healthy tissue followed by a 1 cm target volume, again followed by healthy tissue. Derive the energy distribution of the incident protons such that the dose is maximum in the target and before and behind only a minimal dose is delivered.
- Position a 0.1 cm piece of bone between skin and target. Derive the properties of the new proton beam suitable for radiation therapy. Does the result depend on the position of the piece of bone?
- Try to extend your simulation such that also the secondary electrons are considered. Do the results of your simulation change?

10.5.3 Details

A reader of your project paper will certainly have some question when thinking about Monte Carlo simulations and radiation therapy. Your paper at least should provide him with the information relevant to answer the following questions:

- is the effort put into a Monte Carlo simulation compared to the numerical solution of the Bethe–Bloch equation validated in this case? Are there particular advantages in the use of the MC simulation?
- the beam tailoring you have performed in your model has the advantage of a rather small exposure of the healthy tissue surrounding the target. But does this method not also invoke the risk of errors in therapy if there is unexpected tissue with different absorption properties in the path of the beam? Discuss.
- I am the patient, you are the therapist. Can you give me a crude estimate on the exposure of my healthy tissue in the particle therapy compared to conventional radiation therapy with a γ emitter.
- There is some talk about radiation therapy with heavy ions, see e.g. <http://www.gsi.de/portrait/Broschueren/Therapie/Krebstherapie.htm>). What are the advantages and disadvantages of heavy ions compared to protons? Can you modify your Monte Carlo simulation such that it considers a certain species of heavy ions instead of the protons?

Chapter 11

Closure

This text is neither a formal introduction into modeling nor into numerical methods. Most concepts have been introduced in examples. As in modeling, this closure loops back to the beginning: it summarizes some concepts and methods and rechecks with the beginning whether our goals have been attained or not.

11.1 Transport Modeling in General

The first aspect of this lecture, the introduction into modeling, was focus of chap. 2. Here we have learned about the basic ingredients of modeling, that are: (1) identification of the relevant quantities and processes and the volume under study; (2) mathematical formulation of the problem; (3) reduction and simplification, (4) formulation and solution of the numerical/analytical model, (5) test of the results and (6) closure. This scheme has been discussed in some examples in chap. 2. In addition, many of the examples in later chapters, such as the longitudinal tank in chap. 3, the focused transport in interplanetary space in chap. 5 or the simulation of a dike in chap. 6 are introduced and discussed in the scheme outlined above.

Special emphasis has been paid to two aspects of simplification, the stirred tank concept and the limitation to steady-state. Both concepts allow the reduction of a PDE to a ODE or the reduction of an ODE to an algebraic equation because they reduce the dimensionality of the problem: the stirred tank can be used to reduce spatial dimensionality, in steady-state time vanishes as dimension.

Successful simplification thus often leads to a much simpler mathematical model – and thus often allows for simpler methods to solve it. Solutions to a numerical model can be analytical or numerical. Analytical solutions are preferable for models described by algebraic equations or ODEs; for PDEs, and also for many ODEs, numerical solutions are preferable because either no analytical solution is available or analytical solutions can be obtained only for a few special cases and very restricted boundary conditions.

Another important aspect to consider in modeling, borrowing and selling, is not strongly enough emphasized throughout the text. However, I hope that the examples in chap. 1 and some of the comments/examples at the end of chap. 5, chap. 7 and chap. 8 might help you to appreciate this important aspect of modeling: it is not necessary to derive any model new but it might be more economic to adopt and modify an existing and tested (!) model to the own problem.¹

¹Once the idea of the wheel was discovered and understood, many different realizations of the wheel were manufactured, depending on the required size, the required strength and the materials available and manageable. Although some high-tech wheels are quite exotic and advanced, hopefully none of its constructors had to invent the wheel completely new.

11.2 Numerical Methods

The second focus of this lecture was the introduction to different kinds of numerical methods. The focus of this text was the introduction to finite difference methods (FDM) in chaps. 3–5. These methods are most common in physics. However, the finite element method (FEM) with its broad range of technical applications has been introduced in chaps. 6 and chap. 7.

Finite difference methods are the oldest standard methods in numerics. They divide the simulation space into equidistant steps and evolve the solution from one node to the next (Euler, Runge-Kutta) or by using the two adjacent nodes (centered differences). The boundary conditions are considered in the difference equations for the outer nodes. FDMs are robust, however, their usability is limited because at least in conventional methods equidistant grids are required – and in higher dimensional problems the grids have to be rectangular. In the numerical model, however, small step sizes are required in places where gradients are large while for small gradients larger step sizes will suffice. Some adaptive schemes have been developed for ODEs, however, in a PDE with more than one spatial dimension, adaptive methods in general are not very efficient. In addition, in FDMs the grid cannot easily be adapted to boundary conditions and geometries not aligned with the grid.

A much better adaptation to geometries and varying elements is provided by the finite element methods (FEM). It requires some kind of tessellation pattern for the simulation volume – triangles are a first good approach in a 2D problem but shapes can be much more complex. Weighting functions that are 1 in one node and vanish in all other nodes have to be defined on this grid and applied to the weak form of the equation. This finally leads to a large set of algebraic equations that can be solved by conventional methods.

While FDM and FEM both are strongly deterministic methods leading to a unique solution to the problem (at least in case of successful model formulation and numerical implementation), Monte Carlo simulations follow an entirely different approach: here the modeler just rolls the dice to determine what happens next. The number of faces of the dice as well as the probabilities for each face depend on the interaction cross sections or probabilities of the different processes under study. In simple cases, such as radioactive decay, the dice has just two sides reflecting decay or survival of the particle. Since the approach basically is stochastic, Monte Carlo simulations are useful if stochastic processes are involved (such as diffusion, decay or heat transport) but are not useful in strongly deterministic processes, such as advection or the motion of a charged particle in an electromagnetic field under influence of the Lorentz force only.

The stochastic approach in the Monte Carlo simulation leads to a fundamental difference to FDM and FEM: the solution cannot be repeated because you will never exactly repeat the results from multiple throws of a dice.² Thus the solution of a Monte Carlo simulation is not exact. But this non-exactness also is an advantage of the method: different runs give an average result that is close to the real one and the distribution of the results gives the variability of the expected results.

11.3 Finite Difference Method: Schemes

Some standard finite difference methods for ODEs are graphically depicted in Fig. 11.1. The accuracy of the methods depends on the step size Δx or the number n of steps. These accuracies and the occurrence of the methods throughout this text are given in Table 11.1.

The basic classification of the methods is that into explicit or implicit. Explicit methods only use the known values at the begin of the interval to calculate the value at its end. Thus the scheme can advance straight forward. In consequence, compact schemes result that advance step by step without requiring excessive storage space or even matrix inversion. The situation is different in the implicit schemes: here also nodes not considered so far enter the

²Well, that's not exactly true: if you gamble long enough, eventually the same row of results will be found again. And in numerical methods of rolling a dice you also might be able to repeat the result if the random number generator is initialized with the same value.

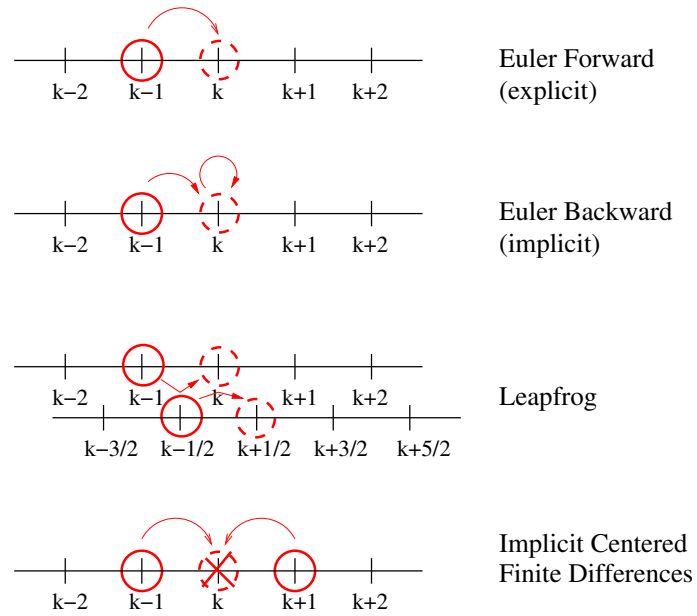


Figure 11.1: Summary FDMs for ODEs

Table 11.1:	Euler forward	explicit	$\mathcal{O}(\Delta x)$	(D.27)
Summary	Euler backward	implicit	$\mathcal{O}((\Delta x)^2)$	(D.29)
of FDM for	Leapfrog	explicit, alternating	$\mathcal{O}(\Delta x)^2)$	(D.34), (D.35)
ODEs	Runge–Kutta 4 th order	explicit	$\mathcal{O}(\Delta x)^4)$	(D.36)
	centered diff	implicit	$\mathcal{O}(\Delta x)^2)$	sect. 3.1

calculation of a given node. In case of the Euler backward method, the resulting problem of iteration can be circumvented by introducing a predictor step using the Euler forward method. Thus as in the explicit methods, the scheme advances step by step. In the centered difference scheme, on the other hand, the equations for all nodes have to be solved simultaneously. Thus a rather large (but sparse) matrix must be inverted.

FDM schemes for PDEs differ from that for ODEs in such that the least a second independent variable: either time in addition to space or a second spatial coordinate. Some schemes discussed in this text are presented in Fig. 11.2; their accuracy and their appearance in the text are given in Table 11.2. All schemes discussed here are (at least partially) implicit because they use the centered difference scheme already known from the ODEs for the spatial coordinate. The simplest scheme is the FTCS scheme: forward in time and centered in space. This scheme is a direct continuation from the centered difference scheme in the ODE: for each time step, the centered scheme is solved while the advance in time is by a simple forward process. This scheme, therefore is easily coded: once you have a numerical solution for the simple centered difference scheme, time just is wrapped around it in a loop according to Euler forward. The Crank–Nicolson scheme, on the other hand, also is a kind of centered scheme: although time advances only from t^l to t^{l+1} , the centered aspects enters through the time at which the spatial transport occurs: $t^{l+\frac{1}{2}}$, that is in the middle of the time step. Although the accuracy in transport in time is now increased, the numerical implementation still is similar to the one in FTCS: we only need to solve the matrix for the centered differences in space but the transport in time still is straight forward.

The five-point scheme (or seven-point scheme in a 3D problem) also is concerned with two independent variables. In this case, however, both are spatial variables and the scheme

Table 11.2:	FTCS	explicit/implicit	$\mathcal{O}(\Delta t, (\Delta x)^2)$	sect. 3.2.1
Summary FDMs	Crank–Nicolcon	implicit	$\mathcal{O}((\Delta t)^2), (\Delta x)^2)$	sect. 3.2.2
for PDEs	Five-point scheme	implicit	$\mathcal{O}((\Delta x)^2), (\Delta y)^2)$	sect. 4.2.1

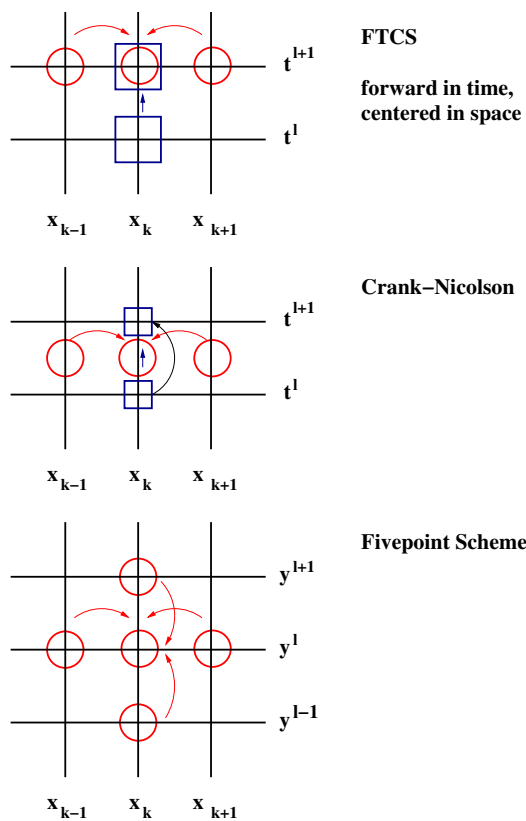


Figure 11.2: Summary FDMs for PDEs

is centered in both variables at the grid points and not in the middle of an interval. In consequence, a 3D matrix would be required to solve the problem. Instead, the matrix is given in lexicographical order. This leads to an extremely large five-diagonal matrix which requires efficient solvers. Here iterative methods such as the Jacobi method or Gauß-Seidel are used instead of the standard of Gaussian elimination.

11.4 Some Final Words

We have started this lecture boldly with a large set of examples, mainly from natural transport problems. Thus some of the readers might feel disappointed that they still are not able to develop a model of a glacier under changing climate conditions or to build a fine nice climate model for their notebook.

However, if you have navigated carefully through the text, I hope that you have started to develop some ideas regarding the complexity of natural systems and the requirements of numerical modeling. Probably you will now start to develop a more critical view on complex models, in particular models entering the political stage such as climate models. But I also hope that you have started to think a little bit more about physics and the view of physics on a problem: physics is based on reductionism. And in consequence, our experiments and models do not reflect the world but only some aspects. If you start to think about these aspects of your profession, you probably have learned something more important than just coding a centered difference scheme.

Appendix A

Useful Things

A.1 List of symbols

α	pitch angle	Pitchwinkel
α	heat transfer coefficient	Wärmeübergangszahl
β	v/c speed in units of the speed of light c	
γ	spectral index	Spektralindex
γ	decay coefficient	Zerfallskonstante
ϵ	rate of energy dissipation	Energiedissipationsrate
ϵ	property of space	Raumeigenschaft
ϵ	energy density	Energiedichte
ϵ	porosity	Porosität
ϵ_0	absolute permeability	absolute Permeabilität
$\epsilon_{\vec{B}}$	energy density in the magnetic field	Energiedichte im magnetischen Feld
$\epsilon_{\vec{E}}$	energy density in the electric field	Energiedichte im elektrischen Feld
$\bar{\epsilon}$	average emissivity	mittleres Emissionsvermögen
φ_{12}		Einstrahlzahl
κ	pitch angle diffusion coefficient	Pitchwinkeldiffusionskoeffizient
λ	mean free path	mittlere freie Weglänge
λ	thermal conductivity	Wärmeleitvermögen
λ_D	Debye length	debye-Länge
λ_r	radial mean free path	radiale mittlere freie Weglänge
λ_{\parallel}	parallel mean free path	parallele mittlere freie Weglänge
λ_c	Coulomb logarithm	Coulomb Logarithmus
λ_D	Debye length	Debye-Länge
μ	Pitch cosine	Kosinus des Pitchwinkels
μ	absorption coefficient	Absorptionskoeffizient
μ	viscosity	Viskosität
ν	collision frequency	Stoßfrequenz
ν	kinematic viscosity	kinematische Viskosität
ω	angular speed	Winkelgeschwindigkeit
ω	relaxation factor	Relaxationsfaktor
ω_{\odot}	angular velocity of the Sun	Winkelgeschwindigkeit der Sonne
Ω	solid angle	Raumwinkel
ψ	spiral angle	Spiralwinke
ψ	probability function	Wahrscheinlichkeitsfunktion
ρ	iteration parameter	Iterationsparameter
ϱ	mass density	Dichte

ϱ_c	charge density	Ladungsdichte
σ	scattering cross section	Wirkungsquerschnitt
ζ	focusing length	Fokussierungslänge
\vec{B}	magnetic field	magnetische Flussdichte
\vec{C}	velocity of a point in phase space	Geschwindigkeit im Phasenraum
A	area, cross section	Fläche
c	speed of light	Lichtgeschwindigkeit
c	specific heat capacity	spez. Wärmekapazität
c_{12}	radiation exchange coefficient	Strahlungsaustauschkoeffizient
c	concentration	Konzentration
D	diffusion coefficient	Diffusionskoeffizient
D	rate of evaporation	Verdunstungsrate
D_r	radial diffusion coefficient	radialer Diffusionskoeffizient
D_{\parallel}	parallel diffusion coefficient	paralleler Diffusionskoeffizient
D	dispersion coefficient	Dispersionskoeffizient
e	elementary charge	Elementarladung
E	energy	Energie
$\langle E_B \rangle$	average bond energy	mittlere Bindungsenergie
\vec{E}	electric field	elektrische Feldstärke
$f(\vec{q}, \vec{p}, t)$	phase space density	Phasenraumdichte
f	flow	
F	flow rate	
F	distribution function	Verteilungsfunktion
f_x	discharge rate of x	
g	amplification factor	
h	step size	Schrittweite
H	conditioning matrix	Konditionierungsmatrix
I	information	Information
I	differential intensity	differentielle Intensität
i	index for spatial coordinate (subscript)	
i	current (time dependent)	Strom (zeitabhängig)
j_{conv}	convective heat flow density	Wärmestromdichte
j_Q	heat flow density due to thermal conductivity	Wärmestromdichte
J	differential flux	differentieller Fluss
k	index for spatial coordinate (subscript)	
k	wave number	Wellenzahl
k	permeability	Permeabilität
K	efficient permeability	effektive Permeabilität
K	dispersion coefficient	Dispersionskoeffizient
l	index for time (superscript)	
L	scale length	Skalenlänge
L_k	Kolmogoroff scale	
\mathcal{L}	differential operator	Differentialoperator
N	particle number (density)	Teilchenzahl(dichte)
n	index iteration step (superscript)	
n_e	electron density	Elektronendichte
m	mass	Masse
m_e	mass of the electron	Elektronenmasse
\vec{o}	surface of a volume element	
\vec{p}	momentum	Impuls
p_i	generalized momentum	generalisierter Impuls
\vec{p}	momentum	Impuls
p	probability	Wahrscheinlichkeit
p	pressure	Druck

$P(x)$	Gauß distribution	Gauß-Verteilung
q_i	generalized coordinates	generalisierte Koordinate
q	charge	Ladung
q	radiation flow	Strahlungsstrom
q	spectral index	Spektralindex
Q	heat	Wärmemenge
Q	source term	Quellterm
\bar{Q}	point in phase space	Punkt im Phasenraum
\vec{r}	spatial coordinate	räumliche Koordinate
r	reaction rate	Reaktionsrate
R	resistance	Widerstand
s	length along a path	Länge entlang eines Pfades
S	saturation	Sättigung
\vec{S}	streaming	
\vec{S}	energy flux density	Energiestromdichte
t	time	Zeit
t_m	time to maximum	Zeit zum maximum
T	temperature	Temperatur
T_{eff}	effective temperature	Effektivtemperatur
	mean radiant temperature	Strahlungstemperatur
u	voltage (time dependent)	Spannung (zeitabhängig)
U	particle number density	Teilchenzahldichte
u	bulk speed	Strömungsgeschwindigkeit
u'	fluctuating speed component	
u_t	turbulent speed	
u	unknown quantity (scalar, vector ...)	
v_{\parallel}	parallel speed	Geschwindigkeit parallel
v_{\perp}	perpendicular speed	Geschwindigkeit senkrecht
\vec{v}	speed of a particle	Geschwindigkeit
v_{th}	thermal speed	thermische Geschwindigkeit
V	volume	Volumen
W	total number of moles	
x_0	average	Mittelwert
Z	charge	Ladung

A.2 List of Acronyms

ADI	alternating direction implicit
CFD	computational fluid dynamics
CFL	Courant–Friedrichs–Lewy
ENSO	El Nino Southern Oscillation
FCT	flux corrected transport
FD	finite difference
FDE	finite difference equation
FDM	finite difference method
FEM	finite element method
FTCS	forward in time centered in space scheme
GCM	general circulation model
IMF	interplanetary magnetic field
LET	linear energy transfer
ODE	ordinary differential equation
PDE	partial differential equation
SEP	solar energetic particles

TE	truncation error
TM	transport model

A.3 Useful Numbers

Boltzmann constant k_B	1.3807×10^{-23} J/K
gravitational constant γ	6.67×10^{-11} N m ² /kg ²
permittivity constant ε_0	8.85×10^{-12} C ² /(N m ²)
Stefan–Boltzmann constant σ	5.67×10^{-8} W/(m ² K ⁴)

A.4 Exponential Function and Related Stuff

- Euler’s formula:

$$e^{ix} = \cos x + i \sin x \quad \text{and} \quad e^{-ix} = \cos x - i \sin x . \quad (\text{A.1})$$

- trigonometric functions:

$$\cos x = \frac{e^{ix} + e^{-ix}}{2} \quad \text{and} \quad \sin x = \frac{e^{ix} - e^{-ix}}{2i} . \quad (\text{A.2})$$

- hyperbolic functions:

$$\sinh x = \frac{e^x - e^{-x}}{2} , \quad \cosh x = \frac{e^x + e^{-x}}{2} \quad \text{and} \quad \tanh x = \frac{e^x - e^{-x}}{e^x + e^{-x}} . \quad (\text{A.3})$$

A.5 Vector Calculus

- vector identities:

$$\vec{A} \cdot (\vec{B} \times \vec{C}) = \vec{C} \cdot (\vec{A} \times \vec{B}) = \vec{B} \cdot (\vec{C} \times \vec{A}) \quad (\text{A.4})$$

$$\vec{A} \times (\vec{B} \times \vec{C}) = \vec{B}(\vec{A} \cdot \vec{C}) - \vec{C}(\vec{A} \cdot \vec{B}) \quad (\text{A.5})$$

$$\vec{A} \times (\vec{B} \times \vec{C}) + \vec{B} \times (\vec{C} \times \vec{A}) + \vec{C} \times (\vec{A} \times \vec{B}) = 0 \quad (\text{A.6})$$

$$(\vec{A} \times \vec{B}) \cdot (\vec{C} \times \vec{D}) = (\vec{A} \cdot \vec{C})(\vec{B} \cdot \vec{D}) - (\vec{A} \cdot \vec{D})(\vec{B} \cdot \vec{C}) \quad (\text{A.7})$$

$$(\vec{A} \times \vec{B}) \times (\vec{C} \times \vec{D}) = (\vec{A} \times \vec{B} \cdot \vec{D})\vec{C} - (\vec{A} \times \vec{B} \cdot \vec{C})\vec{D} \quad (\text{A.8})$$

- gradient

$$\text{grad } A = \frac{\partial A}{\partial x} \vec{e}_x + \frac{\partial A}{\partial y} \vec{e}_y + \frac{\partial A}{\partial z} \vec{e}_z = \begin{pmatrix} \partial A / \partial x \\ \partial A / \partial y \\ \partial A / \partial z \end{pmatrix} = \nabla A . \quad (\text{A.9})$$

$$\text{grad } A = \nabla A = \frac{\partial A}{\partial \varrho} \vec{e}_\varrho + \frac{1}{\varrho} \frac{\partial A}{\partial \varphi} \vec{e}_\varphi + \frac{\partial A}{\partial z} \vec{e}_z . \quad (\text{A.10})$$

$$\text{grad } A = \nabla A = \frac{\partial A}{\partial r} \vec{e}_r + \frac{1}{r} \frac{\partial A}{\partial \theta} \vec{e}_\theta + \frac{1}{r \sin \theta} \frac{\partial A}{\partial \varphi} \vec{e}_\varphi , \quad (\text{A.11})$$

- divergence

$$\text{div } \vec{A} = \nabla \cdot \vec{A} = \frac{\partial A_x}{\partial x} + \frac{\partial A_y}{\partial y} + \frac{\partial A_z}{\partial z} . \quad (\text{A.12})$$

$$\text{div } \vec{A} = \nabla \cdot \vec{A} = \frac{1}{\rho} \frac{\partial(\rho A_\rho)}{\partial \rho} + \frac{1}{\rho} \frac{\partial A_\varphi}{\partial \varphi} + \frac{\partial A_z}{\partial z} . \quad (\text{A.13})$$

$$\text{div } \vec{A} = \nabla \cdot \vec{A} = \frac{1}{r^2} \frac{\partial(r^2 A_r)}{\partial r} + \frac{1}{r \sin \vartheta} \frac{\partial(\sin \vartheta A_\vartheta)}{\partial \vartheta} + \frac{1}{r \sin \vartheta} \frac{\partial A_\varphi}{\partial \varphi} , \quad (\text{A.14})$$

- Laplace operator

$$\Delta = \nabla^2 = \left(\frac{\partial^2}{\partial x^2} + \frac{\partial^2}{\partial y^2} + \frac{\partial^2}{\partial z^2} \right) \quad (\text{A.15})$$

$$\Delta A = \frac{1}{\rho} \frac{\partial}{\partial \rho} \left(\rho \frac{\partial A}{\partial \rho} \right) + \frac{1}{\rho^2} \frac{\partial^2 A}{\partial \varphi^2} + \frac{\partial^2 A}{\partial z^2}. \quad (\text{A.16})$$

$$\begin{aligned} \Delta A &= \frac{1}{r^2} \frac{\partial}{\partial r} \left(r^2 \frac{\partial A}{\partial r} \right) + \frac{1}{r^2 \sin \vartheta} \frac{\partial}{\partial \vartheta} \left(\sin \vartheta \frac{\partial A}{\partial \vartheta} \right) \\ &\quad + \frac{1}{r^2 \sin^2 \vartheta} \frac{\partial^2 A}{\partial \varphi^2}, \end{aligned} \quad (\text{A.17})$$

- curl

$$\text{curl} \vec{A} = \nabla \times \vec{A} = \begin{pmatrix} \partial/\partial x \\ \partial/\partial y \\ \partial/\partial z \end{pmatrix} \times \begin{pmatrix} A_x \\ A_y \\ A_z \end{pmatrix} = \begin{pmatrix} \partial A_z/\partial y - \partial A_y/\partial z \\ \partial A_x/\partial z - \partial A_z/\partial x \\ \partial A_y/\partial x - \partial A_x/\partial y \end{pmatrix}. \quad (\text{A.18})$$

$$\begin{aligned} \text{curl} \vec{A} &= \nabla \times \vec{A} = \left(\frac{1}{\varrho} \frac{\partial A_z}{\partial \varphi} - \frac{\partial A_\varphi}{\partial z} \right) \vec{e}_\varrho + \left(\frac{\partial A_\varrho}{\partial z} - \frac{\partial A_z}{\partial \varrho} \right) \vec{e}_\varphi \\ &\quad + \frac{1}{\varrho} \left(\frac{\partial(\varrho A_\varphi)}{\partial \varrho} - \frac{\partial A_\varrho}{\partial \varphi} \right) \vec{e}_z. \end{aligned} \quad (\text{A.19})$$

$$\begin{aligned} \text{curl} \vec{A} &= \nabla \times \vec{A} = \frac{1}{r \sin \vartheta} \left(\frac{\partial(\sin \vartheta A_\varphi)}{\partial \vartheta} - \frac{\partial A_\vartheta}{\partial \varphi} \right) \vec{e}_r \\ &\quad + \frac{1}{r} \left(\frac{1}{\sin \vartheta} \frac{\partial A_r}{\partial \varphi} - \frac{\partial(r A_\varphi)}{\partial r} \right) \vec{e}_\vartheta + \frac{1}{r} \left(\frac{\partial(r A_\vartheta)}{\partial r} - \frac{\partial A_r}{\partial \vartheta} \right) \vec{e}_\varphi \end{aligned} \quad (\text{A.20})$$

- Gauss theorem

$$\oint_{\mathcal{O}(\mathcal{V})} \vec{F} \cdot d\vec{A} = \int_{\mathcal{V}} \text{div} \vec{F} \, dV. \quad (\text{A.21})$$

- Stokes theorem

$$\oint_{\mathcal{C}(\mathcal{A})} \vec{F} \cdot d\vec{r} = \int_{\mathcal{A}} \text{rot} \vec{F} \cdot d\vec{A}. \quad (\text{A.22})$$

A Little Mathematical Reminder

B.1 Analytical Strategies for Ordinary Differential Equations

Ordinary differential equations (ODEs) are conditional equations for functions $y = f(x)$ of one variable in the form

$$f'(x) = c(x) f(x) + g(x) \quad (\text{B.1})$$

for a first order ODE or

$$f''(x) = d(x) f'(x) + c(x) f(x) + g(x) \quad (\text{B.2})$$

for a second order one.

ODEs can be solved by many different strategies, depending on the order of the ODE and the coefficients and inhomogeneities. Solution strategies can be summarized as follows (cf. [5]):

1. *Separable ODEs* are of the form

$$y' = \frac{f(x)}{g(y)} \quad \text{or} \quad y'' = \frac{f(x)}{g(y')} . \quad (\text{B.3})$$

Note that the 2nd order ODE in fact is a first order ODE for y' .¹

The solution is obtained by separation of the variables and subsequent integration:

$$\int g(y) dy = \int f(x) dx + C \quad \text{or} \quad \int g(y') dy' = \int f(x) Dx + C . \quad (\text{B.4})$$

2. *Linear homogeneous 2nd order ODE with constant coefficients* are of the form

$$ay'' + by' + cy = 0 . \quad (\text{B.5})$$

Eigenwerte λ_i can be determined with an exponential ansatz, giving the solution

$$y = c_1 e^{\lambda_1 x} + c_2 e^{\lambda_2 x} . \quad (\text{B.6})$$

3. A *linear inhomogeneous 2nd order ODE with constant coefficients* has an additional inhomogeneity $g(x)$:

$$ay'' + by' + cy = g(x) . \quad (\text{B.7})$$

The solution is obtained as a superposition of the solution $y_H = c_1 e^{\lambda_1 x} + c_2 e^{\lambda_2 x}$ of the homogeneous ODE and a particulate solution y_p for the inhomogeneity. Some particulate solutions are listed in table B.1.

¹The standard example is linear motion with friction. The equation of motion then reads $m\ddot{x} = -\beta v = -\beta\dot{x}$ or rewritten as 1st order ODE for $v = \dot{x}$: $m\dot{v} = -\beta v$.

$g(x)$	ansatz for y_P	coefficients of y_P
a_0	$K = \text{const}$	$K = \frac{a_0}{c}$
$a_0 + a_1x + a_2x^2 + \dots a_nx^n$	$A_0 + A_1x + A_2x^2 + \dots A_nx^n$	insert into ODE
$a_0 e^{rx}$	$A_0 e^{rx}$	$A_0 = \frac{a_0}{ar^2+br+c}$
$a_0 \sin(nx) + b_0 \cos(nx)$	$A_0 \sin(nx) + B_0 \cos(nx)$	$A_0 = \frac{(c-n^2a)a_0+nbb_0}{(c-n^2a)^2+n^2b^2}$ $B_0 = \frac{(c-n^2a)b_0-nba_0}{(c-n^2a)^2+n^2b^2}$

Table B.1: Particulate integrals for a 2nd order ODE of form $ay'' + by' + cy = g(x)$

4. *Linear homogeneous 2nd order ODE with variable coefficients* of the form

$$a(x)y'' + b(x)y' + c(x)y = 0. \quad (\text{B.8})$$

The standard solution is an ansatz by a power series yielding a solution

$$y = c_1 \sum_{n=1}^{\infty} a_n x^{n+k_1} + c_2 \sum_{n=1}^{\infty} b_n x^{n+k_2}. \quad (\text{B.9})$$

5. *Inhomogeneous initial value ODEs with variable coefficients* can be solved by Laplace transformation (cf. B.3).

Asides from these major schemes there are also some minor schemes for solving ODEs:

6. *Linear inhomogeneous 1st order ODE with variable coefficients* have the form

$$y' + f(x)y = g(x). \quad (\text{B.10})$$

Using the technique of variation of the constant, the general solution can be determined to be

$$y = \exp \left\{ \int -f(x) dx \left[\int g(x) \exp \left(\int f(x) dx \right) dx + C \right] \right\}. \quad (\text{B.11})$$

7. A *general 1st order ODE* has the form

$$\frac{y' + f(x, y)}{g(x, y)} = 0. \quad (\text{B.12})$$

There are two basic methods to derive a solution:

- (a) A substitution $y = vx$ might yield a separable ODE in v and x only with the solution

$$\ln x = C - \int \frac{g(1, v) dv}{f(1, v) + vg(1, v)}. \quad (\text{B.13})$$

- (b) In case of an exact ODE, that is

$$\frac{\partial f}{\partial y} = \frac{\partial g}{\partial x} \quad (\text{B.14})$$

the solution is directly given as

$$\int f(x, c) dx + \int g(c, y) \frac{\partial}{\partial y} \int f(x, c) dx dy = C. \quad (\text{B.15})$$

8. A *nonlinear 2nd order ODE with first derivative and terms in x missing* has the form

$$y'' = f(y). \quad (\text{B.16})$$

It can be solved by multiplying with

$$2 \frac{dy}{dx} dx$$

to obtain the equation

$$y' = \left[2 \int f(y) dy + C \right]^{\frac{1}{2}}. \quad (\text{B.17})$$

This equation is separable and thus can be solved by separation of variables.

9. A *nonlinear 2nd order ODE with missing dependent variable* can be written as

$$f(y'', y', x) = 0. \quad (\text{B.18})$$

The solution is obtained by reduction to a 1st order ODE by *p-substitution*

$$p = \frac{dy}{dx}.$$

Integration of the 1st order ODE can be done by any of the methods above and yields p . A second integration is required to obtain y .

10. A *nonlinear 2nd order ODE with missing independent variable* can be written as

$$f(y'', y', y) = 0. \quad (\text{B.19})$$

Again, the solution is obtained by reduction to a 1st order ODE by *p-substitution*

$$\frac{d^2y}{dx^2} = \frac{dp}{dx} = \frac{dp}{dy} \frac{dy}{dx} = p \frac{dp}{dy}. \quad (\text{B.20})$$

Subsequent procedure as in 9.

B.2 Partial Differential Equations – Classification

A n th-order ODE has a general solution depending on n arbitrary integration constants. The general solution of a PDE, on the other hand, does not depend on arbitrary constants but on arbitrary functions. Their number, in general, equals the order of the PDE. The arbitrary functions depend on one variable less than the solution itself.

B.2.1 Characteristics of a PDE

A system of k PDEs for k unknown functions $\vec{u} = (u^i)$ ($i = 1 \dots k$) of n independent variables $\vec{x} = (x_\nu)$ ($\nu = 1 \dots n$) can be written as

$$L_j(u) = a^{ij\nu} \frac{\partial u^i}{\partial x_\nu} + b^j = r^j = 0 \quad j = 1, \dots, k. \quad (\text{B.21})$$

Here repeated indices require summation. Coefficients $a^{ij\nu}$ depend on \vec{x} ; coefficients b^j depend on \vec{x} and eventually also on \vec{u} . A shorthand notation is

$$\vec{L}(\vec{u}) = \mathbf{A}^\nu \frac{\partial \vec{u}}{\partial x_\nu} + \vec{b} = 0 \quad \text{with} \quad \frac{\partial \vec{u}}{\partial x_\nu} = \frac{\partial \vec{u}}{\partial \nu}. \quad (\text{B.22})$$

Here \mathbf{A}^ν is a $k \times k$ matrix $(a^{ij})^\nu$; the operators \vec{L} and \vec{b} are vectors. Equation (B.22) also is called the matrix form of the system.

On a surface \mathcal{C} : $\Phi(x) = 0$ and $\nabla\Phi \neq 0$, the characteristic matrix is defined as

$$\mathbf{A} = \frac{\partial \Phi}{\partial \nu} \mathbf{A}^\nu. \quad (\text{B.23})$$

A characteristic determinant or characteristic form is defined as

$$Q \left(\frac{\partial \Phi}{\partial x_1}, \dots, \frac{\partial \Phi}{\partial x_n} \right) = |\mathbf{A}|. \quad (\text{B.24})$$

For a Cauchy problem, the initial value of \vec{u} , also called the Cauchy data, is given on the Cauchy surface \mathcal{C} . If $Q \neq 0$ on \mathcal{C} , (B.22) determines in a unique way all partial derivatives $\partial \vec{u} / \partial \nu$ for arbitrary initial data. In this case, \mathcal{C} is called a free surface. If $Q = 0$, \mathcal{C} is a characteristic surface and there exists a characteristic linear combination $\lambda L(\vec{u}) = \lambda_j L_j(\vec{u}) = \Lambda(\vec{u})$ of the differential operators L_j such that in Λ the derivative of \vec{u} on \mathcal{C} depends only on \vec{u} on \mathcal{C} . Since $\Lambda(\vec{u})$ imposes a relation between the initial data, these cannot be chosen arbitrarily.

B.2.2 Types of PDEs – Examples

We will now analyze the types and characteristics of some PDEs, using typical examples for illustrations.

Linear Convection Equation – A Hyperbolic Equation

The linear convection equation

$$\frac{\partial u}{\partial t} + c \frac{\partial u}{\partial x} = r = 0 \quad (\text{B.25})$$

is a first-order PDE of hyperbolic type. Its characteristic matrix is the 1×1 -matrix

$$\mathbf{A} = \left(\frac{\partial \Phi}{\partial t} + c \frac{\partial \Phi}{\partial x} \right). \quad (\text{B.26})$$

The characteristic form is

$$Q = \frac{\partial \Phi}{\partial t} + c \frac{\partial \Phi}{\partial x} \quad (\text{B.27})$$

and the characteristic curve has the slope

$$\left(\frac{d\vec{x}}{dt} \right)_c = - \frac{\frac{\partial \Phi}{\partial t}}{\frac{\partial \Phi}{\partial x}} = c. \quad (\text{B.28})$$

The characteristics thus are straight lines \mathcal{C} : $x - ct = \text{const.}$ The compatibility relation, $r = 0$, is the equation itself. The linear convection equation represents a derivative along the characteristics. If $u_{\mathcal{C}}$ is the value of u on \mathcal{C} , the total derivative is

$$\left(\frac{du}{dt} \right)_c = \frac{\partial u}{\partial t} + \left(\frac{dx}{dt} \right)_c \frac{\partial u}{\partial x} = \frac{\partial u}{\partial t} + c \frac{\partial u}{\partial x} = 0. \quad (\text{B.29})$$

The total derivative vanishes and thus $u_{\mathcal{C}} = \text{const.}$ The solution to (B.25) thus can be written as

$$u(x, t) = f(x - ct) \quad (\text{B.30})$$

with $f(\xi)$ being an arbitrary function of the new variable $\xi = x - ct$.

Wave Equation – A Totally Hyperbolic Equation

The wave equation

$$\frac{\partial^2 u}{\partial t^2} - c^2 \frac{\partial^2 u}{\partial x^2} = 0 \quad (\text{B.31})$$

best can be studied after transformation into a system of first-order PDEs. With $v = \partial u / \partial t$ and $w = \partial u / \partial x$, the system reads

$$\frac{\partial v}{\partial t} - c^2 \frac{\partial w}{\partial x} = r_1 = 0 \quad \text{and} \quad \frac{\partial w}{\partial t} - \frac{\partial v}{\partial x} = r_2 = 0. \quad (\text{B.32})$$

The matrix form of the system depends on \mathbf{A}^t and \mathbf{A}^x :

$$\begin{pmatrix} 1 & 0 \\ 0 & 1 \end{pmatrix} \frac{\partial}{\partial t} \begin{pmatrix} v \\ w \end{pmatrix} + \begin{pmatrix} 0 & -c^2 \\ -1 & 0 \end{pmatrix} \frac{\partial}{\partial x} \begin{pmatrix} v \\ w \end{pmatrix} = 0. \quad (\text{B.33})$$

The characteristic matrix then reads

$$\mathbf{A} = \begin{pmatrix} \partial \Phi / \partial t & -c^2 \partial \Phi / \partial x \\ -\partial \Phi / \partial x & \partial \Phi / \partial t \end{pmatrix} \quad (\text{B.34})$$

with the determinant $|\mathbf{A}| = Q$:

$$Q = \left(\frac{\partial \Phi}{\partial t} \right)^2 - c^2 \left(\frac{\partial \Phi}{\partial x} \right)^2 = \left(\frac{\partial \Phi}{\partial t} - c \frac{\partial \Phi}{\partial x} \right) \left(\frac{\partial \Phi}{\partial t} + c \frac{\partial \Phi}{\partial x} \right) = 0. \quad (\text{B.35})$$

The factors of Q are known from (B.27). Following the procedure there, we obtain two families of characteristic curves with slope $(dx/dt)_C = \pm c$. The characteristics \mathcal{C}^\pm are straight lines $x \mp ct = \text{const}$; the equation is a totally hyperbolic PDE.

The compatibility relations are obtained from the determinant

$$\begin{vmatrix} r_1 & -c^2 \partial\Phi/\partial x \\ r_2 & \partial\Phi/\partial t \end{vmatrix} = 0. \quad (\text{B.36})$$

Since $\partial\Phi/\partial t = \mp c \partial\Phi/\partial x$, we obtain two relations

$$\frac{\partial(v - cw)}{\partial t} + c \frac{\partial v - cw}{\partial x} = 0 \text{ on } \mathcal{C}^+ \quad \text{and} \quad \frac{\partial(v + cw)}{\partial t} - c \frac{\partial v + cw}{\partial x} = 0 \text{ on } \mathcal{C}^-. \quad (\text{B.37})$$

Integration yields

$$v - cw = f(x - ct) \quad \text{and} \quad v + cw = g(x + ct). \quad (\text{B.38})$$

Further integration yields d'Alembert's solution for $u(x, t)$

$$u(x, t) = F(x - ct) + G(x + ct) \quad (\text{B.39})$$

with F and G being arbitrary functions of a single argument $\xi_i = x \mp ct$.

Laplace Equation – An elliptic PDE

Laplace's equation

$$\frac{\partial^2 u}{\partial x^2} + \frac{\partial^2 u}{\partial y^2} = 0 \quad (\text{B.40})$$

can be analyzed in the same way as the wave equation by substituting t for y and i for c . The characteristic form then becomes

$$Q = \left(\frac{\partial\Phi}{\partial x} \right)^2 + \left(\frac{\partial\Phi}{\partial y} \right)^2. \quad (\text{B.41})$$

In this case, $Q = 0$ cannot be satisfied by any real function except for the trivial solution. As a consequence, no real characteristic directions exist. Laplace's equation therefore is elliptic.

Heat Conduction Equation – A Parabolic PDE

The heat conduction equation

$$\frac{\partial u}{\partial t} = \alpha \frac{\partial^2 u}{\partial x^2} \quad \text{for} \quad \alpha > 0 \quad (\text{B.42})$$

can be rewritten into a first-order system using $v = \partial u/\partial x$:

$$\frac{\partial u}{\partial t} - \alpha \frac{\partial v}{\partial x} = 0 \quad \text{and} \quad \frac{\partial u}{\partial x} = 0. \quad (\text{B.43})$$

In matrix form we get

$$\begin{pmatrix} 1 & 0 \\ 0 & 0 \end{pmatrix} \frac{\partial}{\partial t} \begin{pmatrix} u \\ v \end{pmatrix} + \begin{pmatrix} 0 & -\alpha \\ 1 & 0 \end{pmatrix} \frac{\partial}{\partial x} \begin{pmatrix} u \\ v \end{pmatrix} = \begin{pmatrix} 0 \\ 0 \end{pmatrix}. \quad (\text{B.44})$$

The characteristic matrix is

$$\mathbf{A} = \begin{pmatrix} \partial\Phi/\partial t & -\alpha \partial\Phi/\partial x \\ \partial\Phi/\partial x & 0 \end{pmatrix}. \quad (\text{B.45})$$

The characteristic form $Q = |\mathbf{A}| = -\alpha(\partial\Phi/\partial x)^2$ is degenerated because it does not contain the derivative $\partial\Phi/\partial t$. $Q = 0$ requires $\partial\Phi/\partial x = 0$; $\partial\Phi/\partial t$ is arbitrarily chosen to be 1, which is a double root. The characteristics then are straight lines $t = \text{const}$ and only one compatibility relation can be obtained. The slope of the characteristic is $(dx/dt)_C = \pm\infty$: the speed of propagation is infinite in both directions along the x -axis.

The heat conduction equation is parabolic.

B.2.3 Summary 2D

The most general form of a 2D PDE is

$$a_1(x, y) \frac{\partial^2 u}{\partial x^2} + a_2(x, y) \frac{\partial^2 u}{\partial x \partial y} + a_3(x, y) \frac{\partial^2 u}{\partial y^2} + a_4(x, y) \frac{\partial u}{\partial x} + a_5(x, y) \frac{\partial u}{\partial y} + f(x, y, u) = 0. \quad (\text{B.46})$$

The type of the PDE depends on the coefficients in front of the derivatives of highest order, in this case on a_1 , a_2 and a_3 . The classification then is

$$\begin{vmatrix} a_1 & a_2/2 \\ a_2/2 & a_3 \end{vmatrix} = \begin{cases} > 0 & \text{elliptic (positive definit)} \\ = 0 & \text{parabolic (positive definit but not definit)} \\ < 0 & \text{hyperbolic (indefinit)} \end{cases} \quad (\text{B.47})$$

Note that the type of the PDE depends on (x, y) . Consequently, also mixed types of PDEs are possible. For instance, the Euler–Tricomi equation

$$\frac{\partial^2}{\partial x^2} = x \frac{\partial^2}{\partial y^2}$$

is an elliptic–hyperbolic PDE because it is elliptic in the region $x < 0$, hyperbolic in the region $x > 0$ and degenerate parabolic on the line $x = 0$.

B.3 Laplace Transformation

The Laplace transformation, or Laplace transform for short, is one example of an integral transform. Another example is the Fourier transform.

B.3.1 Integral Transforms

In an integral transform a function $F(t)$ is multiplied by a kernel $K(s, t)$ and integrated between the limits a and b :

$$\mathfrak{T}\{F(t)\} = \int_a^b F(t) K(s, t) dt = f(s). \quad (\text{B.48})$$

The Kernel K and the integration limits (a, b) define the type \mathcal{T} of transformation. For a *Laplace transform* the kernel is e^{-st} (with $s \in \mathbb{C}$) and the integration interval is $(0, \infty)$:²

$$\mathcal{L}\{F(t)\} = \int_0^\infty F(t) e^{-st} dt = f(s). \quad (\text{B.49})$$

The inverse transform is written as

$$\mathcal{L}^{-1}\{f(s)\} = F(t). \quad (\text{B.50})$$

The function $F(t)$ to be transformed can be any function, derivative of a function or even an integral. The Laplace transforms for some important functions are listed in table B.2.

The Laplace transform is used to solve ODEs. If an ODE is transformed, each term of the ODE is transformed. The transformed differential equation then is a simple algebraic equation in s -space and can be solved easily. Note that the variables t and s are corresponding variables, for instance spatial coordinate and momentum or time and energy/frequency. The advantages of a Laplace transform over the methods discussed in Sect. B.1 are the following:

- an inhomogeneous ODE can be solved directly without first solving the homogeneous part of the ODE.
- a wide range of inhomogeneities can be handled without recourse to particular integrals.
- even discontinuous inhomogeneities, such as described by a δ or Heavyside function, can be solved.
- the initial conditions are automatically incorporated into the solution.

²For comparison, the Fourier transform has the kernel $e^{i\omega t}$ and the integration interval $-\infty$ to $+\infty$.

$F(t)$	$f(s)$	Table B.2: Laplace transforms for some important functions
1	s^{-1}	
t	s^{-2}	
e^{-at}	$(s+a)^{-1}$	
t^n	$n!/s^{n+1}$	
$\sin(kt)$	$k/(s^2+k^2)$	
$t^n e^{-at}$	$n!/(s+a)^{n+1}$	
$\cos(kt)$	$s/(s^2+k^2)$	
$\sinh(kt)$	$k/(s^2-k^2)$	
$e^{-at} \cos(kt)$	$[s+a]/[(s+a)^2+k^2]$	
$\cosh(kt)$	$s/(s^2-k^2)$	
$e^{-at} \sin(kt)$	$k/[(s+a)^2+k^2]$	

B.3.2 Properties of the Laplace Transform

The general properties of a Laplace transform can be summarized as:

1. Definition of the Laplace transform:

$$F(t) \quad \rightarrow \quad \int_0^{\infty} F(t) e^{-st} dt . \quad (\text{B.51})$$

2. Inverse transform:

$$\frac{1}{2\pi i} \lim_{\beta \rightarrow 0} \int_{\gamma-i\beta}^{\gamma+i\beta} e^{tz} f(z) dz \quad \rightarrow \quad f(s) . \quad (\text{B.52})$$

3. Transform of a constant:

$$C \quad \rightarrow \quad C/s . \quad (\text{B.53})$$

4. Transform of a sum:

$$a F(t) + b G(t) \quad \rightarrow \quad a f(s) + b g(s) . \quad (\text{B.54})$$

5. Transform of a derivative:

$$\begin{aligned} F'(t) &\rightarrow s f(s) - F(0) \\ F''(t) &\rightarrow s^2 f(s) - s F(0) - F'(0) \\ F^{(n)}(t) &\rightarrow s^n f(s) - s^{n-1} F(0) - s^{n-2} F'(0) \dots F^{(n-1)}(0) . \end{aligned} \quad (\text{B.55})$$

6. Transform of an integral:

$$\int_0^t F(t) dt \quad \rightarrow \quad \frac{f(s)}{s} . \quad (\text{B.56})$$

7. Convolution theorem (inverse of a product):

$$\int_0^t F(\tau) G(t-\tau) d\tau = F(t) * G(t) \quad \rightarrow \quad f(s) g(s) . \quad (\text{B.57})$$

8. Heavyside expansion (inverse of a ratio of polynomials):

$$\sum_{n=1}^{\infty} \frac{(s-a_n)p(a_n)}{q(a_n)} e^{a_n t} = \sum_{n=1}^{\infty} \frac{p(a_n)}{q'(a_n)} e^{a_n t} \quad \rightarrow \quad \frac{p(s)}{q(s)} \quad (\text{B.58})$$

with order of $p(s) < q(s)$ and a_n being the roots of $q(s)$.

9. Inverse of derivatives:

$$\begin{aligned} -t F(t) &\rightarrow f'(s) \\ (-1)^n t^n F(t) &\rightarrow f^{(n)}(s). \end{aligned} \quad (\text{B.59})$$

10. Inverse of an integral:

$$\frac{F(t)}{t} \rightarrow \int_s^\infty f(x) dx. \quad (\text{B.60})$$

11. Translation (shifting properties):

$$e^{at} F(t) \rightarrow f(s - a) \quad (\text{B.61})$$

and

$$\begin{cases} f(t - a) & t > a \\ 0 & t < a \end{cases} \rightarrow e^{-as} f(s). \quad (\text{B.62})$$

12. Initial value theorem:

$$F(0) \rightarrow \lim_{s \rightarrow \infty} s f(s). \quad (\text{B.63})$$

13. Final value theorem:

$$\lim_{t \rightarrow \infty} F(t) \rightarrow \lim_{s \rightarrow 0} s f(s). \quad (\text{B.64})$$

The harmonic oscillator with external forcing is a typical example for an inhomogeneous 2nd order ODE. With an arbitrary forcing $F(t)$ the equation of motion is

$$\ddot{x} + \omega_0^2 x = F(t)/m \quad (\text{B.65})$$

with $\omega_0 = \sqrt{k/m}$ and the initial conditions $v(0) = v_0$ and $x(0) = x_0$. Its Laplace transform is

$$s^2 x(s) - s x_0 - v_0 + \omega_0^2 x(s) = f(s)/m \quad (\text{B.66})$$

with the solution

$$x(s) = \frac{x_0 s + v_0}{s^2 + \omega_0^2} + \frac{f(s)}{m} \frac{1}{s^2 + \omega_0^2}. \quad (\text{B.67})$$

Inversion yield the solution

$$x(t) = x_0 \cos(\omega_0 t) + \frac{v_0}{\omega_0} \sin(\omega_0 t) + \frac{1}{m \omega_0} \int_0^t \sin(\omega_0 t) F(t - \tau) d\tau. \quad (\text{B.68})$$

The first two terms on the right are the well-known general solution for the harmonic oscillator without external forcing. The last term contains the modification of this solution due to the existence of an arbitrary external forcing $F(t)$.

If the forcing function is $F(t) = F_0 \sin(\omega t)$, B.66 can be written as

$$s^2 x(s) - s x_0 - v_0 + \omega_0^2 x(s) = \frac{F_0}{m} \frac{\omega}{s^2 + \omega^2}. \quad (\text{B.69})$$

Its solution is

$$x(s) = \frac{x_0 s + v_0}{s^2 + \omega_0^2} + \frac{F_0}{m} \frac{\omega}{(s^2 + \omega_0^2)(s^2 + \omega^2)}. \quad (\text{B.70})$$

The inverse transform of the first term on the right is the same as used in (B.67), the second term yields to a Heavyside expansion:

$$x(t) = x_0 \cos(\omega_0 t) + \frac{1}{\omega_0} \left[v_0 + \frac{F_0 \omega}{m(\omega^2 - \omega_0^2)} \right] \sin(\omega_0 t) - \frac{F_0}{m(\omega^2 - \omega_0^2)} \sin(\omega t). \quad (\text{B.71})$$

A singularity (resonance) arises for $\omega = \omega_0$.

Exercises

Aufgabe 15 Solve the equation of motion

$$\ddot{x} + \gamma\dot{x} + \omega_0^2 x = F(t)/m$$

of an harmonic oscillator with damping and external forcing using a Laplace transform. Use the above example as guideline.

Appendix C

A Little Remainder on Some Physics Basics

C.1 Some Fundamental Laws

Table C.1 lists some of the fundamental laws in physics together with some auxiliary relations.

The most fundamental laws are the conservation of mass, momentum and energy. Conservation laws can be written in different forms. To understand the idea, consider a volume element. Any change of a property ε inside this volume is due to sources or sinks $S(\varepsilon)$ and the convergence $\vec{C}(\varepsilon)$ of the flow of mass across the volume's boundary:

$$\frac{\partial \varepsilon}{\partial t} + \nabla \cdot \vec{C}(\varepsilon) = S(\varepsilon). \quad (\text{C.1})$$

The flow density \vec{j} of the flow across the boundary is the product of the density ρ_ε and the flow speed \vec{v} : $\vec{j} = \rho_\varepsilon \vec{v}$:

$$\frac{\partial \rho_\varepsilon}{\partial t} - \nabla \cdot (\rho_\varepsilon \vec{v}) = S \quad \text{or for } S = 0: \quad \frac{\partial \rho_\varepsilon}{\partial t} = -\nabla \cdot (\rho_\varepsilon \vec{v}) = -\nabla \cdot \vec{j}. \quad (\text{C.2})$$

Mass conservation is a special case of the latter equation: at least on the macroscopic level, mass has no sources and sinks. With ρ as mass density and under consideration of relation (2.30) between partial and total derivative, mass conservation can be written as

$$\frac{d\rho}{dt} = \frac{\partial \rho}{\partial t} + \vec{v} \cdot \nabla \rho = -\rho \nabla \cdot \vec{v}, \quad (\text{C.3})$$

Integration and consideration of Gauss' law (A.21) leads to the integral form

$$\frac{\partial}{\partial t} \int_{\mathcal{V}} \rho \, dV = - \oint_{\mathcal{O}(\mathcal{V})} \vec{j} \cdot d\vec{A}. \quad (\text{C.4})$$

If we use the charge density ρ_e instead of the mass density ρ , these equation give the conservation of charge which can also be written as Kirchoff's 1st law: for a node in an electrical circuit, the sum of currents into and out of it must be zero.

Energy conservation can be described with the same formalism, replacing the mass density ρ by the energy density ε :

$$\frac{d\varepsilon}{dt} = \frac{\partial \varepsilon}{\partial t} + \vec{v} \cdot \nabla \varepsilon = -\varepsilon \nabla \cdot \vec{v}, \quad (\text{C.5})$$

and in integral form

$$\frac{\partial}{\partial t} \int_{\mathcal{V}} \varepsilon \, dV = - \oint_{\mathcal{O}(\mathcal{V})} \vec{j} \cdot d\vec{A}. \quad (\text{C.6})$$

		Table C.1: Some fundamental laws of physics
conservation of mass (eq. of continuity)	$\frac{d\rho}{dt} = \frac{\partial \rho}{\partial t} + \vec{v} \cdot \nabla \rho = -\rho \nabla \vec{v}$	
conservation of energy	$\frac{d\varepsilon}{dt} = \frac{\partial \varepsilon}{\partial t} + \vec{v} \cdot \nabla \varepsilon = -\varepsilon \nabla \vec{v}$	
Newton's law (conservation momentum)	$\vec{F} = m \frac{d\vec{v}}{dt} = \frac{dp}{dt}$	
Universal gravitation	$\vec{F} = \gamma \frac{m_1 m_2}{r^2} \vec{e}_r$	
Ohm's law	$u = \frac{i}{R}$	
Kirchhoff's law 1 (conservation charge)	$(\sum i)_{\text{junction}} = 0$	
Kirchhoff's law 2 (conservation energy)	$(\sum u)_{\text{loop}} = 0$	
Coulomb's law	$\vec{F} = \frac{1}{4\pi\varepsilon_0} \frac{q_1 q_2}{r^2} \vec{e}_r$	
Fick's law	$N = -DA \frac{dc}{dx}$	
Fourier's law	$q = -kA \frac{dT}{dx}$	
Newton's law of cooling	$\frac{d}{dt} \Delta T = -K \Delta T$	
Newton's viscosity law	$\tau = -\mu \frac{dv}{dx}$	
Chemical reaction rate, 1 st order	$r = k_r C$	
Chemical reaction rate, 2 nd order	$r = K_R C^2$ or $r = k_r C_A C_B$	
Chem. reaction rate, Michaelis–Menton	$r = \frac{r_{\max} S}{k_m + S}$	
Interphase transport, mass	$N = k_c A \Delta C$	
Interphase transport, heat	$q = h A \Delta T$	
frictional pressure drop in a pipe	$\Delta p_f = 4f_p \frac{v^2}{2} \frac{L}{d}$	
drag in flow around a body	$F_D = c_D \rho A_c \frac{v^2}{2}$	
thermal enthalpy change	$\Delta H = c_p \Delta T$	
enthalpy of reaction	$H_{\text{products}} - H_{\text{reactants}}$	
enthalpy of vaporization	$H_{\text{vapor}} - H_{\text{liquid}}$	
enthalpy of solidification	$H_{\text{liquid}} - H_{\text{solid}}$	

Special cases are the conservation of mechanical energy or the conservation of thermal energy. Also related to the conservation of energy is Kirchhoff's 2nd law, which states that the sum of the voltage drops u in a closed loop in an electric circuit is zero. This can be interpreted as a special form of the conservation of potential energy. The mathematical expression for some energy forms is given in Tab. C.2.

Newton's 2nd law gives the equation of motion or momentum balance, that is the change in momentum (or the acceleration) as a function of the acting forces. It leads to the *conservation of momentum*

$$\sum \vec{p} = 0, \quad (\text{C.7})$$

the *conservation of angular momentum*

$$\sum I\omega = 0 \quad (\text{C.8})$$

ε_{pot}	$= \rho gh$	potential energy density
ε_{kin}	$= \frac{1}{2} \rho u^2$	kinetic energy density
$\varepsilon_{\vec{B}}$	$= \frac{1}{2\mu_0} B^2$	energy density in the magnetic field
$\varepsilon_{\vec{E}}$	$= \frac{1}{2} \varepsilon_0 E^2$	energy density in the magnetic field

Table C.2: Mathematical expressions for different forms of energy

and to the *conservation of moment*

$$\sum \vec{r} \times \vec{F} = 0. \quad (\text{C.9})$$

The remaining laws in table C.1, although fundamental, are not concerned with conservations. Two laws are important for the interaction between bodies: Newton's universal law of gravitation gives the gravitational force between two masses m_1 and m_2 separated by a distance r . Its direct counterpart in the realm of charged particles is Coulomb's law which gives the force between two charges q_1 and q_2 separated by r .

Fick's law and *Fourier's law* are transport equations related to diffusive processes. They give the rate of flux of mass N (mol/s) and thermal energy q (J/s). In both laws the driving force is a gradient (in concentration C or in temperature T), which, together with a coefficient D or k , can be interpreted as a kind of conductivity or the reciprocal of a resistance to transport. Mathematically, both laws are equivalent. They are even equivalent in the sense that the essence of the underlying physical process is described by the same law. The details of the process and the physical quantities, however, are different.

C.2 Distributions and Phase Space Density

Transport processes deal with bulk transport. Thus we do not transport individual bodies of mass m but volume elements with density ρ . But density inside a volume element might change. And although the volume element moves at speed \vec{u} into one direction, owing to the thermal motion none of the particles inside the volume element might move at that speed. For a formal description, we therefore have to agree on some terms such as phase space density and velocity distribution.

C.2.1 Phase space density

When we are concerned with the transport of matter, we are aware of the fact that matter is composed of smaller units. In a gas or liquid the smallest units relevant to transport are the atoms or molecules. To extend our discussion later to other media, we can also use the more general term particles.

Kinetic theory starts from the physics of individual particles (the microscopic approach). The macroscopic phenomena then can be described by averaging over a sufficiently large number of particles, an approach which also is used in statistical mechanics.

Phase Space and Distribution Function

The mechanical properties of each particle are described completely by its position and momentum. The *phase space* is a six-dimensional space defined by the three spatial coordinates q_1, q_2, q_3 and the three generalized momenta p_1, p_2, p_3 . Each particle is related unambiguously to one *point* in phase space:

$$\vec{Q} = (q_1, q_2, q_3; p_1, p_2, p_3) = (\vec{q}, \vec{p}). \quad (\text{C.10})$$

The *speed* of the particle in phase space, i.e. the combined change in its position and momentum in ordinary three-dimensional space, then is

$$\vec{C} = \frac{d\vec{Q}}{dt} = \left(\frac{dq_1}{dt}, \frac{dq_2}{dt}, \frac{dq_3}{dt}; \frac{dp_1}{dt}, \frac{dp_2}{dt}, \frac{dp_3}{dt} \right) = \left(\frac{d\vec{q}}{dt}, \frac{d\vec{p}}{dt} \right). \quad (\text{C.11})$$

A particle ensemble of N particles thus occupies N such points in phase space. The number N_{V_i} of particles inside the phase space volume V_i can be used to define a *phase space density* $f(\vec{q}, \vec{p}, t)$ that gives the number of particles inside a volume element $V_i = [(q_i, q_i + dq_i), (p_i, p_i + dp_i)]$. This density function also is called a *distribution function*.

C.2.2 Averaging

The ordinary particle density in 3D space can be obtained from the phase space density by integration over the generalized momenta:

$$n(\vec{q}, t) = \int_{-\infty}^{+\infty} f(\vec{q}, \vec{p}, t) d^3\vec{p}. \quad (\text{C.12})$$

The *number density* is used in the definition of averages. These describe the macroscopic properties of the particle ensemble. If $a(\vec{q}, \vec{p}, t)$ is a function in phase space, its average is defined as

$$\langle a(\vec{q}, t) \rangle = \frac{1}{n(\vec{q}, t)} \int_{-\infty}^{\infty} a(\vec{q}, \vec{p}, t) f(\vec{q}, \vec{p}, t) d^3\vec{p}. \quad (\text{C.13})$$

The average or bulk speed of the particle ensemble, for instance, is given as

$$\vec{u}(\vec{q}, t) = \langle \vec{v}(\vec{q}, t) \rangle = \frac{1}{n(\vec{q}, t)} \int_{-\infty}^{\infty} \vec{v}(\vec{p}, \vec{q}, t) f(\vec{q}, \vec{p}, t) d^3\vec{p}. \quad (\text{C.14})$$

Application of this averaging scheme to the equation of motion yields the fundamental equations for the description of the particle ensemble. A prominent example is the *Vlasov equation* which provides a statistical description of a plasma.

C.2.3 Maxwell's Velocity Distribution

The average speed $\langle \vec{v} \rangle$ of the particles in the ensemble is defined by (C.14). This speed is also the flow speed \vec{u} of the gas or fluid. The speeds \vec{v}_i of individual particles, however, can be substantially different; in particular, in a hot gas, such as a plasma, speeds of individual particles can exceed the flow speed by orders of magnitude. In addition, a particle ensemble might contain different particle species s which all have their own average speed \vec{u}_s .

To derive the velocity distribution of the particles, let us first determine the kinetic energy contained in a volume element. The kinetic energy of the flow is determined by the average speed \vec{u} , while the entire kinetic energy is the sum of the kinetic energies of all particles. Since the latter always is larger, there is also kinetic energy contained in the stochastic motion of the particles, which can be described by

$$\left\langle \frac{m}{2} (\vec{v} - \vec{u})^2 \right\rangle = \frac{\int m(\vec{v} - \vec{u})^2 f(\vec{r}, \vec{v}, t) d\vec{v}}{2 \int f(\vec{r}, \vec{v}, t) d\vec{v}}. \quad (\text{C.15})$$

This *random kinetic energy* is related to the hydrostatic pressure by

$$\frac{p}{n} = \frac{2}{N} \left\langle \frac{m}{2} (\vec{v} - \vec{u}_s)^2 \right\rangle, \quad (\text{C.16})$$

where N is the number of degrees of freedom, normally three.

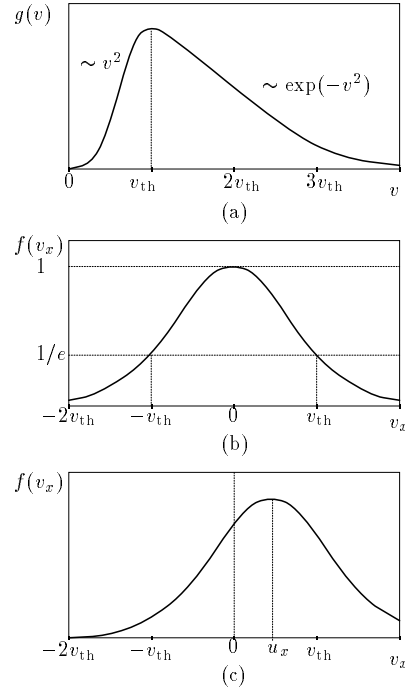
If the system is in thermal equilibrium, the velocity distribution is given by the Maxwell distribution:

$$f(\vec{r}, \vec{v}, t) = n \sqrt{\left(\frac{m}{2\pi k_B T} \right)^3} \exp \left\{ -\frac{m(\vec{v} - \vec{u})^2}{2k_B T} \right\} \quad (\text{C.17})$$

where T is the temperature and k_B is the Boltzmann constant. According to (C.17), the relative number of particles with large stochastic speeds $|\vec{v} - \vec{u}|$ increases with T . The distribution's maximum is at the most probable thermal speed v_{th} :

$$v_{\text{th}} = \sqrt{\frac{2k_B T}{m}}. \quad (\text{C.18})$$

Figure C.1: Maxwell distribution. (a) Distribution $g(\vec{v}, r)$ for the particle speeds in a plasma at rest. (b) Maxwell distribution of one velocity component for a plasma at rest, the other velocity components have been removed by integration. (c) Same as above but for a plasma moving with average speed u_x in the x -direction. Note that an increase in temperature would not affect the position of the maximum in (b) and (c) but would shift the maximum towards the right in (a), combined with an increase of the maximum



In a one-atomic gas in equilibrium, the temperature is related to the kinetic energy of the stochastic motion by

$$\left\langle \frac{1}{2} m (\vec{v} - \vec{u})^2 \right\rangle = \frac{1}{2} N k_B T. \quad (\text{C.19})$$

Note that the combination of (C.16) and (C.19) yields the ideal gas law $p = nk_B T$.

Occasionally, we are concerned only with particle speeds and not with the direction of motion. This might be the case if the particle ensemble is at rest, i.e. \vec{u} equals zero. The distribution function (C.17) then is

$$\iint f(\vec{r}, \vec{v}, t) d\Omega_v v^2 dv = (4\pi f(\vec{r}, |v|, t) v^2) dv = g(\vec{r}, v) dv \quad (\text{C.20})$$

where Ω is the solid angle. Equation (C.20) gives the number of particles inside a volume element with speeds between v and $v + dv$. The function $g(\vec{r}, v)$ gives the number of particles per velocity unit, again with speeds between v and $v + dv$. For small speeds, this function increases with the square of v while for large speeds it decreases exponentially (see upper panel in Fig. C.1). If not the speed, but only one component of the velocity is considered, the distribution is symmetric around zero if the ensemble is at rest (middle) or symmetric around the flow speed in that particular direction if the ensemble is in motion (lower panel).

Reminder: the Maxwell–Boltzmann distribution requires a thermal equilibrium. If this is not the case, it can not be applied to the description of a particle population. For most terrestrial examples given in this script, the assumption of thermal equilibrium is valid. Occasionally, we will also use space plasmas or energetic particles in space as examples. The plasmas often can be described as Maxwellian or bi-Maxwellian, too, while the energetic particle population often can be described as an exponential tail on the Maxwellian. Such a distribution is called kappa-distribution or Lorentz distribution.

C.2.4 Distribution Function and Measured Quantities

While the distribution function is important for our theoretical treatment of the particle ensemble, it is a quantity which cannot be measured directly. Instead, observations give

the *differential flux* $J(E, \vec{\Omega}, \vec{r}, t)$ of particles within a solid angle $d\vec{\Omega}$ and an energy interval $(E, E + dE)$. Thus the quantity

$$J(E, \vec{\Omega}, \vec{r}, t) d\vec{A} d\vec{\Omega} dt dE$$

is the number of particles in the energy band from E to $E + dE$ coming from the direction $\vec{\Omega}$ within a solid angle $d\vec{\Omega}$, going through a surface $d\vec{A}$ perpendicular to $d\vec{\Omega}$ during the time interval dt . The differential flux therefore can be measured in units of particles per $(\text{m}^2 \text{ sr s MeV})$. Since J depends on $\vec{\Omega}$, it can also be interpreted as the angular distribution of the particles. The *omnidirectional intensity* can be obtained from the differential flux by averaging over all directions:

$$J_{\text{omni}}(E, \vec{r}, t) = \frac{1}{4\pi} \int J(E, \vec{\Omega}, \vec{r}, t) d\vec{\Omega} . \quad (\text{C.21})$$

The number density of particles with velocity v in a phase space element is given as $dn = f v^2 d\vec{v} d\vec{\Omega}$. Multiplication by v gives the differential flux of particles with velocity v as $f(\vec{v}, \vec{p}, t) v^3 d\vec{v} d\vec{\Omega}$. Comparison with the same quantity expressed by the differential flux yields

$$J(E, \vec{\Omega}, \vec{r}, t) dE d\vec{\Omega} = f(\vec{r}, \vec{p}, t) v^3 dv d\vec{\Omega} . \quad (\text{C.22})$$

Since the energy is related to speed, dE is related to dv by $dE = mvdv$. The relation between the differential flux and the distribution function therefore can be written as

$$J(E, \vec{\Omega}, \vec{r}, t) = \frac{v^2}{m} f(\vec{r}, \vec{p}, t) . \quad (\text{C.23})$$

C.3 Fundamental Transport Equations in Phase Space

The basic equations that describe the evolution of the particle ensembles can be derived from the equation of motion for the individual particle and application of the averaging scheme C.13. The Boltzmann equation is the fundamental equation of motion in statistic theory, the Fokker–Planck equation is most suitable when scattering is concerned. Thus we will meet this latter one frequently during the script.

C.3.1 Boltzmann equation

The Boltzmann equation is the fundamental equation of motion in phase space. The only assumption inherent in the Boltzmann equation is that only external forces \vec{F} act on the particles while internal forces vanish: there are no collisions between the particles.

The Boltzmann equation is a direct consequences of the equation of continuity in phase space:

$$\frac{\partial f}{\partial t} + \nabla_6 \cdot (f\vec{C}) = 0 \quad (\text{C.24})$$

which also can be written as

$$\frac{\partial f}{\partial t} + \nabla_{\vec{r}} \cdot (\vec{v}f) + \nabla_{\vec{v}} \cdot (\vec{a}f) = 0 , \quad (\text{C.25})$$

where ∇_6 , $\nabla_{\vec{r}}$, and $\nabla_{\vec{v}}$ are the divergence in phase space, in ordinary space, and in momentum space, respectively, and \vec{v} and \vec{a} are velocity and acceleration. In phase space, \vec{r} and \vec{v} are independent variables. If we further assume that the acceleration \vec{a} , and therefore also the force \vec{F} , is independent of \vec{v} , (C.25) can be simplified:

$$\frac{\partial f}{\partial t} + \vec{v} \cdot \nabla_{\vec{r}} f + \vec{a} \cdot \nabla_{\vec{v}} f = 0 \quad (\text{C.26})$$

or

$$\frac{\partial f}{\partial t} + \vec{v} \cdot \nabla f + \frac{\vec{F}}{m} \cdot \frac{\partial f}{\partial \vec{v}} = 0 . \quad (\text{C.27})$$

Equation (C.27) is called the collisionless Boltzmann equation. It also can be written as

$$\frac{df}{dt} = 0, \quad (\text{C.28})$$

which states that the convective derivative of the phase space density is always zero for a collisionless assembly of particles. Thus for an observer moving with the flow, the phase space density is constant. Or, in other words: the substrate of points in phase space behaves like an incompressible fluid. This is also called *Liouville's theorem*.

The general form of the Boltzmann equation can be written as

$$\frac{\partial f}{\partial t} + \vec{v} \cdot \nabla f + \frac{\vec{F}}{m} \cdot \frac{\partial f}{\partial \vec{v}} = \left(\frac{\partial f}{\partial t} \right)_{\text{coll}}, \quad (\text{C.29})$$

where the term on the right-hand side is the rate of change in phase space density due to collisions (see below).

If changes in f due to collisions are small, e.g. in the case of a thermodynamic equilibrium, the *reduced Boltzmann equation* can be written as

$$\left(\frac{\partial f}{\partial t} \right)_{\text{coll}} = 0. \quad (\text{C.30})$$

The solution of this equation is the Maxwell distribution.

C.3.2 Fokker–Planck equation

The Fokker–Planck equation considers the short-range, local interactions between particles. In a plasma, collisions arise from many small Coulomb interactions between charged particles. The collision term has its mechanical analogy in the Brownian motion of particles in a gas; however, both are not equivalent as will be discussed below.

Collisions are not a deterministic but a stochastic process. Thus for a given particle, although we might know its momentary position and velocity, we cannot determine its future motion. Only for an assembly of particles the collective behavior can be determined. This can be done by means of probabilities. Let $\psi(\vec{v}, \Delta\vec{v})$ be the probability that a particle with velocity \vec{v} after many small collisions during a time interval dt has changed its velocity to $\vec{v} + \Delta\vec{v}$. The phase space density $f(\vec{r}, \vec{v}, t)$ also is a probability function. At a time t it can be written as the product of the phase space density at an earlier time $t - \Delta t$ multiplied by the probability of changes during this time interval and integrated over all possible velocity changes $\Delta\vec{v}$:

$$f(\vec{r}, \vec{v}, t) = \int f(\vec{r}, \vec{v} - \Delta\vec{v}, t - \Delta t) \psi(\vec{v} - \Delta\vec{v}, \Delta\vec{v}) d(\Delta\vec{v}). \quad (\text{C.31})$$

Since we only consider scattering by small angles, i.e. $|\Delta\vec{v}| \ll |\vec{v}|$, Taylor expansion to second order of the product $f\psi$ yields

$$\begin{aligned} f(\vec{r}, \vec{v}, t) &= \int \left[f(\vec{r}, \vec{v}, t - \Delta t) \psi(\vec{v}, \Delta\vec{v}) - \Delta\vec{v} \cdot \frac{\partial(f\psi)}{\partial \vec{v}} \right] d(\Delta\vec{v}) \\ &+ \int \left[\frac{\Delta\vec{v}\Delta\vec{v}}{2} \odot \frac{\partial^2(f\psi)}{\partial \vec{v}\partial \vec{v}} \right] d(\Delta\vec{v}). \end{aligned} \quad (\text{C.32})$$

Note that the \odot in the last term indicates a product between two tensors.¹ The resulting matrix is the Hess matrix.

Because some interactions always take place, the probability can be normalized: $\int \psi d(\Delta\vec{v}) = 1$. Equation (C.32) then can be simplified to

$$f(\vec{r}, \vec{v}, t) = f(\vec{r}, \vec{v}, t - \Delta t) - \frac{\partial(f\langle\Delta\vec{v}\rangle)}{\partial \vec{v}} + \frac{1}{2} \frac{\partial}{\partial \vec{v}\partial \vec{v}} \odot (f\langle\Delta\vec{v}\Delta\vec{v}\rangle), \quad (\text{C.33})$$

¹The product $\mathbf{S} \odot \mathbf{T}$ of two tensors \mathbf{S} and \mathbf{T} itself is a tensor and can be obtained by application of the rules of matrix multiplication.

with

$$\langle \Delta \vec{v} \rangle = \int \psi \Delta \vec{v} d(\Delta \vec{v}) \quad \text{and} \quad \langle \Delta \vec{v} \Delta \vec{v} \rangle = \int \psi \Delta \vec{v} \Delta \vec{v} d(\Delta \vec{v}). \quad (\text{C.34})$$

By definition, the collision term as written down in (C.29) is

$$\left(\frac{\partial f}{\partial t} \right)_{\text{coll}} = \frac{f(\vec{r}, \vec{v}, t) - f(\vec{r}, \vec{v}, t - \Delta t)}{\Delta t}. \quad (\text{C.35})$$

Thus the Fokker–Planck equation can be written as

$$\left(\frac{\partial f}{\partial t} \right)_{\text{coll}} \Delta t = -\frac{\partial}{\partial \vec{v}} \cdot (f \langle \Delta \vec{v} \rangle) + \frac{1}{2} \frac{\partial^2}{\partial \vec{v} \partial \vec{v}} \odot (f \langle \Delta \vec{v} \Delta \vec{v} \rangle). \quad (\text{C.36})$$

The first term on the right basically contains $\langle \Delta \vec{v} \rangle / \Delta t$, which is an acceleration. Thus the term describes the frictional forces leading to an acceleration of the slower and a deceleration of the faster particles, which tends to equalize the speeds. The negative divergence in velocity space describes this narrowing of the distribution function. The second term, $\langle \Delta \vec{v} \Delta \vec{v} \rangle / \Delta t$, is a diffusion in velocity space. This term describes the broadening of a narrow velocity distribution, e.g. a beam, as a result of the collisions. The two terms therefore operate in the opposite sense. They are in balance in an equilibrium distribution, e.g. the Maxwell distribution. The physics of the collision processes is contained in the probability function ψ .

Equation (C.36) also can be written as

$$\left(\frac{\partial f}{\partial t} \right)_{\text{coll}} \Delta t = -\nabla_{\vec{v}} \cdot (\mathbf{D} \cdot \nabla_{\vec{v}} \cdot f) \quad (\text{C.37})$$

with the diffusion tensor \mathbf{D} derived from the first- and second-order fluctuations of the particle velocity.

C.3.3 Vlasov equation

The Vlasov equation is the basic equation in the kinetic theory of a plasma.

The Vlasov equation is the application of the Boltzmann equation to a plasma on which only electromagnetic forces act. These forces are described by the Lorentz force

$$\ddot{\vec{r}} = \frac{q}{m} \left(\vec{E} + \vec{v} \times \vec{B} \right). \quad (\text{C.38})$$

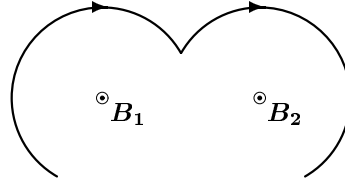
In the derivation of (C.27) we have made the assumption of a force independent on \vec{v} . At first glance, the Lorentz force violates this assumption and therefore should not be considered in (C.27). Closer inspection, however, shows that this is not true. Since the Lorentz force contains the cross product of speed and magnetic field, the resulting force is perpendicular to the speed. Thus each individual component of the force does not depend on the same component of the velocity. Since in (C.25) a scalar product is considered, the only derivatives of \vec{a} are of the form $\partial a_x / \partial v_x$ and therefore vanish. Thus the Lorentz force can be inserted into (C.27):

$$\frac{\partial f}{\partial t} + \vec{v} \cdot \nabla f + \frac{q}{m} \left(\vec{E} + \frac{\vec{v} \times \vec{B}}{c} \right) \cdot \frac{\partial f}{\partial \vec{v}} = 0. \quad (\text{C.39})$$

Equation (C.39) is called the Vlasov equation. Because of its simplicity, this is the equation most commonly studied in kinetic theory.

The Vlasov equation is derived under the assumption of non-interacting particles. On the other hand, interactions are the very essence of a plasma. Thus we have to discuss whether the Vlasov equation can be applied as often as it is. As we shall see, the Vlasov equation is a valid approach. It does not consider collisions in the sense of short-range, local interactions, such as collisions between two billiard balls or Coulomb collisions between two charged particles. Nonetheless, that kind of interaction, which is essential in a plasma, is

Figure C.2: Collisions in a plasma can shift the gyro-center of a particle onto another field line, here illustrated for a collision of a charged particle with a neutral one



considered: each particle moves in the average Coulomb field created by thousands of other particles. Thus the fields in the Vlasov equation are due to the rest of the plasma and describe the interaction of the particles. These fields often are called self-consistent fields. External fields can be included in (C.39), too. Since the fields \vec{E} and \vec{B} are determined by the rest of the plasma, they depend on the distribution function f .

The Vlasov equation thus is non-linear; analytical solutions in general are not possible. But Jeans' theorem identifies some solutions. It states: any function of the constants of motion is a solution of the Vlasov equation. For instance, if there are no electric fields, the kinetic energy is a constant of motion. Thus any function of $mv^2/2$ is a solution of the Vlasov equation. In particular, the Maxwell distribution (C.17) is a solution.

Jeans' theorem therefore shows the equivalence of kinetic theory and orbit theory. Following an approach given by Boyd and Sanderson [18], this equivalence can be shown easily. The basic equation of orbit theory is Newton's second law $\vec{F} = m d^2 \vec{r} / dt$. This is a second-order differential equation in three dimensions and therefore the general solution must contain six constants of integration, $\gamma_1, \dots, \gamma_6$. Thus the solutions of Newton's second law can be written as $\vec{r} = \vec{r}(\gamma_1, \dots, \gamma_6, t)$ and $\vec{v} = \vec{v}(\gamma_1, \dots, \gamma_6, t)$. These six scalar equations can be solved in principle to give the γ_i : $\gamma_i = \gamma_i(\vec{v}, \vec{r}, t)$. Jeans' theorem then states that each function $f = f(\gamma_1, \dots, \gamma_6)$ is a solution of the fundamental equation of kinetic theory, the Boltzmann equation (C.27). This can be seen easily by inserting the γ_i into the Boltzmann equation:

$$\sum_i \left(\frac{\partial \gamma_i}{\partial t} + \vec{v} \cdot \nabla \gamma_i + \frac{\vec{F}}{m} \cdot \frac{\partial \gamma_i}{\partial \vec{v}} \right) = \sum_i \frac{\partial f}{\partial \gamma_i} \frac{d \gamma_i}{dt} = 0. \quad (\text{C.40})$$

The result is identically zero because the γ_i are constants.

C.4 Excursion: Collisions

We have mentioned collisions twice in this chapter. In Sect. C.2.3 we introduced the Maxwell distribution. The basic requirement for such a distribution is thermal equilibrium, which requires collisions between the particles. If we have a distribution with a suprathermal tail, such as the kappa distribution, in time collisions will transform it into a Maxwellian. This time scale depends, of course, on the time scales of the collisions. We have also mentioned collisions in connection with the Fokker–Planck equation. We have even mentioned that the collisions should lead to small changes in speed only. But we did not talk explicitly about the nature of these collisions. This section is supplementary, briefly introducing some of the basics of collisions.

Collisions are also important in the energy transfer between different components in a plasma: imagine a plasma which also contains neutral particles. The charged particles might be accelerated by an electric field. In time, collisions between charged and neutral particles will equalize the two distributions, leading to an acceleration of the neutrals. Collisions also are related to macroscopic properties of the plasma, such as conductivity, resistance and viscosity.

As in a neutral gas, collisions in a plasma change the path of the individual particle. In a magnetized plasma, collisions between a charged particle and a neutral can shift the gyro-center of a particle onto another field line (see Fig. C.2). Collisions between charged particles can also lead to a shift in the gyro-center and/or changes in pitch angle.

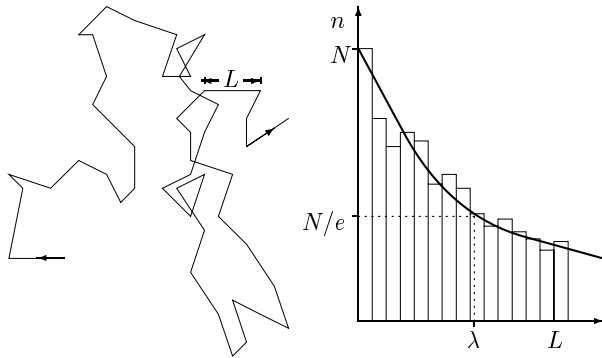


Figure C.3: Statistical path of a particle under the influence of collisions (*left*) with other particles (Brownian motion) and distribution of the path length between two collisions (*right*)

C.4.1 Collisions Between Neutrals

Collisions between neutral particles give rise to the Brownian motion in a gas. The individual process is a collision between two hard spheres. The hard sphere model is a simple and quite useful approximation. The full treatment of the collisions between neutrals requires a quantum-mechanical approach considering the attracting van der Waals forces and the repulsing Coulomb forces of the electron shells of the two atoms. The van der Waals potential varies roughly with r^{-6} , the repulsing potential with r^{-12} [181]. Combination of both leads to an extremely steep potential surrounded by a very shallow potential depression in the order of meV compared with the typical eV range in molecule formation. A hard sphere therefore is a reasonable approach to describe the collision of neutrals.

The basic equations are the conservation of momentum and the conservation of energy. The changes in momentum and direction depend on the masses and speeds of the particles and on the angle between their velocities. The change in momentum is largest in a head-on collision: when mass is equal, the particle loses twice its initial momentum as its velocity is reversed. Thus scattering by a large angle up to 180° is possible in collisions between neutrals.

The relevant parameters to describe the scattering process are the mean free path and the scattering cross section. The particle mean free path λ is defined as the average distance traveled by a particle between two subsequent collisions. If we could follow a smoke particle in air, we would detect a path similar to the one depicted on the left-hand side of Fig. C.3. The statistical motion is composed of many straight lines with different length L . The right-hand side of Fig. C.3 shows the distribution of these L . This probability distribution can be described by a function $p(L) = a \exp(-L/\lambda)$ with a being a constant depending on the total number of collisions and λ being the particle mean free path.

The number of collisions, and therefore the mean free path, depends on the number density of particles and on their ‘size’ as described by the scattering cross section. Consider a fast particle with radius r_1 moving in a gas of slow particles with radii r_2 . A collision happens if the distance between the two particles has decreased below $r_1 + r_2$. Alternatively, we can assume the fast particle to be a mass point. Then we have to attribute a radius of $r_1 + r_2$ to the gas molecules. Thus for the fast particle, a gas molecule is equivalent to a disk with the scattering cross section $\sigma = \pi(r_1 + r_2)^2$.

Now consider a beam of particles incident on a slab of area A and thickness dx . The number density of molecules in this slab is n_s , the total number of molecules in the slab is $n_s A dx$. The fraction of the slab blocked by atoms therefore is $\sigma n_s A dx / A = \sigma n_s dx$. Out of N particles incident on the slab, $\Delta N = N n_s \sigma dx$ will experience a collision, leading to a reduction in N according to $dN/N = -\sigma n_s dx$. Integration yields

$$N(x) = N_0 \exp(-\sigma n_s x) = N_0 \exp(-x/\lambda), \quad (\text{C.41})$$

where the mean free path λ is defined as

$$\lambda = \frac{1}{n_s \sigma}. \quad (\text{C.42})$$

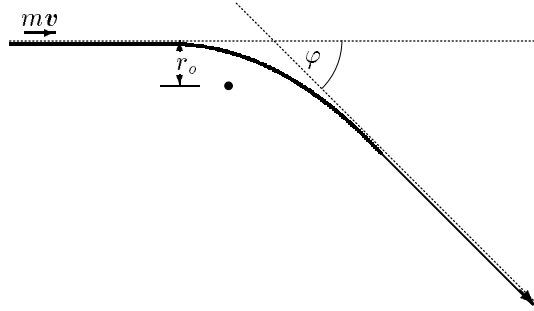


Figure C.4: Coulomb scattering: orbit of an electron in the Coulomb field of an ion

Thus, the mean free path can also be interpreted as the distance over which the number of particles decreases to $1/e$ of its initial value. After traveling a distance λ , the particle will have a high probability of colliding. The average time between two collisions is

$$\tau = \frac{\lambda}{\langle v \rangle} = \frac{1}{n_s \sigma \langle v \rangle}. \quad (\text{C.43})$$

This also can be written as a collision frequency ν_c :

$$\nu_c = n_s \sigma \langle v \rangle. \quad (\text{C.44})$$

The formalism for interactions between a charged particle and a neutral is the same as for a collision between two neutral particles because the charge on one collision partner only does not change the forces during the collision.

C.4.2 Collisions Between Charged Particles

Collisions between charged particles do not require a direct contact, instead the interaction takes place as each particle is deflected in the electric field of the other one. Since the Coulomb force has a long range such an interaction leads to a gradual deflection. Nonetheless, one can derive a kind of cross section for this process. Following the attempt given in Chen [30], we shall only make an order-of-magnitude estimate.

The geometry of a Coulomb collision is shown in Fig. C.4: an electron with velocity \vec{v} approaches an ion with charge e . If no Coulomb force acts, the electron will pass the ion at a distance r_0 , the impact parameter. But the Coulomb force $F = -e^2/(4\pi r^2)$ leads to a deflection of the electron from its original direction by an angle φ . The force acts on the electron for a time $T \approx r_0/v$ when it is in the vicinity of the ion. The change in electron momentum then can be approximated by $\Delta p = |FT| \approx e^2/(4\pi r_0 v)$. For a 90° collision, the change in momentum is of the order of mv . Thus it is $\Delta p \cong mv \cong e^2/(4\pi r_0 v)$. A deflection by 90° results for an impact parameter $r_{90^\circ} = e^2/(4\pi m v^2)$. The cross section for a deflection of at least 90° therefore can be written as

$$\sigma_{>90^\circ} = \pi r_0^2 = \frac{e^4}{16\pi m^2 v^4}, \quad (\text{C.45})$$

leading to a collision frequency of

$$\nu_{ei, >90^\circ} = n\sigma v = \frac{ne^4}{16\pi m^2 v^3}. \quad (\text{C.46})$$

In a real plasma the situation is more complex. Let us consider the motion of one particle, a test particle, in the field created by the other particles, the field particles. The fields of these particles add to a stochastic field that changes continuously in time and space. Therefore, the test particle will not move in a hyperbolic orbit as in the interaction between two charged particles, instead it basically follows its original direction of motion, though not on a straight line but on a jittery trajectory. Because of the stochastic nature of the collisions,

test particles with nearly identical start conditions will diverge in space and velocity. Most of these collisions result in small changes in the particle path only. Occasionally, also large deviations of the original direction result. These are called large-angle collisions.

To understand the different types of collisions, we have to consider the typical spatial scales. One characteristic scale is the Debye length λ_D : the test particle is screened from the electric field of the charges outside the Debye sphere. The Debye length can be interpreted as the range of microscopic electric fields and separates the field particles into two groups: (i) particles at distances larger than the Debye length can influence the test particle by the macroscopic fields only, leading to gyration, drift, and oscillations; and (ii) particles inside the Debye sphere create a microscopic field leading to the stochastic motion of the test particle.

The other spatial scale is related to the scattering angle, which in turn is related to the impact parameter. In the derivation of the Fokker–Planck equation we have assumed scattering by small angles only. The deflection angle will be small if the kinetic energy $m_T v_T^2/2$ of the test particle is large compared with the electrostatic potential $Z_T Z_F e^2/r_0$, where r_0 is the impact parameter (see Fig. C.4). The test particle will be deflected by a small angle only if the impact parameter r_0 fulfills the condition $r_{90^\circ} < r_0 < \lambda_D$, with r_{90° being the impact parameter for a deflection by 90° defined as $r_{90^\circ} = Z_T Z_F e^2/(m_T v_T^2)$. The ratio for deflections by small and large angles can be determined from the ratio of cross sections for both processes:

$$\frac{\lambda_D^2 - r_{90^\circ}^2}{r_{90^\circ}^2} \leq \frac{\lambda_D^2}{r_{90^\circ}^2} \approx \left(\frac{9}{Z_T Z_F} \right)^2 \left(\frac{4\pi}{3} n \lambda_D^3 \right)^2 =: \Lambda^2 . \quad (\text{C.47})$$

The expression inside the second parentheses is the number of particles inside a Debye sphere. If we assume this number to be large, (C.47) states that collisions leading to deflections by a small angle by far outnumber the collisions with large-angle deflection. A careful calculation shows that small-angle interactions are about two orders of magnitude more efficient in the deflection of test particles than the few large-angle interactions [13]. Thus, the Fokker–Planck formalism can be applied to the Coulomb collisions in a plasma too. The logarithm of the above quantity, $\lambda_c = \ln \Lambda$, is called the Coulomb logarithm.

C.5 Scale Analysis

Scale analysis is a method to judge the relative importance of different terms in an equation. As an example we will use the general equation of motion in a fluid such as the atmosphere or an ocean, that is the Navier–Stokes equation already encountered in chap. 7, in particular in sect. 7.1.

C.5.1 Equation of motion in Oceans and in the Atmosphere

The general equation of motion for a mass density ϱ and a force density \vec{f} reads

$$\vec{f} = \varrho \frac{d\vec{p}}{dt} . \quad (\text{C.48})$$

In a continuous medium the relevant forces are

$$\begin{aligned} \frac{d\vec{u}}{dt} = & \quad -\nabla p && (1) \text{ pressure gradient force} \\ & \quad +\vec{g} && (2) \text{ gravitation} \\ & \quad +\nu \nabla^2 \vec{u} && (3) \text{ friction (incompressible)} \\ & \quad +\frac{1}{3} \nabla(\nabla \times u) && (4) \text{ friction (kompressible)} \\ & \quad -2\vec{\Omega} \times \vec{u} && (5) \text{ Coriolis force} \\ & \quad -\vec{\Omega} \times (\vec{\Omega} \times \vec{r}) && (6) \text{ centrifugal force} . \end{aligned} \quad (\text{C.49})$$

For applications in oceanography and meteorology the equation often is rewritten for local coordinates \vec{i} and \vec{j} in the horizontal plane pointing eastward and northward, respectively,

and \vec{k} pointing upwards. With u and v being speeds in the horizontal and w in the vertical direction, the equation of motion can be written as

$$\begin{aligned} \frac{du}{dt} - \frac{uv \tan \phi}{a} + \frac{uw}{a} &= -\frac{1}{\rho} \frac{\partial p}{\partial x} + 2\Omega v \sin \phi - 2\Omega w \cos \phi + F_x \\ \frac{dv}{dt} + \frac{u^2 \tan \phi}{a} + \frac{vw}{a} &= -\frac{1}{\rho} \frac{\partial p}{\partial y} - 2\Omega u \sin \phi + F_y \\ \frac{dw}{dt} - \frac{u^2 + v^2}{a} &= -\frac{1}{\rho} \frac{\partial p}{\partial z} - g + 2\Omega u \cos \phi + F_z . \end{aligned} \quad (\text{C.50})$$

Typical scales in the atmosphere (left) and in the oceans (right) are

10 m s ⁻¹	horizontal speed U	1 m s ⁻¹
1 cm s ⁻¹	vertical speed W	1 mm s ⁻¹
10 ⁶ m	horizontal length scale L	10 ⁶ m
10 ⁴ m	vertical length scale D	10 ⁴ m
10 ³ m ² s ⁻²	horizontal pressure fluctuations $\Delta p/\rho$	10 ² m ² s ⁻²
10 ⁵ s	time scales L/U	10 ⁶ s
10 ⁻⁴ s ⁻¹	Coriolis parameter $f_o = 2\Omega \sin \phi$	10 ⁻⁴ s ⁻¹

Scale analysis for the atmosphere thus yields for the horizontal components of the equation of motion

$$\begin{array}{l} \text{x - component} \\ \text{y - component} \\ \text{Scales} \\ \text{OoM [m/s}^{-2}\text{]} \end{array} \quad \begin{array}{l} \frac{du}{dt} \\ \frac{dv}{dt} \\ \frac{U^2}{L} \\ 10^{-4} \end{array} \quad \begin{array}{l} -2\Omega v \sin \phi \\ +2\Omega u \sin \phi \\ f_o U \\ 10^{-3} \end{array} \quad \begin{array}{l} +2\Omega w \cos \phi \\ \\ f_o W \\ 10^{-6} \end{array} \quad \begin{array}{l} +\frac{uw}{a} \\ +\frac{uw}{a} \\ \frac{UW}{a} \\ 10^{-8} \end{array} \quad \begin{array}{l} -\frac{uv \tan \phi}{a} \\ +\frac{u^2 \tan \phi}{a} \\ \frac{U^2}{a} \\ 10^{-5} \end{array} \quad \begin{array}{l} = \\ = \\ \frac{\Delta p}{\rho L} \\ 10^{-3} \end{array} .$$

The last column gives the order of magnitude of the respective term: in the atmosphere, therefore, pressure gradient force and the Coriolis force dominate. Both are one order of magnitude larger than the inertia term. In fact, both forces are sufficient to describe the fundamentals of air motion around pressure regions in the geostrophic approximation.

For the vertical component we obtain

$$\begin{array}{l} \text{z - component} \\ \text{Scales} \\ \text{OoM [m s}^{-2}\text{]} \end{array} \quad \begin{array}{l} \frac{dw}{dt} \\ \frac{UW}{L} \\ 10^{-7} \end{array} \quad \begin{array}{l} -2\Omega u \cos \phi \\ f_o U \\ 10^{-3} \end{array} \quad \begin{array}{l} -\frac{u^2+v^2}{a} \\ \frac{U^2}{a} \\ 10^{-5} \end{array} \quad \begin{array}{l} = \\ = \\ 10 \end{array} \quad \begin{array}{l} -\frac{1}{\rho} \frac{\partial p}{\partial z} \\ \frac{P_o}{\rho H} \\ 10 \end{array} \quad \begin{array}{l} -g \\ g \\ 10 \end{array} .$$

the dominating forces are pressure gradient force and gravitation – thus the essence of the equation also is captured by the hydrostatic equation which consists of exactly these two terms.

For the ocean we obtain for the horizontal component

$$\begin{array}{l} \text{x - component} \\ \text{y - component} \\ \text{Scales} \\ \text{OoM [m/s}^{-2}\text{]} \end{array} \quad \begin{array}{l} \frac{du}{dt} \\ \frac{dv}{dt} \\ \frac{U^2}{L} \\ 10^{-6} \end{array} \quad \begin{array}{l} -2\Omega v \sin \phi \\ +2\Omega u \sin \phi \\ f_o U \\ 10^{-4} \end{array} \quad \begin{array}{l} +2\Omega w \cos \phi \\ \\ f_o W \\ 10^{-7} \end{array} \quad \begin{array}{l} +\frac{uw}{a} \\ +\frac{uw}{a} \\ \frac{UW}{a} \\ 10^{-10} \end{array} \quad \begin{array}{l} -\frac{uv \tan \phi}{a} \\ +\frac{u^2 \tan \phi}{a} \\ \frac{U^2}{a} \\ 10^{-7} \end{array} \quad \begin{array}{l} = \\ = \\ \frac{\Delta p}{\rho L} \\ 10^{-4} \end{array} .$$

and for the vertical one

$$\begin{array}{l} \text{z - component} \\ \text{Scales} \\ \text{OoM [m s}^{-2}\text{]} \end{array} \quad \begin{array}{l} \frac{dw}{dt} \\ \frac{UW}{L} \\ 10^{-9} \end{array} \quad \begin{array}{l} -2\Omega u \cos \phi \\ f_o U \\ 10^{-4} \end{array} \quad \begin{array}{l} -\frac{u^2+v^2}{a} \\ \frac{U^2}{a} \\ 10^{-7} \end{array} \quad \begin{array}{l} = \\ = \\ 1 \end{array} \quad \begin{array}{l} -\frac{1}{\rho} \frac{\partial p}{\partial z} \\ \frac{P_o}{\rho H} \\ 10 \end{array} \quad \begin{array}{l} -g \\ g \\ 10 \end{array} .$$

Thus the relevant terms in the equation of motion are the same as in the atmosphere.

Some in-between calculation 5 Apply a scale analysis to a cup of tea and to a bathtub.

Questions

Frage 45 What is the relation between density, phase space density and flux?

Frage 46 Explain the equation of continuity in ordinary space and in phase space.

Frage 47 What is the mean free path? Explain formally and descriptive.

Frage 48 Describe the basic equations of statistical theory. Explain similarities and differences, state the underlying assumptions.

Frage 49 What does the Fokker–Planck equation describe?

Frage 50 What's the meaning of a scattering cross section?

Frage 51 Explain the difference in scattering between neutrals and scattering between charged particles.

Appendix **D**

A Little Remainder on Some Numeric's Basics

Since this text deals with transport equations, at least in advanced model the basic equations are PDEs. Their solution often requires numerical methods. In this chapter some simple, although important methods are repeated briefly.

D.1 Discretization

The essence of numerical solutions of differential equations is discretization. In calculus we have learned that the derivative is a difference quotient with the difference in the denominator approaching zero. Infinitesimal small differences, however, cannot be handled numerically. Thus at the beginning of numerical treatment of a differential equation, the differential quotient has to be converted back to a difference quotient, a process called discretization.

Consider a function $f(x)$ in an interval $[a, b]$. A discretization divides the interval in M constant steps of width $h = (b - a)/M$. The continuous interval thus is mapped onto a series of $M + 1$ discrete supporting points $x_i = a + (i - 1)h$. The continuous function $f(x)$ then is evaluated only at these points, yielding a series of $M + 1$ values $u_i = f(x_i)$.

D.1.1 First- and Second-Order Derivatives

A derivative in this supporting space can be introduced from a Taylor expansion of the original function at a point x_i :

$$u_{i+1} = f(x_{i+1}) = f(x_i + h) = f(x_i) + h f'(x_i) + \frac{h^2}{2!} f''(x_i) + \frac{h^3}{3!} f'''(x_i) + \mathcal{O}(h^4). \quad (\text{D.1})$$

Rewrite with $f(x_i) = u_i$ as

$$\frac{u_{i+1} - u_i}{h} = f'(x_i) + \frac{h}{2!} f''(x_i) + \frac{h^2}{3!} f'''(x_i) + \mathcal{O}(h^3). \quad (\text{D.2})$$

As $h \rightarrow 0$, the left hand side is the definition of the derivative. Thus it can be used as a *finite-difference approximation* on the first derivative. The leading term in the error is $h f''(x_i)/2! = \mathcal{O}(h)$. Thus the scheme is accurate to first-order. Such a scheme can be used as one-sided, advanced or forward finite-difference scheme.

Replacing h by $-h$ yields

$$u_{i-1} = f(x_{i-1}) = f(x_i - h) = f(x_i) - h f'(x_i) + \frac{h^2}{2!} f''(x_i) - \frac{h^3}{3!} f'''(x_i) + \mathcal{O}(h^4). \quad (\text{D.3})$$

instead of (D.1). The resulting approximation on the derivative

$$\frac{u_i - u_{i-1}}{h} = f'(x_i) - \frac{h}{2!} f''(x_i) + \frac{h^2}{3!} f'''(x_i) + \mathcal{O}(h^3) \quad (\text{D.4})$$

again is of first-order accuracy and one-sided, although it is retarded or backward.

The average of the two previous schemes

$$\frac{u_{i+1} - u_{i-1}}{2h} = f'(x_i) + \frac{h^2}{3!} f'''(x) + \mathcal{O}(h^4) \quad (\text{D.5})$$

is a centered difference and it is accurate of second-order with a remainder of forth-order.

The difference of (D.2) and (D.4) gives the second derivative

$$\frac{u_{i+1} - 2u_i + u_{i-1}}{h^2} = f''(x_i) + \frac{h^2}{4!} f''''(x_i) + \mathcal{O}(h^4) \quad (\text{D.6})$$

as a centered scheme of second-order accuracy.

Taylor expansion for a function of two or more variables can be obtained as Taylor expansion in one variable followed by a Taylor expansion in the other variable followed by ... and so on. Performing the same calculations as above for a function $f(x, y)$, we can show that partial derivatives can be approximated in the same fashion as described above for the total derivatives.

D.1.2 Consistency and Accuracy

The step back from the differential equation to the finite difference equation (FDE) implies truncation of the higher order terms of the Taylor expansion.

Definition 7 *The truncation error (TE) ε_i^n is obtained by putting the exact solution \hat{u}_i^n in the FDE in place of the approximate solution.*

For instance, the PDE for diffusion or heat conduction can be written as

$$\frac{\partial u}{\partial t} = \alpha \frac{\partial^2 u}{\partial x^2} \quad \text{with } \alpha > 0. \quad (\text{D.7})$$

The FDE on the other hand reads

$$\frac{u_i^{n+1} - u_i^n}{\Delta t} - \alpha \frac{u_{i+1}^n - 2u_i^n + u_{i-1}^n}{(\Delta x)^2} = 0 \quad (\text{D.8})$$

with the subscript indicating the position in space and the superscript that in time. The truncation error then is

$$\varepsilon_i^n = \frac{\hat{u}_i^{n+1} - \hat{u}_i^n}{\Delta t} - \alpha \frac{\hat{u}_{i+1}^n - 2\hat{u}_i^n + \hat{u}_{i-1}^n}{(\Delta x)^2} \neq 0. \quad (\text{D.9})$$

Taylor expansion of the original equation (the FDE cannot be expanded because it is defined only in the supporting points) yields

$$\varepsilon_i^n = \left(\frac{\partial \hat{u}_i^n}{\partial t} - \alpha \frac{\partial^2 \hat{u}_i^n}{\partial x^2} \right) + \frac{\Delta t}{2} \frac{\partial^2 \hat{u}_i^n}{\partial t^2} - \alpha \frac{(\Delta x)^2}{12} \frac{\partial^4 \hat{u}_i^n}{\partial x^4} + \mathcal{O}((\Delta t)^2, (\Delta x)^4). \quad (\text{D.10})$$

The exact solution satisfies the PDE and the terms in the bracket cancel. The remaining truncation error then is

$$\varepsilon_i^n = \frac{\Delta t}{2} \frac{\partial^2 \hat{u}_i^n}{\partial t^2} - \alpha \frac{(\Delta x)^2}{12} \frac{\partial^4 \hat{u}_i^n}{\partial x^4} + \mathcal{O}((\Delta t)^2, (\Delta x)^4). \quad (\text{D.11})$$

The leading terms in the truncation error are of first-order in time and second-order in space, that is our accuracy is $\mathcal{O}(\Delta t, (\Delta x)^2)$.

Definition 8 *A finite-difference scheme is consistent if $\varepsilon_i^n \rightarrow 0$ for $\Delta t \rightarrow 0$ and $\Delta x \rightarrow 0$ independently. If the TE is of form $\varepsilon_i^n = \mathcal{O}((\Delta t)^p, (\Delta x)^q)$ the scheme is said to be of the order p in t and q in x .*

Note that both, accuracy and consistency, are independent on the point chosen for Taylor expansion.

D.1.3 Stability

Consistency and accuracy are fundamental properties of a FDE in such that they define the convergence of the finite difference scheme:

Definition 9 Lax's Equivalence Theorem: *given a properly posed initial value problem and a finite difference approximation to it that satisfies the consistency condition, stability is the necessary and sufficient condition for convergence.*

Here convergence means that the difference between the exact and discrete solution will tend to zero as the discretization step sizes tend to zero:

$$|\hat{u}(x_i, t^n) - u_i^n| \rightarrow 0 \quad \text{for} \quad \Delta t, \Delta x \rightarrow 0. \quad (\text{D.12})$$

Asides from the truncation error, there is also a round-off error involved in a numerical scheme because a computer only has a finite accuracy. Stability is concerned with this problem; a simple and flexible tool at hand is Von Neumann analysis.¹ Since the method relies on the superposition of wave modes, its application is limited to (systems of) linear homogenous equations. Nonlinear equations must be linearized by freezing the coefficients of the partial derivatives.

Again the heat conduction equation will serve as example. In update form, the new values of the unknowns can be calculated directly:

$$u_i^{n+1} = u_i^n + \alpha \frac{\Delta t}{(\Delta x)^2} (u_{i+1}^n - 2u_i^n + u_{i-1}^n). \quad (\text{D.13})$$

Each Fourier mode will be analyzed separately in a complex fashion:

$$u_i^n = g^n e^{i i \beta} = g^n (\cos(i\beta) + i \sin(i\beta)). \quad (\text{D.14})$$

Here g is the complex amplitude raised to the n th power with n corresponding to time and β is the wave number corresponding to the Fourier mode. Substituting into (D.13) yields

$$g^{n+1} e^{i i \beta} = g^n e^{i i \beta} + \sigma g^n (e^{i(i+1)\beta} - 2e^{i i \beta} + e^{i(i-1)\beta}) \quad \text{with} \quad \sigma = \frac{\alpha \Delta t}{(\Delta x)^2}. \quad (\text{D.15})$$

Solving for the amplification factor

$$g = 1 - 2\sigma(1 - \cos \beta) \quad (\text{D.16})$$

allows to determine stability conditions. The scheme is stable, that is round-off errors are damped, only if $|g| \leq 1 \forall \beta$:

$$-1 \leq 1 - 2\sigma(1 - \cos \beta) \leq 1 \quad \forall \beta. \quad (\text{D.17})$$

Since $\sigma \geq 0$, the right inequality is always satisfied. The left side requires $\sigma(1 - \cos \beta) \leq 1$ or $\sigma \leq \frac{1}{2}$. With the definition of σ in (D.15), stability is obtained if the following relation between spatial and temporal step size is fulfilled:

$$\Delta t \leq \frac{(\Delta x)^2}{2\alpha}. \quad (\text{D.18})$$

For the linear convection equation

$$\frac{\partial u}{\partial t} + c \frac{\partial u}{\partial x} = 0 \quad (\text{D.19})$$

Lax' scheme reads

$$\frac{u_i^{n+1} - \frac{u_{i-1}^n + u_{i+1}^n}{2}}{\Delta t} + c \frac{u_{i+1}^n - u_{i-1}^n}{2\Delta x} = 0, \quad (\text{D.20})$$

which is stable as long as the Courant–Friedrichs–Lewy (CFL) condition

$$\Delta t \leq \frac{\Delta x}{|c|} \quad (\text{D.21})$$

is fulfilled.

¹Other tools, such as matrix eigenvalue analysis methods exist, too. The interested reader is referred to standard texts on numerical solutions of PDEs such as [53, 76, 94, 107, 128, 143, 146]

D.2 Numerical Integration – The Basics

In most calculus courses the concept of integration is introduced as numerical integration: integration is not introduced as the reverse operation to differentiation but as the area under the graph of a function. And numerical integration comes in when the students are asked to evaluate the area with the aid of rectangles or trapezoids.

Numerical integration is the formalized version of this game. Our goal is to determine the definite integral of a function $f(x)$ between the limits a and b :

$$I = \int_a^b f(x) \, dx . \quad (\text{D.22})$$

As in its graphical counterpart, the integration interval $[a, b]$ is divided into M steps of length $\Delta x = (b - a)/M$. In the central method the function is assumed to be constant within Δx with the functional characteristics $f(x_{k-\frac{1}{2}})$ taken in the middle of the respective intervals $[x_{k-1}, x_k]$. The integral therefore is

$$I_{\text{cm}} = \sum_{k=1}^M f(x_{k-\frac{1}{2}}) \Delta x \quad \text{with} \quad x_{k-\frac{1}{2}} = \frac{x_{k-1} + x_k}{2} . \quad (\text{D.23})$$

While the graphical description of the central method is the rectangle, the trapezoid integration uses, as its name suggests, the trapezoid. Thus the functional characteristics at the lower and upper limit of each interval are taken into account and the integral can be written as

$$I_{\text{ti}} = \frac{1}{2} \sum_{k=1}^M (f(x_k) + f(x_{k-1})) \Delta x . \quad (\text{D.24})$$

While the trapezoid method is a linear approximation on the function within each step, Simpson integration uses a second-order polynomial as approximation:

$$I_{\text{Si}} = \frac{1}{6} \sum_{k=1}^M \left(f(x_k) + 4f(x_{k-\frac{1}{2}}) + f(x_{k-1}) \right) \Delta x . \quad (\text{D.25})$$

The most important technical aspects are the correct discretization of the relevant equations and an efficient choice of the step size Δx : the latter has to be small enough to reduce numerical uncertainties but large enough to avoid unreasonably long computation times. While in classical numerical schemes the step size is constant, today often methods are used that adapt step size: if the function does not vary very much, larger steps lead to satisfactory and fast results. But in intervals with large variations, smaller step sizes are required to preserve accuracy. Examples for adaptive methods are the MatLab functions `quad` that uses an adaptive Simpson method and `quad1` that uses an adaptive Lobotta method.

D.3 Numerical Solutions of ODEs – Finite Differences

The numerical solution of an ODE is a straightforward application of the numerical integration. Again, conventional methods start from equally space grid points while modern programm package also use adaptive methods. And again, discretization, choice of a suitable method, and choice of an adequate step size are the challenges presented to the modeler. The conventional methods for numerical solutions of ODEs are closely related to the methods for numerical integration.

Numerical methods for the solution of ODEs can be limited to first order ODEs since all ODEs of higher order n can be decomposed into a set of n ODEs of first order. Therefore a general formulation of the problem of obtaining a numerical solution of an ODE can follow

these lines: find a numerical solution of the initial value problem $\dot{x} = f(x, t)$ with initial value $x(0) = x_0$ in the interval $a \leq t \leq b$. Discretization yields for the ODE

$$\frac{\Delta x}{\Delta t} = \frac{x_k - x_{k-1}}{\Delta t} = f(x, t). \quad (\text{D.26})$$

The simplest scheme is Euler's method which comes in the flavors of a forward and a backward method. Both methods are comparable to the central method in numerical integration in such that they assume one value, in the case the gradient \dot{x} , to be constant in each step. In Euler's forward method we take the gradient at the begin of each interval and thus get

$$x(t_{k+1}) = x(t_k) + \Delta t f(x_k, t_k) \quad \text{with } x(0) = x_0 \quad \text{and} \quad t_k = t_0 + k\Delta t. \quad (\text{D.27})$$

The right-hand side of the integration interval thus is evaluated from the initial values. The truncation error in this scheme is

$$\varepsilon_i = \frac{x_{i+1} - x_i}{h} - f(t_i, x_i) = \dot{x}_i + \frac{h}{2} \ddot{x}_i - f(t_i, x_i) + \mathcal{O}(h^2) = \frac{h}{2} \ddot{x}_i + \mathcal{O}(h^2). \quad (\text{D.28})$$

The Euler scheme thus is accurate to first-order.

Euler's backward method uses the rise at the end of the interval:

$$x(t_{k+1}) = x(t_k) + \Delta t f(x_{k+1}, t_{k+1}). \quad (\text{D.29})$$

The backwards method poses a problem: $f(x_{k+1}, t_{k+1})$ is required to calculate one of its arguments, $x(t_{k+1})$. The method therefore is termed implicit while the forward method is explicit. The problem of the unknown gradient $f(x_{k+1}, t_{k+1})$ can be circumvented, for instance, by using an Euler forward method als predictor step. This x_{k+1}^P than is inserted into (D.29):

$$x(t_{k+1}) = x(t_k) + \Delta t f(x_{k+1}^P, t_{k+1}). \quad (\text{D.30})$$

Eliminating the provisional value x_{k+1}^P from the scheme, the TE becomes

$$\begin{aligned} \varepsilon_i &= \frac{x_{i+1} - x_i}{h} - \frac{1}{2} (f(t_i, x_i) + f(t_i + h, x_i + hf(t_i, x_i))) \\ &= \dot{x}_i + \frac{h}{2} \ddot{x}_i + \frac{h^2}{3!} \frac{\partial^3 x_i}{\partial t^3} + \mathcal{O}(h^3) - f(t_i, x_i) \\ &\quad - \frac{h}{2} \frac{\partial f(t_i, x_i)}{\partial t} - \frac{hf(t_i, x_i)}{2} \frac{\partial f(t_i, x_i)}{\partial x} + \mathcal{O}(h^2) \\ &= \frac{4}{2} \left(\ddot{u}_i - \frac{\partial f(t_i, x_i)}{\partial t} - f_i \frac{\partial f(t_i, x_i)}{\partial x} \right) + \mathcal{O}(h^2) = \mathcal{O}(h^2). \end{aligned} \quad (\text{D.31})$$

The implicit Euler scheme thus is of second-order accuracy.

Both methods are combined in the explicit/implicit Crank–Nicolson method:

$$x(t_{k+1}) = x(t_k) + \frac{1}{2} (f(t_k, x_k) + f(t_{k+1}, x_{k+1})) \quad (\text{D.32})$$

with

$$x(0) = x_0 \quad \text{and} \quad t_k = t_0 + k\Delta t. \quad (\text{D.33})$$

The Leapfrog method uses Euler's forward method but with a two grids, offset by half a step. The resulting equations are

$$x_{k+\frac{1}{2}} = x_{k-\frac{1}{2}} + f(t_i, x_i) \Delta t \quad \text{with} \quad x_{-\frac{1}{2}} = x_0 - \frac{1}{2} f(t_0, x_0) \Delta t \quad (\text{D.34})$$

and

$$x_{k+1} = x_k + f(t_{k+\frac{1}{2}}, x_{k+\frac{1}{2}}) \Delta t \quad \text{with} \quad x(0) = x_0. \quad (\text{D.35})$$

Both equations are iterated by turns.

The Runge–Kutta method, 4th order, uses a higher order approximation on the gradient in each step. The method comes in different flavors, depending on the order of the approximation. The most common method is a 4th order approximation using the gradient at both limits and at the center of each interval:

$$x_k = x_{k-1} + \frac{1}{6} (h_1 + 2h_2 + 2h_3 + h_4) \quad (\text{D.36})$$

with

$$\begin{aligned} h_1 &= f(t_{k-1}, x_{k-1}) \Delta t, \\ h_2 &= f(t_{k-\frac{1}{2}}, x_{k-1} + \frac{1}{2}h_1) \Delta t, \\ h_3 &= f(t_{k-\frac{1}{2}}, x_{k-1} + \frac{1}{2}h_2) \Delta t, \\ h_4 &= f(t_k, x_{k-1} + h_3) \Delta t. \end{aligned} \quad (\text{D.37})$$

The method is accurate to fourth order.

D.4 Numerical Solutions of PDEs – Finite Difference Methods

A classification of PDEs already has been introduced in sect. B.2.2. Here some typical numerical approaches for the corresponding equations are summarized and compared regarding accuracy and stability.

D.4.1 Linear Hyperbolic Equations

The typical examples for hyperbolic equations are the linear convection equation and the wave equation. Within the framework of this text, we will focus on the convection equation and neglect the wave equation.

Linear Convection Equation

The linear convection equation, a hyperbolic PDE, can be written as

$$\frac{\partial u}{\partial t} + c \frac{\partial u}{\partial x} = 0 \quad \text{with } c > 0 \quad (\text{D.38})$$

because the x -axis of our coordinate system always can be adjusted such that the convection speed c is positive. To advance the solution in time, u_k^{l+1} must appear in the time derivative; the scheme for $\partial u/\partial t$ therefore must be a forward scheme.

Centered Scheme

In the centered scheme, discretization gives the difference equation

$$\frac{u_k^{l+1} - u_k^l}{\Delta t} + c \frac{u_{k+1}^l - u_{k-1}^l}{2\Delta x} = 0. \quad (\text{D.39})$$

The TE is

$$\varepsilon_k^l = \frac{\Delta t}{2} \frac{\partial^2 u_k^l}{\partial t^2} + c \frac{(\Delta x)^2}{6} \frac{\partial^3 u_k^l}{\partial x^3} + \mathcal{O}((\Delta t)^2, (\Delta x)^4) = \mathcal{O}(\Delta t, (\Delta x)^2), \quad (\text{D.40})$$

the scheme therefore is accurate of first-order in time and second-order in space. The scheme is conditionally unstable because $g = 1 - i\sigma \sin \alpha$ with $\sigma = c(\Delta t/\Delta x)$ and thus $|g| > 1$ for $\sigma \neq 0$. Although the scheme therefore is not useful for accurate analysis, it still is a simple scheme suitable for first approaches on a problem.

Upwind Scheme

A better numerical approach is the upwind scheme which is a retarded scheme. The difference equation is

$$\frac{u_k^{l+1} - u_k^l}{\Delta t} + c \frac{u_k^l - u_{k-1}^l}{\Delta x} = 0. \quad (\text{D.41})$$

The TE is

$$\varepsilon_k^l = \frac{\Delta t}{2} \frac{\partial^2 u_k^l}{\partial t^2} - c \frac{\Delta x}{2} \frac{\partial^2 u_k^l}{\partial x^2} + \mathcal{O}((\Delta t)^2, (\Delta x)^2) = \mathcal{O}(\Delta t, \Delta x); \quad (\text{D.42})$$

the scheme thus is first-order accurate in both space and time. In addition, the scheme is consistent. Stability is given if the CFL criterion (D.21) is met. This is also the case if the Lax scheme (D.20).

Lax–Wendroff Scheme

A second-order accurate scheme is the Lax–Wendroff scheme. It can be derived from a Taylor expansion of u_k^{l+1} and reads

$$\frac{u_k^{l+1} - u_k^l}{\Delta t} + c \frac{u_{k+1}^l - u_{k-1}^l}{2\Delta x} - c^2 \frac{\Delta t}{2} \frac{u_{k+1}^l - 2u_k^l + u_{k-1}^l}{(\Delta x)^2} = 0 \quad (\text{D.43})$$

or in update form

$$u_k^{l+1} = u_k^l - c \Delta t \frac{u_{k+1}^l - u_{k-1}^l}{2\Delta x} + c^2 \frac{\Delta t}{2} \frac{u_{k+1}^l - 2u_k^l + u_{k-1}^l}{(\Delta x)^2}. \quad (\text{D.44})$$

D.4.2 Linear Parabolic Equations

The standard examples for linear parabolic equations are the diffusion equation and the heat conduction equation:

$$\frac{\partial u}{\partial t} = \alpha \frac{\partial^2 u}{\partial x^2}. \quad (\text{D.45})$$

The equation also allows to describe viscous effects. Exact solutions can be obtained by separation of variables as demonstrated for the Laplace equation in sect. 4.2.

Simple Explicit Scheme

A simple explicit scheme based on centered differences in space and an upward step in time can be written as

$$\frac{u_k^{l+1} - u_k^l}{\Delta t} = \alpha \frac{u_{k+1}^l - 2u_k^l + u_{k-1}^l}{(\Delta x)^2}. \quad (\text{D.46})$$

The scheme is similar to the implicit scheme used in sect. 3.2.1; the difference is the time step at which the spatial difference scheme is evaluated. Here we discuss an explicit scheme and thus the centered time difference is evaluated from the known quantities at time l . In sect. 3.2.1 and Fig. 3.1 we have discussed an implicit scheme where the centered spatial difference is evaluated at the following time step $l+1$.

The explicit scheme is consistent and of first-order accuracy in time and second-order accuracy in space, as can be seen from the TE

$$\begin{aligned} \varepsilon_k^l &= \frac{\partial u_k^l}{\partial t} + \frac{\Delta t}{2} \frac{\partial^2 u_k^l}{\partial t^2} + \frac{(\Delta t)^2}{3!} \frac{\partial^3 u_k^l}{\partial t^3} + \mathcal{O}((\Delta t)^3) \\ &- \alpha \left(\frac{\partial^2 u_k^l}{\partial x^2} + \frac{(\Delta x)^4}{4!} \frac{\partial^4 u_k^l}{\partial x^4} + \mathcal{O}((\Delta x)^4) \right) = \mathcal{O}(\Delta t, (\Delta x)^2). \end{aligned} \quad (\text{D.47})$$

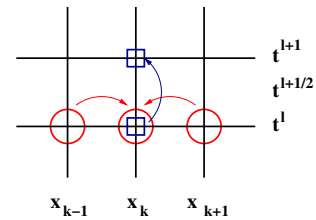


Figure D.1: Explicit scheme

Since the stability conditions for this scheme is $\sigma \leq \frac{1}{2}$, the relation between the step sizes must be

$$\Delta t \leq \frac{(\Delta x)^2}{2\alpha}. \tag{D.48}$$

Simple Implicit Scheme

The implicit scheme (Laasonen scheme), see also Fig. 3.1, differs from the explicit scheme in such that the spatial derivative is derived at the target time step $l + 1$ and not at the lower interval boundary l . The difference equation reads

$$\frac{u_k^{n+1} - u_k^n}{\Delta t} = \alpha \frac{u_{k+1}^{n+1} - 2u_k^{n+1} + u_{k-1}^{n+1}}{(\Delta x)^2}. \tag{D.49}$$

The TE can be derived from (D.47) by substituting $-\Delta t$ for Δt . The implicit scheme thus also is consistent and of first-order accuracy in time and second-order accuracy in space.

While the explicit scheme can be solved forward, the implicit scheme requires a simultaneous solution and therefore a matrix based algorithm as described in sect. 3.2.1.

Combined Methods, e.g. Crank-Nicolson

The simple explicit and implicit schemes are special cases of the more general scheme

$$\frac{u_k^{l+1} - u_k^l}{\Delta t} = (1-\vartheta)\alpha \frac{u_{k+1}^l - 2u_k^l + u_{k-1}^l}{(\Delta x)^2} + \vartheta\alpha \frac{u_{k+1}^{l+1} - 2u_k^{l+1} + u_{k-1}^{l+1}}{(\Delta x)^2} \quad 0 \leq \vartheta \leq 1. \tag{D.50}$$

The general scheme thus takes a weighted average of the spatial derivatives at the time step l and the following step $l + 1$ with weight ϑ . The simple explicit scheme arises for $\vartheta = 0$, the simple implicit scheme for $\vartheta = 1$. The combined method again is second-order in space and first-order in time, except for a few special cases:

- the Crank–Nicolson scheme takes the arithmetic mean of the two spatial derivatives, thus $\vartheta = \frac{1}{2}$, and is of second-order accuracy in both time and space.
- a weight

$$\vartheta = \frac{1}{2} - \frac{(\Delta x)^2}{12\alpha\Delta t} \tag{D.51}$$

gives a scheme of second order in time and fourth order in space.

- the same weight combined with a stability criterion, that is

$$\vartheta = \frac{1}{2} - \frac{(\Delta x)^2}{12\alpha\Delta t} \quad \text{and} \quad \frac{(\Delta x)^2}{\alpha\Delta t} = \sqrt{20}, \tag{D.52}$$

even yields a scheme of second order in time and sixth order in space.

Since the implicit scheme is included in this combined scheme, the equations have to be solved simultaneously

D.4.3 Linear Elliptic Equations

The Poisson equation

$$\frac{\partial^2 u}{\partial x^2} + \frac{\partial^2 u}{\partial y^2} = f(x, y) \tag{D.53}$$

is one example for an elliptic equation. It differs from the previous PDEs in such that we do not encounter one spatial and one temporal derivative but two spatial derivatives.

If we choose the approach of centered finite differences for the scheme, the difference equation reads

$$\frac{u_{i+1,k} - 2u_{i,k} + u_{i-1,k}}{(\Delta x)^2} + \frac{u_{i,k+1} - 2u_{i,k} + u_{i,k-1}}{(\Delta y)^2} = f_{i,k}, \tag{D.54}$$

see also (4.40) and Fig. 4.8. Such a scheme also is called a five-point scheme. Taylor expansion around the center point gives for the TE

$$\begin{aligned}\varepsilon_{i,k} &= \frac{\partial^2 u_{i,k}}{\partial x^2} + \frac{(\Delta x)^2}{4!} \frac{\partial^4 u_{i,k}}{\partial x^4} + \mathcal{O}((\Delta x)^4) + \frac{\partial^2 u_{i,k}}{\partial y^2} + \frac{(\Delta y)^2}{4!} \frac{\partial^4 u_{i,k}}{\partial y^4} + \mathcal{O}((\Delta x)^4) \\ &= \mathcal{O}((\Delta x)^2, (\Delta y)^2).\end{aligned}\quad (\text{D.55})$$

Numerical solutions of this scheme are discussed in detail in sect. 4.2.

D.4.4 Diffusion–Convection Equation

The diffusion–convection equation has been discussed in detail in chap. 3. It can be written as

$$\frac{\partial u}{\partial t} + c \frac{\partial u}{\partial x} + D \frac{\partial^2 u}{\partial x^2} = 0. \quad (\text{D.56})$$

The equation consists of a temporal derivative, a first spatial derivative and a second spatial derivative. It consists of a hyperbolic part (the convection term) and a parabolic part (the diffusion term).

A standard scheme here is the FTCS method (forward in time and centered in space) method:

$$\frac{u_k^{l+1} - u_k^l}{\Delta t} + c \frac{u_{k+1}^l - u_{k-1}^l}{2\Delta x} - D \frac{u_{k+1}^l - 2u_k^l + u_{k-1}^l}{(\Delta x)^2} = 0. \quad (\text{D.57})$$

The TE is

$$\begin{aligned}\varepsilon_k^l &= \frac{\partial u_k^l}{\partial t} + \frac{\Delta t}{2} \frac{\partial^2 u_k^l}{\partial t^2} + \mathcal{O}((\Delta t)^2) + c \left(\frac{\partial u_k^l}{\partial x} + \frac{(\Delta x)^2}{3!} \frac{\partial^3 u_k^l}{\partial x^3} + \mathcal{O}(\Delta x^4) \right) \\ &\quad - D \left(\frac{\partial^2 u_k^l}{\partial x^2} + \frac{(\Delta x)^2}{4!} \frac{\partial^4 u_k^l}{\partial x^4} + \mathcal{O}((\Delta x)^3) \right) = \mathcal{O}(\Delta t, (\Delta x)^2); \end{aligned}\quad (\text{D.58})$$

the scheme thus is of first-order in time and second-order in space.

D.5 Thomas Algorithm for Tridiagonal Matrices

We have encountered a tridiagonal matrix in the solution of the ODE in sect. 3.1. A tridiagonal matrix is any matrix which has elements only on the diagonal, the subdiagonal and the superdiagonal. Such kind of matrix often results in solutions of ODEs. In principle, it could be solved by Gaussian elimination but this would involve of the order $\mathcal{O}(n^3/3)$ operations. In addition, Gaussian elimination is an inefficient algorithm because the matrix is sparse, that is many entries are zero.

Instead, the Thomas algorithm provides an efficient method which requires only $\mathcal{O}(n)$ operations. The algorithm works on a tridiagonal system such as

$$\mathbf{A}\vec{x} = \begin{bmatrix} \alpha_1 & \gamma_1 & 0 & \dots & 0 \\ \beta_2 & \alpha_2 & \gamma_2 & \ddots & \vdots \\ 0 & \beta_3 & \alpha_3 & \ddots & 0 \\ \vdots & \ddots & \ddots & \ddots & \gamma_{n-1} \\ 0 & \dots & 0 & \beta_n & \alpha_n \end{bmatrix} \begin{bmatrix} x_1 \\ x_2 \\ \vdots \\ x_{n-1} \\ x_n \end{bmatrix} = \begin{bmatrix} b_1 \\ b_2 \\ \vdots \\ b_{n-1} \\ b_n \end{bmatrix}. \quad (\text{D.59})$$

The matrix \mathbf{A} can be decomposed into two matrices with non-zero elements only on the

diagonal and on either the sub- or the superdiagonal:

$$\begin{aligned}
 \mathbf{A} &= \begin{bmatrix} \alpha_1 & \gamma_1 & 0 & \dots & 0 \\ \beta_2 & \alpha_2 & \gamma_2 & \ddots & \vdots \\ 0 & \beta_3 & \alpha_3 & \ddots & 0 \\ \vdots & \ddots & \ddots & \ddots & \gamma_{n-1} \\ 0 & \dots & 0 & \beta_n & \alpha_n \end{bmatrix} \\
 &= \begin{bmatrix} l_1 & 0 & 0 & \dots & 0 \\ \beta_2 & l_2 & 0 & \ddots & \vdots \\ 0 & \beta_3 & l_3 & \ddots & 0 \\ \vdots & \ddots & \ddots & \ddots & 0 \\ 0 & \dots & 0 & \beta_n & l_n \end{bmatrix} \begin{bmatrix} 1 & \mu_1 & 0 & \dots & 0 \\ 0 & 1 & \mu_2 & \ddots & \vdots \\ 0 & 0 & 1 & \ddots & 0 \\ \vdots & \ddots & \ddots & \ddots & \mu_{n-1} \\ 0 & \dots & 0 & 0 & 1 \end{bmatrix}. \tag{D.60}
 \end{aligned}$$

This process is called LU decomposition. The coefficients of the original and the two new matrices are related by

$$\begin{aligned}
 \alpha_1 &= l_1 \\
 \alpha_i &= l_i + \beta_i \mu_{i-1} & i = 2, 3, \dots, n \\
 l_i \mu_i &= \gamma_i & i = 1, 2, \dots, n-1.
 \end{aligned} \tag{D.61}$$

The solution is obtained by forward and back substitution:

$$\begin{aligned}
 z_1 &= b_1/l_1 & i = 2, 3, \dots, n \\
 z_i &= (b_i - \beta_i z_{i-1})/l_i & i = 2, 3, \dots, n \\
 x_n &= z_n & i = 1, 2, \dots, n-1 \\
 x_i &= (z_i - \mu_i z_{i+1})/l_i & i = 1, 2, \dots, n-1
 \end{aligned} \tag{D.62}$$

Appendix E

Solutions to some questions

Chapter 2

Ex. 3: the logistic law can be written as

$$\frac{dp}{dt} = ap - bp^2,$$

which is a first-order ODE. Separation of variable yields

$$\int dt = \int \frac{dp}{p(a - bp)} \quad \Rightarrow \quad p(t) = \frac{1}{b} \left[\frac{p(t_0) e^{a(t-t_0)}}{\frac{1}{a} - p(t_0) + p(t_0) e^{a(t-t_0)}} \right].$$

List of Figures

2.1	Mass balance (top) and copper balance (bottom)	24
2.2	Comfort range: influences	28
2.3	Comfort temperature	29
2.4	Thermal balance of a building as matryoshka problem	30
2.5	Heat conduction	30
2.6	Convection	31
2.7	Radiative transfer	31
2.8	Radiation exchange coefficients	32
2.9	Radiative losses during a window at night	33
2.10	Transient simulation of a building: night setbacks	35
3.1	Centered finite difference scheme	44
3.2	Concentration versus distance along vertical axis of a cylindrical reactor in steady-state for different values of the dispersion coefficient	46
3.3	FTCS scheme	47
3.4	Crank–Nicolson scheme	48
3.5	Concentration versus distance along the vertical axis of a cylindrical reactor for different times	51
3.6	0D compartment models: water and atmosphere	51
3.7	1D atmosphere model	52
3.8	2D atmosphere model	53
4.1	Gains and losses tossing a coin	58
4.3	Broadening of a Gauß distribution	59
4.2	Galton board	59
4.4	Diffusion requires a gradient to transport	60
4.5	Diffusive profiles for different λ	61
4.6	Isotropic turbulence	62
4.7	Temperature distribution in a rectangular plate	64
4.8	Finite centered differences in 2D	65
4.9	Snow Leopard	72
4.10	Porous medium	74
4.11	Oil layer above soil	75
4.12	Reacting solid particle with external ash layer	77
5.1	Interplanetary magnetic field	82
5.2	Magnetic field power-density spectrum	82
5.3	Resonance scattering	86
5.4	Resonant wave–particle interaction	86

5.5	Example for a fit with the focused transport model	88
5.6	Time-splitting	90
5.7	Comparison of solutions of focused transport with and without solar wind effects	92
5.8	Temporal evolution of the energy spectrum at the observer's site	92
5.9	Geometry of a propagating shock	93
5.10	Shock with and without solar wind effects	94
5.11	Same as Fig. 5.10 but the shock efficiency decreases as r^{-2}	94
5.12	Spatial variation of particle events at shocks	95
5.13	Simulated spatial dependence of particle events	96
5.14	Deformation of the interplanetary magnetic field by a magnetic cloud	96
5.15	Modification of intensity times profiles by magnetic clouds	96
5.16	Wendelstein	98
6.1	Room with boundaries	101
6.2	Temperature distribution in room from Fig. 6.1	102
6.3	Discretization in 1D FEM and basis functions	104
6.4	Tessellation according to Escher	104
6.5	FEM to determine π	105
6.6	Dike during normal and high water levels	108
6.7	Different dikes	110
6.8	Boundary conditions at the dike	111
6.9	Discretization of the dike	112
6.10	Fluid height levels, stationary conditions	113
6.11	Subsoil flow speeds, stationary conditions	114
6.12	Moisture content, stationary conditions	116
6.13	Concentrations and flows of pollutants, stationary conditions	117
7.1	Forces and stresses acting on a volume	119
7.2	Velocities of two fluid layers for different times	125
7.3	CFD and Columbia accident	127
7.4	Flow around an obstacle for different Reynolds' numbers	127
7.5	Coronal structure during a solar eclipse	132
7.6	Sun in soft X-rays	132
7.7	MHD dynamo	134
8.1	Numerical integration: π	137
8.2	Variation of π with number of shots	138
8.3	Variation of π with number of shots	138
8.4	Test of a random number generator	140
8.5	Radioactive decay: Monte Carlo simulation	141
8.6	Bastille Day event	143
8.7	Bethe–Bloch equation	145
8.8	Bastille Day event: particle intensities and ionization rates	146
8.9	Bastille Day event: observed and modeled NO_x production and ozone depletion	146
8.10	Tracks of electrons and protons in a model atmosphere	148
8.11	Energy losses of protons: Monte Carlo vs. Bethe–Bloch	149
8.12	Energy losses of electrons: Monte Carlo vs. Bethe–Bloch	150
8.13	Ionization rates: combined electrons and protons	150
8.14	Ozone depletion following the October/November 2003 event series	152
8.15	October 1989 event and the atmosphere	153
8.16	Ionization during the solar cycle	155
8.17	Total ozone column during the solar cycle	156
8.18	Ozone variation without geomagnetic field	156
8.19	Variation in ozone and temperature	157

9.1	Ordered to random net	164
9.2	Examples for networks	165
9.3	Wikipedia as a hub	168
9.4	World Wide Web	168
9.5	Spread of a disease on random and scale free nets	169
9.6	Spread of Money	170
11.1	Summary FDMs for ODEs	180
11.2	Summary FDMs for PDEs	181
C.1	Maxwell distribution	200
C.2	Shift of the gyro-center by a collision	204
C.3	Brownian motion and mean free path	205
C.4	Coulomb scattering	206
D.1	Explicit scheme for parabolic PDE	216

List of Tables

11.1	Summary of FDM for ODEs	180
11.2	Summary FDMs for PDEs	180
B.1	Particulate integrals for 2 nd order ODEs	188
B.2	Laplace transforms	193
C.1	Fundamental laws	197
C.2	Mathematical Expressions for different forms of energy	197

Bibliography

- [1] Agostinelli, S., et al., Geant4 - a simulation toolkit. Nuclear Instruments and Methods in Physics Research Section A, 250–303, 2003. 148
- [2] H. Alfvén and G. Fälthammar: *Cosmical electrodynamics*, Oxford, 1963 83
- [3] P. Baccini and H.P. bader: *Regionaler Stoffhaushalt*, Spektrum, 1996 53
- [4] P. Baccini and P.H. Brunner: *Metabolism of the anthroposphere*, Springer, 1991 53
- [5] D. Basmadjian: *Mathematical modeling of physical systems*, Oxford University Press, Oxford, 2003 15, 17, 187
- [6] K.-J. Bathe: *Finite-Elemente-Methoden*, Springer, 1986 117
- [7] B. Baumann and U. Stein, 2004: *FEM-Starterkit*, <http://www.haw-hamburg.de/pers/Baumann/fem.pdf> 117, 174
- [8] M. Baurmann, W. Ebenhöh und U. Feudel: Bakterien-Nährstoffmodell: Muster im Wattsediment, *Einblicke Nr. 41*, Carl von Ossietzky Universität Oldenburg, 2005; <http://www.uni-oldenburg.de/presse/einblicke/41/7-bauermann.pdf> 172
- [9] J. Bear: *Dynamics of fluids in porous media*, Dover, 1972 3, 74
- [10] J. Bear and A. Verruijt: *Modeling groundwater flow and pollution*, Reidel, 1987 3, 74
- [11] J. Beebe-Wang, P. Vaska, F.A. Dilmanian, S.G. Peggs and D.J. Schlyer: Simulation of Proton Therapy Treatment Verification via PET imaging of Induced Positron-Emitters, in *IEEE Nuclear Science Symposium/Medical Imaging Conference October 2003*; http://www.agsrhichome.bnl.gov/AP/ap_notes/ap_note_122.pdf 176
- [12] M. Beniston: *From turbulence to climate*, Springer, 1998
- [13] A.O. Benz: *Plasma astrophysics*, Kluwer, Dordrecht, 1993 207
- [14] I. Berenstein, M. Dolnik, L. Yang, A. Zhabotinsky and I.R. Epstein: Turing pattern formation in a two-layer system: superposition and superlattice patterns, *Phys. Rev.* **70**, 046219, 2004; http://hopf.chem.brandeis.edu/yanglingfa/paper/PhysRevE_70.046219.pdf 172
- [15] I. Bialynicki-Birula and I. Bialynicki-Birula: *Modeling reality*, Oxford, 2004 39
- [16] R.B. Bird, W.E. Stewart and E.N. Lightfott: *Transport phenomena*, Wiley, 1960 79
- [17] M. Boots and A. Sasaki: Small worlds and the evolution of virulence: Infection occurs locally and at a distance. *Proc. R. Soc. London Ser. B* **266**, 1933–38, 1999
- [18] T.J.M. Boyd, and J.J. Sanderson: *Plasma dynamics*, Barnes and Noble, New York, 1969 204
- [19] D. Brockmann, L. Hufnagel and T. Geisel: The scaling laws of human travel, *nature* 439, 16 Jan 2006. doi:10.1038/nature04292 169, 170
- [20] J. Caldwell and D.K.S. Ng: *Mathematical modeling*, Kluwer, 2004 39, 41, 79
- [21] Callis, L.B., Boughner, R.E., Baker, D.N. et al., Precipitating electrons: evidence for effects on mesospheric odd nitrogen, *Geophys. Res. Lett.* 23, 1901, 1996. 151
- [22] Callis, L.B., Baker, D.N., Natarajan, M., et al., A 2-D model simulation of downward transport of NO_y into the stratosphere: effects on the austral spring O₃ and NO_y, *Geophys. Res. Lett.* 23, 1905, 1996. 151

- [23] H.V. Cane, D.V. Reames, and T.T. von Roseninge: The role of interplanetary shocks in the longitude distribution of energetic particles, *J. Geophys. Res.* **93**, 9555, 1988 95
- [24] R. Capra: Physics processes: Software process and OOAD, *4th Workshop on Geant4 Biomedical Developments and Geant4 Physics Validation*, 2005, <http://www.ge.infn.it/geant4/events/july2005/agenda.html> 176
- [25] R. Carter: *Mapping the Mind*, Seven Dials, London, 1998 159
- [26] R.W.G. Carter: *Coastal environments – an introduction to the physical, ecological and cultural systems of coastlines*, Academic Press, 1999 5
- [27] R.W.G. Carter and C.D. Woodroffe (eds.): *Coastal evolution*, Cambridge, 1997 5
- [28] CERN: *Physics reference Manual*, 2005, <http://wwwasd.web.cern.ch/wwwasd/geant4/G4UsersDocuments/UsersGuides/PhysicsReferenceManual/print/PhysicsReferenceManual.pdf> 158, 176, 177
- [29] J.-J. Chattot: *Computational aerodynamics and fluid dynamics*, Springer, 2002 135
- [30] F.F. Chen: *Plasma physics and controlled fusion*, vol. 1, Plenum Press, New York, 1984 119, 206
- [31] Chipperfield, M., The TOMCAT offline chemical transport model, UGAMP International Report 44a, <http://www.env.leeds.ac.uk/martyn/slimcat.html>, 1996. 147
- [32] J. Crank: *The Mathematics of Diffusion*, Oxford University Press, 1979 79
- [33] Crutzen, P.J., I.S.A. Isaksen, and G.C. Reid (1975): Solar proton events: stratospheric sources of nitric oxide, *Science* **189**, 457. 144
- [34] H. D'Arcy: *Les fontaines publiques de la ville de Dijon*, 1852 74
- [35] R.G. Dean: *Beach nourishment – Theory and practice*, World Scientific, 2002 5
- [36] Denskat, K.U., H.J. Beinroth, and F.M. Neubauer (1983): Interplanetary magnetic field power spectra with frequencies from $2.4 \cdot 10^{-5}$ Hz to 470 Hz from Helios-observations during solar minimum conditions, *J. Geophys. Res.* **87**, 2215 82
- [37] R.A. Dietrich: *Nichtlineare Finite-Element-Modellierungen von Sickerströmungen und Schadstofftransporten in ungesättigten und gesättigten oberflächennahen Zonen von Deichregionen bei extremen Ereignissen*, Dissertation, Uni Lüneburg, 1999 4, 108, 110, 111, 112, 113, 114, 116, 117
- [38] M.W. Dingemans: *Water wave propagation over uneven bottoms – 1. Linear wave propagation*, World Scientific, 1997 3
- [39] M.W. Dingemans: *Water wave propagation over uneven bottoms – 1. Non-linear wave propagation*, World Scientific, 1997 3
- [40] O.S. Dohm: *Monte-Carlo Simulation der Dosimetrie kleiner Felder in der Strahlentherapie mit hochenergetischen Photonen*, Dissertation, Uni Tübingen, 2005, http://w210.ub.uni-tuebingen.de/dbt/volltexte/2005/1651/pdf/Diss_Dohm.pdf 176
- [41] DVWK: *Anwendung hydrogeochemischer Modelle*, Parey, 1992 74
- [42] T.E. Faber: *Fluid dynamics for physicists*, Cambridge University Press, Cambridge, 1995 22, 135
- [43] M. Fippel, M. Alber, M. Birkner, W. Laub, F. Nüsslin, and I. Kawrakow: Inverse Treatment Planning for Radiation Therapy Based on Fast Monte Carlo Dose Calculation, in .. (eds.), Springer, Berlin, 2001; http://www.irs.inms.nrc.ca/papers/MC2000/Fippel_et_al_MC2000_217_222.pdf 176
- [44] Forman, M.A., and Webb, G.M., Acceleration of energetic particles, in: Stone R.G. and Tsurutani B.T. (Eds.), *Collisionless shocks in the heliosphere*, AGU Geophys. Mon. 34, 1985. 148
- [45] J. Fredsøe and R. Deigaard: *Mechanics of coastal sediment transport*, World Scientific, 1995 6
- [46] P.W. French: *Coastal defences*, Routledge, 2001 5
- [47] Geant4, <http://wwwasd.web.cern.ch/wwwasd/geant4/geant4.html>, 2003. 148
- [48] N. Gershenfeld: *The nature of mathematical modeling*, Cambridge University Press, Cambridge, 2003
- [49] M. Gladwell: *Blink*, Allen Lane/Penguin Books, 2005 23

- [50] Goeckler, G., Characteristics of solar and heliospheric ion populations observed near Earth, *Adv. Space Res.* 4, (2-3)127, 1984. 148
- [51] Gosling, J., Asbridge, J.R., Bame, S.J., et al., Interplanetary ions during an energetic storm particle event, *J. Geophys. Res.* 86, 547, 1981. 148
- [52] T.E. Graedel and P.J. Crutzen: *Chemie der Atmosphäre*, Spektrum, 1993 51, 52, 53
- [53] Ch. Großmann and H.-G. Roos: *Numerik partieller Differentialgleichungen*, Teubner, 1994 98, 212
- [54] C. Gutfinger (ed.): *Topics in Transport Phenomena*, Wiley, 1975
- [55] C.L. Hartmann Siantar and E.I. Moses: The PEREGRINETM program: using physics and computer simulation to improve radiation therapy for cancer, *Eur. J. Phys.* 19, 513–521, 1998; <http://ej.iop.org/links/q34/ckX94ztapJQmaPOAiw46vA/ej8604.pdf>. 176
- [56] R. Hatzky: *Winkelverteilungen energiereicher geladener Teilchen und die Streueigenschaften des interplanetaren Mediums*, Dissertation, IfKKi, Uni Kiel 89, 90
- [57] R. Hatzky, M.-B. Kallenrode, J. Schmidt: The effect of adiabatic deceleration on angular distributions of solar energetic particles, *Proc. 25th ICRC* 1, 245, 1997 89
- [58] R. Hatzky and M.-B. Kallenrode: Numerics of interplanetary transport, *Proc. 26th ICRC* 6, ... 1999 92
- [59] E. Hering, R. Matrin and M. Stohrer: *Physikalisch-technisches Taschenbuch*, vdi-Verlag, Düsseldorf (more recent editions at Springer Verlag) 32
- [60] H.J. Herrmann: Spuren im Sand, *Physik Journal* 4, (8/9)57 5
- [61] N. Herrmann, J. Siefer, E.P. Stephan and R. Wagner: *Mathematik und Umwelt*, Edition Universität Hannover, Theodor Oppermann Verlag, Hannover, 1994
- [62] E. Holzbecher: *Modellierung dynamischer Prozess in der Hydrologie*, Springer, 1996 3, 74, 75
- [63] R.L. Hooke: *Principles of glacier mechanics*, Cambridge, 2005 5
- [64] S. Howinson: *Practical applied mathematics – Modeling, analysis, approximation*, Cambridge University Press, Cambridge, 2005
- [65] A. von Humboldt: *Der Kosmos*, Nachdruck, Eichborn, 2004 39
- [66] A.J. Hundhausen: *Coronal expansion and the solar wind*, Springer, Berlin, 1972 82
- [67] D.M. Imboden and S. Koch: *Systemanalyse*, Springer, 2003
- [68] P. Imkeller, Jin-Song von Storch (eds.): *Stochastic climate models*, Birkhäuser, 2001 162
- [69] Intergovernmental Panel on Climate Change IPCC: *Climate Change 2001: The Scientific Basis*, Genf, 2001, www.ipcc.ch 12, 13
- [70] Intergovernmental Panel on Climate Change IPCC: *Climate Change 2001: Impacts, Adaption and Vulnerability*, Genf, 2001, www.ipcc.ch
- [71] Intergovernmental Panel on Climate Change IPCC: *Climate Change 2001: Mitigation*, Genf, 2001, www.ipcc.ch
- [72] Intergovernmental Panel on Climate Change IPCC: *Climate Change 2001: Synthesis Report*, Genf, 2001, www.ipcc.ch
- [73] ISL-Info; http://www.hmi.de/isl/isl_info/98-1/paganetti.html 176
- [74] Jackman, C.H., and McPeters, R.D., The response of ozone to solar proton events during solar cycle 21: a theoretical interpretation. *J. Geophys. Res.* 90, 7955–7966, 1985. 151
- [75] Jackman, C.H., R.D. McPeters, G.J. Labow, C.J. Praderas, and E.L. Fleming (2001): Measurements and model predictions of the atmospheric effects due to the July 2000 solar proton event, *Geophys. Res. Lett.* 28, 2883 143
- [76] Y. Jaluria and K.E. Torrance: *Computational heat transfer*, Hemisphere & Springer, 1986 7, 212
- [77] E. Javierre, C. Vuik, F.J. Vermolen, and S. van der Zwaag: A comparison of numerical models for 1D Stefan problems, Uni Delft, Tech-Rep 05-03; <http://ta.twi.tudelft.nl/nw/users/vuik/papers/Jav05VVZ.pdf> 173

- [78] Jones, F. C., and Ellison, D. C., The plasma physics of shock acceleration, *Space Sci. Rev.* **58**, 259, 1991. 148
- [79] D. Jost and K. Nagel: Traffic jam dynamics in traffic flow models, *STRC 3 Conf.*, 2003; <http://www.strc.ch/Paper/jost.pdf> 173
- [80] A. Jüngel: *Das kleine Finite-Elemente-Skript*, <http://www.numerik.mathematik.uni-mainz.de/~juengel/scripts/femscript.pdf> 101, 102, 117, 174
- [81] R. Kainhofer: *Simulation der Wärmeleitungsgleichung: Vergleich zwischen Quasi-Monte-Carlo Simulationen, Monte-Carlo-Simulation und numerischer Lösung mittels Differenzenschema*, Techn. Uni Graz, 1999, <http://reinhold.kainhofer.com/Students/Mathematik/EDV-Projekt%20Simulation/Simulation.pdf>
- [82] M.-B. Kallenrode: The temporal and spatial development of MeV proton acceleration at interplanetary shocks, *J. Geophys. Res.* **102**, 22347 - 22363, 1997 **93**, 95, 148
- [83] M.-B. Kallenrode: A statistical study of shock evolution and subsequent particle propagation, *J. Geophys. Res.* **102**, 22335 - 22345, 1997 **93**, 95
- [84] M.-B. Kallenrode: *Bauphysik – Bau und Energie*, Vorlesungsskript, Uni Lüneburg, 1999 32
- [85] M.-B. Kallenrode: Shock as a black box II: Effects of adiabatic deceleration and convection included, *J. Geophys. Res.* **106**, 24 989, 2001 **88**, **93**, **96**
- [86] M.-B. Kallenrode: Magnetic clouds and interplanetary transport: a numerical model, *J. Atm. Solar-Terr. Phys.* **64**, 1973–1978, 2002 **96**
- [87] Kallenrode, M.-B., Current views on impulsive and gradual solar energetic particle events, *J. Phys. G* **29**, 965–981, 2003. 147
- [88] M.-B. Kallenrode: *Space Physics*, Springer, 2004 **83**, **99**, **133**
- [89] M.-B. Kallenrode and R. Hatzky: Energetic particle events at traveling interplanetary shocks: modeling between 20 keV and 500 MeV, *Proc. 26th Int. Cosmic Ray Conf.*, **6**, **93**, **94**
- [90] M.-B. Kallenrode and G. Wibberenz: Propagation of particles injected from interplanetary shocks: a black-box model and its consequences for acceleration theory and data interpretation, *J. Geophys. Res.* **102**, 22311 - 22334, 1997 **93**, **94**, **95**
- [91] M.-B. Kallenrode, G. Wibberenz, and S. Hucke : Propagation conditions for relativistic electrons in the inner heliosphere, *Astrophys. J.* **394**, 351, 1992 **88**
- [92] T.U. Kämpfer: *Modeling of macrosegregation using an adaptive domain decomposition method*, Dissertation, EPFL Lausanne, 2002 5
- [93] B.S. Kerner and H. Rehborn: Experimental properties of phase transitions in traffic flow, *Phys. Rev. Lett.*, **79**, 4030, 1997; http://prola.aps.org/pdf/PRL/v79/i20/p4030_1 173
- [94] P. Knabner and L. Angermann: *Numerik partieller Differentialgleichungen*, Springer, 2000 **98**, **212**
- [95] W. Kinzelbach: *Numerische Methoden zur Modellierung des Transports von Schadstoffen im Grundwasser*, Oldenbourg, 1992 **3**, **74**
- [96] W. Kinzelbach and R. Rausch: *Grundwassermodellierung*, Borntraeger, 1995 **3**, **74**
- [97] P.E. Kloeden and E. Platen: *Numerical solution to stochastic differential equations*, Springer, 1999 **162**
- [98] D. Kuzmin, R. Löhner, and S. Turek (eds): *Flux-corrected transport*, Springer, 2005 **99**
- [99] F. Lampa: *Numerik des 2-D-Transports von geladenen Teilchen in fluktuierenden Magnetfeldern*, Diplomarbeit, Osnabrück, 2006 **98**
- [100] D.P. Landau and K. Binder: *Monte carlo simulations in statistical physics*, Cambridge UP, 2000 **162**
- [101] K. Lang: *Sun, earth and sky*, Springer, 1996 **132**
- [102] B. Lapeyre, E. Pardeaux, and R. Sentis: *Introduction to Monte-Carlo methods for transport and diffusion equations*, Oxford, 2003 **162**
- [103] Lecture on Monte Carlo simulations, <http://www.ualberta.ca/~cdeutsch/images/Lec04-MonteCarlo.pdf>

- [104] T. Leppänen: *Computational studies of pattern formation in turing systems*, Dissertation, Univ. Helsinki, 2004; <http://lib.tkk.fi/Diss/2004/isbn9512273969/isbn9512273969.pdf> 73, 172
- [105] T. Leppänen, *The theory of Turing pattern formation*, Imperial College Press, 2004. http://www.lce.hut.fi/////research/polymer/turing_review.pdf 73, 74
- [106] , Deterministic Nonperiodic Flow, *J. Atmospheric Sciences* **20**, März 1963 (hier ist der Schmetterling zwar noch eine Möwe, aber er entwickelt sich 11
- [107] G.I. Marchuk, *Methods of Numerical Mathematics*. In: Balakrishnan, A.V. and Hildebrand, W. (Eds.): *Applications of Mathematics*. Vol. 2. Springer, 1975. 89, 212
- [108] S.R. Massel: *Ocean surface waves: their physics and prediction*, World Scientific, 1998 3
- [109] S.R. Massel: *Fluid mechanics for marine ecologists*, Springer, 1999 135
- [110] K. McGrattan: *Computational fluid dynamics and fire modeling*, Fall 2001, http://fire.nist.gov/fds/docs/fds_class_notes.pdf 127, 128
- [111] C.C. Mei: *The applied dynamics of ocean surface waves*, World Scientific, 1999 3
- [112] G.N. Milstein and M.V. Tretyakov: *Stochastic numerics for mathematical physics*, Springer, 2004 162
- [113] M. Minnaert: *de natuurkunde van 't vrije veld*, 3 Bände, Thieme (Zuphten), 1974 39
- [114] C.N.K. Mooers (ed.): *Coastal ocean prediction*, AGU, 1999 5
- [115] H. Moor: *Bau und Energie – Physikalische Grundlagen*, vdf, 1993 7
- [116] T. Nagatani: Chaotic jam and phase transition in traffic flow with passing, *Phys. Rev. E* **60**, 1535, 1999; http://prola.aps.org/pdf/PRE/v60/i2/p1535_1 173
- [117] K. Nagel, P. Wagner and R. Woessler: Still flowing: approaches to traffic flow and traffic jam modeling, *Operations Research* **51**, 681–710; <http://www.extenza-eps.com/INF/doi/pdf/10.1287/opre.51.5.681.16755> 79, 173
- [118] R.K. Nagle, E.B. Saff and A.D. Snider: *Fundamentals of differential equations*, Pearson/Addison Wesley 2004
- [119] M.E.J. Newman: The structure and function of complex networks, *SAM Rev.* **45**, 2, 167–256, <http://arxiv.org/abs/cond-mat/0303516> 164, 165
- [120] M.E.J. Newman and G.T. Barkema: *Monte Carlo methods in statistical physics*, Clarendon Press, 1999 162
- [121] P. Nielsen: *Coastal bottom boundary layers and sediment transport*, World Scientific, 1992
- [122] T.G. Northrop: *The adiabatic motion of charged particles*, Interscience, New York, 1963 83
- [123] J. Ockendon, S. Howinson, A. Lacey, and A. Movchan: *Applied partial differential equations*, Oxford, 1999
- [124] J. de D. Ortúzar and L.G. Willumsen: *Modeling Transport*, Wiley, 1994 1
- [125] R.J. Ott, M.A. Flower, J.W. Babich, and P.K. Marsden: The physics of radio-isotope imaging, in *The physics of medical imaging* (ed. S. Webb), IOP Publishing, Bristol, 1988 159
- [126] Y. Perrot, S. Incerti, Z. Francis, G. Montarou, R. Capra and M.G. Pia: GEANT 4 DNA physics processes: overview and current status, *GEANT 4 DNA Meeting*, 2005, <http://www.ge.infn.it/geant4/events/july2005/agenda.html> 176
- [127] J. Oedlowsky: *Geophysical fluid dynamics*, Springer, 1987 135
- [128] Y. Pinchover and J. Rubinstein: *Partial differential equations*, Cambridge, 2005 98, 212
- [129] W. Pistohl: *Handbuch der Gebäudetechnik*, Werner-Verlag, 1996 28, 30, 31
- [130] H.N. Pollack: *Uncertain Science ... Uncertain World*, Cambridge, 2003 12, 16
- [131] Porter, H.S., Jackman, C.H., and Green, A.E.S., Efficiencies for production of atomic nitrogen and oxygen by relativistic proton impact in air, *J. Chem. Phys.* **167**, 154–167, 1976. 148
- [132] Ir.J.A. Potting: *Stromingsleer*, 1999, Delta Press
- [133] Ir.J.A. Potting: *Warmteoverdracht*, 1999, Delta Press 7

- [134] M. Quack: *Wechselwirkung solarer energiereicher Teilchen mit der Atmosphäre*, Diplomarbeit, Uni Osnabrück, 2001 145, 146
- [135] Quack, M., Kallenrode, M.-B., von König, M., et al., Ground level events and consequences for stratospheric chemistry, Proceedings of ICRC, 4023–4026, 2001. 147
- [136] J. Quest, M.C. Wright, H. Hansen and G.G. Mesuro: First measurements on an Airbus High Lift Configuration at ETW up to flight Reynolds numbers, AIAA-2002-0423, 2002. 126
- [137] A. Rapoport and L.I. Rebhun: On the mathematical theory of rumor spread, *Bull. Math. Biol.* **14**, 4, 375–383, 1952 166
- [138] H. Riedrich: *Nukleation auf vinkinalen Oberflächen*, BA thesis, Osnabrück, 2006 74
- [139] J.C. Robinson: *Ordinary differential equations*, Cambridge, 2004 40
- [140] E.C. Roelof: Propagation of solar cosmic rays in the interplanetary magnetic field, in *Lectures in high energy astrophysics* (eds. H. Ögelmann and J.R. Wayland), NASA SP-a99, p. 111, 1969 87
- [141] G. Rohen, C. von Savigny, M. Sinnhuber, E.J. Llewellyn, J.W. Kaiser, C.H. Jackman, M.-B. Kallenrode, J. Schroter, K.U. Eichmann, H. Bovensmann, and J.P. Burrows: Ozone depletion during the solar proton events of October/November 2003 as seen by SCIAMACHY, *J. geophys. Res.* **100**, A09S39, 2005 152
- [142] H.-G. Roos, M. Stynes, and L. Tobiska, *Numerical methods for singularly perturbed differential equations*, Springer 1996. 89
- [143] I. Rubinstein and L. Rubinstein: *Partial differential equations in classical mathematical physics*, Cambridge, 1998 98, 212
- [144] D. Ruffolo: Effect of adiabatic deceleration on the focused transport of solar cosmic rays, *Astrophys. J.* **442**, 861, 1995 88, 89, 91
- [145] C.T. Russell: Solar wind and interplanetary magnetic field: a tutorial, in Song, P., H.J. Singer, and G.L. Siscoe (eds.) *Space weather*, Geophys. Monogr. 125, American Geophysical Union, Washington, DC, p. 71, 2001 82
- [146] A.A. Samarskii, and P.N. Vabishchevich, P.N., *Computational Heat Transfer, Vol. 1*, Wiley, 1995. 91, 212
- [147] K.H. Schatten, J.M. Wilcox, and N.F. Ness: A model of interplanetary and coronal magnetic fields, *Solar Phys.* **6**, 442, 1969 82
- [148] R. Schmidt: *Untersuchung verschiedener digitaler Geländemodelle hinsichtlich ihrer Eignung für die dynamische Lawinensimulation mit dem dreidimensionalen zweiphasigen Simulationsprogramm SAMOS*, Dissertation, Leopold-Franzens-Universität Innsbruck 5
- [149] J. Schröter, B. Heber, F. Steinhilber, and M. B. Kallenrode: Energetic particles in the atmosphere: A Monte-Carlo simulation, *Adv. Space Res.*, in press, 2005 148, 149, 150
- [150] D. Schuemann: *Maßnahmen zur Reduktion des Wärmebedarfs – Anwendung der dynamischen Gebäudesimulation*, Diplomarbeit, IfKKi, Uni Kiel 33, 35
- [151] R. Schwenn: Large-scale structure of the interplanetary medium, in Schwenn, R. and E. Marsch (eds.) *Physics of the inner heliosphere, vol. I*, Springer, Berlin, p. 99, 1990 82
- [152] T.M. Shih: *Numerical properties and methodologies in heat transfer*, Hemisphere Publ. Washington, 1983
- [153] R. Silvester and J.R.C. Hsu: *Coastal stabilization*, World Scientific, 1999 5
- [154] M. Sinnhuber, J.P. Burrows, M.P. Chipperfield, C.H. Jackman, M.-B. Kallenrode, K.F. Künzi, and M. Quack: A model of the impact of magnetic field structure on atmospheric composition during solar proton events, *Geophys. Res. Lett.* **39**, 1818, doi:10.1029/2003GL017265, 2003 157
- [155] W.A. Sirigano: *Fluid dynamics and transport of droplets and sprays*, Cambridge, 1999
- [156] A.V. Skorokhod: *Studies in the theory of random processes*, Dover, 1965
- [157] J.C. Slattery: *Advanced Transport Phenomena*, Cambridge University Press, 1999 2, 38

- [158] Srivastava, N., and R. Schwenn: The origin of the solar wind: an overview, in Scherer, K., H. Fichtner, and E. Marsch (eds.) *The outer heliosphere: beyond the planets*, Copernicus Ges., Katlenburg-Lindau, p. 13, 2000 82
- [159] F. Steinhilber: *Simulation der solaren Aktivität auf Zeitskalen von Solarzyklen bis zu Jahrhunderten*, Diplomarbeit, Uni Osnabrück, 2005 140
- [160] M. Stoffel and P. Bartelt: Modeling snow slab release using a temperature-dependent viscoelastic finite element model with weak layers, *Surveys in Geophysics* **24**, 417, 2003
- [161] J. Strackee and N. Westerhoff: *The physics of heart and circulation*, IOP, 1993 2
- [162] F. Tiefenbacher: *Vom konstituiven Verhalten fließenden Schnees*, Dissertation, Basel, 2003
- [163] S. Trapp and M. Matthies: *Dynamik von Schadstoffen – Umweltmodellierung mit CemoS*, Springer, 1996
- [164] A. Tveito and R. Winther: *Einführung in partielle Differentialgleichungen – Ein numerischer Zugang*, Springer, 2002 99
- [165] A. Turing: Computing machinery and intelligence, *Mind* **59**, 433, 1950 11
- [166] A. Turing: The Chemical Basis of Morphogenesis, *Phil. Trans. R. Soc. Lond.*, **B237**, 37-72, 1952 72, 73, 172
- [167] M. Twain: *A tramp abroad*, Penguin Classics, 1997 4
- [168] J. Tyndall: *The forms of water in clouds and rivers, ice and galciers*, Appleton & Co, 1897 4, 39
- [169] B.W. van de Fliert and R. van der Hout: A generalized Stefan problem in a diffusion model with evaporation, *SIAM J. Appl. Math.* **60**, 1128, 2000; <http://epubs.siam.org/sam-bin/getfile/SIAP/articles/32759.pdf> 173
- [170] D. Vandervelde: Emergent phenomena in congested traffic flow, Final Term Paper, http://guava.physics.uiuc.edu/~nigel/courses/463/Essays_2004/files/vandervelde.pdf 173
- [171] F.J. Vermolen, C. Vuik, E. Javierre, and S. van der Zwaag: Review on some Stefan Problems for Particle Dissolution in Solid Metallic Alloys, *Nonlinear Analysis: Modelling and Control*, **10** (3)257; <http://ta.twi.tudelft.nl/nw/users/vuik/papers/Ver05VJZ.pdf> 173
- [172] Verronen, P.T., Turunen E., Ulich T., and Kyrölä E., Modelling the effects of the October 1989 solar proton event on mesospheric odd nitrogen using a detailed ion and neutral chemistry model, *Ann. Geophys.* **20**, 1967–1976, 2002. 151
- [173] H. von Storch, S. Güss, and M. Heimann: *Das Klimasystem und seine Modellierung*, Springer, Heidelberg, 1998 16, 160
- [174] W.M. Washington and C.L. Parkinson: *An introduction to three-dimensional climate modeling*, University Science Books, Mill Valley, CA, 1986 16
- [175] D.J. Watts: Networks, dynamics and the small-world phenomenon, *AJS* **105**, 2, 493–527, 1999 164
- [176] D.J. Watts: The new science of networks, *Annu. Rev. Sociol.*, **30**, 243-270, doi: 10.1146/annurev.soc.30.020404.104342, 2004 164, 165, 166, 169
- [177] D.J. Watts and S.H. Strogatz: Collective dynamics of ‘small-world’ networks, *Nature* **393**, 440–42, 1998 166
- [178] S. Webb: *The physics of three-dimensional radiation therapy*, IOP, Bristol, 1993 162, 176
- [179] D.J. Wollkind and L.E. Stephenson: Chemical Turing pattern formation analysis: comparison of theory with experiment, *SIAM J. Appl. Math.* **61**, 387–431; <http://epubs.siam.org/sam-bin/dbq/article/32621> 74, 172
- [180] Xin-She Yang: Turing pattern formation for catalytic reaction-diffusion systems in engineering application, *Modeling Simul. Mater. Sci. Eng.* **11**. 321, 2003; <http://www.iop.org/EJ/abstract/0965-0393/11/3/305/> 73, 74, 172
- [181] R. Zare: *Chem. Phys.* **40**, 1934, 1964 205
- [182] C. Zürcher und T. Frank: *Bau und Energie – Bauphysik*, vdf, 1998 7, 28, 29

Index

- $\alpha\Omega$ dynamo, 134
- α -effect, 134
- absorption, 6
- abstraction, 38
- acceleration
 - stochastic, 86, 87
- acceleration efficiency, 93
- accuracy, 45, 211
 - first-order, 210
 - second-order, 211
- ADI, 69
- ADI method, 69
- adiabatic deceleration, 81, 87, 91, 94
- adiabatic invariants, 83
- advection, 161
- advection–dispersion eq.
 - first-order reaction, 42
- air shower, 158
- air temperature, 29, 33
- albedo, 6
- Alfvén wave, 83
- alternating direct method (ADI), 69
- ambient temperature, 29, 33
- amplification factor, 67, 69, 212
- angular distribution, 201
- anisotropic diffusion, 60
- anisotropy, 87
- ansatz by a power series, 188
- Archimedian spiral, 82
- art of modeling, 20
- art of simplifying, 15
- artesian pressure, 109
- autobahn, 1
- avalanche, 5, 11
- average bond energy, 145
- average displacement, 58
- average emissivity, 32
- average speed, 199
- average squared distance, 58
- averaging, 161, 162, 198, 199, 201
- Böschungsbruch, 109
- Böschungsrutschen, 109
- basis function, 104
- basis functions, 104
- Bastille Day event, 143, 146
- beam tailoring, 160, 177
- bell curve, 59
- Bernoulli, 58
- Bernoulli distribution, 139
- Bernoulli’s equation, 174
- Bernoulli’s law, 1, 3, 38
- best-case–worst-case scenario, 15, 21
- Bethe–Bloch equation, 145, 146, 149, 176, 177
- bi-Maxwellian, 200
- black body, 31
- black box model, 93
- Bohr, 38
- Boltzmann equation, 85, 201, 203, 204
 - collision term, 86, 202
 - collisionless, 202
 - reduced, 202
- Bouger–Lambert–Beer law, 176
- boundary condition, 3, 173
 - Dirichlet, 102, 112
 - mixed Dirichlet–Neumann, 102
 - Neumann, 102
 - Robin, 102
- boundary conditions
 - Cauchy, 112
- boundary immobilization method (BIM), 79
- boundary value problem, 102
- boundary-value problem, 78
- bracketing the solution, 15, 21, 31
- Bragg peak, 145, 151, 176
- Bremsstrahlung, 147, 151
- bremsstrahlung, 147, 149, 159
- Brownian motion, 202, 205
- brute-force reductionism, 11
- bulk speed, 119, 199
- buoyancy, 109
- butterfly effect, 11

- calculated ion–pair production rate, 145
 CAMMPUS, 174
 cardiovascular system, 2
 cascade, 158
 Cauchy boundary conditions, 112
 Cauchy data, 189
 Cauchy problem, 189
 Cauchy surface, 189
 CAWSES, 142, 144, 157
 cellular automata, 174
 centered finite difference, 43
 centered scheme, 215
 central method, 213
 centrifugal force, 121, 122
 Cerenkov detector, 159
 Challenger, 18
 chaotic behavior, 162
 characteristic determinant, 189
 characteristic form, 189
 characteristic matrix, 189
 characteristic path length, 164
 characteristic surface, 189
 characteristics, 190
 - elliptic PDE, 191
 - hyperbolic PDE, 190
 - parabolic PDE, 191
 - totally hyperbolic PDE, 190
 Chernobyl, 12
 climate model, 6, 70
 climate modeling, 160
 clo, 29
 closure, 16
 clustering coefficient, 164
 coastal defence, 5
 coastal evolution, 5
 cobpoint, 93
 collision, 57, 204
 collision frequency, 62, 206
 collision term, 86, 203
 collisionless viscosity, 121
 collisions
 - large-angle, 207
 comfort range, 28
 compartment, 24
 compartment concept, 20
 compartment model, 41
 compatibility relation, 190
 compatibility relations, 191
 Compton scattering, 149
 computational fluid dynamics, 118
 computer tomography, 159
 conditioning matrix, 66–68
 conductivity, 204
 confinement of a plasma, 98
 conservation
 - angular momentum, 197
 - charge, 197
 - energy, 196, 197, 205
 - mass, 196, 197
 - mechanical energy, 197
 - moment, 198
 - momentum, 197, 205
 - potential energy, 197
 - thermal energy, 197
 conservation laws, 16, 36, 196
 conservation of momentum, 38
 conservations law, 161
 consistency, 211
 consolidation coefficient, 111
 constituting equations, 111
 contact erosion, 109
 continuity
 - equation of
 - phase space, 201
 convection, 7, 28, 31, 81, 87, 91
 - with the solar wind, 87
 convection in momentum space, 85
 convective cooling, 31
 convective streaming, 71
 convergence, 67, 212
 convolution theorem, 193
 Coriolis force, 121, 122, 208
 corresponding variables, 192
 cosmogenic nuclide, 159
 cosmogenic nuclides, 143
 Coulomb collision, 206, 207
 Coulomb collisions, 84
 Coulomb interaction, 202
 Coulomb logarithm, 207
 Coulomb scattering, 84
 - cross section, 206
 Coulomb's law, 197, 198
 Courant–friedrich–Lewis, 216
 Courant–Friedrichs–Lewy, 212
 Cowling's theorem, 133
 Cramer's rule, 66
 Crank–Nicolson, 48, 50, 214
 Crank–Nicolson scheme, 217
 critical Reynolds' number, 22
 cross section, 205, 206
 - Coulomb scattering, 206
 - large-angle deflection, 206
 Crutzen, 144
 current acceleration, 131
 d'Alembert's solution, 191
 D'Arcy speed, 74, 111
 D'Arcy's law, 74, 75
 Dalton's law, 27

- data models, 17
- dead-end pores, 74
- Debye length, 207
- decay, 42
- decay probability, 140
- decay radiation, 159
- degenerated, 191
- Deichverteidigungstraße, 110
- deposition, 5
- derivative, 210
 - second, 211
- difference quotient, 210
- differential flux, 201
- differential quotient, 210
- differential rotation, 134
- diffusion, 7, 56, 57, 62, 71, 76, 160, 166
 - anisotropic, 60
 - definition, 55
 - homogenous medium, 61
 - in momentum space, 57, 85
 - in pitch angle, 84
 - isotropic, 60, 61
 - pitch angle, 84
 - spatial, 57, 84
- diffusion coefficient, 58–62, 166
 - eddy, 62
 - field parallel, 62
 - in momentum space, 85
 - pitch angle, 84
 - radial, 61, 62
 - turbulent, 62
- diffusion equation, 9, 60, 216
 - solution for δ -injection, 61
 - source term, 61
 - spherical symmetric, 61
- diffusion in momentum space, 57, 85, 86
- diffusion plus advection, 56
- diffusion tensor, 60, 61, 203
- diffusion–convection, 166
- diffusion–convection equation, 42, 55, 71, 81, 84, 87, 89, 218
- diffusion–convection model, 1, 56
- diffusion–reaction equation, 172
- diffusion–reaction model, 72
- dike, 4, 107
 - discretization, 112
 - fluid pressure height, 113
- dimensional analysis, 22
- dimensionless variable, 127
- Dirichlet boundary condition, 102, 112
- discretization, 103–105, 112, 210, 213
- disease, 166
- dispersion, 42, 56, 62, 71, 160
- dispersion coefficient, 45, 62
- dispersion–advection equation, 71
- dissipation range, 83
- distribution function, 57, 119, 198, 201
- drunkards walk, 57, 137
- dunes, 5
- dyad, 120
- dynamical systems, 163
- dynamo
 - $\alpha\Omega$, 134
 - homogeneous, 133
 - MHD, 129
- eddy, 56
- eddy diffusion, 39, 62
- eddy diffusion coefficient, 62
- edge, 164
- effective permeability, 75
- effective porosity, 111
- effective temperature, 31
- efficient porosity, 74
- einstrahlzahl, 32
- El Nino, 161
- Elbeflut, 108
- electromagnetic cascade, 159
- electron trajectory, 149
- elliptic PDE, 101, 191
 - ADI, 69
 - centered finite difference, 217
 - characteristics, 191
 - five-point scheme, 218
 - numerical schemes, 217
- elliptical boundary problem, 102
- embankment
 - breaking, 109
 - sliding, 109
 - surface erosion, 109
- embankment spring, 108, 109, 114
- emergence, 163
- emergent phenomena, 173
- energy balance, 38
- energy conservation, 16, 38, 196
- energy density, 16, 17
- energy flux density, 16, 17
- energy loss distribution, 147
- energy spectrum, 92
- energy transport, 6
- enhanced fractional time step and time splitting method, 89
- enthalpy, 79
- enthalpy method, 79
- envelope, 19
- eq. of continuity, 197
- equation of continuity, 36, 41, 60
 - soil, 111
 - water, 111

- equation of motion, 38, 118, 122
 erosion, 5, 109, 115
 Erosionsgrundbruch, 109, 115
 Euler's backward method, 214
 Euler's equation, 118, 120, 174
 Euler's forward method, 214
 Euler's method, 214
 Euler–Tricomi equation, 192
 evaporation, 7, 26, 28
 expected displacement, 59
 expected distance, 58
 expected value, 139
 explicit, 214
 explicit centered five-point scheme in space
 and an advanced scheme in time, 67
 explicit scheme, 216
 exponential ansatz, 187
 external force, 118

 FDM, 41
 FEM, 41
 Fermi, 40
 Feuchtigkeitsgehalt, 111
 Feynman, 18
 Fick's law, 31, 42, 43, 162, 197, 198
 field reversal, 143
 filament
 solar, 129
 filtering, 162
 filtration speed, 74
 finite difference scheme
 consistent, 211
 finite difference equation, 211
 finite difference scheme
 accuracy, 211
 advanced, 210
 backward, 211
 centered, 211
 consistency, 211
 convergence, 212
 forward, 210
 one-sided, 210, 211
 retarded, 211
 finite element, 101, 104
 finite-difference approximation, 210
 fire modeling, 128
 fire simulation, 8
 first principle, 16
 five-point scheme, 218
 flash-over, 128
 flow speed, 199
 fluid pressure height, 113
 flux corrected transport, 9, 99
 flux limiter, 97
 flux limiter method, 89, 91

 flux-tube structure, 83
 focused transport, 81, 87
 focused transport equation, 84
 focusing, 81, 83, 87, 100
 focusing length, 87, 95
 Fokker–Planck equation, 201–204, 207
 forward in time and centered in space, 218
 Fourier transform, 192
 Fourier's law, 31, 197, 198
 fractionalization, 103, 104, 112, 174, 175
 friction, 121
 frictional forces, 203
 frozen-in field, 131
 FTCS method, 69, 218
 FTCS scheme, 47
 functional imaging, 159

 galactic cosmic rays, 148, 158, 159
 Galton board, 59, 60
 game theory, 58
 Gauß distribution, 59
 Gauß' distribution, 59
 Gauss–Seidel method, 67
 Gauss-Seidel algorithm, 103
 Gauss-Seidel method, 68
 Gaussian elimination, 66, 103
 GEANT 4, 148, 158, 176
 general circulation model, 161
 geomagnetic field, 143, 151
 geostrophic approximation, 208
 glacier, 4
 global circulation, 7
 global coupled ocean–atmosphere model, 7
 global growth phase, 169
 graph theory, 163
 gray body, 31
 Green's function, 8, 9, 82
 greenhouse gas, 157
 groundwater, 74
 growing core, 76
 gyration, 83

 Hadley cell, 122
 hadronic interaction, 147, 158, 159
 Hall effect, 132
 HAMMONIA, 157
 Hangquelle, 108, 109
 heat
 latent, 7
 sensible, 7
 heat balance integral method, 79
 heat conduction, 28, 30, 56, 76, 101
 heat conduction equation, 17, 63, 67, 191, 216
 steady-state, 63
 heat flow, 101

- heat flow density, 31
 heat transfer coefficient, 31
 heat transport, 7
 Heavyside expansion, 193, 194
 Heizkörper, 30
 Hess matrix, 202
 HIV, 165
 HO_x, 144, 151, 153, 154
 holistic approach, 11
 hub, 167
 hydraulic base failure, 109, 115
 hydraulic gradient, 111
 hydraulischer Grundbruch, 109, 115
 hydrological cycle, 4, 7
 hydrostatic equation, 208
 hydrostatic pressure, 199
 hyperbolic PDE, 89, 91, 190
 - centered scheme, 215
 - characteristics, 190
 - Lax–Wendroff scheme, 216
 - numerical schemes, 215
 - totally, 190, 191
 - characteristics, 190
 - upwind scheme, 216
- ideal fluid, 120
 Iljin scheme, 90, 91
 impact parameter, 206, 207
 implicit, 214
 implicit scheme, 90, 217
 incompressible fluid, 121
 inertial range, 83
 information, 2, 23
 initial boundary value problem, 47
 initial distribution, 173
 initial vector, 66
 input variables, 19
 integral transform, 192
 integro-interpolation scheme, 91
 interaction cross section, 147
 internal force, 118
 interplanetary magnetic field, 82
 interplanetary propagation, 82, 98
 interplanetary shock, 93
 interplanetary space
 - diffusion coefficient, 62
- intertwined models, 4
 ion acoustic wave, 83
 ion–pair production, 144, 145, 149
 ion–pair production rate, 144
 ionization, 143, 144, 147, 176
 Iraqi war, 12
 isolated pores, 74
 isotropic diffusion, 61
 isotropic turbulence, 62
- iteration parameters, 69
 iterative method, 66
 Jacobi method, 66, 103
 Jeans’ theorem, 204
 kappa distribution, 204
 kappa-distribution, 200
 Katrina, 8, 12, 17
 kernel, 192
 kinematic viscosity, 120, 121
 kinetic energy, 199, 200
 kinetic theory, 198
 Kirchhoff’s law, 196
 Kirchhoff’s law 1, 197
 Kirchhoffs law, 197
 knee, 101
 Kolmogoroff scale, 63
 Laasonen scheme, 217
 Ladevektor, 105
 laminar, 22
 Laplace equation, 63, 191, 216
 Laplace transform, 188, 192, 193
 - properties, 193
- large-angle collisions, 207
 large-angle interactions, 84, 207
 Larmor radius, 83, 121
 latent heat, 7
 law of large numbers, 58
 Lax scheme, 216
 Lax’ scheme, 212
 Lax’s Equivalence Theorem, 212
 Lax–Wendroff scheme, 216
 Leapfrog method, 214
 lexicographical ordering, 65
 linear convection equation, 190, 215
 linear energy transfer, 148
 linear system, 22
 linearizing, 21
 Liouville’s theorem, 202
 local growth phase, 169
 logistic law, 40, 220
 Lorentz, 11
 Lorentz distribution, 200
 Lorentz force, 203
 Lorentz’ butterfly, 11
 Lorentz’ force, 83
 LU decomposition, 219
- macroscopic phenomena, 198
 magnetic bottle, 83
 magnetic cloud, 95, 97
 magnetic field fluctuations, 82
 magnetic field reversal, 156

- magnetic mirror, 83
- magnetic moment, 83
- magnetic pressure, 131
- Malthus' law, 40
- mass balance, 36
- mass conservation, 196
- mass matrix, 105
- mathematical model, 15
- matrix
 - pentadiagonal, 66
- matrix form, 189
- Maxwell distribution, 119, 121, 199, 202–204
- Maxwell–Boltzmann distribution, 200
- mean free path, 45, 60, 62, 121, 205, 206
 - and rigidity, 86
 - estimate, 62
 - parallel to the field, 62, 84
 - radial, 62
- mean radiant temperature, 31
- met, 29
- metabolism, 29
- MHD
 - one-fluid description, 130
 - two-fluid description, 131
- MHD dynamo, 122, 129, 135
- Michaelis–Menton, 197
- microscopic approach, 198
- mixed Dirichlet–Neumann boundary, 102
- mixing length theory, 62
- mobility, 60
- model
 - data, 17
 - first principle based, 16
 - phenomenological, 17
- modeling
 - definition, 15
- moisture content, 111
- momentum balance
 - two-fluid description, 131
- momentum balance, 38, 118, 122
 - fictitious forces, 121
 - pressure-gradient force, 119
 - stress tensor, 120
 - viscosity, 121
- momentum transport, 7, 91
- Monte Carlo differential equation, 160
- Monte Carlo simulation, 57, 105, 136, 176, 177
 - π , 136
 - accuracy, 137, 139
 - advection and decay, 142
 - radioactive decay, 140
 - radiation therapy, 175
 - radioactive decay, 141
- moving boundary, 173
- multiple equilibria, 162
- multiple scattering, 146, 149
- Navier–Stokes equation, 75, 118, 120, 122, 126, 207
- Navier–Stokes equations, 69
- network, 164
- Neumann boundary condition, 102
- Newton, 38
- Newton's law, 197
- Newton's law of cooling, 25, 197
- Newton's universal law of gravitation, 198
- Newton's viscosity law, 197
- nitrite oxides, 144
- NO_x, 144, 146, 151, 153, 154
- nodal integration method (NIM), 79
- nonlinearity, 161
- normal force, 119
- nuclear physics, 158
- number density, 199
- numerical integration, 136
- ODE, 41
 - 1st order
 - general, 188
 - inhom, variable coeff., 188
 - 2nd order
 - hom., const. coeff., 187
 - hom., variable coeff., 188
 - inhom., const. coeff., 187
 - nonlin, 188, 189
 - ansatz by a power series, 188
 - Crank–Nicolson, 214
 - Euler backwards, 214
 - Euler forwards, 214
 - Euler's method, 214
 - exponential ansatz, 187
 - finite difference methods, 213
 - Laplace transform, 188
 - Leapfrog, 214
 - p-substitution, 189
 - particulate integral, 187
 - Runge–Kutta, 215
 - separable, 187
 - separation of variables, 187
 - startegies, 187
 - variation of the constant, 188
- Oderflut, 108
- Ohm's law, 197
 - current acceleration, 131
 - Hall term, 132
 - pressure diffusion, 132
 - two-fluid description, 131
- omnidirectional intensity, 201

- one-dimensional Maxwell distribution, 119
- one-dimensional pipe, 20
- one-dimensional pipe model, 20
- output variables, 19
- over-relaxation method, 68
- ozone, 143, 144, 146, 153, 157
- p-substitution, 189
- pair production, 147, 159
- parabolic PDE, 42, 89, 191
 - characteristics, 191
 - Crank–Nicolson, 217
 - explicit scheme, 216
 - Iljin scheme, 90
 - implicit scheme, 90, 217
 - Laasonen scheme, 217
 - numerical schemes, 216
- parallel mean free path, 62, 84
- parameter study, 8
- partial differential equation, 9
- particle, 198
- particle number conservation, 91
- particle precipitation, 143
- particulate integral, 187, 188
- PDE, 41
 - Cauchy problem, 189
 - characteristic determinant, 189
 - characteristic form, 189
 - characteristics, 189
 - classification, 190
 - elliptic, 101, 191
 - ADI, 69
 - centered finite difference, 217
 - characteristics, 191
 - five-point scheme, 218
 - numerical schemes, 217
 - finite differences, 215
 - FTCS method, 218
 - hyperbolic, 89, 91, 190
 - centered scheme, 215
 - characteristic, 190
 - Lax–Wendroff scheme, 216
 - numerical schemes, 215
 - upwind scheme, 216
 - parabolic, 42, 89, 191
 - characteristics, 191
 - Crank–Nicolson, 217
 - explicit scheme, 216
 - Iljin, 90
 - implicit scheme, 90, 217
 - Laasonen scheme, 217
 - numerical schemes, 216
 - totally hyperbolic, 190, 191
 - characteristics, 190
 - types, 190
- Peaseman–Rachford ADI, 69
- penetration depth, 75
- pentadiagonal matrix, 66
- permeability, 74, 75, 111
 - effective, 75
- perturbation method, 79
- perturbation theory, 85
- phase space, 198
 - equation of continuity, 201
 - equation of motion, 201
 - point, 198
 - speed, 198
- phase space density, 84, 85, 198
- phase transition, 173
- phenomenological model, 17
- phonon, 56
- photoionization, 149
- pipeline, 2
- pitch angle, 83, 84
- pitch angle coefficient, 91
- pitch angle diffusion, 84
- pitch angle diffusion coefficient, 84, 86
- pitch angle scattering, 81, 82, 87
- pitch angle transport, 89
- plasma, 129
- plasma confinement, 83, 98
- plasma fusion, 98
- plasma- β , 131
- point in phase space, 198
- Poisson equation, 217
- polar cap, 143, 151
- polar front, 7
- pores
 - dead-end, 74
 - isolated, 74
- porosity, 74, 75, 111
 - efficient, 111
- porous media, 100
- positron, 159
- post-facto modeling, 17
- power density spectrum, 82, 86
- power law, 148
- precipitating particles
 - energy spectra, 148
- pressure, 120
- pressure diffusion, 132
- pressure gradient force, 208
- pressure-gradient force, 118–120
- probability function, 203
- proton trajectory, 149
- quasi-linear theory, 85
- quasi-neutral, 128
- radial mean free path, 62

- radiation exchange coefficient, 32
 radiation therapy, 175
 radiation therapy planing, 176
 radiation transport, 6
 radiative heat exchange, 7
 radiative heat transfer, 28, 31
 radiator, 7, 30
 radioactive decay
 Mont Carlo simulation, 141
 Monte Carlo simulation, 140
 radiocarbon, 159
 random kinetic energy, 199
 random number, 139
 repetition, 139
 random number generator, 139
 reaction rate, 54
 real fluid, 120
 reduced Boltzmann equation, 202
 reduction, 161, 178
 reflection, 6
 relaxation factor, 68
 reputation, 23
 resistance, 204
 resonance, 194
 resonance catastrophe, 23
 resonance condition, 86
 resonance frequency, 86
 resonance gap, 91
 resonance interaction, 86
 resonance scattering, 86
 resonant wave–particle interaction, 86
 Reynolds' number, 22, 75, 127
 rigidity, 86
 Robin boundary condition, 102
 room temperature, 101
 round-off error, 212
 rumor, 166
 run-off ditch, 108–110, 114
 runaway, 23
 Runge–Kutta method, 4th order, 215

 SARS, 170
 saturated zone, 74
 saturation, 74, 111, 113
 saturation line, 108
 scale analysis, 21, 63, 207
 atmosphere, 208
 scale-free net, 164
 scale-free network, 167, 168
 scattering, 6
 resonance, 86
 scattering at plasma waves, 84
 scattering cross section, 205
 scattering in momentum space, 86
 secondary electron, 149, 176

 secondary electrons, 146
 sediment, 2
 self generated turbulence, 93
 self-consistent fields, 204
 self-excited waves, 85
 self-organization, 163
 self-stabilizing system, 85
 sensible heat, 7, 31
 sensitivity analysis, 16
 separable ODE, 187
 separation ansatz, 63, 93
 separation of the variables, 187
 separation of variables, 189
 shear failure, 109, 115
 shear stress, 119, 120
 shell-and-tube heat exchanger, 40
 shock, 93, 95
 acceleration efficiency, 93
 as black box, 93
 in interplanetary space, 93
 shock in interplanetary space
 as Stefan problem, 97
 shrinking core, 76
 Sickerlinie, 108
 Sickerpunkt, 108
 Sickerströmung, 74, 109
 simplification, 15, 178
 simplifying as an art, 15
 simplifying assumptions, 19
 Simpson integration, 213
 singular perturbed problem, 89
 six degrees of separation, 164
 slab model, 86
 SLIMCAT/TOMCAT model, 147
 small world, 166
 small-angle interactions, 84, 207
 small-angle scattering, 86
 small-world, 164
 small-world phenomenon, 163
 smokestack, 56
 solar constant, 6
 solar cycle, 154
 solar energetic particle, 61, 81, 97, 143, 157
 energy spectra, 148
 solar energetic particle event, 81
 ozone depletion, 143
 solar wind, 82
 solar wind effects, 91
 solar wind expansion, 83, 87
 sound wave, 161
 Southern Oscillation, 161
 spallation, 159
 sparse, 218
 sparse matrix, 45

- spatial diffusion, 57, 84
- spatial scale, 10
- spatial transport, 89
- specific energy loss, 145
- specific heat, 17
- spectral index, 148
- speed
 - average, 199
 - bulk, 199
 - flow, 199
 - relative to soil, 111
 - stochastic, 199
 - thermal, 199
 - turbulent, 63
- speed in phase space, 198
- spiral angle, 62
- splitting scheme, 89
- stability, 212
 - parabolic PDE
 - explicit scheme, 217
- stability conditions, 97
- standard deviation, 59, 139
- statistical mechanics, 198
- steady-state, 23, 42, 50
- Stefan problem, 78, 81, 97, 173, 174
 - shock in interplanetary space, 97
- Stefan–Boltzmann law, 31
 - gray body, 31
- Steifigkeitsmatrix, 105
- Stephan number, 78
- sterile modeling, 17
- stiffness matrix, 105
- stirred tank, 20, 24, 25, 41, 76, 178
- stochastic acceleration, 86, 87
- stochastic differential equation, 160
- stochastic motion, 199, 200
- stochastic partial differential equation, 161
- stochastic process, 56, 57, 82
- stochastic speed, 199
- stochastic transport process, 55
- stochasticity, 161
- Stoffstrommanagement, 53
- stream structure, 83
- streaming, 60, 71, 85
 - convective, 71
 - diffusive, 60
- stress tensor, 120, 121
- subsoil flow, 74, 109
- suffosion, 109
- sunspot, 129
- supergranular motion, 82
- supergranulation, 83
- surface erosion, 109
- surface temperature, 33
- surface wave, 2, 6
- system variables, 19
- Taylor expansion, 210
- TE, 211
 - Euler backwards, 214
 - Euler forward, 214
 - hyperbolic PDE
 - centered scheme, 215
 - upwind scheme, 216
 - parabolic PDE
 - centered finite difference, 218
 - explicit scheme, 216
 - PDE
 - FTCS method, 218
- temperature, 119, 200
 - effective, 31
 - mean radiant, 31
 - room, 101
- temporal scale, 10
- tensor, 120
- test, 22
- thermal comfort, 33
- thermal conductivity, 31
- thermal equilibrium, 200, 204
- thermal motion, 57, 119
- thermal speed, 119, 121
 - most probable, 199
- thermohaline circulation, 7, 70, 161
- Thomas algorithm, 48, 125, 218
- three-decade-standard, 4
- time scale, 161
- time splitting, 90
- time splitting scheme, 81, 89
- time to maximum, 61
- total squared displacement, 58
- totally hyperbolic PDE, 191
- traffic, 2
- traffic jam, 173
- translation, 194
- transmission probability, 166
- transport
 - definition, 9
 - in momentum, 91, 119
 - in pitch angle, 89
- transport model, 9
- transport through porous media, 74
- trapezoid integration, 213
- triangulation, 104
- tridiagonal matrix, 45, 48, 107, 125, 218
- truncation error, 211, 212
 - Euler backwards, 214
 - Euler forward, 214
 - hyperbolic PDE
 - centered scheme, 215

- upwind scheme, 216
- parabolic PDE
 - centered finite difference, 218
 - explicit scheme, 216
- PDE
 - FTCS method, 218
- tsunami, 3
- turbulence, 2, 24, 82, 83, 162
 - isotropic, 62
- turbulent, 22
- turbulent diffusion coefficient, 62
- turbulent energy dissipation, 63
- turbulent mixing, 62
- turbulent speed, 63
- Turing, 11, 72
- Turing pattern, 172, 173
 - 1D, 173
 - initial distribution, 173
- Turing's avalanche, 11

- unconditionally stable, 69
- under-relaxation method, 68
- unsaturated zone, 74
- update form, 212
- upwind scheme, 216

- vardose zone, 74
- variation of the constant, 188
- vector-borne disease, 169
- velocity distribution, 198, 199
- vertex, 164
- viscosity, 75, 111, 121, 204
 - collisionless, 121
 - kinematic, 120, 121
- viscosity coefficient, 121
- Vlasov equation, 85, 199, 203, 204
 - average, 85
- volume dilation, 111
- Von Neumann analysis, 212
- von Neumann ansatz, 67
- von Neumann method, 68
- Vorfluter, 108–110

- wave
 - Alfvén, 83
 - ion acoustic, 83
 - ion-cyclotron, 83
 - Whistler, 83
- wave equation, 190
- wave-particle interaction, 84, 85
- weak form, 103
- weak problem, 112
- Weichselflut, 108
- weight function, 175
- weighting function, 103

- Wendelstein, 98
- Whistler, 83
- wind-chill, 29
- working model, 11
- World Wide Web, 168

- X-ray, 159

- z88, 174
- Zeltfunktion, 104